

Single Molecule Catalysis of Organic Ions
Studied by
Mass Spectrometry and Computational Chemistry

For Lindsay

Single Molecule Catalysis of Organic Ions
Studied by
Mass Spectrometry and Computational Chemistry

By

KARL JOHN JOBST, B.Sc.

A Thesis

Submitted to the School of Graduate Studies

In Partial Fulfillment of the Requirements

for the Degree

Doctor of Philosophy

McMaster University

© Copyright by Karl John Jobst, May 2011

Abstract

During the past fifty years, mass spectrometry, often hyphenated with chromatography, has developed into the most widely used technique for the quantitative and qualitative analysis of increasingly complex mixtures of (bio)organic molecules.

One important aspect of this development concerns the relationship between the structure (atom connectivity) of a molecule and the mass spectrum obtained by electron ionization (EI). In this context, from 1960 - 1990, a wealth of studies has appeared that uses a variety of novel experimental techniques, often in conjunction with isotope labelling, to probe the structure, stability, reactivity and dissociation characteristics of the radical cations generated by EI of various classes of molecules. One highlight was the discovery of surprisingly stable distonic ions and the role they play in the dissociation chemistry of ionized molecules.

However, mechanistic proposals based upon experimental observations can often only be considered as tentative. Synergy between experiment and theory would be ideal to remedy this situation, but it was not until recent spectacular advances in computer technology and software that this approach could be implemented. It has led to the growing realization that many rearrangement reactions of radical cations in the rarefied gas-phase involve catalysis. Proton-transport catalysis (PTC) is a prime example : here, a neutral species induces an ion to isomerize via hydrogen-bridged radical cations (HBRCs) as intermediates. An exemplary case described in this thesis concerns the ion-molecule reaction of the cyanamide ion $\text{NH}_2\text{-C}\equiv\text{N}^{\bullet+}$ with a single H_2O molecule : experiment and theory indicate that the H_2O molecule catalyzes the swift transformation of $\text{NH}_2\text{-C}\equiv\text{N}^{\bullet+}$ into the more stable carbodiimide ion $\text{HN}=\text{C}=\text{NH}^{\bullet+}$.

The thesis exploits the synergy of tandem mass spectrometry and computational chemistry to study the role of catalysis in the association and dissociation reactions of several systems of radical cations. During these studies, a new type of a catalyzed reaction was discovered: "ion-catalysis", where an organic cation promotes the otherwise

prohibitive rearrangement of a neutral. Ion-catalysis is proposed to explain the unexpected loss of $\text{NH}_2\text{O}^\bullet$ from low-energy N-hydroxyacetamide ions $\text{CH}_3\text{C}(=\text{O})\text{NHOH}^{+\bullet}$: the molecular ion rearranges into the HBRC $[\text{O}=\text{C}-\text{C}(\text{H}_2)-\text{H}-\text{N}(\text{H})\text{OH}]^{+\bullet}$ whose acetyl (cation) component catalyzes the transformation $\text{NHOH}^\bullet \rightarrow \text{NH}_2\text{O}^\bullet$. Another highlight involves a hybrid reaction, in which both the ion and the neutral component of an incipient HBRC catalyze one another to rearrange into more stable isomers.

Catalysis may also play an important role in astrochemistry and a question addressed in this context is whether pyrimidine, a key component of DNA, may be generated by ion-molecule reactions. It appears that the acrylonitrile ion (AN) does not react with HCN to produce ionized pyrimidine, instead it isomerizes by PTC. However, the reaction of the ion with its neutral counterpart does not involve catalysis, but rather cyclization into the pyrimidine ion! A related topic concerns the structures of covalently bound dimers of the ubiquitous interstellar molecules HCN and HNC. Neutralization-Reionization Mass Spectrometry in conjunction with model chemistry calculations leaves little doubt that the elusive dimers $\text{HN}=\text{C}=\text{C}=\text{NH}$ and $\text{HC}=\text{N}-\text{C}=\text{NH}$ are kinetically stable in the rarefied gas-phase, whereas $\text{HC}=\text{N}-\text{N}=\text{CH}$ is not.

The structure of ions may also be probed by interactions with selected neutral molecules rather than dissociative collision experiments (MS/MS). An exciting case involves the differentiation of isomeric heterocyclic ions by ion-molecule reactions with dioxygen. Here, too, model chemistry calculations play an essential role in understanding the mechanism and the scope of the reaction.

Preface

The larger part of the experimental and computational results reported in this thesis were obtained by the author during five years of research in gas-phase ion chemistry. This field is ideally suited to be subjected to both experimental and theoretical investigation : theoretical chemistry and mass spectrometry are complementary approaches for the examination of isolated molecules and ions. Such investigations necessitate the collaboration of both experimental and theoretical chemists. Collaborative contributions from Prof. Richard D. Bowen (Chapters 8 and 9), Dr. Pascal Gerboux (Chapters 2, 5 and 13) and Prof. Robert Flammang (Chapter 13) are greatly appreciated. The computational contributions of Dr. Henri Ervasti (Chapters 3 and 5) are also greatly appreciated.

Finally, two individuals deserve special mention in the context of collaboration : Dr. Peter C. Burgers (Chapters 3, 5 and 6) and Prof. Paul J.A. Ruttink (Chapters 2, 3, 5 – 7 and 11). Their contributions, insights, suggestions and critical evaluations have significantly shaped the way the results have been presented.

The permission of Elsevier Science to reproduce data and text which has been previously published is also appreciated.

List of Publications

1. K.J. Jobst, R.D. Bowen, J.K. Terlouw, *Int. J. Mass Spectrom.* (in press).
The dissociation chemistry of low-energy N-formylethanolamine ions : hydrogen-bridged radical cations as key intermediates
2. K.J. Jobst, S. Jogee, R.D. Bowen, J.K. Terlouw, *Int. J. Mass Spectrom.* (in press).
A mechanistic study of the prominent loss of H₂O from ionized 2-hydroxy-aminoethanol
3. K.J. Jobst, J.K. Terlouw, *Chem. Phys. Lett.* 497 (2010) 7.
The covalently bound dimer ion HC=N-C=NH⁺ and its neutral counterpart.
4. H.K. Ervasti, K.J. Jobst, P. Gerbaux, P.C. Burgers, P.J.A. Ruttink, J.K. Terlouw
Chem. Phys. Lett. 482 (2009) 211.
The reaction of the acrylonitrile ion CH₂=CH-C≡N⁺ with HCN : Proton-transport catalysis vs formation of ionized pyrimidine.
5. K.J. Jobst, P. Gerbaux, G. Dimopoulos-Italiano, P.J.A. Ruttink, J.K. Terlouw
Chem. Phys. Lett. 478 (2009) 144.
The quest for the elusive carbodiimide ion HN=C=NH⁺ and its generation by proton-transport catalysis.
6. K.J. Jobst, J. De Winter, R. Flammang, J.K. Terlouw, P. Gerbaux
Int. J. Mass Spectrom. 286 (2009) 83.
Differentiation of the pyridine radical cation from its distonic isomers by ion-molecule reactions with dioxygen.
7. K.J. Jobst, M.R. Hanifa, P.J.A. Ruttink, J.K. Terlouw
Chem. Phys. Lett. 473 (2009) 257.
The covalently bound HCN dimer ions HC=N-N=C-H⁺ and HC=N-C(=N)H⁺ are stable species in the gas-phase, but the neutral counterparts are not.
8. J.L. Holmes, K.J. Jobst, J.K. Terlouw, *Eur. J. Mass Spectrom.* 15 (2009) 261.
Small (poly)unsaturated oxygen containing ions and molecules : a brief assessment of their thermochemistry based on computational chemistry.
9. K.J. Jobst, M.R. Hanifa, J.K. Terlouw, *Chem. Phys. Lett.* 462 (2008) 152.
The covalently bound HNC dimer ion HN=C=C=NH⁺ has a kinetically stable neutral counterpart.

10. K.J. Jobst, J.K. Terlouw, T. Luider, P.C. Burgers, *Anal. Chim. Acta.* 627 (2008) 136.
On the interaction of peptides with calcium ions as studied by MALDI-FTMS : towards peptide fishing using metal ion baits.
11. K.J. Jobst, S.A. Hasan, J.K. Terlouw, *Chem. Phys. Lett.* 450 (2008) 243.
Does the ion-molecule reaction between $HC\equiv CH^{+}$ and HCN lead to $CH_2=CH-C\equiv N^{*+}$?*
12. K.J. Jobst, P.J.A. Ruttink, J.K. Terlouw, *Int. J. Mass Spectrom.* 269 (2008) 165.
The remarkable dissociation chemistry of 2-aminoxyethanol ions $NH_2OCH_2CH_2OH^{+}$ studied by experiment and theory.*
13. J.L. Holmes, K.J. Jobst, J.K. Terlouw
J. Label. Compd. Radiopharm. 50 (2007) 1115.
Isotopic Labelling in mass spectrometry as a tool for studying mechanisms of ion dissociations.
14. K. Levsen, H. Schiebel, J.K. Terlouw, K.J. Jobst, M. Elend, A. Preiß, H. Thiele, A. Ingendoh, *J. Mass Spectrom.* 42 (2007) 1024.
Even electron ions : a systematic study of the neutral species lost in the dissociation of quasi-molecular ions.
15. K.J. Jobst, T.R. Khan, J.K. Terlouw, *Int. J. Mass Spectrom.* 264 (2007) 146.
The loss of DCN from OD-labelled 4-hydroxypyridine radical cations : a rearrangement reaction unraveled by theory and experiment.
16. H.K. Ervasti, K.J. Jobst, P.C. Burgers, P.J.A. Ruttink, J.K. Terlouw
Int. J. Mass Spectrom. 262 (2006) 88.
The acrylonitrile dimer ion : a study of its dissociation via self-catalysis, self-protonation and cyclization into the pyrimidine radical cation.
17. K.J. Jobst, P.C. Burgers, P.J.A. Ruttink, J.K. Terlouw
Int. J. Mass Spectrom. 254 (2006) 127.
The loss of NH_2O^ from the N-hydroxyacetamide radical cation : an ion-catalyzed rearrangement.*

Acknowledgements

First and foremost, I am indebted to Dr. J.K. Terlouw for his mentorship during the past five years. JKT : your devotion to learning and well being of your students is remarkable and I credit much of my success as a graduate student to the experience and confidence that you instilled in me. Hartelijk Dank !

I am also grateful to my advisory committee members, Dr. Paul Ayers and Dr. Brian McCarry for their encouragement and inspiration during the course of my studies. In particular, I would like to thank Dr. McCarry for many stimulating discussions and Dr. Ayers for inciting my interest (if not aptitude) in theoretical chemistry.

The insight and expertise provided by our collaborators, Dr. Peter C. Burgers (Erasmus University), Dr. Paul J.A. Ruttink (Utrecht University) and Dr. Pascal Gerbaux (University of Mons) also played an important role in my scientific development. The hospitality they showed me during my (ad)ventures abroad is also greatly appreciated. I am also thankful to Dr. Vince Y. Taguchi (Ontario Ministry of the Environment) for involving me in a joint project and provoking my interest in Environmental Mass Spectrometry.

During my studies, I was pleased to have had the opportunity to work with Henri Ervasti and Julien De Winter. I am grateful for your contributions to this thesis as well as the many interesting conversations we have had over a pint (or two) of Belgian beer.

In the McMaster mass spectrometry laboratory, I have also had the opportunity to work with Dr. Kirk Green, Tadek Olech, Gina Dimopoulos-Italiano, Leah Allen, Ewan DeSilva and Richard Lee. I greatly appreciate your contribution to a pleasant lab atmosphere.

I thank the friends that I have, both inside and outside the Department of Chemistry. Your friendship helped me to maintain a positive attitude during the most tumultuous periods of my studies. I am ever thankful to my parents and siblings for their love and support. Finally, I am grateful to my wife Lindsay who was a constant source of encouragement and (financial) support. Lindsay : I love you and I could not have done it without you !

Table of Contents

Abstract	iii
Preface	v
List of Publications	vi
Acknowledgements	viii
Table of Contents	ix
List of Figures	xi
List of Abbreviations	xviii
 CHAPTER 1	
1.1 Introduction, scope of this thesis	1
1.2 Mass spectrometry and computational chemistry for the study of radical cations	3
1.3 Radical cations of unconventional structure and their role in proton-transport catalysis	20
 CHAPTER 2	
The quest for the elusive carbodiimide ion $\text{HN}=\text{C}=\text{NH}^{\bullet+}$ and its generation by proton-transport catalysis	27
 CHAPTER 3	
The acrylonitrile dimer ion : a study of its dissociation via self-catalysis, self-protonation and cyclization into the pyrimidine radical cation	39
 CHAPTER 4	
Does the ion-molecule reaction between $\text{HC}\equiv\text{CH}^{\bullet+}$ and $\text{HC}\equiv\text{N}$ lead to $\text{CH}_2=\text{CH}-\text{C}\equiv\text{N}^{\bullet+}$?	65
 CHAPTER 5	
The reaction of the acrylonitrile ion $\text{CH}_2=\text{CH}-\text{C}\equiv\text{N}^{\bullet+}$ with HCN : Proton-transport catalysis vs formation of ionized pyrimidine	75
 CHAPTER 6	
The loss of $\text{NH}_2\text{O}^\bullet$ from the N-hydroxyacetamide radical cation $\text{CH}_3\text{C}(=\text{O})\text{NHOH}^{\bullet+}$: an ion catalyzed rearrangement	87

CHAPTER 7

The remarkable dissociation chemistry of 2-aminoxyethanol ions HOCH ₂ CH ₂ ONH ₂ ^{•+} studied by experiment and theory.....	103
--	-----

CHAPTER 8

A mechanistic study of the prominent loss of H ₂ O from ionized 2-hydroxyaminoethanol, HOCH ₂ CH ₂ NHOH ^{•+}	125
---	-----

CHAPTER 9

The dissociation chemistry of low-energy N-formylethanolamine ions : hydrogen-bridged radical cations as key intermediates.....	147
--	-----

CHAPTER 10

The covalently bound HNC dimer ion HN=C=C=NH ^{•+} has a kinetically stable neutral counterpart.	181
--	-----

CHAPTER 11

The covalently bound HCN dimer ions HC=N-N=CH ^{•+} and HC=N-C(=N)H ^{•+} are stable species in the gas-phase, but the neutral counterparts are not.	195
--	-----

CHAPTER 12

The covalently bound dimer ion HC=N-C=NH ^{•+} and its neutral counterpart.....	207
---	-----

CHAPTER 13

Differentiation of the pyridine radical cation from its distonic isomers by ion-molecule reactions with dioxygen.....	219
--	-----

CHAPTER 14

Experimental	231
Summary	241

List of Figures

Page	
6	Figure 1.1 Schematic diagram of the VG Analytical ZAB-R mass spectrometer.
7	Figure 1.2 Partial MI spectra of (a) unlabelled and (b) OD-labelled 4-hydroxypyridine ions.
8	Figure 1.3 Partial MI mass spectrum of protonated methyl oxamate.
9	Figure 1.4 Energy diagram of an endothermic reaction.
11	Figure 1.5 (a) MI and (b) CID mass spectra of ionized 4-hydroxypyridine.
12	Figure 1.6 Partial CID mass spectrum of ionized 4-hydroxypyridine.
14	Figure 1.7 Schematic representation of a CIDI experiment.
15	Figure 1.8 Schematic representation of a NR experiment.
24	Figure 1.9 Schematic diagram of the Autospec 6F mass spectrometer.
29	Figure 2.1 Optimized geometries of the cyanamide ion 1 and its principal isomers obtained at the B3LYP/CBSB7 level of theory; bond lengths in Å. Also shown is the geometry of the crossing 6 → 6Q discussed in Section 2.2.
31	Figure 2.2 Potential energy diagram for the loss of N(⁴ S) from the cyanamide ion 1 and its principal isomers. The numbers in square brackets refer to CBS-QB3 derived 298 K enthalpy values in kcal mol ⁻¹ .
34	Figure 2.3 (a) Partial CID spectrum and (b) NR-CID spectrum of cyanamide ions 1 ; (c) Partial CID spectrum of nitrilimine ions 5 generated from 1,3,4-triazole; (d) Partial CID spectrum of carbodiimide ions 2 generated by the dissociative ionization of 2-imidazolecarboxaldehyde; (e) partial CID spectrum of the CIDI experiment on <i>N</i> -methylguanidine derived ions, see text; (f) Partial CID spectrum of the <i>m/z</i> 42 ions generated in the ion-molecule reaction of ions 1 with H ₂ O.
37	Figure 2.4 Proton-transport catalysis (PTC) of the cyanamide ion 1 .
42	Figure 3.1 (a) Chemical ionization mass spectrum of a mixture of gaseous acrylonitrile and CO ₂ . The MI and the CID spectra of the <i>m/z</i> 106 acrylonitrile dimer ions of this spectrum are shown as items (b) and (c) respectively. The insets in (b) and (c) refer to the spectra of the <i>m/z</i> 108 dimers ions of acrylonitrile-2-d.

- 47 **Figure 3.2** Structures of stable acrylonitrile dimer ions and their stabilization energies (kcal/mol) relative to the dissociation level $\text{CH}_2=\text{CH}-\text{C}\equiv\text{N}^{\bullet+}$ (AN) + $\text{CH}_2=\text{CH}-\text{C}\equiv\text{N}$; the values in square brackets refer to CBS-QB3 calculations (298 K enthalpies).
- 48 **Figure 3.3** (a and b) Potential energy diagrams (CBS-QB3 calculations) describing the self-protonation reaction and the occurrence of proton-transport catalysis in acrylonitrile dimer ions. The relative energies are in kcal/mol.
- 51 **Figure 3.4** CID mass spectra of product ions generated from metastable acrylonitrile dimer ions: (a) m/z 53 ions (loss of acrylonitrile); (b) m/z 79 ions (loss of HCN); (c) m/z 80 ions (loss of C_2H_2); (d) m/z 105 ions (loss of H^\bullet).
- 53 **Figure 3.5** Isomerization pathways of acrylonitrile dimer ions **D1** into ions **D7**. The relative energies are in kcal/mol and were obtained from CBS-QB3 calculations (Table 3.2).
- 56 **Figure 3.6** Energy diagram derived from CBS-QB3 298K calculations (in kcal/mol) describing the losses of C_2H_2 , HCN and H^\bullet from metastable acrylonitrile dimer ions **D1**. Note #1 : dissociation from **VP1a** and **VP2a**, see text; Note #2 : exchange vinyl H atoms via **VP1b**, see text.
- 58 **Figure 3.7** Selected optimized geometries (CBSB7 basis set) for stable intermediates and transition states involved in the dissociation chemistry of low-energy acrylonitrile dimer radical cations.
- 68 **Figure 4.1** (a) MI and (b) CID spectra of m/z 53 acrylonitrile ions **AN**; the inset displays the partial MI spectrum of $\text{CH}_2=\text{CH}-^{13}\text{C}\equiv\text{N}$ (c) CID spectrum of **AN-4**, generated by HCN loss from pyrazine ions; (d) CID spectrum of **AN-2**, generated by HCN loss from metastable pyridine ylid-ions; (e,f) CID spectra of m/z 52 ions $\text{HC}=\text{C}=\text{C}=\text{NH}^+$ generated from metastable ions **AN** and **AN-4**, respectively; (g) CID spectrum of ions $\text{HC}\equiv\text{C}-\text{N}=\text{CH}^+$ generated from collisionally energized ions **AN-4**; (h) CID spectrum of ions $\text{CH}_2=\text{C}-\text{C}\equiv\text{N}^+$ generated by dissociative ionization of 2-bromoacrylonitrile.
- 69 **Figure 4.2** Dissociation pathways leading to the loss of HCN and H^\bullet from acrylonitrile ions and two of its principal isomers **AN-2** and **AN-4**. Energy diagram (kcal/mol) based on CBS-APNO calculations.
- 78 **Figure 5.1** The mechanistic proposal for the formation of ionized pyrimidine in the ion-molecule reaction of HCN and ionized acrylonitrile (**AN**). The numbers refer to CBS-QB3 derived 298 K enthalpies in kcal/mol.

- 80 **Figure 5.2** CID mass spectra of the C_3H_3N ions generated from : (a) low-energy (metastable) pyrimidine (**PY**); (b) pyrimidine-4-ylid (**PY1**) ions; (c) ionized acrylonitrile (**AN**) and (d) the ion-molecule reaction **AN** + HCN.
- 82 **Figure 5.3** (a) Chemical ionization mass spectrum of a mixture of $CH_2=CH-C\equiv N$, HCN and CO_2 ; (b) mass spectrum of the products of the ion-molecule reaction **AN** + HCN performed in the hexapole reaction chamber of the Autospec; (c) MI and partial CID spectra of m/z 81 ions **AN**/ $H^{13}CN$; (d) partial CID spectra of adduct ions **AN**/HCN and **AN**(^{15}N)/HCN.
- 84 **Figure 5.4** Proton-transport catalysis (PTC) of the acrylonitrile ion (**AN**) with HCN as the catalyst. The numbers refer to CBS-QB3 derived 298 K enthalpies in kcal/mol.
- 91 **Figure 6.1** (a) MI spectrum of ionized N-hydroxyacetamide, $CH_3C(=O)NHOH^{+\bullet}$ (**HA-1**); (b) partial MI spectrum of $CH_3C(=O)NDOD^{+\bullet}$ (**HA-1d₂**); (c) partial CID spectrum of $CH_3C(=O)NDOD^{+\bullet}$ (**HA-1d₂**); (d) CIDI spectrum of the $m = 32$ neutrals generated from metastable ions **HA-1**; (e) the m/z 14 – 18 region of the CIDI spectrum of the $m = 32$ neutrals generated from metastable ions **HA-1**; (f) the m/z 14 – 18 region of the CID spectrum of the m/z 32 reference ions of the structure $NHOH^+$.
- 95 **Figure 6.2** Energy-level diagram derived from CBS-QB3 calculations describing the elimination of NH_2O^{\bullet} from metastable N-hydroxyacetamide ion **HA-1** via *quid-pro-quo* mechanism. The numbers refer to 298K enthalpy values in kcal/mol.
- 100 **Figure 6.3** Selected optimized geometries (CBSB7 basis set) for stable intermediates and transition states involved in the elimination of NH_2O^{\bullet} from ionized N-hydroxyacetamide (**HA-1**).
- 106 **Figure 7.1** (a) 70 eV EI mass spectrum of $NH_2OCH_2CH_2OH$ (2-aminoxyethanol); the MI and CID spectra of the molecular ion are represented by items (b) and (c) respectively, whereas item (d) shows the MI spectrum of $ND_2OCH_2CH_2OD^{+\bullet}$; items (e) to (h) are CID spectra of respectively m/z 61, 60, 47 and 46 ions generated from metastable ions $NH_2OCH_2CH_2OH^{+\bullet}$.
- 109 **Figure 7.2** Optimized geometries (B3LYP/CBSB7 method) of selected stable intermediates and connecting transition states involved in the dissociation of 2-aminoxyethanol ions **AE1**.
- 113 **Figure 7.3a** Energy diagram depicting the isomerization of ionized 2-aminoxyethanol (**AE-1**) into the hydrogen-bridged radical cation **HBRC-2**. The numbers refer to 298 K enthalpies (in kcal mol⁻¹) derived from CBS-QB3 calculations.

- 114 **Figure 7.3b** Energy diagram depicting the various dissociation mechanisms initiated from **HBRC-2**. The numbers are 298 K enthalpies (in kcal mol⁻¹) derived from CBS-QB3 calculations.
- 117 **Figure 7.4** Transformation of the glycolaldehyde ion **2a** into the 1,2-dihydroxyethene ions **2b** by proton-transport catalysis. The numbers are 298 K enthalpies (in kcal mol⁻¹) derived from CBS-QB3 calculations.
- 128 **Figure 8.1** Structures of *m/z* 59 C₂H₅NO⁺ product ions and their enthalpies of formation (298 K values in kcal mol⁻¹ derived from CBS-QB3 calculations, see Table 8.1).
- 129 **Figure 8.2** 70 eV EI mass spectrum of 2-hydroxyaminoethanol hydrochloride.
- 129 **Figure 8.3** MI and CID spectra of molecular ions HOCH₂CH₂NHOH⁺, items (a) and (b) respectively. The insets refer to the corresponding spectra of the isotopologue DOCH₂CH₂NDOD⁺. Item (c) is the CID spectrum of the *m/z* 59 ions generated from metastable ions HOCH₂CH₂NHOH⁺ while items (d) and (e) represent the corresponding partial spectra of the *m/z* 60 and 61 ions from DOCH₂CH₂NDOD⁺ and HOCH₂CD₂NHOH⁺, respectively. Spectra (c) and (d) contain a partially resolved peak for loss of H[•] with an intensity of ~ 30 % of the base peak.
- 132 **Figure 8.4** Optimized geometries of various conformers of ionized 2-hydroxyaminoethanol (**HE1a-e**) and their neutral counterparts (**HEN1a-e**).
- 134 **Figure 8.5** Energy diagram depicting the C-C bond cleavage of the 2-hydroxyaminethanol ion **HE1a**. The numbers are CBS-QB3 derived 298 K enthalpies (in kcal mol⁻¹).
- 135 **Figure 8.6** Energy diagram depicting the proposed mechanism for loss of water from 2-hydroxy-aminoethanol ions **HE1a**. The numbers are CBS-QB3 derived 298 K enthalpies (in kcal mol⁻¹).
- 139 **Figure 8.7** Alternative mechanisms for the loss of water from 2-hydroxyaminoethanol ions **HE1a**. The numbers in square brackets are CBS-QB3 derived 298 K enthalpies (in kcal mol⁻¹).
- 144 **Figure 8.8** Optimized geometries (B3LYP/CBSB7) of minima and transition states involved in the water loss from ionized 2-hydroxy-aminoethanol (**HE-1**).
- 151 **Figure 9.1** EI mass spectrum of N-formylethanolamine HOCH₂CH₂NHCHO
- 151 **Figure 9.2** (a) MI and (b) CID mass spectra of the N-formylethanolamine radical cation (**FE1**); (c) MI and (d) CID mass spectra of protonated N-formylethanolamine (**PFE**); note : a weak peak (*c.* 5%) at *m/z* 89 in Fig. 9.2d is not shown.

- 153 **Figure 9.3** Left column: (a), (b) and (c) are CID mass spectra of the source generated m/z 46, m/z 59 and m/z 71 ions from N-formylethanolamine; (d) CID spectrum of the m/z 71 ions generated by thermal decomposition. Right column : CID spectra with the collision chamber at -1 kV of m/z 71 ions generated from (e) N-vinyl-formamide; (f) N-formylethanolamine and (g) N-formyl-O-methylethanolamine $\text{CH}_3\text{OCH}_2\text{CH}_2\text{NHCHO}$; (h) CID spectrum of the m/z 73 ions generated from ^{18}O -labelled N-formylethanolamine $\text{HOCH}_2\text{CH}_2\text{NHCHO}^{18}$.
- 154 **Figure 9.4** $\text{C}_3\text{H}_5\text{NO}^{*+}$ (m/z 71) ion structures and their 298 K enthalpies of formation in kcal mol^{-1} derived from CBS-QB3 calculations.
- 178 **Figure 9.5** Optimized geometries of selected minima and transition states involved in the dissociation chemistry of ionized N-formylethanolamine. Numbers in brackets are CBS-QB3 derived 298 K enthalpies in kcal mol^{-1} .
- 183 **Figure 10.1** Proposed fragmentation pathways of precursor ions which yield the HCN dimer ions **1** and **2**.
- 185 **Figure 10.2** (Front) 3ffr CID mass spectra of m/z 54 ions generated by dissociative ionization of (a) xanthine, (b) aminomalononitrile and (c) diaminomaleonitrile. The m/z 53 peak in spectra (b) and (e) is not shown; it is four times as intense as the m/z 27 peak. (Back) the corresponding NR-CID mass spectra of the m/z 54 ions (d) $\text{HN}=\text{C}=\text{C}=\text{NH}^{*+}$ (**1**) and (e) $\text{H}_2\text{N}-\text{C}-\text{C}\equiv\text{N}^{*+}$ (**2**).
- 187 **Figure 10.3** Computational results pertaining to the isomerization and dissociation of the $\text{C}_2\text{H}_2\text{N}_2$ ions **1-4** (top) and their neutrals **N1-N4** (bottom). The numbers in square-brackets refer to CBS-APNO derived 298 K enthalpies in kcal mol^{-1} . Vertical recombination energies (RE_v) are given in eV.
- 190 **Figure 10.4** NR mass spectra of m/z 54 ions generated by dissociative ionization of (a) xanthine, (b) aminomalononitrile and (c) diaminomaleonitrile. Insets show an expanded view of the m/z 23 – 29 region.
- 192 **Figure 10.5** Mechanistic proposal rationalizing the generation of ions **1** and **2** from ionized diaminomaleonitrile. The numbers refer to 298 K enthalpies in kcal mol^{-1} calculated by the CBS-QB3 model chemistry.
- 198 **Figure 11.1** (left) Measurements on *s*-tetrazine : (a) 70 eV EI mass spectrum; (b,c) CID mass spectra (O_2) of the m/z 54 ions generated in the ion source and from metastable molecular ions; (d) NR mass spectrum of the m/z 54 ions. (right) Measurements on *s*-triazine : (e) 70 eV EI mass spectrum; (f,g) CID mass spectra (O_2) of the m/z 54 ions generated in the ion source and from metastable molecular ions; (h) NR mass spectrum of the m/z 54 ions. Partial CID spectra (He) of the m/z 38- 40 region are shown in the insets.

- 199 **Figure 11.2** Mechanistic proposal for the formation of m/z 54 and m/z 28 ions from low-energy *s*-tetrazine ions (**TET-1**). Numbers in square and round brackets refer to 298 K enthalpies (in kcal mol⁻¹) derived from CBS-APNO and CBS-QB3 calculations respectively.
- 202 **Figure 11.3** Mechanistic proposal for the formation of m/z 54 ions from low-energy *s*-triazine ions (**TRI-1**). Numbers in brackets refer to 298 K enthalpies (in kcal mol⁻¹) from CBS-APNO calculations.
- 203 **Figure 11.4** Mechanistic proposal for the formation of m/z 28 ions and m/z 53 ions from the low-energy HCN dimer ions **1** and **2**. The numbers refer to CBS-APNO derived 298 K enthalpies in kcal mol⁻¹.
- 209 **Figure 12.1** EI mass spectrum of 2-methoxy-*s*-triazine
- 210 **Figure 12.2** The formation of C₂H₂N₂⁺⁺ ions **1** and **2** by dissociative ionization of *s*-triazine and 2-methoxy-*s*-triazine. The numbers in square brackets are 298 K enthalpies in kcal mol⁻¹.
- 211 **Figure 12.3** (left) CID mass spectra of the m/z 54 ions generated from (a) *s*-triazine; (b) 2-methoxy-*s*-triazine and (c) CD₃-labelled 2-methoxy-*s*-triazine. (right) NR mass spectra of the m/z 54 ions generated from (d) *s*-triazine and (e) 2-methoxy-*s*-triazine. Item (f) shows the m/z 20 – 30 region of the NR mass spectrum of HC=N–C=ND⁺⁺.
- 213 **Figure 12.4** Model chemistry results of Table 13.1 showing the dissociation and isomerization chemistry of C₂H₂N₂⁺⁺ ions **1** - **4** and their neutral counterparts. The 298K enthalpies are in kcal mol⁻¹; the vertical recombination energies (RE_v) shown are in eV.
- 216 **Figure 12.5** (a) NR-CID and (b) 3ffr CID mass spectra of the m/z 54 ions from 2-methoxy-*s*-triazine.
- 220 **Figure 13.1** Structures of the pyridine ion **1** and its α -, β - and γ -distonic isomers **2-4**. Relative energies are in kcal/mol and taken from Ref. 4.
- 221 **Figure 13.2** The generation of pyridine-2-ylid ions by dissociative ionization of 2-acetylpyridine.
- 222 **Figure 13.3** Mass spectra of the products of the ion-molecule reactions of pyridine-2-ylid ions with : (a) water vapour; (b) dioxygen [O₂ pressure = 2 x 10⁻⁴ mbar] and (c) dioxygen [O₂ pressure = 8 x 10⁻⁴ mbar]. Items (d-f) are CID mass spectra of the m/z 95, m/z 94 and m/z 111 ions, generated in the above ion-molecule reactions with dioxygen.
- 223 **Figure 13.4** The ion-molecule reaction of the pyridine-2-ylid ion **2** with H₂O. The numbers refer to 298 K enthalpies in kcal/mol derived from CBS-QB3 calculations.

- 225 **Figure 13.5** Potential energy diagrams describing the associative ion-molecule reactions of (a) the pyridine-2-ylid ion **2** and (b) the pyridine-3-ylide ion **3** with dioxygen. Numbers in square brackets refer to CBS-QB3 derived 298 K enthalpies in kcal/mol.
- 227 **Figure 13.6** The generation of pyridine-3-ylid ions by dissociative ionization of 2,3-diacetylpyridine.
- 228 **Figure 13.7** Mass spectra of the products of the ion-molecule reactions of pyridine-3-ylid ions with dioxygen. (a) [O_2 pressure = 2×10^{-4} mbar] and (b) [O_2 pressure = 8×10^{-4} mbar]; (c) CID mass spectrum of the m/z 95 ions generated in the above ion-molecule reaction.

List of Abbreviations

AE	=	appearance energy
B	=	magnetic sector
B3LYP	=	hybrid Hartree-Fock/density functional theory
CA	=	collisional activation
CCSD(T)	=	coupled cluster singles doubles and triples
CE	=	charge exchange
CI	=	chemical ionization
CID	=	collision-induced dissociation
CIDI	=	collision-induced dissociative ionization
CS	=	charge-stripping
CBS-APNO	=	composite theoretical method (model chemistry)
CBS-QB3	=	composite theoretical method (model chemistry)
DFT	=	density functional theory
EI	=	electron ionization
ESA	=	electrostatic analyzer
eV	=	electron Volt (1 eV = 23.061 kcal/mol or 96.387 kJ/mol)
ffr	=	field-free region
G3	=	Gaussian-3 theoretical method
HBRC	=	hydrogen-bridged radical cation
ΔH_f	=	enthalpy of formation
HF	=	Hartree-Fock
$IE_{(a/v)}$	=	ionization energy (adiabatic/vertical)
KER	=	kinetic energy release
MI	=	metastable ion
MO	=	molecular orbital
MP	=	Møller-Plesset (perturbation theory)
MS	=	mass spectrometry
NDMA	=	N,N-dimethylaniline
m/z	=	mass to charge ratio
NR(MS)	=	neutralization-reionization (mass spectrometry)
PA	=	proton affinity
q	=	charge
r	=	radius
$RE_{(a/v)}$	=	recombination energy (adiabatic/vertical)
SCF	=	self-consistent field
T	=	kinetic energy release (value)
TPEPICO	=	threshold photoelectron photoion coincidence
TS	=	transition state
ZAB-R	=	BEE three-sector mass spectrometer
ZPVE	=	zero-point vibrational energy

Chapter 1

1.1 Introduction, scope of this thesis

Catalytic processes have been used widely for thousands of years, for example in the age-old practice of fermentation. However, a rational theory of catalysis was not proposed until the early 19th century [1]. This discovery heralded unprecedented advances in chemistry and presently, catalysis is recognized as a widespread natural phenomenon that is highly important in multiple scientific disciplines.

This thesis explores the role of catalysis in the chemistry of organic radical cations using mass spectrometry-based experiments and computational chemistry.

Radical cations ($M^{\bullet+}$) may conveniently be generated by ionization of organic molecules (M) under the high-vacuum conditions of the mass spectrometer. Compared to their neutral counterparts, radical cations display dramatically altered unimolecular reactivity, often leading to the isomerization of ions $M^{\bullet+}$ into (more) stable isomers, which are frequently of unconventional structure [2]. In general, unconventional ions have neutral counterparts that are either very weakly bound or else represent unstable or transient species. Examples of these include distonic ions [2a], ion-dipole complexes [2b] and the structurally related hydrogen-bridged radical cations (HBRCs) [2c].

Where the isomerization of a solitary ion is associated with a prohibitive energy barrier, an important question of general interest is whether a single ‘solvent’ molecule may catalyze the reaction. The concept coined ‘proton-transport catalysis’ (PTC) [3] is a prime example : in this *catalysis*, the encounter complex generated in the interaction of a radical cation with a neutral molecule, adopts the configuration of a HBRC wherein the neutral promotes the isomerization of the ion into a more stable (distonic) hydrogen shift isomer. This intriguing topic is explored in Chapters 2 – 5 .

As stated above, conventional radical cations may isomerize into HBRCs, the key intermediates in PTC, en route to their dissociation. In Chapter 6 – 9, the important role of catalysis is explored in the dissociative ionization of various organic molecules.

The available experimental (and computational) methodologies are not confined to the study of ions, but these can also be advantageously used to study highly reactive neutral molecules. In the short studies described in Chapters 10 – 12, the technique of neutralization-reionization mass spectrometry (NRMS) [4] is used to probe the structure and stability of the covalently bound HCN dimers, species of potential interest in astrochemistry. Here too, the theme of catalysis emerges in the generation of the corresponding dimer ions.

Finally, an important aspect of the studies in catalysis is the structure analysis of organic ions. Chapter 13 deals with an interesting method to characterize distonic ions using ion-molecule reactions with dioxygen.

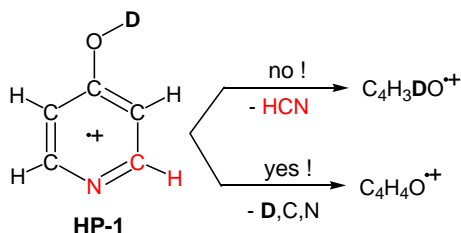
The studies described in this thesis and reported in the literature (see page vi), were obtained as part of joint projects with various international research groups. In this mutually beneficial arrangement, it was possible to address challenging scientific problems requiring complementary experimental and theoretical information (and expert intellectual input !) not available in our research group. Indeed, for the studies of Chapters 2, 5 and 13, unambiguous results could only be obtained using the sophisticated six-sector mass spectrometer (Autospec 6F) in the laboratory of Dr. Pascal Gerboux (Mons University, Belgium). Nevertheless, the better part of the measurements and calculations has been performed and interpreted by the author using the ZAB-R and Autospec 6F mass spectrometers and the SHARCNET computer network at McMaster University .

For the benefit of the non-expert reader, the various experimental and computational methods are briefly introduced and discussed in Section 1.2. This is followed in Section 1.3 by a brief introduction to radical cations of unconventional structure and their relationship to proton-transport catalysis.

1.2 Mass spectrometry and computational chemistry for the study of radical cations

Electron ionization (EI) mass spectrometry is a powerful method for the structure analysis of organic molecules and since its inception in the early 1960s, a variety of experimental procedures has been designed to establish the structure, stability, reactivity and dissociation characteristics of a great many radical cations [5]. The use of these techniques as well as the present knowledge of the structure and reactivity of small organic ions ($C_1 - C_3$) has been recently summarized in the book ‘Assigning Structures to Ions in Mass Spectrometry’ [5]. This book forms the basis for the outline below, where it deals with the various experimental procedures used in the studies of this thesis.

Experiments have been widely used to study the reaction mechanisms of organic ions, but experimental results alone frequently lead to tentative proposals at best. A case in point concerns the study [6] of the dissociation chemistry of ionized 4-hydroxypyridine (**HP-1**). Perhaps unsurprisingly, low-energy ions **HP-1** dissociate by losing CO and hydrogen (iso)cyanide. However, when the time-honoured method of isotopic labelling [7] is used to probe the mechanism, a confounding result is obtained : the OD-labelled ion of Scheme 1.1 loses DCN (or DNC) specifically !



Scheme 1.1

This puzzling observation would have remained unexplained, were it not that spectacular advances in computer technology and software in the early 1990s paved the way for the advent of the CBS, Gaussian and Weizmann model chemistries [8]. These computational tools allow reaction mechanisms to be studied in considerable detail, often with chemical accuracy (± 1 kcal/mol).

Throughout the introduction to the mass spectrometry-based experiments described in Sections 1.2.1 – 1.2.3, selected results from the study of the dissociation chemistry of ions **HP-1** are interspersed to facilitate the explanation of the methodology. Section 1.2.4 provides a brief description of the computational tools that played a crucial role in the studies of this thesis and in unravelling the mysterious D,C,N loss from ions **HP-1**.

1.2.1 The principles of the mass spectrometer and the study of metastable ions

The interaction of a fast moving electron with a gaseous sample molecule may lead to ejection of an electron from the neutral, its ionization, within 10^{-16} seconds [9].

This process is orders of magnitude faster than a molecular vibration (10^{-13} to 10^{-14} seconds) and thus, in line with the Franck-Condon principle, the nuclear framework of the molecule remains fixed. The kinetic energy of the impinging electrons ($E_{\text{el}} \cong 50 - 100$ eV) greatly exceeds the ionization energy (IE) of the target organic molecule, typically 7 – 14 eV. As a result, the EI experiment yields ‘odd-electron’ molecular ions, whose internal energy distribution peaks at around 3 eV and effectively extends to ~ 7 eV.

The incipient molecular ions may undergo various rearrangement reactions and also dissociate, provided that they have sufficient internal energy. However, where and when a given reaction can be *observed* in the experiments also depends on the time-scale of the events listed in Table 1.1. It follows from the Table that the ions reside in the source for about 1 μs before they are converted into a fast moving ion beam of typically 8 keV translational energy that reaches the detector about 20 μs later.

This implies that a minimum rate constant of 10^6 s^{-1} obtains for the *unstable* molecular ions that dissociate within the source. The maximum rate constant depends on the type of reaction and varies from 10^{14} s^{-1} for direct bond cleavage reactions to 10^{10} s^{-1} for certain rearrangement processes.

In contrast, the *stable* ions are defined as having insufficient internal energy to achieve a rate constant $> 10^5$ s^{-1} and thus, these ions reach the detector before they fragment.

The fraction of molecular ions that dissociate en route to the detector (with rate constants

$10^5 < k < 10^6 \text{ s}^{-1}$) are called *metastable* ions [9]. These distinguish themselves from the *unstable* ions as having a narrow, well-defined internal energy distribution.

Table 1.1. Time-scale of events in μs following the EI ionization of a molecule in a magnetic deflection type instrument.

Event	Total time elapsed in μs (time of event)
Ionization	10^{-10}
Vibration (chemistry begins)	$10^{-7} - 10^{-9}$
Rotation	10^{-2}
Ions leave source	1
Ions pass field-free region 1	3
Ions reach collision cell 4 in field-free region 2	13
Collisional excitation	$10^{-8} - 10^{-10}$
Time for ions to traverse a collision cell	10^{-1}
Ions reach detector 1	23

ZAB-R mass spectrometer, for m/z 100 ions, accelerated by 8 kV

Theoretical treatments (QET and RRKM theory) have been developed which could, in principle, predict the appearance of an EI mass spectrum, but only if the mechanisms and the associated energy requirements of all of the competing fragmentations has been established [9]. Moreover, for processes that take place in the ion source, such an analysis is further complicated by the broad internal energy distribution of the ions.

Analysis of the (low-energy) metastable ions is therefore quite attractive because the potential mechanisms that need be considered are confined to those whose energy requirements fall into a narrow energy domain. A sector mass spectrometer configured with the magnet (B) preceding the electrostatic analyzer (E) is the ideal instrument to study dissociating metastable ions. The VG ZAB-R instrument [10] used in the studies of this thesis has such a BE configuration, as shown in Figure 1.1. The instrument is in fact a unique three-sector mass spectrometer capable of performing a wide array of

sophisticated experiments on mass-selected ions, broadly referred to as MS/MS techniques [5]. The first MS/MS technique that will be discussed is the metastable ion kinetic energy (MIKE or MI) experiment.

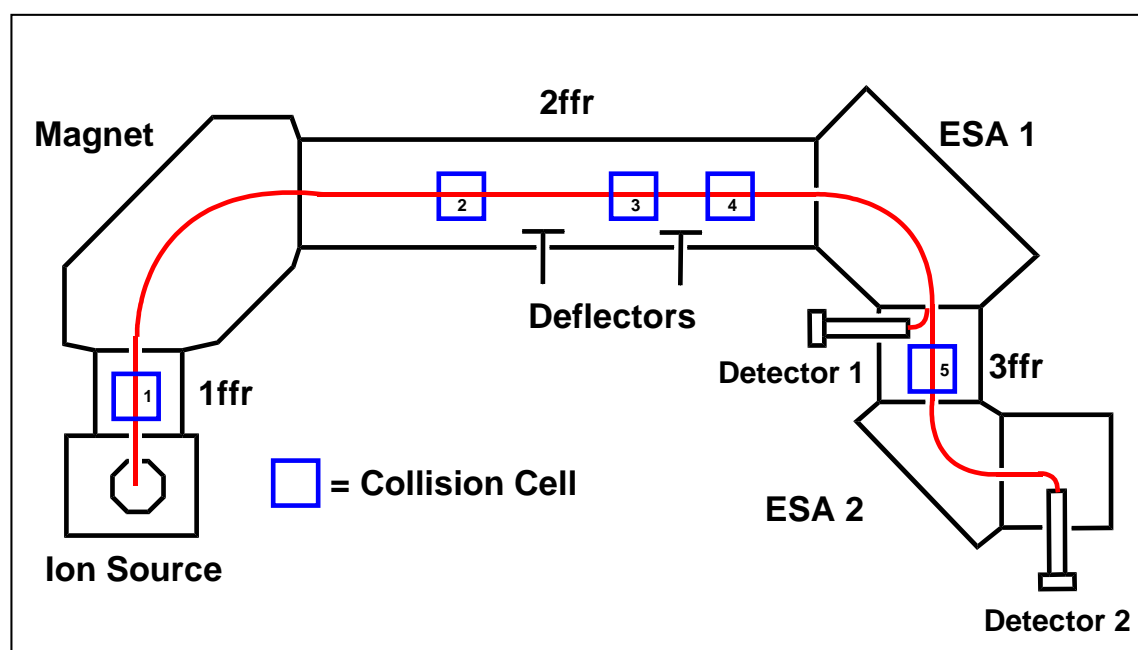


Figure 1.1. Schematic diagram of the VG Analytical ZAB-R instrument. The positive ions generated in the ion source are extracted by a small positive potential applied to a repeller electrode inside the ionization chamber. Upon exiting the source, the ions are accelerated by a 6-10 keV potential drop V into a drift region preceding the magnet. This drift region is termed the first field free region (ffr) as it is free of any applied magnetic or electric fields. There are two additional field free regions in this instrument, the 2ffr and the 3ffr, and it is within these field free regions where the chemistry of the ions is explored.

Metastable ion (MI) mass spectra are obtained by selectively transmitting the stable and metastable precursor ions m_1^+ through the magnetic sector, into the second field free region (2ffr). This is achieved using a fixed accelerating voltage (V) and by setting the magnetic field strength (B) so that only ions m_1^+ are deflected along a radius (r) according to the fundamental equation: $m/z = B^2 r^2 / 2V$. Upon dissociation of ion m_1^+ in the 2ffr, its kinetic energy is distributed amongst the products $m_2^+ + m_3$, in line with the law of conservation of momentum. In this scenario, ions m_2^+ will pass through ESA1 with a

kinetic energy equal to the mass weighted fraction of the kinetic energy of the precursor ion, $(m_2/m_1)V$. Thus, mass separation of the products arising from mass selected metastable ions, which account for *c.* 1% of the total ion current, may be achieved by scanning the ESA voltage.

Figure 1.2a displays the MI mass spectrum of the 4-hydroxypyridine molecular ions **HP-1**. The peaks at m/z 67 and 68 are the only signals in the spectrum and these arise from the losses of CO and [H,C,N]. In Figure 1.2b, it is seen that the OD-labelled **HP-1** ions lose CO and [D,C,N] to yield a single peak at m/z 68, whose shape is clearly a composite of the two peaks in Figure 1.2a. This nicely illustrates how the composite shape of a peak is telltale sign that (at least) two different processes are operative [9] in forming either isobaric or isomeric product ions.

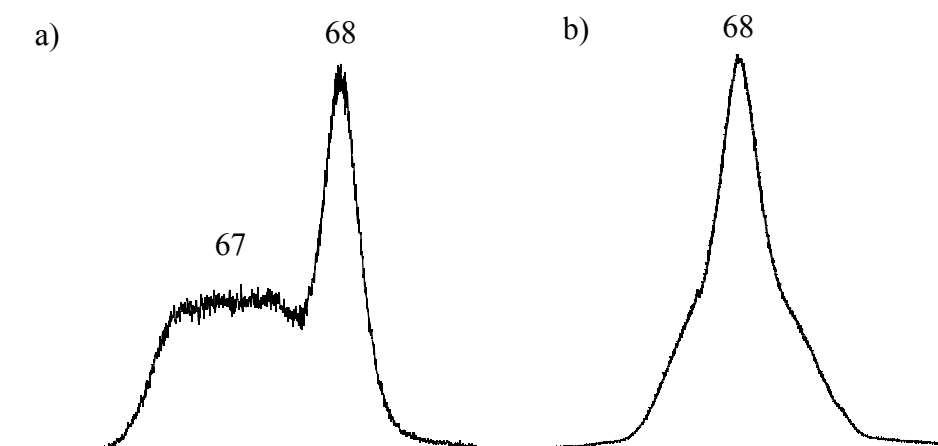


Figure 1.2 Partial MI spectra of (a) unlabelled and (b) OD-labelled 4-hydroxypyridine ions **HP-1**.

An interesting example of a ‘triple’ composite peak is shown in Figure 1.3. It concerns the metastable peak at m/z 76 obtained from metastable m/z 104 ions resulting from the self-protonation reaction of ionized methyl oxamate $[\text{NH}_2\text{-C(=O)-C(=O)OCH}_3]^{\bullet+} : \text{M}^{\bullet+} (m/z 103) + \text{M} \rightarrow [\text{M+H}]^+ (m/z 104) + [\text{M-H}]^\bullet$. The three components must arise from three different processes that have not yet been established.

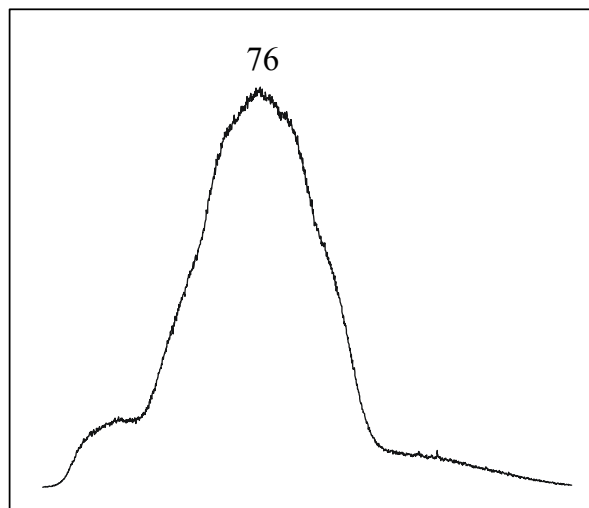


Figure 1.3 Partial MI spectrum of protonated methyl oxamate

A general phenomenon in MI mass spectra is that the product ion peaks are broadened relative to the precursor ion peak. This reflects the fact that kinetic energy is released during the dissociation [9]. The origin of this energy is made clear below.

The dissociation of metastable ions m_1^+ is typically an endothermic process as depicted in the energy diagram of Figure 1.4. (Some ionized molecules may undergo exothermic dissociation, but this typically occurs in the ion source and not the 2ffr). In many cases, particularly for rearrangement processes, the activation barrier for dissociation lies above the combined enthalpy of the products and this so-called ‘reverse activation energy’ is denoted as ϵ_{rev} . The forward reaction requires a minimum energy (ϵ_0) plus a slight excess (ϵ_{excess}) to raise the rate constant to the appropriate value ($\sim 10^5 - 10^6 \text{ s}^{-1}$) so that dissociation occurs in the metastable time-frame. Hence, upon dissociation of the metastable ions, the combined energy $\epsilon_{\text{rev}} + \epsilon_{\text{excess}}$ is deposited into the products $m_2^+ + m_3$ as internal energy and kinetic energy. The partitioning of the deposited energy is strongly dependent upon the shape of the potential energy surface for the reaction [11].

The kinetic energy release T is obtained from the width of the metastable ion peak at height h , using the equation: $T_h = m_1^2 V(\Delta E_h)^2 / 16m_2m_3E^2$, where E is the electric sector

Using the above procedure, it follows that the measured T values for the losses of CO and [H,C,N] from ions **HP-1** are 12 and 1 kcal mol⁻¹ respectively. These values represent the minimum reverse activation energies ($\epsilon_{\text{rev}} + \epsilon_{\text{excess}}$) of the reactions, assuming all of the excess energy is partitioned and released as kinetic energy.

The height of the reaction barrier (ϵ_0) could be probed directly by a (metastable) appearance energy (AE) measurement. The AE value is obtained from the onset of the plot of a selected m/z abundance as a function of the energy of the ionizing electrons. This deceptively simple technique requires dedicated custom-built instrumentation to obtain meaningful results [5]. In the study of 4-hydroxypyridine, an appearance energy was not available, but AEs reported in the literature are referred to throughout the thesis and the reader is directed to a recent review [12] for a more complete description of the methodology.

In summary, the MI experiment is used to probe the spontaneous dissociation reactions of the low-energy molecular ions. The kinetic energy releases and metastable ion peak shapes provide important information about the fragmentation processes. In the case of OD-labelled 4-hydroxypyridine, the MI experiment indicates that the low-energy ions lose [D,C,N] and CO and that the associated reaction mechanisms must involve minimum reverse barriers of 1 and 12 kcal mol⁻¹.

1.2.2 Collision Induced Processes

The controlled introduction of a gas like He or O₂ into the 2ffr, while performing a MI experiment, leads to intense signals in the resulting spectrum [13]. This is illustrated by comparing the MI spectrum of ions **HP-1** shown in Fig. 1.5a *vis-à-vis* the collision-induced dissociation (CID) spectrum of Fig. 1.5b.

In the CID experiment, the result of glancing collisions of the fast-moving mass-selected ions with the stationary target gas (contained in a 1cm x 1cm cell) is monitored. These collisions typically lead to an internal energy gain of up to about 10 eV in the ions. The vast majority of the ions sampled in this experiment are stable ions that lack sufficient

internal energy to dissociate on their own. Upon collisional excitation however, a small fraction of the ions dissociates via a great many pathways on a time-scale (similar to the EI event in the source) that extends from zero (the collision event) to the μs timeframe [5].

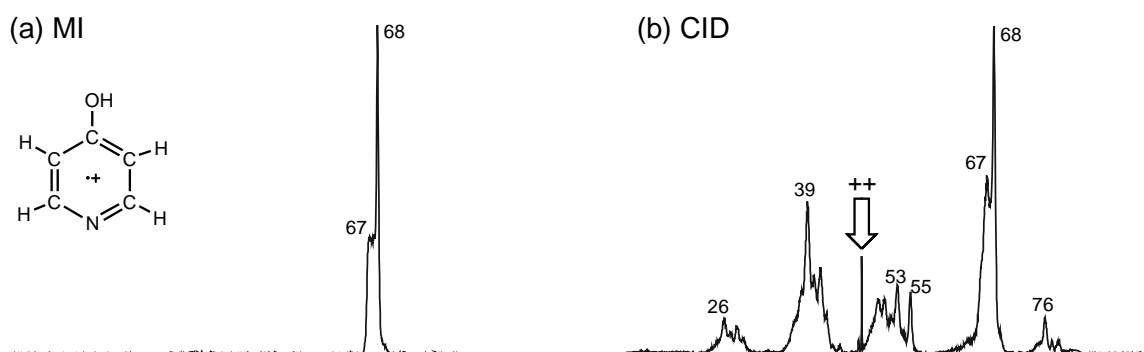


Figure 1.5 (a) MI and (b) CID mass spectra of ions **HP-1**

Under these conditions, fast simple bond cleavages often prevail over slow rearrangement processes. Thus, the CID spectrum ideally yields a picture of structure characteristic direct bond cleavage reactions of ions of low internal energy and of a well-defined structure. The careful selection of precursor molecules has led to the acquisition of reproducible CID mass spectra for a great many (isomeric) organic cations [5]. Thus, the interpretation of a CID spectrum is often facilitated by a comparison with reference spectra obtained under the same experimental conditions. In this way, the structure of the m/z 67 and 68 ions generated from ions **HP-1** could be established, the m/z 68 ion being ionized vinyl ketene, $\text{CH}_2=\text{CH}-\text{CH}=\text{C}=\text{O}^+$.

The collision event may also give rise to Charge Stripping (CS) [14], that is, the loss of one (or more) electrons from the ions with a negligible kinetic energy release as illustrated by the very narrow doubly-charged signal (++) in Figure 1.5b. The CS peak is enhanced by the use of diatomic collision gases (O_2 or N_2) and its presence often enables the differentiation of isomeric ions whose MI and CID characteristics are similar [15].

The many signals observed in the CID spectrum are usually far more intense than those

arising from metastable decompositions. In contrast, the intensity of the m/z 67 and 68 peaks in Fig. 1.5 are hardly influenced by the introduction of the collision gas, indicating that, in this case, metastable dissociations contribute to the ‘true’ CID mass spectrum. This is apparent in the partial CID spectrum of ions **HP-1** shown in Fig. 1.6 : the m/z 67 peak is a composite of the flat-topped metastable peak and the narrow collision induced component emerging from the centre. In cases where the MI interference is not negligible, it is possible to remove the unimolecular component by applying an external voltage to the collision cell [16].

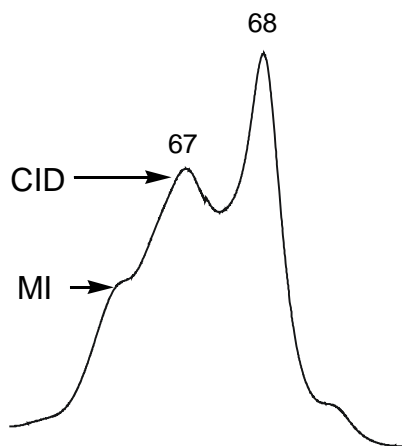


Figure 1.6 Partial CID mass spectrum of ions **HP-1**

Other important considerations that affect the appearance of the CID mass spectrum are the collision gas and collision gas pressure.

Helium is the most widely used collision gas because of its high target collision efficiency and the ease by which it is removed by differential pumping. Oxygen, argon and nitrogen are also commonly used and although the choice of collision gas usually has little effect on the appearance of the CID spectrum, oxygen sometimes yields unique, structure diagnostic peaks. The mechanism for this so-called ‘oxygen effect’ [17] is proposed to involve energy transfer from the excited states of O_2 and its radical cation in the short-lived collision complex.

The *pressure* of the collision gas is an important variable affecting to the number of collisions the mass-selected ions are subject to in the ffr. Single-collision conditions are achieved when the pressure is sufficient to reduce the flux of ions by approximately 10%. These conditions are desirable because the CID mass spectra obtained thereunder are more reproducible and structure specific than those obtained under multiple-collision conditions [18]. A reduction of the main beam by ~30 % is generally a good compromise between signal intensity and single collision conditions.

In summary, the high translational energy collisions that characterize the above-described CID experiment result in short-lived collision complexes in which the ion may become highly energized. The fragmentation processes that occur in the ion are fast and structure specific. Thus, (high-energy) CID is an important tool to differentiate (isomeric) ions.

In contrast, CID experiments performed using the popular quadrupole and ion-trap type instruments involve low translational energy, multiple-collision conditions [14a]. The resulting low-energy CID mass spectra do not display the same quality of structure diagnostic fragmentations. However, the generation of long-lived collision complexes raises the possibility that associative ion-molecule reactions may occur that do provide valuable structure information [19]. On the other hand, the structure analysis may also be frustrated if the collision gas molecule promotes isomerization of the substrate ion.

Studies of associative ion-molecule reactions are ideally performed using an instrument designed to generate the ion-molecule collision complex at low-translational energies and characterize the resulting reaction products using high-energy CID. The instrumentation for such an experiment is not routinely available : it is a special feature of the dedicated six-sector Autospec 6F mass spectrometer (Mons University, Belgium). This instrument has been used in the studies described in Chapters 2, 5 and 13 and the basic principles of its operation are described in Section 1.4.

1.2.3. Mass spectrometry of fast neutrals

Collision-induced dissociative ionization

In the dissociation of an organic ion m_1^+ , $m_1^+ \rightarrow m_2^+ + m_3$, the structure of the neutral is usually inferred from the difference in the masses of ions m_1^+ and m_2^+ , leading to the notion that Mass Spectrometry is ‘blind’ to neutrals. However, the introduction of the Collision-Induced Dissociative Ionization (CIDI) technique [20] in the mid 1980s dispelled this erroneous notion.

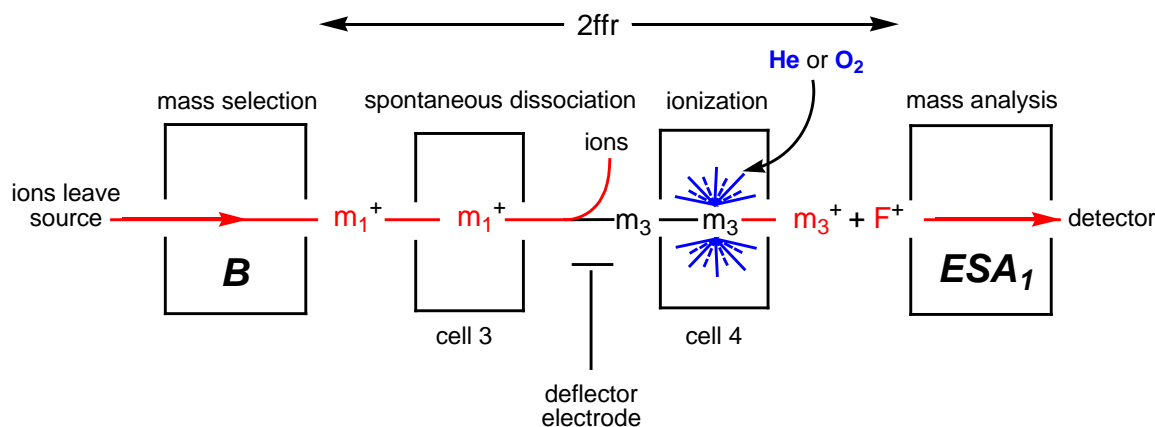


Figure 1.7 The 2fr of the instrument set up for a collision-induced dissociative ionization experiment, where B is the magnet and ESA_1 is the first electrostatic analyzer.

A CIDI experiment is performed with the instrumental setup for MI but with charging of the deflector electrode (see Figure 1.7). As the ions of interest m_1^+ enter the 2fr, a small fraction (the metastable ions) spontaneously dissociates into $m_2^+ + m_3$. Upon arrival at the positively charged electrode, all of the ions m_1^+ and m_2^+ are deflected away so that only the neutrals m_3 enter collision cell 4, where they are ionized by collisions with either He or O_2 target gas. The collisionally-ionized neutrals m_3^+ and the fragment ions F^+ generated therefrom are recorded as the CIDI spectrum by scanning ESA_1 .

The fragment ions may be used to characterize the structure of the neutral. This technique has, for example, shown that NH_2O^\bullet rather than $NHOH^\bullet$ is lost from metastable ions $CH_3C(=O)NHOH^{*\bullet}$. The mechanism for this unexpected reaction is studied in Chapter 6.

Although conceptually simple, a CIDI spectrum is not easy to obtain because the signal strength is usually quite low. Moreover, peaks arising from collision-induced dissociation may also obscure the spectrum.

Neutralization-reionization mass spectrometry

Neutralization-reionization (NR) mass spectrometry [4] is an MS/MS technique eminently suited to explore the structure and dissociation characteristics of highly reactive neutrals. The NR experiment is performed with the same experimental setup for CIDI but with the admission of a collision gas into the cell ahead of the deflector electrode (see Fig. 1.8).

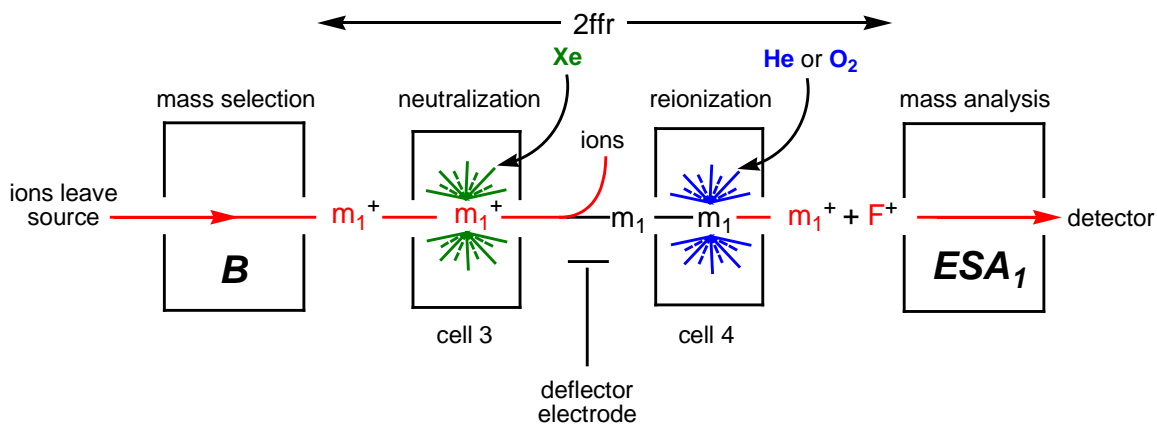


Figure 1.8 The 2fr of the instrument set up for a neutralization-reionization experiment.

In the experiment, ions m_1^+ are mass selected and transmitted into the 2fr where collisions with the gaseous neutralization reagent, Xe, in cell 3 results in reduction of part of the ions to neutrals m_1 . Other commonly used neutralization reagents are Hg vapour and polyatomic organics such as N,N-dimethylaniline (NDMA) or dimethyldisulphide.

An important criterion for efficient charge-transfer is that the difference between the ionization energy (IE) and the recombination energy (RE) of the target gas and the ion lie in the range 0 – 4 eV [4]. The ions m_1^+ that are not neutralized and the relatively minor fraction of their ionic dissociation products are deflected by the positively charged

electrode so that only neutrals m_1 and their uncharged dissociation products are transmitted to the next collision chamber, cell 4. The neutrals are subsequently reionized by collisions with He or O_2 and the reionized species m_1^+ and the (structure characteristic) fragments F^+ generated therefrom are registered as signals in the NR mass spectrum by scanning ESA1.

The presence of a signal corresponding to m_1^+ in the NR mass spectrum suggests that the neutral m_1 has remained intact for $> 1\mu s$. The mere presence of this so-called ‘survivor’ signal does not exclude the possibility that the incipient neutrals spontaneously rearrange prior to being reionized. Nevertheless, it stands to reason that such rearrangements do not occur if the NR and CID mass spectra of the ion under investigation are closely similar.

This contention hinges on the assumption that the fragment peaks in the NR spectrum arise from the (collision-induced) dissociation of the reionized neutral. However, it is important to realize that the peaks in the NR spectrum may also originate from (i) reionized dissociation products of neutralized ions m_1^+ ; and (ii) reionized neutral fragments of metastable and collision induced dissociations which may occur before the ions reach the deflector electrode.

The signals generated from (i) may aid the interpretation of the NR mass spectrum as is the case in the studies of Chapters 10 and 12. However, in situations where signals from (i) and (ii) obscure the interpretation and the identity of the reionized species is in doubt, an elegant solution is to obtain a CID spectrum of the survivor ions provided there is sufficient signal intensity : the peaks in the NR-CID spectrum are typically ~ 1000 fold weaker than those in the CID spectrum.

In the NR-CID experiment, the survivor ions are transmitted into the 3ffr where they are induced to dissociate by collisions with the target gas in cell 5. The observation that the resulting NR-CID spectrum is closely similar to the CID spectrum of the source generated ions provides strong evidence that the initial ion flux was pure and that the neutrals m_1 have survived the NR process without isomerization.

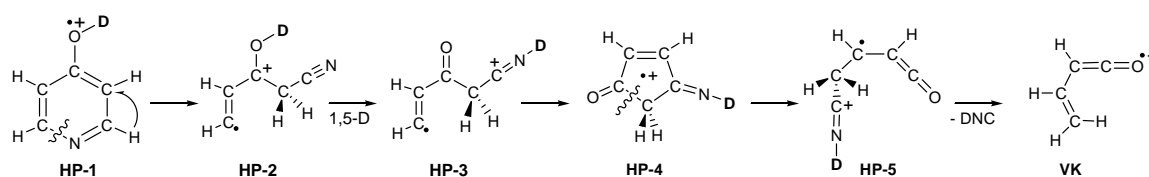
1.2.4 Calculation of thermodynamic properties

Accurate thermochemical data are essential to provide insight into chemical reactivity. However, it is often not possible to obtain such data from experiment for many of the highly reactive species that play a role in the chemistry of organic neutrals and ions.

The dissociation chemistry of ionized 4-hydroxypyridine serves as a salutary reminder that experimental observations provide limited insight into reaction mechanisms. The mass spectrometry techniques described in the previous sections are well suited to characterize the precursor and product ions as well as to define the energy domain in which the reaction occurs.

However, information on the structures and energies of the key intermediates and connecting transition states involved in the reaction, cannot be probed directly by experiment. In the same vein, an answer to the question whether a measured AE corresponds to the thermochemical threshold or reflects the energy of the highest transition-state of a reaction sequence can only come from integrating experiment with theory.

Fortunately, the missing thermochemical data required to construct the potential energy surface (PES) describing the reaction may be obtained using model chemistry calculations such as the CBS-QB3 and CBS-APNO methods. By integrating the results from experiment and theory, the mechanism of Scheme 1.2 was proposed for the loss of DNC from OD-labelled ions **HP-1** [6] :



Scheme 1.2 The proposed mechanism for the loss of DNC from ions **HP-1**

In the paragraphs that follow, the main components of the model chemistry calculations used in the studies of this thesis are described with emphasis placed on the concepts and the *terminology* [21].

The first step in a calculation involves the *geometry optimization* of the molecule or ion. Several optimization procedures have been developed, but in the context of this introduction, it suffices to mention that all of these are iterative processes in which the positions of the atoms in the molecule are repeatedly changed so as to obtain a minimum energy structure on the PES. The next step is to perform a *frequency calculation* to verify the stability of the resulting structure. This calculation generates the vibrational frequencies and these are used to differentiate between minima (all frequencies real) and transition states (one imaginary frequency). The transition state structure can be characterized further by performing an *intrinsic reaction coordinate* calculation, which follows the reaction coordinate of the imaginary frequency and thereby connects the transition state to the minima.

In general, the geometry is less sensitive to the computational method than the energy. Thus, the geometry optimization and frequency calculations are typically performed with a modest level of theory relative to the subsequent *single-point* calculations used to refine the energy of the optimized structure.

The level of accuracy provided by the calculation and the associated costs in time and computational resources are generally a function of two key elements : the choice of *basis set* and the theoretical treatment used to approximate the electron-electron repulsion energy, commonly called the *correlation* energy.

The *basis set* represents a set of mathematical functions, which describe the orbitals of the molecule. Ideally, the number of functions in the set is ‘infinite’, but such an approach is far too resource demanding for all but the smallest systems. Therefore, one has to resort to the use of truncated basis sets. The minimum basis set includes one basis function for every formally or partially occupied orbital in the atoms of the molecule. These are referred to as single-zeta basis sets, but in practice double-zeta basis sets (with two basis

functions per orbital) are used. The CBS model chemistries of our studies employ the split-valence basis sets developed by Pople and co-workers [22]. These sets use single-zeta in the core and double-zeta in the valence orbitals where the chemistry happens. To correct for basis set truncation, the Complete Basis Set (CBS) methods employ an extrapolation procedure [8a], which involves performing a sequence of calculations with basis sets using an increasing number of basis functions.

Electron correlation can be incorporated into a calculation in several ways. Perturbation theory is one common way, which involves expressing the electron-electron potential as a Taylor expansion. Incorporation of the second, third and fourth terms of the expansion in the calculation are denoted as MP2, MP3 and MP4. The other form of electron correlation is configuration interaction, which involves expressing the trial wave-function (or configuration) as a linear combination of (excited-state) determinants with the expansion coefficients obtained by minimizing the energy. The quadratic configuration interaction (QCI) and coupled cluster (CC) methods are related to configuration interaction conceptually, only differing in the formulation of the wave function. The S,D and T annotation in CCSDT and QCISDT indicates that the determinants in the calculations are singly, doubly and triply excited relative to the ground-state configuration.

Density functional theory (DFT) has become a very popular computational method. Instead of using wave-functions, DFT methods are based on the Hohenberg-Kohn theorem that the energy may be computed from general functionals of the electron density. These methods differ from each other in the form of the functional and the main drawback of DFT is that if a chosen functional fails, there is no way to systematically correct its performance. However, it has become clear that DFT methods have many advantages; they implicitly include correlation effects and their accuracy is comparable to other correlation methods, such as MP2, but with a significantly decreased cost in terms of resources. The commonly employed DFT method B3LYP is used in the CBS-QB3 model chemistry for the geometry optimization and frequency calculations.

The CBS methods assume that the effects of ‘infinite’ basis sets and high-order electron correlation treatments may be approximated by additive corrections to a lower-level calculation. Using this approach, the CBS methods provide accurate 298 K enthalpies in a reasonable timeframe : on the order of 2 – 8 hours for an ion of the size of those studied in this thesis. These methods were easily implemented using Windows-based PCs and the SHARCNET computer network loaded with the GAUSSIAN suite of programs [23].

The challenging and time-consuming aspect of the calculations is locating the minimum energy pathway in the multi-step reactions studied in this thesis. A key requirement for the geometry optimization step is that a good initial guess of the structure can be proposed, which is often not available. To obtain a reasonable guess, the potential energy surface in the neighbourhood of the desired structure is explored by performing a series of calculations (called a *scan*) in which a key internal coordinate (such as interatomic distance or angle) is varied while optimizing the other degrees of freedom. Ideally, the entire PES could be obtained by performing scans of all possible coordinates, but this is not practical. Promising methodologies are becoming available that can efficiently deal with 3 – 4 coordinates [24], but a ‘black-box’ approach to deal with the complex reactions described in this thesis is still far away. Thus, the successful elucidation of the minimum energy pathway depends not only on the computational resources but also on careful thought experiments that direct the judicious choice of key internal coordinates.

1.3 Ions of unconventional structure and their role in proton-transport catalysis

The methylene oxonium ion $\bullet\text{CH}_2\text{OH}_2^+$ represents one of the earliest examples of an ion of unconventional structure investigated in great detail using experiment and theory [25]. The corresponding neutral $\text{CH}_2\text{--OH}_2$ resembles a weakly bound complex of CH_2 and H_2O , whose enthalpy lies 84 kcal/mol higher than that of methanol. In contrast, the ion $\bullet\text{CH}_2\text{OH}_2^+$ is characterized by a short (covalent) C-O bond and it is remarkably stable with an enthalpy that lies 7 kcal/mol *below* that of its conventional isomer CH_3OH^+ . The formal separation of the charge and radical sites inspired the classification of $\bullet\text{CH}_2\text{OH}_2^+$ as

a *distonic* ion, a term derived from the Greek *diestos* and Latin *distans*, meaning separate. Since their discovery in the early 1980s, distonic ions have been invoked as key intermediates and products of a great many reactions of radical cations.

The distonic ion $\bullet\text{CH}_2\text{OH}_2^+$, is generated by the loss of CH_2O from $\text{HOCH}_2\text{CH}_2\text{OH}^{*\bullet}$ and it is readily differentiated from $\text{CH}_3\text{OH}^{*\bullet}$ on the basis of a comparison of the MI, CID and NR mass spectra. The ethyleneoxonium ion, $\bullet\text{CH}_2\text{CH}_2\text{OH}_2^+$ is similarly generated from $\text{HOCH}_2\text{CH}_2\text{CH}_2\text{OH}^{*\bullet}$. It readily adopts the structure of an ion-dipole complex (IDC) when its internal energy is raised to the dissociation threshold for its structure characteristic loss of H_2O [26]. The IDC can best be viewed as a positively charged ethene rod interacting with the dipole of the water molecule, which can roam freely along and around the positive rod. Stabilization of ion-dipole species arises from the electrostatic interactions between the ion and dipole, which amounts to about 10-25 kcal/mol.

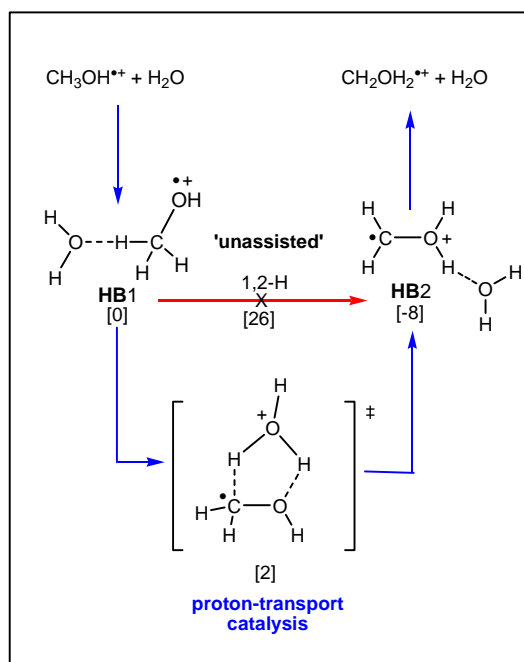
Direct experimental evidence that IDCs act as intermediates in a given reaction is often not available, but when the final intermediate in a multi-step dissociation reaction is an IDC, the reaction is often associated with a very small kinetic energy release ($T_{0.5}$ value). As an illustration, the loss of H_2O from the ethylene oxonium ion $\text{CH}_2\text{CH}_2\text{OH}_2^{*\bullet}$, where the final intermediate is the ion-dipole complex $\text{CH}_2=\text{CH}_2^{*\bullet} / \text{H}_2\text{O}$, is associated with a $T_{0.5}$ value of only ~ 0.2 meV [26]. In contrast, typical values for direct bond cleavage reactions lie in the range 10-30 meV.

Hydrogen-bridged radical cations (HBRCs) are closely related to ion-dipole complexes. One can envisage the generation of an HBRC when the H_2O dipole in the ion-dipole complex $\text{CH}_2=\text{CH}_2^{*\bullet} / \text{H}_2\text{O}$ aligns with the $\text{C}_2\text{H}_4^{*\bullet}$ ion so as to form a C-H-O bridge. In this case, the bridging hydrogen resides much closer to the C than to the O because the proton-affinity (PA) of $\text{CH}_2=\text{CH}^\bullet$ is 15 kcal/mol greater than that of H_2O . As a result, the stability of the HBRC is not much different than the IDC. However, when the PAs are close, the hydrogen bridge supplies an additional ~ 5 kcal/mol of stabilization.

The most important role of the hydrogen-bridging interaction is that it promotes proton-transfers between the ionic and neutral components of the HBRC. Consecutive proton-transfer reactions in HBRC intermediates are the key steps in proton-transport catalysis.

Proton-transport catalysis

The isomerization of ionized methanol into its more stable distonic isomer is prohibited by an energy barrier of 26 kcal/mol. However, detailed computational and experimental studies [27,28] have shown that the interaction of a single water molecule promotes the isomerization $\text{CH}_3\text{OH}^{\bullet+} \rightarrow \bullet\text{CH}_2\text{OH}_2^+$ in a process termed proton-transport catalysis (PTC) [3]. The computational results of Ref. 27a are summarized in Scheme 1.3 and it follows that the unassisted 1,2-H shift barrier is reduced to a mere 2 kcal/mol and that the hydrogen-bridged radical cations **HB1** and **HB2** act as key intermediates.



Scheme 1.3 The transformation $\text{CH}_3\text{OH}^{\bullet+} \rightarrow \bullet\text{CH}_2\text{OH}_2^+$ catalyzed by a single H_2O molecule. The numbers are relative energies (in kcal/mol) taken from Ref. 27a.

Radom and Gault have developed general criteria for successful proton-transport catalysis [27b]. The most important of these stipulates that the transformation of an ion HAB^+ into its more stable H-shift isomer ABH^+ readily occurs if the PA of the interacting solvent molecule (M) lies between those of the radical AB^\bullet at the donor site A and the acceptor site B. In line with this, the PA of H_2O (165 kcal/mol) lies between the PAs of $\text{CH}_2\text{OH}^\bullet$ at C (160 kcal/mol) and at O (167 kcal/mol).

One approach to study proton-transport catalysis in bimolecular reactions is to perform a chemical ionization (CI) experiment in which the substrate and catalyst molecules are introduced into the ion source with a ten-fold excess of a bath gas (such as CO_2). The total pressure in the ion source (*c.* 10^{-4} torr) is kept relatively high so that the energy rich HBRC encounter complexes are stabilized by unreactive collisions. In this way, the acrylonitrile dimer radical cations of Chapter 3 were prepared. It follows that the dissociation and isomerization chemistry of the stable (and metastable) HBRCs can be probed by various collision experiments in the 2ffr.

The CI experiment is seemingly straightforward, but other processes often suppress the desired ion-molecule reaction. For example, ions CH_3OH^+ (and CH_2OH_2^+) are so rapidly protonated by CH_3OH molecules ($\Delta H_{\text{rxn}} = -20$ kcal/mol) that proton-bound ions [$\text{CH}_3\text{OH}-\text{H}^+-\text{OH}_2$], rather than stable HBRCs, dominate the chemistry in the ion source.

An experiment that avoids this complication involves reacting *mass-selected* ions with the reagent molecules in a region separate from the ion-source. Such an experiment can be realized using the Mons Autospec 6F instrument shown schematically in Figure 1.9.

In brief, the experiment involves mass selection of a beam of m/z 32 methanol ions (8 keV) using the first three sectors. Next, the ions are decelerated to ~ 5 eV in front of the hexapole cell to optimize the yield of associative ion-molecule reactions with H_2O vapour. Following reacceleration to 8 keV, the m/z 32 ions leaving the hexapole cell are mass selected by B_2 and subjected to collision-induced dissociation with O_2 in chamber C_3 . That ions CH_2OH_2^+ are generated by catalysis may easily be inferred from the high-energy CID

mass spectrum obtained by scanning sector E_4 . This technique was used to study the ion-molecule reactions of Chapters 2, 5 and 13.

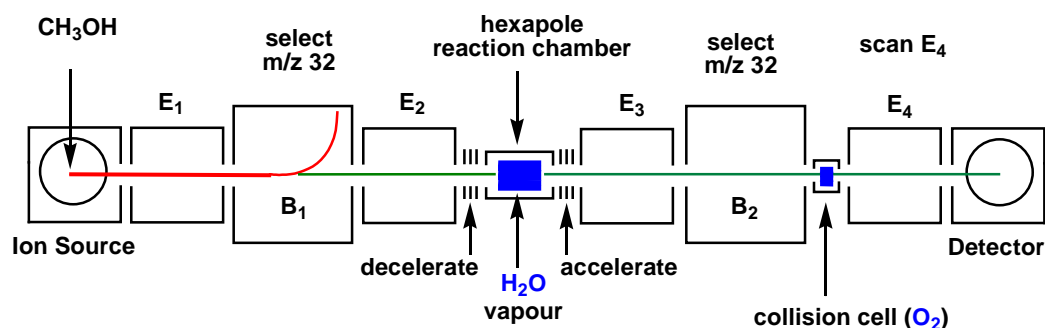
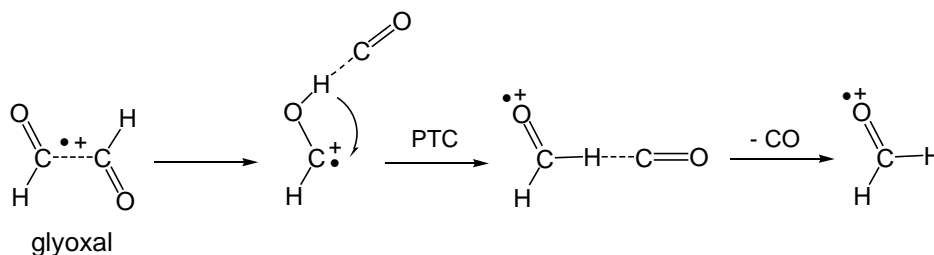


Figure 1.9 Schematic diagram of the Mons Autospec 6F mass spectrometer (Mons University, Belgium).

PTC is not restricted to bimolecular reactions, but can also occur during the course of unimolecular dissociations. An elegant illustration is provided by mechanism for the decarbonylation of low-energy glyoxal ions $\text{O}=\text{C}(\text{H})-\text{C}(\text{H})=\text{O}^{\bullet+}$ shown in Scheme 1.4 :



Scheme 1.4

The combined experimental and theoretical study of Wong *et al.* [29] showed that the ion $\text{CH}_2\text{O}^{\bullet+}$ (and not $\text{HCOH}^{\bullet+}$) is generated. The mechanistic analysis indicated that the molecular ions rearrange into the hydrogen-bridged complex $[\text{HCO}--\text{H}--\text{C}=\text{O}]^{\bullet+}$ wherein the CO molecule catalyzes the transformation $\text{HCOH}^{\bullet+} \rightarrow \text{CH}_2\text{O}^{\bullet+}$.

The prominent role of catalysis in dissociation reactions is explored in Chapters 6 – 9.

In summary, distonic ions, ion-dipole complexes and the related hydrogen bridged radical cations are remarkably stable species that act as key intermediates in the association and dissociation chemistry of organic ions. The involvement of IDCs and HBRCs also raises the possibility that within such complexes, the components may undergo rearrangement via PTC. The role of PTC and its variants in the chemistry of organic radical cations represents the unifying theme of this thesis.

Finally, it should be noted that the FT-ICR technique, Fourier Transform - Ion Cyclotron Resonance, has also played an important role in the study of ion structures and reaction mechanisms [30], including proton-transport catalysis [31]. This very sophisticated technique was used in a collaborative MALDI project on the interaction of Ca^{2+} ions with peptides [32] but, like most modern instruments dedicated to bioanalytical applications, the FT-ICR instrument at the Erasmus University is not equipped to study the fundamental chemistry of radical cations with specific ion-molecule reactions.

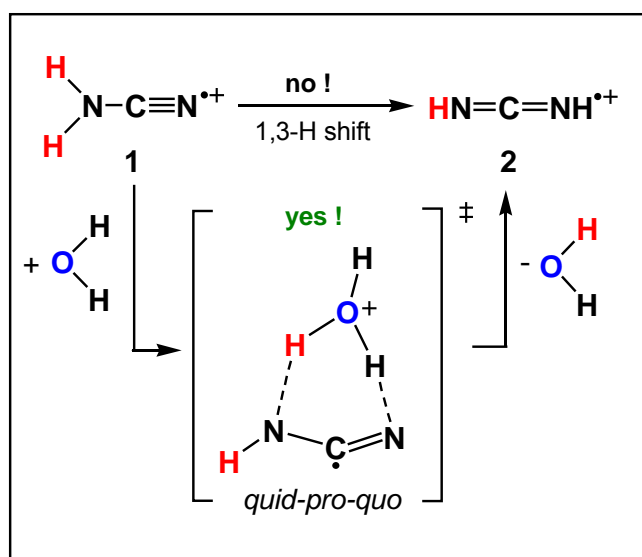
References

- [1] A.J.B. Robertson, *Platinum Metals Rev.*, 19 (1975) 64.
- [2] N.M.M. Nibbering (Ed.), *Encyclopedia of Mass Spectrometry*, vol. 4, Elsevier, Amsterdam, 2005,
 - (a) H.I. Kenttämä, Ion-molecule Reactions of Distonic Radical Cations, p. 160 - 164;
 - (b) T.H. Morton, Theoretical Models for Ion-neutral Complexes in Unimolecular Ion Decompositions, p. 165 - 172;
 - (c) P.C. Burgers, J.K. Terlouw, Hydrogen-bridged Cations, p. 173 - 179.
- [3] D.K. Böhme, *Int. J. Mass Spectrom. Ion Proc.*, 115 (1992) 95.
- [4] R. Tureček, *Top. Curr. Chem.* 225 (2003) 77.
- [5] J.L. Holmes, C. Aubry, P.M. Mayer. *Assigning Structures to Ions in Mass Spectrometry*. CRC Press, Boca Raton, 2007.
- [6] K.J. Jobst, T.R. Khan, J.K. Terlouw, *Int. J. Mass Spectrom.* 42 (2007) 1024.
- [7] J.L. Holmes, K.J. Jobst, J.K. Terlouw, *J. Labelled Compd. Radiopharm.* 50 (2007) 1088.
- [8]
 - (a) J.A. Montgomery, Jr., M.J. Frisch, J.W. Ochterski, G.A. Petersson, *JCP* 112 (2000) 6532;
 - (b) L.A. Curtiss, P.C. Redfern, K. Raghavachari, *J. Chem. Phys.* 126 (2007) 084108;
 - (c) J.M.L. Martin, S. Parthiban, in J. Cioslowski and A. Szarecka (Ed.), *Quantum Mechanical Prediction of Thermochemical Data, Understanding Chemical Reactivity Series*, Vol. 22, Kluwer Academic Publishers, Dordrecht, 2005, p. 31 – 65.
- [9] R.G. Cooks, J.H. Beynon, R.M. Caprioli, G.R. Lester. *Metastable Ions*. Elsevier Scientific Publishing Company, New York, 1973
- [10] H.F. van Garderen, P.J.A. Ruttink, P.C. Burgers, G.A. McGibbon, J.K. Terlouw, *Int. J. Mass Spectrom. Ion Proc.* 121 (1992) 159

- [11] (a) J.L. Holmes, J.K. Terlouw, *Org. Mass Spectrom.*, 15 (1980) 383;
 (b) J. Laskin, C. Lifshitz, *J. Mass Spectrom.*, 36 (2001) 459
- [12] N.M.M. Nibbering (Ed.), *Encyclopedia of Mass Spectrometry*, vol. 4, Elsevier, Amsterdam, 2005, J.C. Traeger, Appearance Energies, p. 19 – 28.
- [13] (a) R.G. Cooks, *J. Mass Spectrom.* 30 (1996) 1216;
 (b) P.M. Mayer, *Mass Spectrom. Rev.*, 28 (2009) 608.
- [14] (a) R.G. Cooks, J.H. Beynon, T.J. Ast, *J. Am. Chem. Soc.* 94 (1972) 1004;
 (b) F.M. Harris, *Int. J. Mass Spectrom. Ion Proc.* 120 (1992) 1.
- [15] G.A. McGibbon, P.C. Burgers, J.K. Terlouw, *Int. J. Mass Spectrom.* 136 (1994) 191.
- [16] J.K. Terlouw, P.C. Burgers, H. Hommes, *Org. Mass Spectrom.*, 14 (1979) 387.
- [17] (a) C. Aubry, J.L. Holmes, *J. Phys. Chem. A* 104 (2000) 10045;
 (b) Y. Lin, P.M. Mayer, *J. Am. Soc. Mass Spectrom.*, 22 (2011) 75.
- [18] J.L. Holmes, *Org. Mass Spectrom.* 20 (1985) 169.
- [19] P. Gerbaux, M. Barbieux-Flammang, J.K. Terlouw, R. Flammang, *Int. J. Mass Spectrom.*, 206 (2001) 91.
- [20] P.C. Burgers, J.L. Holmes, A.A. Mommers, J.K. Terlouw, *Chem. Phys. Lett.* 102 (1983) 1.
- [21] (a) S.M. Bachrach. *Computational Organic Chemistry*. Wiley-Interscience, New Jersey, 2007;
 (b) F. Jensen. *Introduction to Computational Chemistry (2nd Ed.)*, John Wiley & Sons, Ltd, 2007.
- [22] (a) R. Ditchfield, W.J. Hehre, J.A. Pople, *J. Chem. Phys.*, 54 (1971) 724;
 (b) W.J. Hehre, R. Ditchfield, J.A. Pople, *J. Chem. Phys.*, 56 (1972) 2257
- [23] M. J. Frisch et al. *Gaussian 09*, Gaussian, Inc., Wallingford CT, 2004.
- [24] S.K. Burger, P.W. Ayers, *J. Chem. Theory Comput.*, 6 (2010) 1490.
- [25] (a) W.J. Bouma, J.K. McLeod, L. Radom, *J. Am. Chem. Soc.* 104 (1982) 2930;
 (b) J.L. Holmes, F.P. Lossing, J.K. Terlouw, P.C. Burgers, *J. Am. Chem. Soc.* 104 (1982) 2931.
- [26] J.K. Terlouw, W. Heerma, G. Dijkstra, *Org. Mass Spectrom.*, 16 (1981) 326.
- [27] (a) J.W. Gauld, H. Audier, J. Fossey, L. Radom, *J. Am. Chem. Soc.*, 118 (1996) 6299;
 (b) J.W. Gauld, L. Radom, *J. Am. Chem. Soc.*, 119 (1997) 9831;
 (c) A.J. Chalk, L. Radom, *J. Am. Chem. Soc.*, 121 (1999) 1574.
- [28] (a) P. Mourgues, H.E. Audier, D. Leblanc, S. Hammerum, *Org. Mass Spectrom.*, 28 (1993) 1098;
 (b) H.E. Audier, D. Leblanc, P. Mourgues, T.B. McMahon, S. Hammerum, *J. Chem. Soc. Chem. Commun.*, (1994) 2329.
- [29] C.Y. Wong, P.J.A. Ruttink, P.C. Burgers, J.K. Terlouw, *Chem. Phys. Lett.*, 387 (2004) 204.
- [30] N.M.M Nibbering, *Mass Spectrom. Rev.*, 25 (2006) 962.
- [31] G. Van der Rest, L.B. Jensen, S. Abdel Azeim, P. Mourgues, H.E. Audier, *J. Am. Soc. Mass Spectrom.*, 15 (2004) 966 and references cited therein.
- [32] K.J. Jobst, P.C. Burgers, T.M. Luider, J.K. Terlouw, *Anal. Chim. Acta*, 627 (2008) 136.

Chapter 2

The quest for the elusive carbodiimide ion $\text{HN}=\text{C}=\text{NH}^{\bullet+}$ and its generation from ionized cyanamide by proton-transport catalysis



Tandem mass spectrometry based collision experiments and computational chemistry (CBS-QB3/APNO methods) indicate that the elusive carbodiimide ion $\text{HN}=\text{C}=\text{NH}^{\bullet+}$ is a stable species in the gas-phase. The ion is the most stable of the family of $\text{CH}_2\text{N}_2^{\bullet+}$ ions and a very high barrier (87 kcal mol^{-1}) separates it from its tautomer ionized cyanamide, $\text{H}_2\text{N}-\text{C}\equiv\text{N}^{\bullet+}$.

The computations also predict that, in the presence of a single H_2O molecule as the catalyst, the cyanamide ion isomerizes into the carbodiimide ion. Experiments on the ion-molecule reaction of $\text{H}_2\text{N}-\text{C}\equiv\text{N}^{\bullet+}$ and H_2O , a reaction of potential interest in astrochemistry, confirm this prediction.

The work described here has been published previously in an article under the same title : K.J. Jobst, P. Gerbaux, G. Dimopoulos-Italiano, P.J.A. Ruttink, J.K. Terlouw, Chem. Phys. Lett. 478 (2009) 144 – 149.

2.1 Introduction

Cyanamide $\text{H}_2\text{N}-\text{C}\equiv\text{N}$ (**1N**) is a key molecule in prebiotic synthesis [1-3] and one of a small group of molecules that are abundant in interstellar space [4]. IR spectroscopic studies of cyanamide in the gas-phase [5,6] indicate that its tautomer carbodiimide $\text{HN}=\text{C}=\text{NH}$ (**2N**) [7], also a molecule of considerable interest in astrochemistry, is present as a minor constituent. The equilibrium constant derived from these experiments [6] indicates that **1N** is more stable than **2N**, by $3.6 \text{ kcal mol}^{-1}$. However, as pointed out in the recent computational study of Tordini et al. [8], the equilibration of **1N** and **2N** is a bimolecular reaction : the *intramolecular* tautomerization involves a prohibitively high barrier of $\sim 90 \text{ kcal mol}^{-1}$. The study of Ref. 8 further predicts that the cooperative effect of only a few water molecules leads to a drastic reduction of the tautomerization barrier. Indeed, the subsequent matrix isolation experiments of Duvernay et al. [9,10] show that amorphous water-ice readily catalyzes the interconversion of cyanamide (**1N**) and carbodiimide (**2N**).

Other isomeric neutrals identified as stable species in the gas-phase are isocyanamide, $\text{H}_2\text{N}-\text{N}\equiv\text{C}$ (**3N**) [11], nitrilimine, $\text{HC}=\text{N}=\text{NH}$ (**5N**) [12,13], as well as diazomethane, $\text{CH}_2\text{N}=\text{N}$ (**7N**), and its cyclic isomer diazirine, $\text{H}_2\text{C}-\text{N}=\text{N}$ (**8N**) [14]. Isodiazirine, $\text{HC}=\text{N}-\text{NH}$ (**4N**), has not (yet) been identified but, as corroborated by the computational results of our study, cyanamide clearly is the CH_2N_2 isomer of lowest energy.

The CBS-QB3 and APNO model chemistries [15,16] of the present study revealed that a different scenario obtains upon ionization of **1N** and **2N**. The carbodiimide ion $\text{HN}=\text{C}=\text{NH}^{\bullet+}$ (**2**) is more stable than the cyanamide ion $\text{H}_2\text{N}-\text{C}\equiv\text{N}^{\bullet+}$ (**1**). In fact, **2** represents the most stable member of the family of $\text{CH}_2\text{N}_2^{\bullet+}$ ions, whose optimized geometries are shown in Figure 2.1. On the other hand, the *intramolecular* tautomerization of the ions by a 1,3-H shift faces the same high barrier (87 kcal mol^{-1}) as that for the neutrals. Thus, solitary ions **1** and **2** cannot interconvert.

This prompted us to explore whether their isomerization can be achieved by catalysis. Theory predicts, as will be discussed in Section 2.3.2, that a *single* molecule of water promotes the isomerization **1** \rightarrow **2** by a process termed proton-transport catalysis [17]. Tandem mass spectrometry based experiments aimed to verify this prediction, *viz.* the ion-molecule reaction of **1** with H₂O described in the Experimental Section, rely upon an unambiguous assignment of the structure of the putative product ion **2**. In this context, the method of choice involves a comparative analysis of the high-energy collision-induced dissociation (CID) mass spectra [18] of the ion with the reference spectra of **1** and **2**. Reference CID mass spectra are readily available for **1**, as shown in the detailed study of Cacace et al. [19], and for several other isomers including **3** [20] and **5** [13], but the carbodiimide ion HN=C=NH⁺ (**2**) has so far eluded experimental observation. Previous attempts to prepare the ion by either direct ionization of pyrolytically generated gaseous neutrals [20] or dissociative ionization of selected precursor molecules [21] failed to yield (pure) ions **2**.

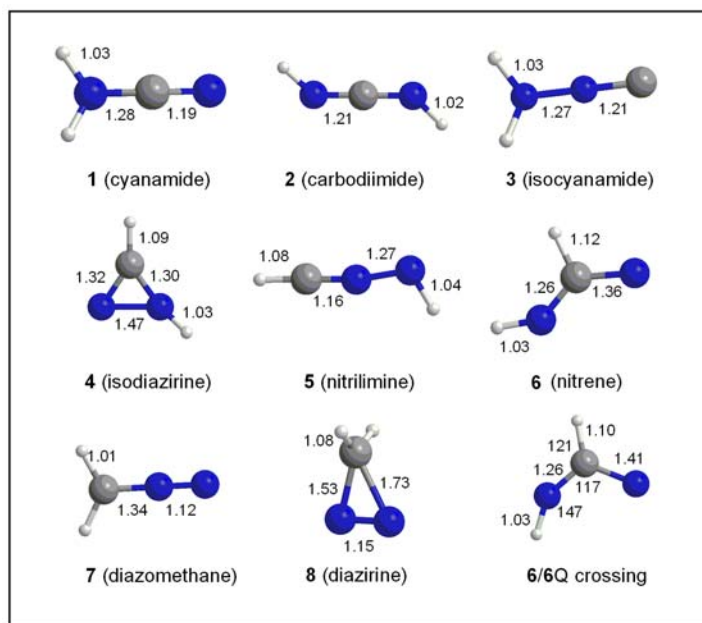


Figure 2.1 Optimized geometries of the cyanamide ion **1** and its principal isomers obtained at the B3LYP/CBSB7 level of theory; bond lengths in Å. Also shown is the geometry of the crossing **6** \rightarrow **6Q** discussed in Section 2.2.

This study describes the dissociation chemistry of $\text{H}_2\text{N}-\text{C}\equiv\text{N}^{\bullet+}$ (**1**) and $\text{HN}=\text{C}=\text{NH}^{\bullet+}$ (**2**), using the results of CID and CIDI (collision-induced dissociative ionization [18]) experiments in conjunction with a computational analysis of the isomerization behaviour of the ions. It will be shown that the elusive carbodiimide ion **2** is readily generated by dissociative ionization of 2-imidazolecarboxaldehyde [22] and also in the ion-molecule reaction of cyanamide ions **1** with H_2O .

2.2 Results and discussion

2.2.1 The characterization of $\text{CH}_2\text{N}_2^{\bullet+}$ ions **1** and **2** using MI/CID mass spectrometry

In our analysis of the experimental results we will use the potential energy diagram of Figure 2.2, which summarizes our calculations on the $\text{CH}_2\text{N}_2^{\bullet+}$ system of ions, as a guide. Enthalpies for the various ions and neutrals are shown in Tables 2.1/2.2.

It is seen that the cyanamide ion **1** lies in a deep potential well and that the barriers for isomerization into the carbodiimide ion **2** and the isocyanamide ion **3** are quite high. The carbodiimide ion **2**, which represents the global minimum on the PES, also lies in a deep well : communication by ring closure/opening with the stable ions **4** and **5** requires 90 kcal mol^{-1} .

The dissociation reaction of lowest energy requirement for these five isomeric ions, **1** - **5**, is a spin-forbidden process involving loss of $\text{N}(^4\text{S})$ to yield $\text{HC}=\text{NH}^+$. Since the dissociation of ion **6** of Fig. 2.2 into m/z 28 ions $\text{HC}=\text{NH}^+$ ($^1\Sigma_g^+$) by loss of $\text{N}(^4\text{S})$, is spin-forbidden, the PESs were scanned in order to find a geometry where the doublet and quartet states are degenerate. Since the B3LYP/CBSB7 wave function optimization for the doublet state appeared to have multiple solutions (depending on the starting orbitals) leading to discontinuities in the PES, it appeared difficult to determine the lowest energy crossing point. Moreover, using the corresponding CBS-QB3 electronic energies leads to changes in the crossing point geometry, which are difficult to predict because no energy gradients are available for this composite method. Nevertheless, a continuous

B3LYP/CBSB7 PES could be obtained by using starting orbitals obtained from a calculation for the neutral $\text{HN}=\text{C}(\text{H})\text{N}$ in its $^3\text{A}''$ state, which does not suffer from the multiple solutions problem. The final crossing geometry shown in Figure 2.1 was then obtained by trial and error. The CBS-QB3 electronic energies for this point differ by 0.5 kcal mol⁻¹. The electronic energy for the crossing (-148.09142) lies 4 kcal mol⁻¹ below TS $6\text{Q} \rightarrow \text{m/z } 28$, so that it is not necessary to locate the minimum in the intersection of the PESs. This TS, see Table 2.1, lies at 352 kcal mol⁻¹ so that the crossing is expected to lie at 348 kcal mol⁻¹.

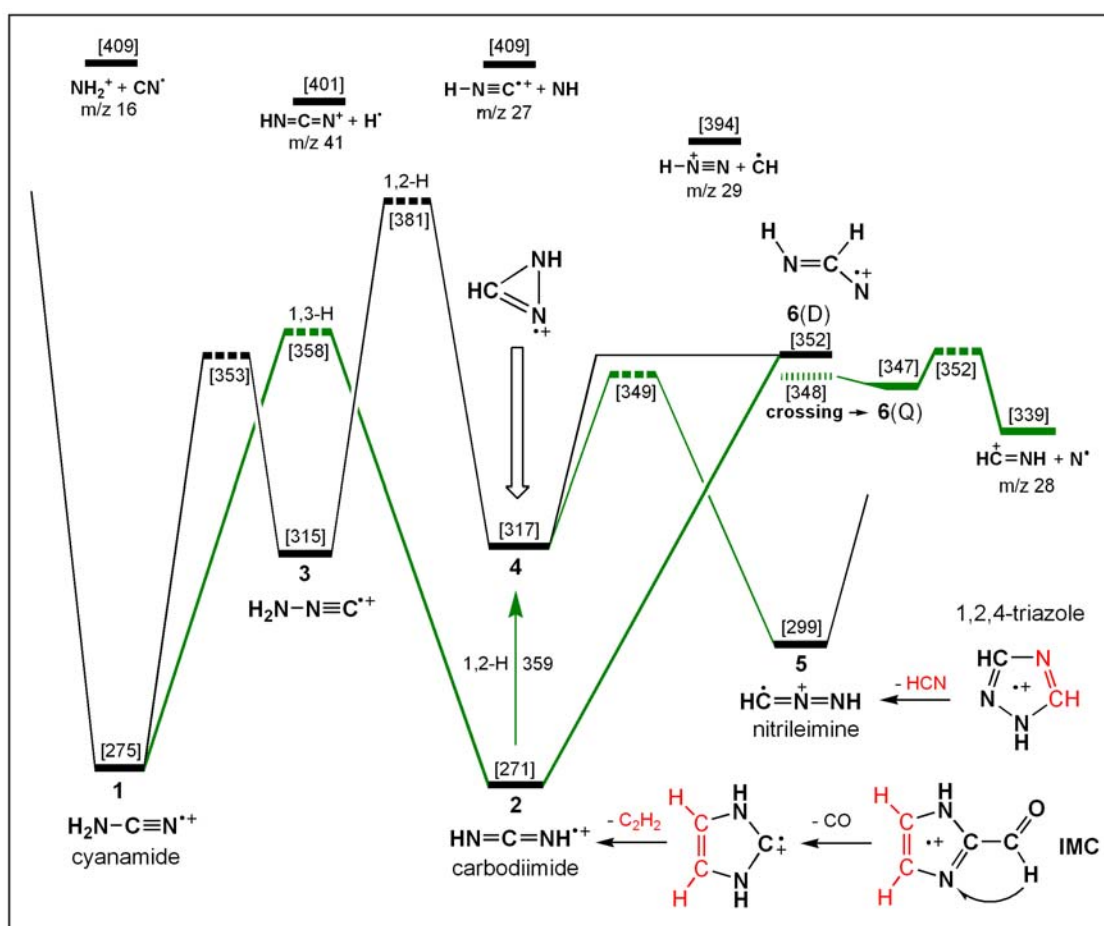
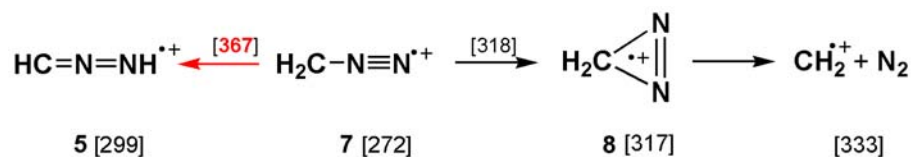


Figure 2.2 Potential energy diagram for the loss of $\text{N}(^4\text{S})$ from the cyanamide ion **1** and its principal isomers. The numbers in square brackets refer to CBS-QB3 derived $\Delta_f H_{298}^\circ$ values in kcal mol⁻¹.

In line with this, the N-atom loss reaction is associated with a significant reverse activation energy, which is reflected in the magnitude of the associated kinetic energy released (KER). For ion **1**, the KER in the formation of N(⁴S) and HC=NH⁺, as measured from the width of the peak at half height is 500 meV (11 kcal mol⁻¹) [18,19]. We further note that the energy requirement for loss of N(⁴S) from ions **1**, **2**, **3**, **4** and **5** are very close. The dissociation characteristics of their *metastable* ions will therefore be closely similar and indeed, for ions **3** [20] and **5** [13,23], a dish-shaped metastable peak has been reported for loss of N(⁴S). In this context we note that the cyclic isodiazirine ion **4** has been proposed to be generated from (substituted) azoles [25]. However, in a later NR study by Goldberg et al. [13], it was established that 1,2,4-triazole generates *m/z* 42 ions having the structure of the nitrilimine ion **5**, as indicated in Fig. 2.2. Thus, the MI spectrum cannot be used to differentiate ions **1** – **5**.

In contrast, see Scheme 2.1, the isomeric ions **7** and **8** are expected to behave differently: these ions could lose N(⁴S) via ion **5**, but the energy requirement for the associated 1,3-H shift greatly exceeds that calculated for the direct bond cleavage into CH₂^{•+} + N₂.



Scheme 2.1

This is indeed borne out by the experimental observations: **7** and **8** both show a Gaussian-type metastable peak at *m/z* 14 (CH₂^{•+}), albeit that the associated KERs are not the same [20]. Since all isomers lie in deep potential wells, their CID spectra may well display peaks of structure diagnostic value [18].

The reported CID spectra all display an intense peak at *m/z* 41 for loss of H[•]. This peak is not of structure diagnostic value but the weaker clusters of peaks in the *m/z* 26-30 and *m/z* 12-17 regions clearly are. For example, a unique peak at *m/z* 30 (N₂H₂^{•+}), corresponding

Table 2.1 Energetic data [a] derived from CBS-QB3 and CBS-APNO calculations of stable ions and connecting transition states involved in the dissociation chemistry of the cyanamide ion **1** and its water-catalyzed isomerization into the carbodiimide ion **2**.

Isomer		CBS-QB3 E(total) [0K]	QB3 $\Delta_f H^0_{298}$	APNO $\Delta_f H^0_{298}$	Transition State	CBS-QB3 E(total) [0K]	QB3 $\Delta_f H^0_{298}$	APNO $\Delta_f H^0_{298}$
$\text{H}_2\text{NC}\equiv\text{N}^{*+}$	1	-148.17933	275.2	276.0	TS 1 \rightarrow 3	-148.05169	352.5	354.9
$\text{HN}=\text{C}=\text{NH}^{*+}$ (cis) [b]	2	-148.18646	271.1	270.9	TS 1 \rightarrow 2	-148.04835	357.7	357.0
$\text{H}_2\text{NN}\equiv\text{C}^{*+}$	3	-148.11690	314.7	314.9	TS 2 \rightarrow 4	-148.04561	359.4	361.1
$\text{HC}=\text{NNH}^{*+}$	4	-148.11197	317.3	317.4	TS 2 \rightarrow 6	-148.05699	351.9	[c]
$\text{HC}=\text{N}=\text{NH}^{*+}$	5	-148.14229	298.6	297.9	TS 3 \rightarrow 4	-148.00993	381.3	379.9
$\text{HN}=\text{C}(\text{H})\text{N}^{*+}$	6	-148.05769	351.7	[c]	TS 4 \rightarrow 5	-148.06165	349.0	348.5
$\text{HN}=\text{C}(\text{H})\text{N}^{*+}$ (quartet)	6Q	-148.06545	346.7	346.5	TS 4 \rightarrow 6	-148.06055	349.8	[c]
$\text{H}_2\text{C}=\text{N}=\text{N}^{*+}$	7	-148.18498	271.7	271.3	TS 7 \rightarrow 8	-148.11187	317.6	[c]
$\text{H}_2\text{CN}=\text{N}^{*+}$	8	-148.11373	316.5	[c]	TS 7 \rightarrow 5	-148.03273	367.1	[c]
					TS 6Q \rightarrow m/z 28	-148.05751	351.7	351.8
$\text{H}_2\text{O}\cdots\text{H}_2\text{NC}\equiv\text{N}^{*+}$	H1	-224.55568	192.3	193.5	TS H1 \rightarrow H2	-224.53377	205.3	204.9
$\text{H}_2\text{O}\cdots\text{HN}=\text{C}=\text{NH}^{*+}$	H2	-224.56694	185.2	186.4				

[a] E(total) in Hartrees, all other components in kcal mol⁻¹; [b] CBS-QB3 predicts the ionic trans isomer to lie at 271.5 kcal mol⁻¹; [c] Geometry optimization could not be achieved.

Table 2.2 Energetic data [a] from CBS-QB3 and CBS-APNO calculations for (i) various dissociation products of the CH_2N_2 ions and (ii) the neutral counterparts of the CH_2N_2 ions of Fig. 2.1.

Ion	m/z	CBS-QB3 E(total) [0K]	QB3 $\Delta_f H^0_{298}$	APNO $\Delta_f H^0_{298}$	Neutral [c]	CBS-QB3 E(total) [0K]	QB3 $\Delta_f H^0_{298}$	APNO $\Delta_f H^0_{298}$
$\text{HNC}\equiv\text{N}^+$	41	-147.48071	349.3	348.7	$\text{H}_2\text{NC}\equiv\text{N}$ 1N	-148.56529	33.0	33.6
$\text{H}_2\text{N}=\text{NH}^+$	31	-110.77246	229.3	229.5	$\text{HN}=\text{C}=\text{NH}$ 2N	-148.56121	35.5	35.4 [b]
$\text{HN}=\text{NH}^{*+}$	30	-110.13127	269.8	268.5	$\text{H}_2\text{NN}\equiv\text{C}$ 3N	-148.49446	77.5	77.9
HN_2^+	29	-109.57988	251.5	[d]	$\text{HC}=\text{NNH}$ 4N	-148.46572	95.2	96.2
$\text{HC}=\text{NH}^+$	28	-93.55430	226.4	226.8	$\text{HC}=\text{N}=\text{NH}$ 5N	-148.47148	89.0	91.3
$\text{HC}\equiv\text{N}^{*+}$	27	-93.78703	345.9	346.6	$\text{H}_2\text{C}=\text{N}=\text{N}$ 7N	-148.51526	64.4	64.2
$\text{HN}\equiv\text{C}^{*+}$	27	-92.82363	323.1	324.0	$\text{H}_2\text{CN}=\text{N}$ 8N	-148.49755	75.1	75.6
NH_2^+	16	-55.38062	302.8	302.5	$\text{HN}=\text{C}=\text{N}^{\bullet}$	-147.91569	76.2	76.9
NH^{*+}	15	-54.65080	396.1	396.7	$\text{HN}\equiv\text{C}$	-93.26616	45.5	46.5
CH_2^{*+}	14	-38.69018	332.9	333.1	CN^{\bullet}	-92.58753	106.6	106.4
H_3O^+	19	-76.59652	143.6	144.6	NH	-55.14448	86.1	86.2
CH^+	13	-38.02397	386.4	387.8	CH^{\bullet}	-38.41267	142.5	142.6

[a] E(total) in Hartrees, enthalpies are in kcal mol⁻¹; [b] A Weizmann-1 calculation yielded 35.0 kcal mol⁻¹; [c] The 298 K enthalpies for H^{\bullet} , N^{\bullet} , H_2O , and HCN (52.1, 113.0, -57.8 and 32.3 kcal mol⁻¹ respectively) were taken from ref. 28; [d] Geometry optimization not achieved; from $\text{PA}(\text{N}_2) = 118$ kcal mol⁻¹ [28] a value of 248 kcal mol⁻¹ is derived.

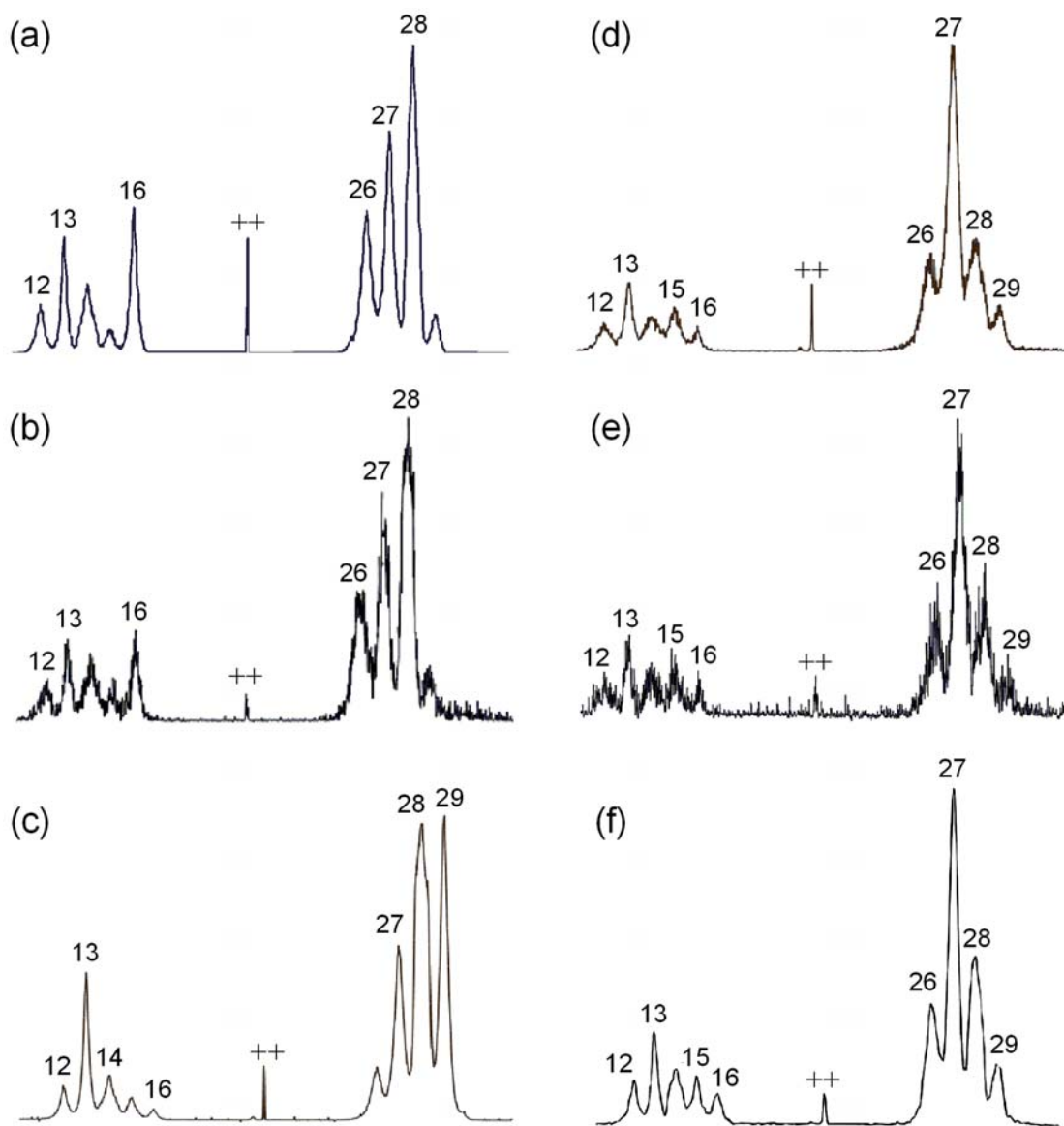


Figure 2.3 (a) Partial (8kV, O₂) CID spectrum and (b) NR-CID spectrum of cyanamide ions **1** ; (c) Partial CID spectrum of nitrilimine ions **5** generated from 1,3,4-triazole; (d) Partial CID spectrum of carbodiimide ions **2** generated by the dissociative ionization of 2-imidazolecarboxaldehyde; (e) partial CID spectrum of the CIDI experiment on *N*-methylguanidine derived ions, see text; (f) Partial CID spectrum of the *m/z* 42 ions generated in the ion-molecule reaction of ions **1** with H₂O.

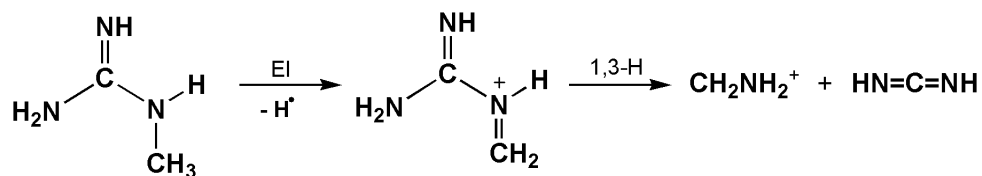
with the high-energy loss of C, easily differentiates the isocyanamide ion **3** from all other isomers [20]. In the same vein, the spectrum of the nitrilimine ion **5**, see Fig. 2.3c, is characterized by peaks at m/z 29 (N_2H^+) and m/z 13 (CH^+) [13,20], while a prominent m/z 14 (CH_2^+) peak characterizes the spectra of **7** and **8** [13, 20].

The CID mass spectrum of **1** (Fig. 2.3a) displays a structure diagnostic peak at m/z 16, indicative of the high-energy direct bond cleavage reaction $\text{H}_2\text{N}-\text{C}\equiv\text{N}^{\bullet+} \rightarrow \text{NH}_2^+ + \text{CN}^\bullet$. This is in line with the prediction of Fig. 2.2 that ions **1** retain their structure prior to metastable or collision-induced dissociation : the high barriers connecting ion **1** with the various CH_2N_2 isomers lie very close to the dissociation threshold for loss of $\text{N}(^4\text{S})$.

To probe the isomeric and isobaric purity of the m/z 42 ions generated by electron ionization of the sublimed cyanamide sample [19], we have used the NR-CID technique described in Refs. 24 and 25. The resulting spectrum of Fig. 2.3b is very close to that of Fig. 2.3a, thereby attesting to the purity of the m/z 42 ion beam.

As mentioned in the introduction, 2-imidazolecarboxaldehyde (IMC) indeed yields carbodiimide ions **2**, by the consecutive loss of CO and C_2H_2 , as depicted in Fig. 2.2.

The CID mass spectrum of these m/z 42 ions lacks the prominent structure diagnostic peaks in the CID mass spectra of ions **1**, **3**, **5** and **7**. Instead, Fig. 2.3d displays peaks at m/z 27 (HNC^+) and m/z 15 (NH^+), which support the carbodiimide ion structure assignment.



Scheme 2.2

Complementary evidence for this structure assignment comes from a previous study [21] in which precursor molecules were examined that may lose *neutral* carbodiimide upon ionization. As indicated in Scheme 2.2, the prominent fragment ions at m/z 72 that result

from loss of H^\bullet from N-methylguanidine molecular ions, served to generate mass 42 neutrals for a collision-induced dissociative ionization (CIDI [18]) experiment.

The $[\text{M-H}]^+$ ion shows a fairly intense peak at m/z 30 in its MI spectrum corresponding to a loss of mass 42. Indeed, a peak at m/z 42 dominates the CIDI mass spectrum of the m/z 72 ion. These m/z 42 ions, upon collisional activation, yield the spectrum of Fig. 2.3e, which is very close to that of Fig. 2.3d.

2.3.2 Proton-Transport Catalysis of the cyanamide radical cation

As discussed in the previous Section, theory predicts that the unassisted isomerization reaction of the cyanamide ion **1** into the more stable carbodiimide ion **2** does not occur spontaneously. This is corroborated by our experiments, which show that ions **1** and **2** have characteristically different CID spectra.

However, the proton-transport catalysis criterion [17] predicts that an efficient isomerization of ions **1** can be realized in an ion-molecule encounter complex with a neutral base, whose proton affinity (PA) lies between that of $\text{HN}=\text{C}=\text{N}^\bullet$ at HN and N, that is between 167 and 171 kcal mol^{-1} (from the data in Table 2.1 and 2.2). The water molecule may well be suitable as a catalyst because its PA, 165 kcal mol^{-1} [26], lies only slightly below the above PA range.

The calculated potential energy diagram of Fig. 2.4 supports this contention. It shows that the interaction of a single water molecule with ion **1** leads to the stable hydrogen-bridged radical cation **H1**. Once formed, ions **H1** can easily overcome the isomerization barrier to generate the more stable species **H2**, which can then dissociate by loss of H_2O to yield ion **2**. The transition state associated with the isomerization **H1** \rightarrow **H2** is easily overcome because it lies lower than the combined enthalpies of ion **1** and H_2O .

Note that the proposed catalysis involves abstraction of a proton from the NH_2 moiety of the cyanamide ion by the H_2O molecule followed by back-donation of another proton from the protonated base. This type of proton-transport catalysis has been coined *quid-pro-quo* [27].

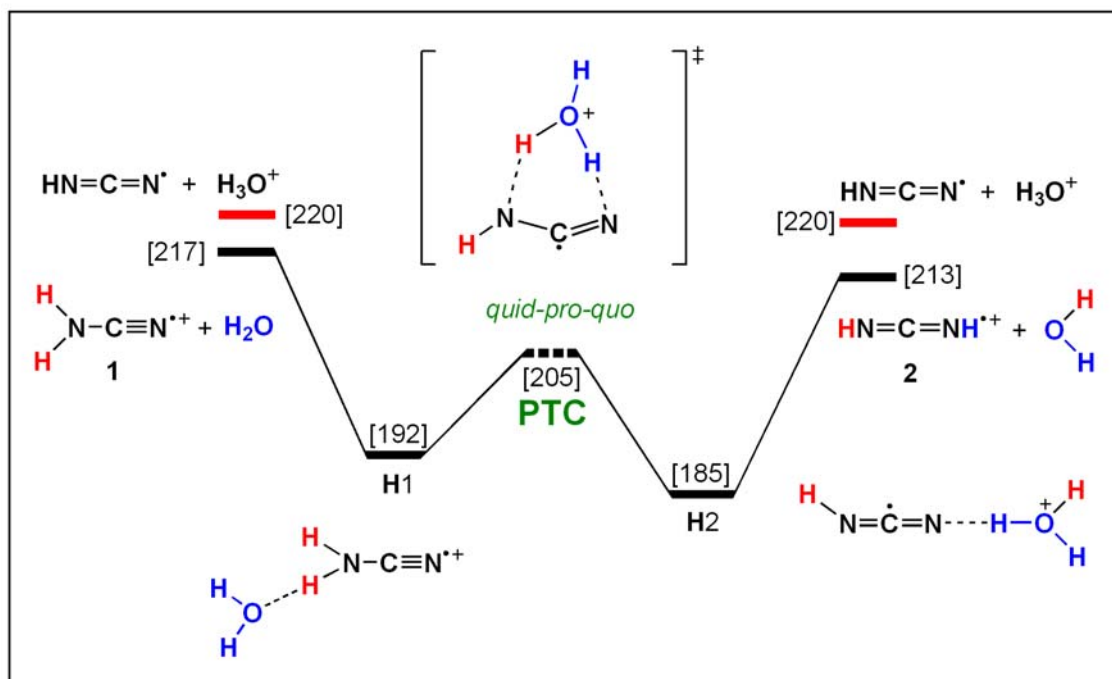


Figure 2.4 Proton-transport catalysis (PTC) of the cyanamide ion **1**. The numbers in square brackets refer to CBS-QB3 derived ΔH_{298}° values in kcal mol⁻¹.

Experimental evidence for this reaction comes from the cyanamide (ion) – water (molecule) reaction in the hexapole cell of our tandem mass spectrometer, described in the Experimental. Fig. 2.3f shows the CID spectrum of the m/z 42 ions that have reacted with H₂O vapour in the hexapole reaction chamber. The observation that the spectrum of Fig. 2.3f is very close to that of Figs. 2.3d/e, demonstrates that water is an efficient catalyst for the isomerization of the cyanamide ion into its more stable carbodiimide tautomer.

References

- [1] A. Schimpl, R.M. Lemmon, M. Calvin. *Science* 147 (1965) 149.
- [2] J. Hulshof, C. Ponnampereuma, *Origins of Life* 7 (1976) 197.
- [3] B.E. Turner, A.G. Kislyakov, H.S. Liszt, K. Kaifu. *Astrophys. J.* 201 (1975) L149.
- [4] E. Herbst, *Annu. Rev. Phys. Chem.* 46 (1995) 27.
- [5] M. Birk and M. Winnewisser. *Chem. Phys. Lett.* 123 (1986) 386.
- [6] M. Birk, M. Winnewisser, A.Z. Cohen. *J. Mol. Spectrosc.* 136 (1989) 402.
- [7] A.W. Allaf, R.J. Suffolk. *J. Chem. Research (S)* 1993, 269.

- [8] F. Tordini, A. Bencini, M. Bruschi, L. De Gioia, G. Zampella, P. Fantucci, *J. Phys. Chem. A* 109 (2005) 603.
- [9] F. Duvernay, T. Chiavassa, F. Borget, J-P. Aycard, *J. Am. Chem. Soc.* 126 (2004) 7772.
- [10] F. Duvernay, T. Chiavassa, F. Borget, J-P. Aycard, *J. Phys. Chem. A* 109 (2005) 603.
- [11] E. Schaefer, M. Winnewisser, J.J. Christiansen, *Chem. Phys. Lett.* 81 (1981) 380.
- [12] M.W. Wong, C. Wentrup, *J. Am. Chem. Soc.* 115 (1993) 7743.
- [13] N. Goldberg, A. Fiedler, H. Schwarz, *Helv. Chim. Acta.* 77 (1994) 2354.
- [14] M.B. Robin, C.R. Brundle, N.A. Kuebler, G.B. Ellison, K.B. Wiberg, *J. Chem. Phys.* 57 (1972) 1758.
- [15] J.A. Montgomery, Jr, M.J. Frisch, J.W. Ochterski, and G.A. Petersson, *J. Chem. Phys.* 112, (2000) 6532.
- [16] J.W. Ochterski, G.A. Petersson, J.A. Montgomery, Jr., *J. Chem. Phys.* 104 (1996) 2598.
- [17] R. Lee, P.J.A. Ruttink, P.C. Burgers, J.K. Terlouw, *Int. J. Mass Spectrom.* 255-256 (2006) 244 (and references cited therein).
- [18] J.L. Holmes, C. Aubry, P.M. Mayer. *Assigning Structures to Ions in Mass Spectrometry*, CRC Press, Boca Raton, 2007.
- [19] F. Cacace, G. de Petris, F. Grandinetti, G. Occhiucci. *J. Phys. Chem.* 97 (1993) 4239.
- [20] B.L.M. van Baar. Ph.D. Dissertation. University of Utrecht, The Netherlands. 1988. Chapter 1.
- [21] G. Dimopoulos-Italiano, MSc Thesis, McMaster University, 2003, Chapter 2.
- [22] G.A. McGibbon, C. Heinemann, D.J. Lavorato, H. Schwarz, *Angew. Chem. Int. Ed.* 36 (1997) 1478.
- [23] A. Maquestiau, Y. van Haverbeke, R. Flammang and J. Elguero. *Org. Mass Spectrom.* 7 (1973) 271.
- [24] L.N. Heydorn, C.Y. Wong, R. Srinivas, J.K. Terlouw, *Int. J. Mass Spectrom.* 225 (2003) 11.
- [25] K.J. Jobst, M.R. Hanifa, J.K. Terlouw, *Chem. Phys. Lett.* 462 (2008) 162.
- [26] E.P.L. Hunter, S.G. Lias. *J. Phys. and Chem. Ref. Data* 27 (1998) No. 3.
- [27] L.N. Heydorn, P.C. Burgers, P.J.A. Ruttink, J.K. Terlouw. *Int. J. Mass Spectrom.* 227 (2003) 453.
- [28] S.G. Lias, J.E. Bartmess, J.F. Liebman, J.L. Holmes, R.O. Levin, W.G. Maillard, *J. Phys. Chem. Ref. Data* 17 (Suppl. 1) (1988).

Chapter 3

The acrylonitrile dimer ion: a study of its dissociation via self-catalysis, self-protonation and cyclization into the pyrimidine radical cation

Large energy barriers prohibit the rearrangement of solitary acrylonitrile ions, $\text{CH}_2=\text{CHC}\equiv\text{N}^{+\bullet}$, into their more stable hydrogen-shift isomers $\text{CH}_2=\text{C}=\text{C}=\text{NH}^{+\bullet}$ or $\text{CH}=\text{CH}-\text{C}=\text{NH}^{+\bullet}$. This prompted us to examine if these isomerizations occur by self-catalysis in acrylonitrile dimer ions. Such ions, generated by chemical ionization experiments of acrylonitrile with an excess of carbon dioxide, undergo five dissociations in the μs time frame, as witnessed by peaks at m/z 53, 54, 79, 80 and 105 in their metastable ion mass spectrum. Collision experiments on these product ions, deuterium labeling, and a detailed computational analysis using the CBS-QB3 model chemistry leads to the following conclusions: (i) the m/z 54 ions are ions $\text{CH}_2=\text{CHC}\equiv\text{NH}^+$ generated by self-protonation in ion-dipole stabilized hydrogen-bridged dimer ions $[\text{CH}_2=\text{CHC}\equiv\text{N}\cdots\text{H}-\text{C}(\text{C}\equiv\text{N})\text{CH}_2]^{+\bullet}$ and $[\text{CH}_2=\text{CHC}\equiv\text{N}\cdots\text{H}-\text{C}(\text{H})\text{C}(\text{H})\text{C}\equiv\text{N}]^{+\bullet}$; the proton shifts in these ions are associated with a small reverse barrier; (ii) dissociation of the H-bridged ions into $\text{CH}_2=\text{C}=\text{C}=\text{NH}^{+\bullet}$ or $\text{CH}=\text{CH}-\text{C}=\text{NH}^{+\bullet}$ by self-catalysis is energetically feasible but kinetically improbable : experiment shows that the m/z 53 ions are ions $\text{CH}_2=\text{CHC}\equiv\text{N}^{+\bullet}$, generated by back dissociation; (iii) the peaks at m/z 79, 80 and 105 correspond with the losses of HCN, C_2H_2 and H^{\bullet} respectively. The calculations indicate that these ions are generated from dimer ions that have adopted the (much more stable) covalently bound “head-to-tail” structure $[\text{CH}_2=\text{CHC}=\text{N}-\text{C}(\text{H}_2)\text{C}(\text{H})\text{C}\equiv\text{N}]^{+\bullet}$; experiments indicate that the m/z 79 ($\text{C}_5\text{H}_5\text{N}$) and m/z 105 ($\text{C}_6\text{H}_6\text{N}_2$) ions have linear structures but the m/z 80 ($\text{C}_4\text{H}_4\text{N}_2$) ions consist of ionized pyrimidine in admixture with its stable pyrimidine-2-ylidene isomer. Acrylonitrile is a confirmed species in interstellar space and our study provides experimental and computational evidence that its dimer radical cation yields the ionized prebiotic pyrimidine molecule.

The work described here has been published previously in an article under the same title : H.K. Ervasti, K.J. Jobst, P.C. Burgers, P.J.A. Ruttink, J.K. Terlouw, *Int. J. Mass Spectrom.* 262 (2007) 88 – 100.

3.1 Introduction

In the context of our experimental and theoretical studies on self-catalysis in dimer radical cations [1] by proton-transport catalysis (PTC) and related mechanisms [2], we observed that dimer ions of acrylonitrile are readily generated in chemical ionization experiments of the monomer in the presence of a large excess of CO₂. The low-energy (metastable) dimer ions primarily dissociate into m/z 54 ions by self-protonation but m/z 53 monomer ions are also generated, either by back dissociation or self-catalysis. Surprisingly, the dimer ions undergo three more competing dissociations. Of these the loss of C₂H₂ aroused our interest because a collision experiment indicated that the resulting m/z 80 ions may well be pyrimidine ions [3]. Acrylonitrile is a confirmed species in astrochemistry [4] – it was first detected in the Sgr B2 cloud [5a] and since then also in the cold cloud TMC-1 [5b] and the atmosphere of Saturn's moon Titan [5c,d] – and a further study of a potential route to the formation of the prebiotic pyrimidine molecule via the above ion-molecule reaction seemed worthwhile.

Ion-molecule interactions have been shown to play a role in the production of larger molecular species in astrochemistry [6] and mass spectrometry has long been an indispensable tool in their study [7]. Ion-molecule reactions are advantageous over neutral-neutral reactions without activation energy because their rate coefficients may be higher by as much as a factor of 10⁴ if the molecule is polar [4]. This is the case with acrylonitrile, which has a large dipole moment.

We further note that the search for prebiotic molecular species in the interstellar medium is a subject of considerable interest. The driving force behind this quest lies in the role these molecules may have played in the formation of life on Earth [8]. Thus far as many as 130 molecular species have been identified, largely in the dense regions of dust clouds. Nevertheless, only a handful of biologically important molecules has yet been confirmed [4,9]. An early search for pyrimidine was unsuccessful [10a] but recently this integral DNA component was tentatively identified in the Sgr B2, Orion KL and W51 interstellar

clouds [10b,c]. A route to its formation has not been established but it has been suggested that it could be formed by the aggregation of HCN and acrylonitrile either in the gas-phase or on the surface of dust grains [10a].

In this study, we report the results of a detailed experimental and computational analysis of the rich and complex chemistry of the acrylonitrile dimer radical cation. It will be shown that interaction of an acrylonitrile ion with its neutral counterpart leads to hydrogen-bridged radical cations. These may undergo self-protonation or isomerize into the very stable distonic ion $\text{CH}_2=\text{CH}-\text{C}\equiv\text{N}^+-\text{CH}_2-\dot{\text{C}}\text{H}-\text{C}\equiv\text{N}$ which can be viewed as a head-to-tail dimer and which acts as precursor for the observed losses of H^+ , HCN and C_2H_2 . The latter process proceeds via cyclization and produces ionized pyrimidine in admixture with its 2-ylide isomer. Self-catalysis, although energetically quite possible, is not observed : this process requires considerable reorientation making it kinetically unfavourable.

3.2 Results and discussion

3.2.1 The occurrence of self-protonation and proton-transport catalysis in the dimer ions

The base peak at m/z 54 in the MI spectrum of the acrylonitrile dimer ion at m/z 106, see Fig. 3.1, corresponds to the generation of protonated acrylonitrile ions. Since the proton affinity (PA) of acrylonitrile, $187.5 \text{ kcal mol}^{-1}$ [11b], is typical of a nitrile rather than an alkene, these ions undoubtedly have the structure $\text{CH}_2=\text{CHC}\equiv\text{NH}^+$ (ANP) and not $\text{CH}_3\text{CHC}\equiv\text{N}^+$. Indeed, it follows from the results of Table 3.1 that the self-protonation $\text{CH}_2=\text{CHC}\equiv\text{N}^+ (\text{AN}) + \text{CH}_2=\text{CHC}\equiv\text{N} \rightarrow \text{CH}_3\text{CHC}\equiv\text{N}^+ + \text{CH}_2=\text{C}^-\text{C}\equiv\text{N}$ is *endothermic*, by 25 kcal mol^{-1} , whereas formation of ANP with either $\text{CH}_2=\text{C}^-\text{C}\equiv\text{N}$ (ANR₁) or $\dot{\text{C}}\text{H}=\text{C}(\text{H})\text{C}\equiv\text{N}$ (ANR₂) is *exothermic*, by 20 and 13 kcal mol^{-1} respectively.

One would therefore expect that in encounter complexes of ionized acrylonitrile with its neutral counterpart, protonation at the cyano group readily occurs and that, when energized, these complexes dissociate into ANP (m/z 54) rather than AN (m/z 53).

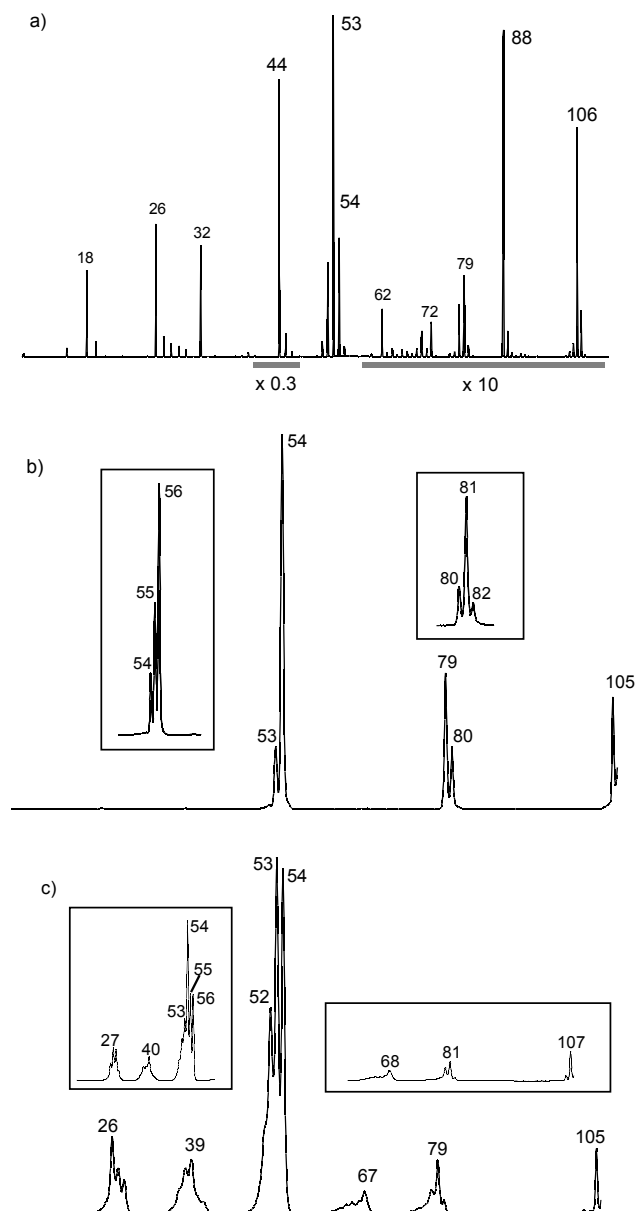


Figure 3.1 (a) Chemical ionization mass spectrum of a *c.* 1:10 molar mixture of gaseous acrylonitrile and CO₂. The total source pressure was $7 - 10 \times 10^{-5}$ Torr. The 2ffr MI and the (8kV, O₂) CID spectra of the *m/z* 106 acrylonitrile dimer ions of this spectrum are shown as items (b) and (c) respectively. The insets in (b) and (c) refer to the spectra of the *m/z* 108 dimer ions of acrylonitrile-2-d.

Table 3.1 Energetic data [a] derived from CBS-QB3 calculations pertinent to the ion chemistry of acrylonitrile and 2-chloroacrylonitrile described in Schemes 3.1 and 3.4.

Ionic/neutral species			CBS-QB3 E(total) [0 K]	ZPE	QB3 $\Delta_f H^0_0$	QB3 $\Delta_f H^0_{298}$	Expt $\Delta_f H^0_{298}$	
CH ₂ =CHC≡N		ANN	-170.53848	31.5	48	46	44	[b]
CH ₂ =CHC≡N ⁺	² A''	AN	-170.13793	30.4	299	298	296	[b]
	² A'	AN	-170.08412	29.6	333	332	-	
CH ₂ =C=C=NH ⁺	² A'	AN1	-170.16624	28.4	282	281	-	
CH=CH-C=NH ⁺	² A'	AN2	-170.15296	29.5	290	289	-	
CH ₂ =C-CH=N ⁺	² A'	AN3	-170.08760	27.9	331	330	-	
HC≡C-C≡NH ⁺			-169.58533	23.5	277	277	-	
TS AN → AN1	(Scheme 3.1)		-169.99871	25.6	387	385	-	
TS AN → AN3	(Scheme 3.1)		-170.06537	26.2	345	344	-	
TS AN3 → AN1	(Scheme 3.1)		-170.06355	25.8	346	345	-	
CH ₂ =CH-C=NH ⁺	¹ A'	ANP	-170.83610	38.2	226	224	223	[c]
CH ₃ CHC≡N ⁺	¹ A'		-170.76564	36.7	271	269	-	
H ₂ C=C-C≡N [•]		ANR₁	-169.87318	22.2	100	100	-	
HC=CH-C≡N [•]		ANR₂	-169.86085	22.7	108	107	-	
TS ANR₁ → ANR₂			-169.78975	18.7	153	152	-	
H ₂ C=CCIC≡N			-629.69426	25.8	42.6	42.5	-	
H ₂ C=CCIC≡N ⁺	(Scheme 3.4)		-629.30609	25.1	286	286	287	[d]
H ₂ C=CCIC=NH ⁺			-629.98240	32.5	227	226	-	
HC=CCI-C≡N [•]			-629.01464	17.3	104	105	-	
D1 (Cl)	(Scheme 3.4)		-801.07231	59.4	(290)	(288)	-	[e]
D4 (Cl)			-801.06640	58.8	(293)	(291)	-	[e]
TS D1 (Cl)→ D4 (Cl)	(Scheme 3.4)		-801.00057	55.9	(332)	(330)	-	[e]
C ₅ H ₅ N ^{•+}	(<i>m/z</i> 79)	(Figure 3.6)	-247.41820	49.6	297	295	-	[f]
PY1	(<i>m/z</i> 80)	(Figure 3.6)	-263.53204	46.8	264	260	260	[b]
PY2	(<i>m/z</i> 80)	(Figure 3.6)	-263.52851	48.1	266	263	-	[f]
TS PY1 → PY2			-263.42505	42.9	331	328	-	
C ₆ H ₅ N ₂ ⁺	(<i>m/z</i> 105)	(Figure 3.6)	-340.19954	58.7	281	278	-	[f]
TS D4 →C ₆ H ₅ N ₂ ⁺ +H [•]	(Figure 3.6)		-340.69641	59.3	335	331	-	

[a] E_(total) in Hartrees, all other components, including the ZPE scaled by 0.99, are in kcal mol⁻¹; [b] From ref. 11e; [c] From PA = 187.5 kcal mol⁻¹ [11b]; [d] From IE = 10.58 eV [11c] and using the calculated enthalpy of the neutral; [e] E_(total) refers to B3LYP/CBSB7 energies; the enthalpies were calculated using the CBS-QB3 values of ANCl + ANN as the anchor; [f] The dissociation levels for the loss of H[•], HCN and C₂H₂ in Figure 3.6 were obtained from the calculated ionic enthalpies of this Table and CBS-QB3 298 K values for H[•], C₂H₂ and HCN of 52.1, 55.2 and 31.7 kcal mol⁻¹ respectively.

Table 3.2 Energetic data [a] derived from CBS-QB3 calculations pertinent to the dissociation chemistry of acrylonitrile dimer ions as described in the Schemes and Figures.

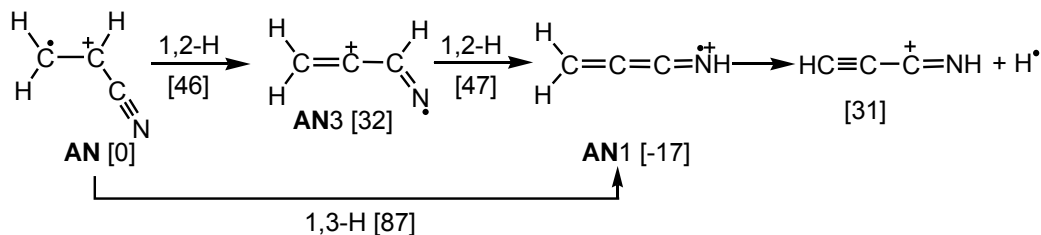
Ionic/neutral species	B3LYP/CBSB7 E(total)	CBS-QB3 E(total) [0 K]	ZPE	QB3 $\Delta_f H^0_0$	QB3 $\Delta_f H^0_{298}$
HBRC-1 (Figure 3.2)	-341.41042	-340.70404	62.5	330	327
HBRC-2 (Figure 3.2)	-341.41065	-340.70269	62.5	331	329
HBRC-3 (Figure 3.3)	-341.44531	[b]	59.7	(314)	(311)
HBRC-4 (Figure 3.3)	-341.43001	-340.74531	60.4	304	301
D1 (Figure 3.2)	-341.45639	-340.76886	64.7	289	286
D2 (Figure 3.2)	-341.42145	-340.73700	63.6	309	306
D3 (Figure 3.2)	-341.42048	-340.73037	64.5	313	310
TS HBRC-1 → D1	-341.41026	-340.7049	62.6	330	327
TS HBRC-2 → D1	-341.41043	-340.7029	62.4	331	328
TS HBRC-1 → HBRC-3	-341.39392	-340.70212	58.9	331	328
TS HBRC-2 → HBRC-4	-341.38607	-340.69777	58.8	334	331
D4 (Figure 3.6)	-341.46192	-340.77004	64.5	289	285
D5 (Figure 3.6)	-341.43638	-340.74755	64.8	303	298
D6 (Scheme 3.3)	-341.43667	-340.74303	65.5	306	302
D7 (Figure 3.5)	-341.44061	-340.74904	64.8	302	298
D8 (Figure 3.7)	-341.42623	-340.73286	62.7	312	308
TS D1 → D4	-341.39405	-340.70471	61.8	330	326
TS D1 → D6	-341.35331	-340.66747	59.8	353	349
TS D4 → D7	-341.37789	-340.68846	60.9	340	336
TS D7 → VP1	-341.43441	-340.74342	64.7	305	301
TS D4 → D5	-341.43278	-340.74516	64.1	304	300
TS D5 → VP1	-341.39167	-340.70135	63.9	332	327
TS D5 → D8	-341.42123	-340.73015	63.2	314	309
VP1 (Figure 3.6)	-341.49269	-340.79467	67.1	273	268
VP1b (Figure 3.6) (text)	-341.43299	-340.72866	65.8	315	310
VP1a (Figure 3.6) (text)	-341.48804	-340.79785	67.7	271	266
VP2 (Figure 3.6)	-341.46800	-340.77584	67.8	285	280
VP2a (Figure 3.6) (text)	-341.46520	-340.77672	67.1	284	280
TS VP1 → VP2	-341.41261	-340.72597	66.0	316	311
TS VP1 → VP1a	-341.44621	-340.76169	63.5	294	289
TS VP2 → VP2a	-341.42553	-340.74089	64.4	307	302
TS VP1 → VP1b	-341.41280	-340.72419	64.6	318	313

[a] $E_{\text{(total)}}$ in Hartrees, all other components, including the ZPE scaled by 0.99, are in kcal mol⁻¹; [b] estimate from a B3LYP/CBSB7 calculation using **HBRC-4** as the anchor; the CCSD(T) component in the CBS-QB3 calculation did not converge.

Yet in the μs time frame metastable dimer ions show four other competing dissociations including loss of acrylonitrile.

One explanation for the presence of the substantial m/z 53 peak in the MI spectrum is that the protonation process leading to m/z 54 involves a significant reverse energy barrier. This would make dissociation of the dimer into its ionic and neutral acrylonitrile components more competitive with the protonation. Alternatively, the m/z 53 ions in the MI spectrum of Fig. 3.1 do not represent ions **AN** but rather ions $\text{CH}_2=\text{C}=\text{C}=\text{NH}^+$ (**AN1**), which are more stable by 17 kcal mol^{-1} , see Table 3.1.

Solitary ions **AN** cannot isomerize into **AN1**: the calculated energy requirement (CBS-QB3 data Table 3.1) for this isomerization – a 1,3-H shift at 87 kcal mol^{-1} or, more economically, two consecutive 1,2-H shifts at 46-47 kcal mol^{-1} – is quite high and well above that for dissociation of the incipient ions **AN1** by H^+ loss into the N-protonated cyanoacetylene ion [3], see Scheme 3.1.



Scheme 3.1

However, the high barrier for the one-step isomerization via a 1,3-H shift in the solitary ion may vanish in the encounter complex if the neutral component catalyses the transformation. Criteria for successful proton-transport catalysis (PTC) have been developed by Böhme [2d] and Radom and co-workers [13]. The most important criterion predicts that a smooth isomerization **AN** \rightarrow **AN1** would occur if the PA of the base (B, acrylonitrile) lies between the PA of $\text{CH}_2=\text{C}^+-\text{C}\equiv\text{N}$ at C and at N. If PA(B) is too low, proton abstraction will not take place. If PA(B) is too high, the incipient ion BH^+ will not release the proton: dissociation to $\text{CH}_2=\text{C}^+-\text{C}\equiv\text{N} + \text{BH}^+$ ($\text{CH}_2=\text{CHC}\equiv\text{NH}^+$ (**ANP**)) will ensue

instead. From the CBS-QB3 results in Table 3.1 we derive values of 168, 185 and 188 kcal mol⁻¹ for PA(CH₂=C[•]-C≡N at C), PA(CH₂=C[•]-C≡N at N) and PA(B) respectively ; the latter value is in excellent agreement with the experimental value. Thus the PA of the base is too high, but only marginally so, which implies that PTC cannot a priori be ruled out.

Various ion-dipole complexes may be formed in the reaction of acrylonitrile with its ionic counterpart which, because of the large dipole moment of the nitrile ($\mu = 3.9$ D), are expected to have stabilization energies in the 10 – 20 kcal mol⁻¹ range. Among these, two hydrogen-bridged dimer ions may be envisaged, *viz.* **HBRC-1** and **HBRC-2** as depicted in Figure 3.2. These C-H-N hydrogen-bridged radical cations [14] are calculated to have stabilization energies of 15-17 kcal mol⁻¹ at the CBS-QB3 level of theory*. They both lie in a very shallow potential well with small barriers for rearrangement into ion-dipole complexes that are not hydrogen-bridged. More importantly, these HBRCs can also rearrange with a negligible barrier into the covalently bound isomer **D1** which enjoys a much larger stabilization energy, 58 kcal mol⁻¹. Two more covalently bound isomers were identified as stable minima *viz.* ions **D2** and **D3** in Fig. 3.2. The latter ion has been proposed as the dimer ion core in an infrared photodissociation study of acrylonitrile cluster ions (CH₂=CHC≡N)_n^{•+} (n = 3-10) [15]. Both isomers are considerably less stable than **D1** and play no obvious role in the dissociation chemistry of the dimer ions.

* **HBRC-1** and **HBRC-2** show a large difference in the stabilization energy (SE) derived from the B3LYP/CBSB7 and CBS-QB3 calculations. The DFT calculation yields an SE of 24 kcal mol⁻¹ for both ions whereas CBS-QB3 predicts much lower values: 17 kcal mol⁻¹ for **HBRC-1** and 15 kcal mol⁻¹ for **HBRC-2**. An explanation for this unusually large discrepancy may involve the following. For the related complex HCN•••H-C(CN)=CH₂^{•+}, in which HCN ($\mu = 3.0$ D)[11a] replaces the acrylonitrile ($\mu = 3.9$ D) [11a] component, the DFT and CBS-QB3 methods yield the same stabilization energy of 15 kcal mol⁻¹. The same value was obtained with the more sophisticated CBS-APNO method. This suggests that the DFT calculation overestimates the stabilization energies for **HBRC-1/2**. The DFT calculation also yields a much more delocalized charge distribution than expected for an ion-dipole complex, probably because the two components of **HBRC-1/2** are identical. In contrast, the DFT charge distribution of the HCN-acrylonitrile complex is as expected: the charge is largely localized on the acrylonitrile moiety. Thus the unrealistic charge distributions and stabilization energies of **HBRC-1/2** may well be connected to the “sameness” of their components [12]. While a poor DFT result for geometries of these complexes may adversely affect the CBS-QB3 derived stabilization, a precise knowledge of their stabilizations is not required for our discussion.

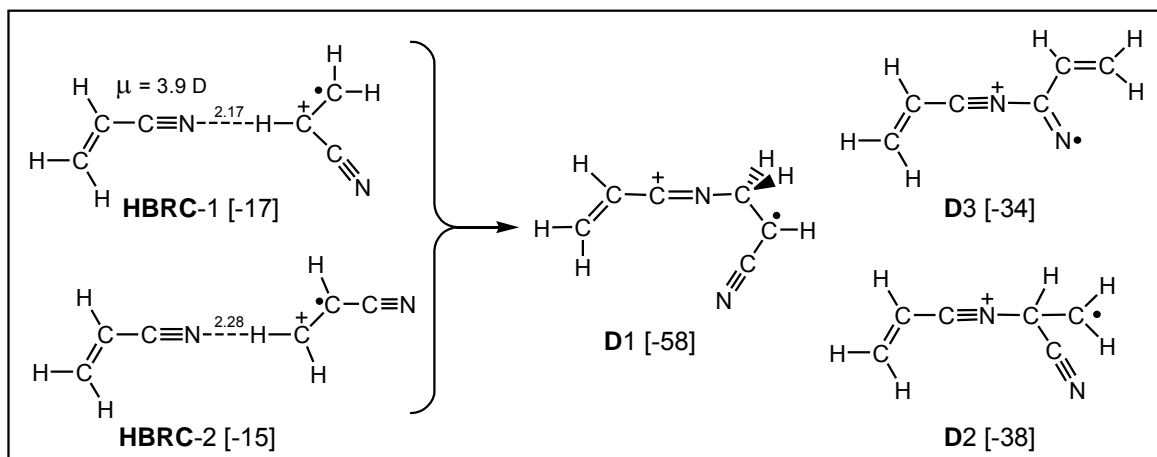


Figure 3.2 Structures of stable acrylonitrile dimer ions and their stabilization energies (kcal mol^{-1}) relative to the dissociation level $\text{CH}_2=\text{CHCN}^+$ (**AN**) + $\text{CH}_2=\text{CHCN}$; the values in square brackets refer to CBS-QB3 (298 K) calculations.

As we shall see in the next section, ion **D1** may act as the reacting configuration for a 1,2-H shift that initiates the observed losses of H^\bullet , HCN and C_2H_2 from the dimer ions.

The self-protonation leading to m/z 54 – and also the formation of m/z 53 if proton-transport catalysis plays a role – most likely involves **HBRC-1** and **HBRC-2**. That the self-protonation reaction in these ions does not proceed spontaneously follows from a consideration of the symmetries of the corresponding electronic wave functions. Radical cation **AN** as well as the radicals **ANR₁** and **ANR₂** are planar. The **AN** ground state ($\Delta_f H_{298} = 298 \text{ kcal mol}^{-1}$) has $^2A''$ symmetry; the lowest $^2A'$ state lies 34 kcal mol^{-1} higher in energy. The ground states of the radicals **ANR₁** and **ANR₂**, however, have $^2A'$ symmetry. The lowest $^2A''$ states for these radicals correspond to excitation energies of 52 and 53 kcal mol^{-1} respectively. Since these excitation energies are much larger than the stabilization energies of **HBRC-1** and **HBRC-2**, the reaction cannot proceed through any of the excited states. As a consequence, the symmetry of the wave function has to change during the proton transfer for the reaction to proceed at energies below the threshold for disproportionation into an acrylonitrile ion and neutral (344 kcal mol^{-1}). Thus, assuming

that the complex is planar, we have to deal with the intersection between the two PESs corresponding to the $^2A'$ and $^2A''$ states of the complex. However, the two states can be connected by lowering the symmetry of the nuclear framework of the $\text{CH}_2=\text{CHC}\equiv\text{N}^{+\bullet}$ moiety. This leads to a TS by distorting the nuclear framework of this moiety such that the $\text{CH}_2=\text{CH}$ π -bond is partially broken. The transition states for the self-protonation reactions depicted in Figure 3.3a/b were found to lie just above the corresponding hydrogen-bridged complexes **HBRC-1/2**. The barrier for formation of ANR_1 is lower than that for ANR_2 , by 3 kcal mol^{-1} , leading to the expectation that ANR_1 is preferentially formed. Note that the two radicals cannot freely interconvert because of a prohibitively high barrier of 52 kcal mol^{-1} , see Table 3.1.

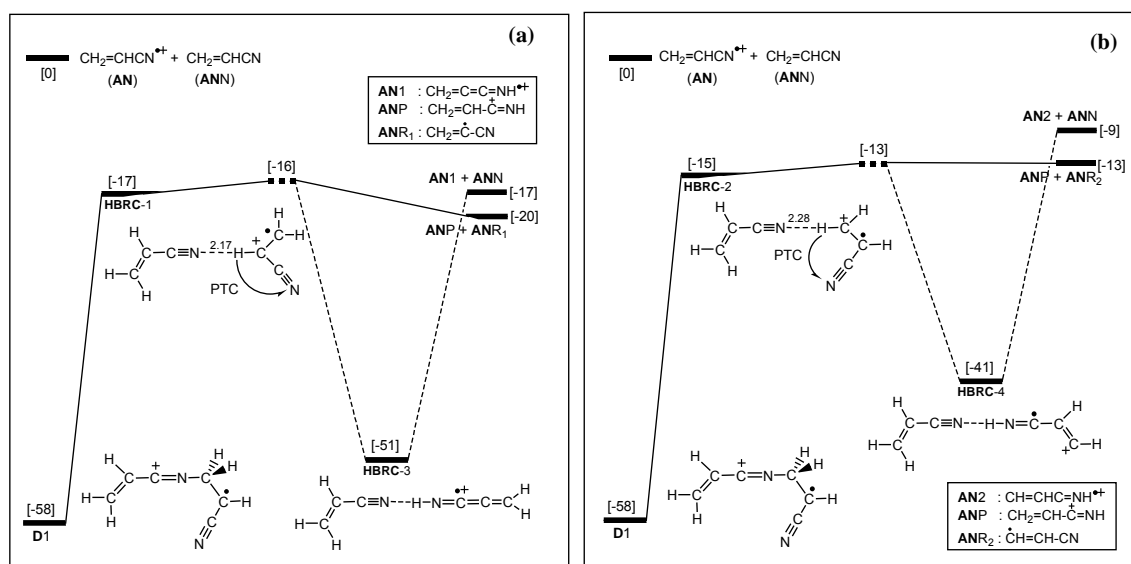


Figure 3.3a/b Potential energy diagrams (CBS-QB3 calculations) describing the self-protonation reaction and the occurrence of proton-transport catalysis in acrylonitrile dimer ions. The energy differences are in kcal mol^{-1} .

Our chemical ionization experiments involving acrylonitrile-2-d, $\text{CH}_2=\text{CDC}\equiv\text{N}$, are in qualitative agreement with the scenario depicted in Fig. 3.3. The deuterated dimer ions dissociate into both $\text{CH}_2=\text{CDC}\equiv\text{ND}^+$ (m/z 56) + $\text{CH}_2=\text{C}^{\bullet}-\text{C}\equiv\text{N}$ (ANR_1) and $\text{CH}_2=\text{CDC}\equiv\text{NH}^{+\bullet}$

(m/z 55) + $\cdot\text{CH}=\text{C}(\text{D})\text{C}\equiv\text{N}$ (ANR_2). This is seen from the inset in the MI spectrum of Fig 3.1b, where the m/z 56 peak is about twice as intense as the m/z 55 peak. Thus both ANR_1 and ANR_2 radicals are formed with a relative abundance of 2 : 1, and note that ANR_1 is thermodynamically the more stable radical. The peak intensity ratio (m/z 56 + m/z 55) : m/z 54 equals the m/z 54 : m/z 53 peak intensity ratio (6.0) in the spectrum of the unlabelled dimer indicating that there is no isotope effect associated with the reactions.

We further note that after passing the transition state, ANP may be formed directly or via N-H-N bridged complexes with ANR_1 or ANR_2 , *viz.* **HBRC-3** and **HBRC-4** in Fig. 3.3. (We note that the stabilization energies calculated for these HBRCs, c. 30 kcal mol⁻¹, is close to that obtained by experiment for the N-H-N bridged proton bound dimer of acrylonitrile, 30.7 kcal mol⁻¹ [16]). However, these HBRCs may also accommodate back-donation of the abstracted proton which would lead to the isomerization of the AN ion into either of its more stable isomers $\text{CH}_2=\text{C}=\text{C}=\text{NH}^{++}$ (AN1) or $\text{CH}=\text{CH}=\text{C}=\text{NH}^{++}$ (AN2). These ions both turn out to have $^2\text{A}'$ ground states, enabling the corresponding proton transfers to take place spontaneously, provided these processes are exothermic. Using the CBS-QB3 derived $\Delta_f H_{298}$ values of the components in Table 3.1, we obtain the following energies for the dissociation products: $\Delta_f H_{298}(\text{AN1} + \text{ANN}) = 327$ kcal mol⁻¹ and $\Delta_f H_{298}(\text{AN2} + \text{ANN}) = 335$ kcal mol⁻¹. These energies are only slightly higher than those for the products of the self-protonations: $\Delta_f H_{298}(\text{ANP} + \text{ANR}_1) = 324$ kcal mol⁻¹ and $\Delta_f H_{298}(\text{ANP} + \text{ANR}_2) = 331$ kcal mol⁻¹. This implies that the PTC processes cannot be ruled out on *energetic* grounds because the energy available in the dimer ions is sufficiently high for either dissociation route. On the other hand, both reactions are exothermic for ions that pass either of the transition states where their configuration is such that formation of ANP involves a mere bond cleavage whereas the formation of the PTC ions AN1 or AN2 requires a significant rearrangement. This makes it unlikely that the PTC processes can effectively compete with the self-protonation reactions. In this context it is important to note that both self-protonation reactions occur and that the self-protonation of Figure 3.3b lies 4 kcal mol⁻¹

higher in energy than the PTC process of Figure 3.4a. Yet, only self-protonation is observed.

Evidence that PTC does not play a significant role comes from an experiment in which we probed the structure of the m/z 53 ions in the MI spectrum of Fig. 3.1 by obtaining their CID mass spectrum. This spectrum is shown in Fig. 3.4a : it is virtually identical with that of acrylonitrile ions generated by electron ionization and characteristically different from that of ions AN1 and AN2 discussed in a previous study [3].

3.2.2 *Back-dissociation vs self-protonation in the acrylonitrile dimer ions HBRC-1/2*

In the previous section we have established that the m/z 53 ions in the MI spectrum do not result from proton-transport catalysis but rather are ions AN resulting from a back-dissociation. It follows from the energy diagram of Figure 3.3, that dimer ions dissociating back into AN + ANN can only do so at energies largely in excess of that required for self-protonation. Prima facie, therefore, the observed competition in the μ s time frame of the back-dissociation with the self-protonation is surprising. However, the following considerations may rationalize why dissociation by self-protonation requires a sizable excess energy.

First, the majority of the reacting configurations do not correspond to **HBRC-1/2**, which lie in very shallow wells, but to the much more stable ion **D1** (at 286 kcal mol⁻¹). According to RRKM theory [17], this implies that a relatively large excess energy is needed. The same argument applies to the dissociations of the very stable ions **HBRC-3/4**. Second, the large dipole moment of acrylonitrile ($\mu = 3.9$ D) and also of the radicals **ANR1/2** ($\mu = 3.8$ and 3.2 D respectively; calculated values) probably leads to a dramatic decrease, by some orders of magnitude, of the dissociation rate constants, as compared to an RRKM (Variational Transition State Theory) estimate. It has been argued that such dissociations do not behave statistically, as classical trajectory calculations have shown

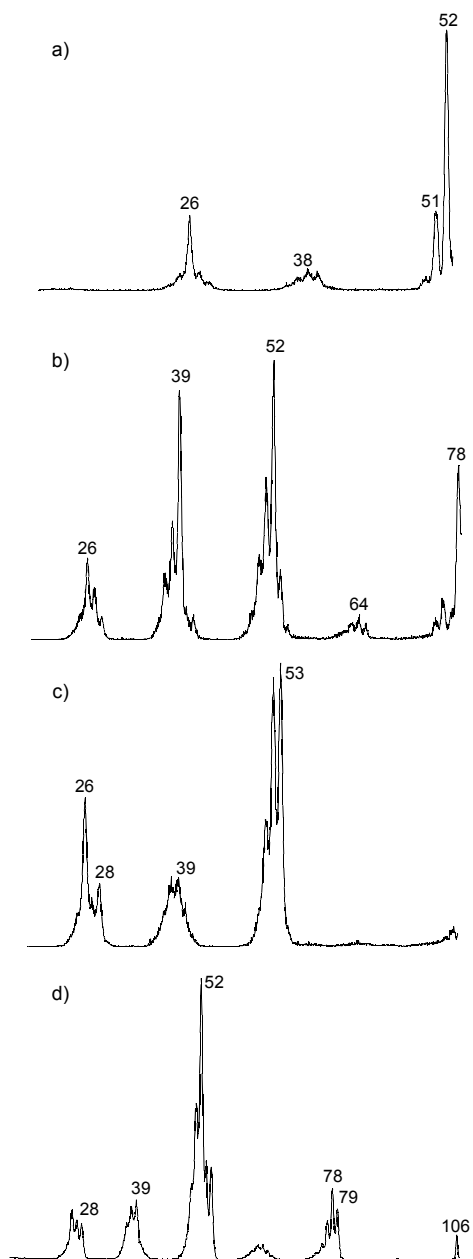


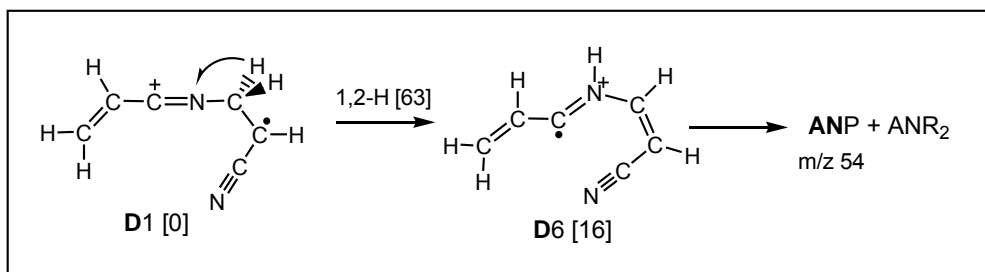
Figure 3.4 CID mass spectra (10kV,3ffr,O₂) of product ions generated from metastable acrylonitrile dimer ions : (a) m/z 53 ions (loss of acrylonitrile) (b) m/z 79 ions (loss of HCN) ; (c) m/z 80 ions (loss of C₂H₂) ; (d) m/z 105 ions (loss of H⁺).

that the trajectories leading to dissociation are quasi-periodical instead of chaotic because of the large ion-dipole stabilization [18]. We suggest that the non-planarity of the transition states connecting **HBRC-1** to **HBRC-3** and **HBRC-2** to **HBRC-4** also contributes to a non-statistical behaviour. Our calculations show that the distortions in the $\text{CH}_2=\text{CHC}\equiv\text{N}^+$ moiety lead to transition states that are 10-13 kcal mol⁻¹ lower in energy than the corresponding (planar) minimum energy crossing points. The self-protonation will then only be effective if the internal rotation of the CH_2 -group in the $\text{CH}_2=\text{CHC}\equiv\text{N}^+$ moiety is excited and the $\text{CH}_2=\text{CHC}\equiv\text{N}$ moiety approaches the ion from the right direction. Because of the large ion-dipole stabilization for all other orientations, the reaction may be substantially slowed down by non-statistical behaviour.

Experimental evidence that the self-protonation is relatively slow comes from a comparison of the MI and CID spectra of the dimer ions presented in Fig. 3.1 : self-protonation dominates the MI spectrum, but in the CID spectrum the m/z 54 peak is diminished with respect to the m/z 53 back-dissociation.

3.2.3 Self-protonation via the covalently bound acrylonitrile dimer ions **D-1** ?

We have also entertained the possibility that protonated acrylonitrile product ions are generated via a hydrogen shift in covalently bound dimer ions. An obvious route for ions **D1** is the one shown in Scheme 3.2, where the second step is a simple bond cleavage.



Scheme 3.2

This route is not feasible: the 1,2-H shift for the isomerization **D1** → **D6** is calculated to be more energy demanding than the formation of **ANP** (m/z 54) via the HBRCs and also, see Figure 3.7, the formation of m/z 105 ions by loss of H^{\bullet} from **D1**. Another possibility is that ions **D6** are generated from ion **D7**, by a 1,4-H shift. The formation of **D7** from **D1**, see Figure 3.5 below, was considered because our calculations indicate that **D7** readily cyclizes into the vinyl pyrimidine type ions **VP1/2** of Figure 3.6. Ion **D7** could thus account for the observed loss of C_2H_2 from the acrylonitrile dimer ions and the formation of m/z 80 pyrimidine type product ions.

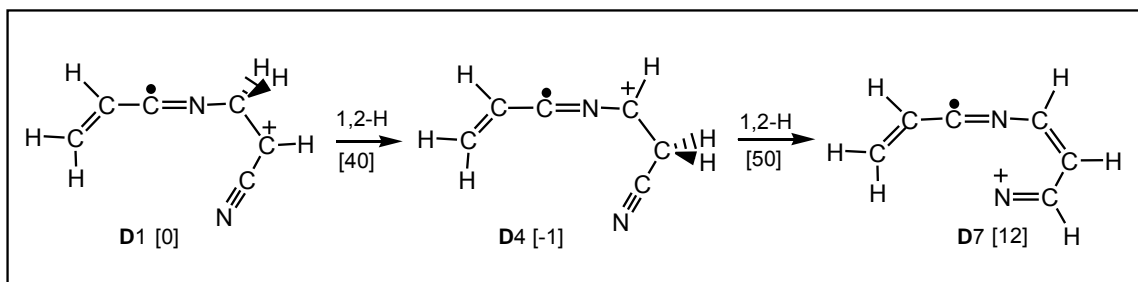


Figure 3.5 Isomerization pathways of acrylonitrile dimer ions **D1** into ions **D7**. The relative energies in square brackets are in kcal mol^{-1} and were obtained from CBS-QB3 calculations (Table 3.2).

This scenario is not a viable option either: the barrier for the isomerization **D1** → **D7** via two consecutive 1,2-H shifts, see Figure 3.5, is so high that it is unlikely that ions **D7** play a role in the dissociation chemistry of the acrylonitrile dimer ions.

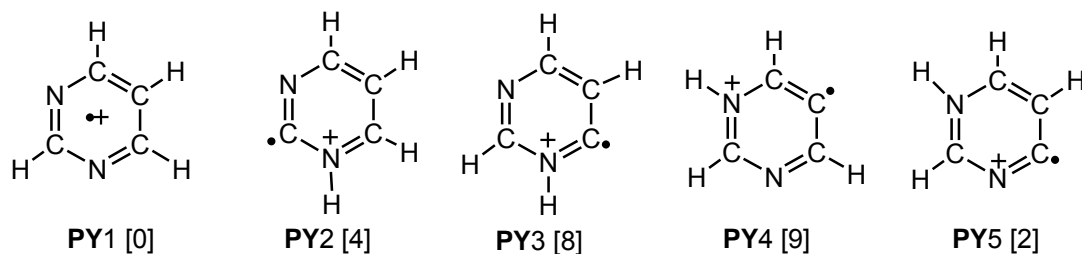
Thus it seems likely that the formation of m/z 54 in the MI spectrum of the dimer ions occurs via **HBRC-1/2**. However, these HBRCs and the related non-hydrogen bridged ion-dipole complexes cannot account for the competing loss of H^{\bullet} and also that of HCN and C_2H_2 , which may well involve a cyclic precursor ion. As we shall see in the next section rearrangement reactions starting from the covalently bound dimer ions **D1** can account for all three losses.

3.2.4 Generation of ionized pyrimidine and its isomer ionized pyrimidine-2-ylidene.

The mechanistic proposal for the dissociation of the dimer ions **D1** by loss of HCN, C₂H₂ and H[•] is presented in Figure 3.6. Its analysis will await the evaluation of the experimental evidence for the proposed product ion structures. That the neutrals lost from **D1** are HCN rather than C₂H₃[•] and also C₂H₂ rather than CN[•] is confirmed by the MI spectrum of the fully deuterated dimer ion (*m/z* 112) which displays a single peak at *m/z* 84 in the *m/z* 80 region.

The CID spectrum of the *m/z* 79 C₅H₅N ions generated by loss of HCN from the metastable dimer ions is shown in Figure 3.4b. The major peaks at *m/z* 52 (loss of HCN and/or C₂H₃[•]), *m/z* 39 (C₃H₃⁺) and *m/z* 26 (C₂H₂⁺) are compatible with the proposed linear C₅H₅N⁺ isomer of Figure 3.6. Reference CID mass spectra of non-cyclic C₅H₅N⁺ isomers are not available so that this structure assignment must remain tentative. We further note that the CID spectrum of Fig. 3.4b is incompatible with that of ionized pyridine or its distonic analogues. These very stable cyclic C₅H₅N⁺ isomers all display CID spectra that are dominated by a peak at *m/z* 52 (loss of HCN) [25].

A different scenario obtains for the structure assignment of the *m/z* 80 ions. Here the overall appearance of the CID mass spectrum of the metastably generated ions is that of a cyclic C₄H₄N₂⁺ ion, *viz.* ionized pyrimidine (**PY1**) and/or one of its ylide counterparts **PY2** – **PY5** shown in Scheme 3.3 (relative energies in kcal mol⁻¹ from ref. 3).



Scheme 3.3

We have previously studied the above system of $C_4H_4N_2^{*+}$ ions in detail, by both theory and experiment [3]. The calculations of this study predict that the five stable pyrimidine isomers have comparable energies but also high interconversion barriers. In spite of this, ions **PY1–PY4** (**PY5** was not experimentally accessible) display similar CID mass spectra. However, the isomers can be differentiated on the basis of the intensity ratios of the m/z 26 ($C_2H_2^{*+}$) and m/z 28 ($HCNH^+$) peaks, which result from high-energy CID dissociations. A comparison of the CID mass spectrum of Fig. 3.4c with the CID mass spectra of **PY1–PY4** of our previous study [3] indicates that the loss of C_2H_2 from **D1** yields ionized pyrimidine in admixture with its ylide isomer **PY2** in a 1 : 1 ratio. The analysis of the CID spectra allows the possibility that the co-generated distonic ion is **PY3** rather than **PY2** but in our quest of mechanistic proposals for the C_2H_2 loss we have not been able to find a plausible pathway for its generation.

The CID mass spectrum of the m/z 105 ions generated by loss of H^* is presented in Fig. 3.4d. Reference spectra are not available for this system of ions. However, the base peak in the spectrum at m/z 52 can readily be rationalized in terms of the structure proposed in Figure 3.6, *viz.* by invoking a simple bond cleavage into $CH=CHC\equiv N^+$ (m/z 52) + $CH_2=CHC\equiv N$. Further support for the structure assignment comes from exploratory calculations which confirm that the least energy demanding H^* loss from **D1** is that of a methylene hydrogen and the discussion of the mixed dimer ions **D1(Cl)** at the end of this section.

We now turn to a discussion of our mechanistic proposals using the energy diagram of Figure 3.6 as a guide.

3.2.5 Formation of pyrimidine via loss of C_2H_2 .

As discussed above, see Figure 3.2, the reaction between two acrylonitrile monomers can lead to a variety of possible dimers. The most stable direct chemically bonded dimer was found to be **D1** which enjoys a stabilization energy of 58 kcal mol^{-1} relative to **AN** + **ANN**.

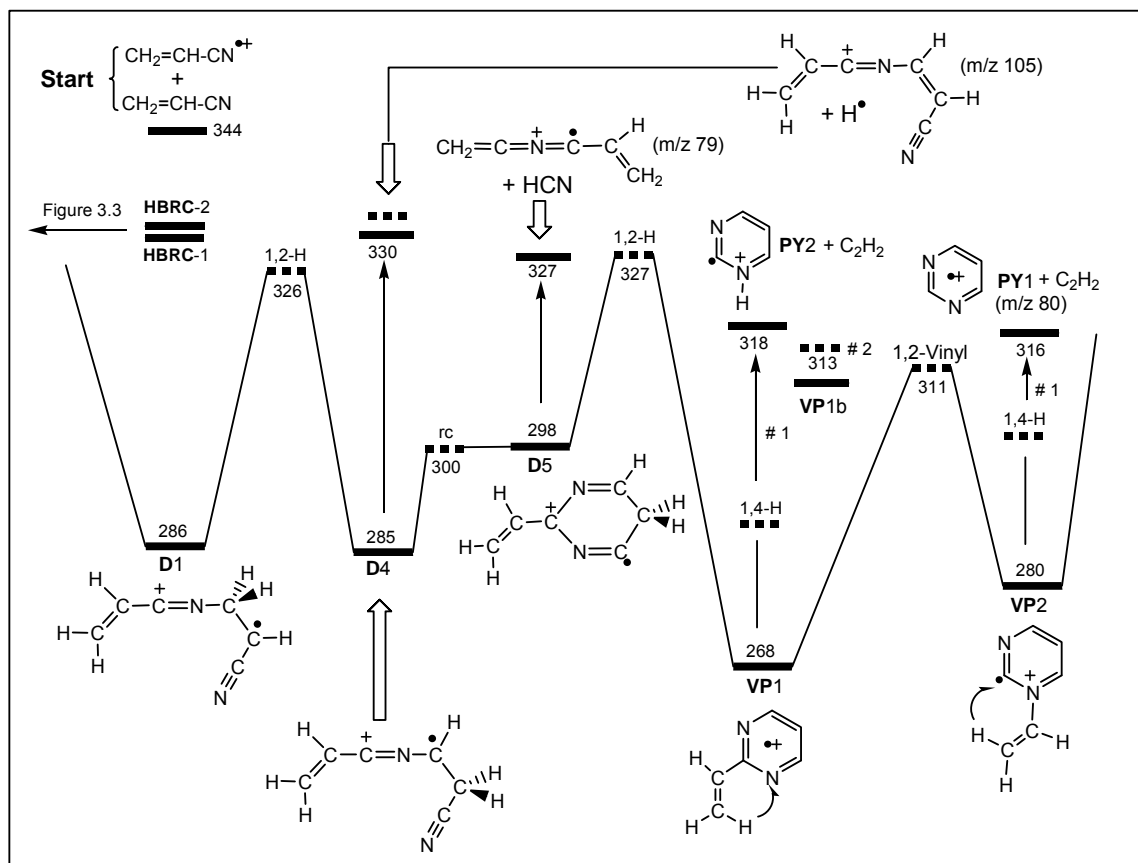


Figure 3.6 Energy diagram derived from CBS-QB3 298 K calculations (kcal mol⁻¹) describing the losses of C₂H₂, HCN and H from metastable acrylonitrile dimer ions **D1**. Note #1 : dissociation from **VP1a** and **VP2a**, see text; Note #2 : exchange vinyl H atoms via **VP1b**, see text.

A six membered ring with the N-C-N connectivity of pyrimidine may be envisaged to occur by ring closure of **D1** but such a species is not a minimum on the potential energy surface. In contrast, ions **D4** generated from a 1,2-H shift in **D1**, can readily lead to the desired ring closure. The fairly energy demanding 1,2-H shift for the transformation **D1** → **D4** (40 kcal mol⁻¹) allows the incipient ions **D4** to cyclize into **D5**. This ion can further rearrange by a 1,2-H shift into the 2-vinylpyrimidine radical cation, **VP1**, which may serve as the immediate precursor for the loss of C₂H₂, see Figure 3.6. Another route to the formation of **VP1** involves the facile ring closure of ions **D7** in Figure 3.5. However, the minimum energy requirement for the transformation **D1** → **D7**, lies at 336 kcal mol⁻¹,

some 10 kcal mol⁻¹ above the transformation **D1** → **D4**. Considering the energy requirements for the competing losses of H[•] and HCN, see Figure 3.6, we see that this transformation is not a viable option.

Ion **VP1** can readily lose C₂H₂ through a simple 1,4-H shift to **VP1a** to generate the distonic pyrimidine isomer **PY2** whose energy level lies at 318 kcal mol⁻¹. To generate the slightly more stable pyrimidine ion **PY1**, the 2-vinylpyrimidine ion **VP1** may first go through a 1,2-vinyl shift at 311 kcal mol⁻¹ (TS **VP1-VP2** in Figure 3.6). The resulting stable distonic isomer **VP2** may then dissociate into **PY1** + C₂H₂ via a low-lying 1,4-H shift analogous to the **VP1-VP1a** shift. Thus, the formation of both **PY1** and **PY2** is energetically possible since the activation energy for the 1,2-vinylidene shift turns out to be relatively small (43 kcal mol⁻¹). Our collision experiments show that the peak at *m/z* 80 in Fig. 3.1b indeed represents a mixture of isomers **PY1** and **PY2**. Note that the interconversion of **PY2** and **PY1** via a 1,2-H shift is not feasible: the activation energy for this isomerization is prohibitively high, 65 kcal mol⁻¹, as has been previously calculated by Lavorato et al. [3].

One further point deserves comment: following the proposal of Figure 3.6, the deuterated dimer ions generated from acrylonitrile-2-d, CH₂=CDC≡N, are expected to lose C₂HD. The *m/z* 81 peak in the inset of Fig. 3.1b, part of which originates from the loss HCN, shows that this is indeed the case. However, loss of C₂H₂ (*m/z* 82) is also observed, indicating that the vinyl hydrogens in ion **VP1** undergo exchange. Our calculations rationalize such an exchange via recurrent 1,2-H shifts between **VP1** and **VP1b** (see Figs. 3.6 and 3.7), with a TS at 313 kcal mol⁻¹.

3.2.6 Loss of H[•] and loss of HCN

Our computational analysis indicates that the loss of H[•] proceeds from **D1** or **D4**, yielding the *m/z* 105 ion structure depicted in Figure 3.6. The thermochemical threshold for these dissociation products lies at 330 kcal mol⁻¹ but this reaction was calculated to have a

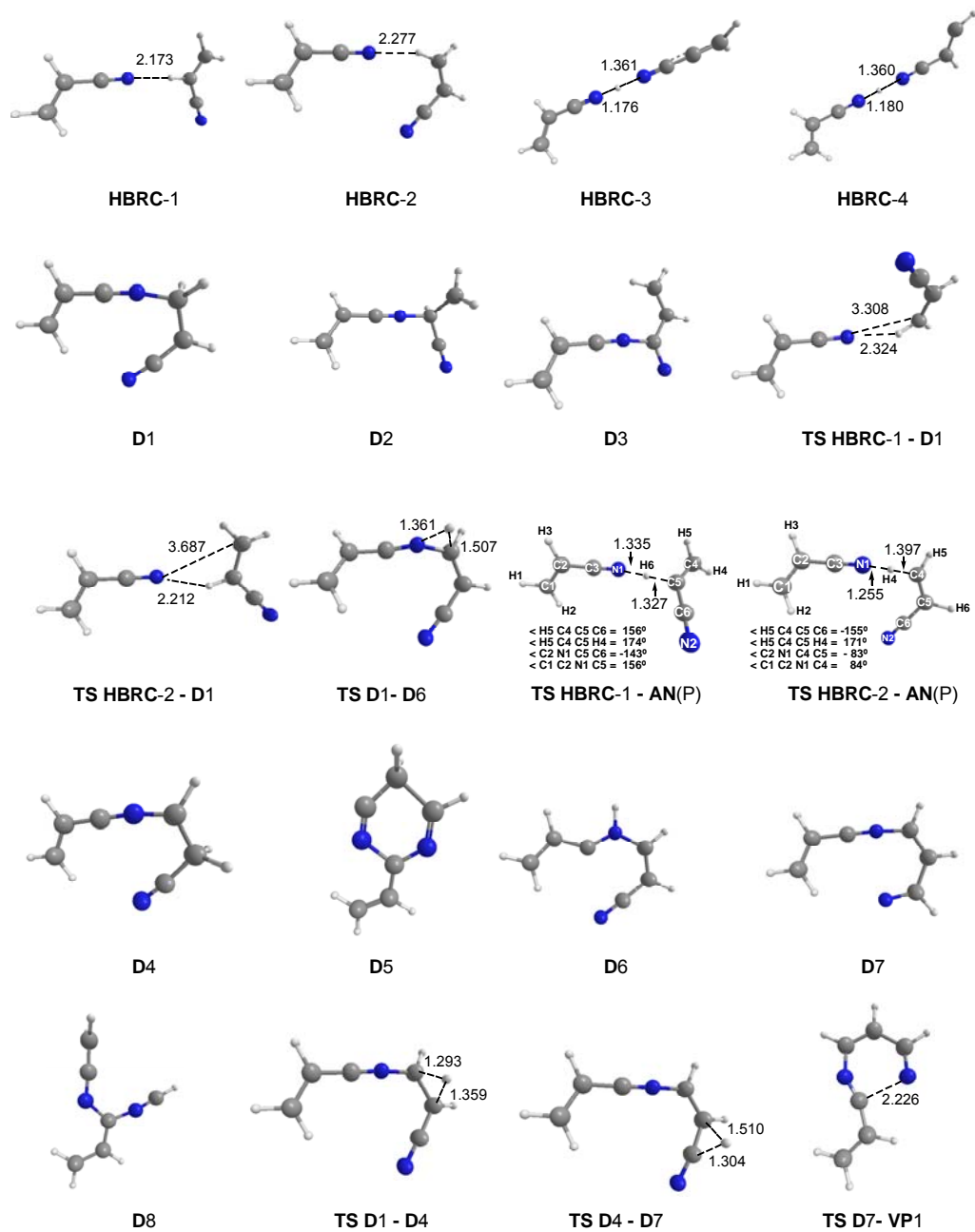


Figure 3.7 Selected optimized geometries (B3LYP/CBSB7 method) of stable intermediates and connecting transition states involved in the dissociation of low-energy acrylonitrile dimer radical cations.

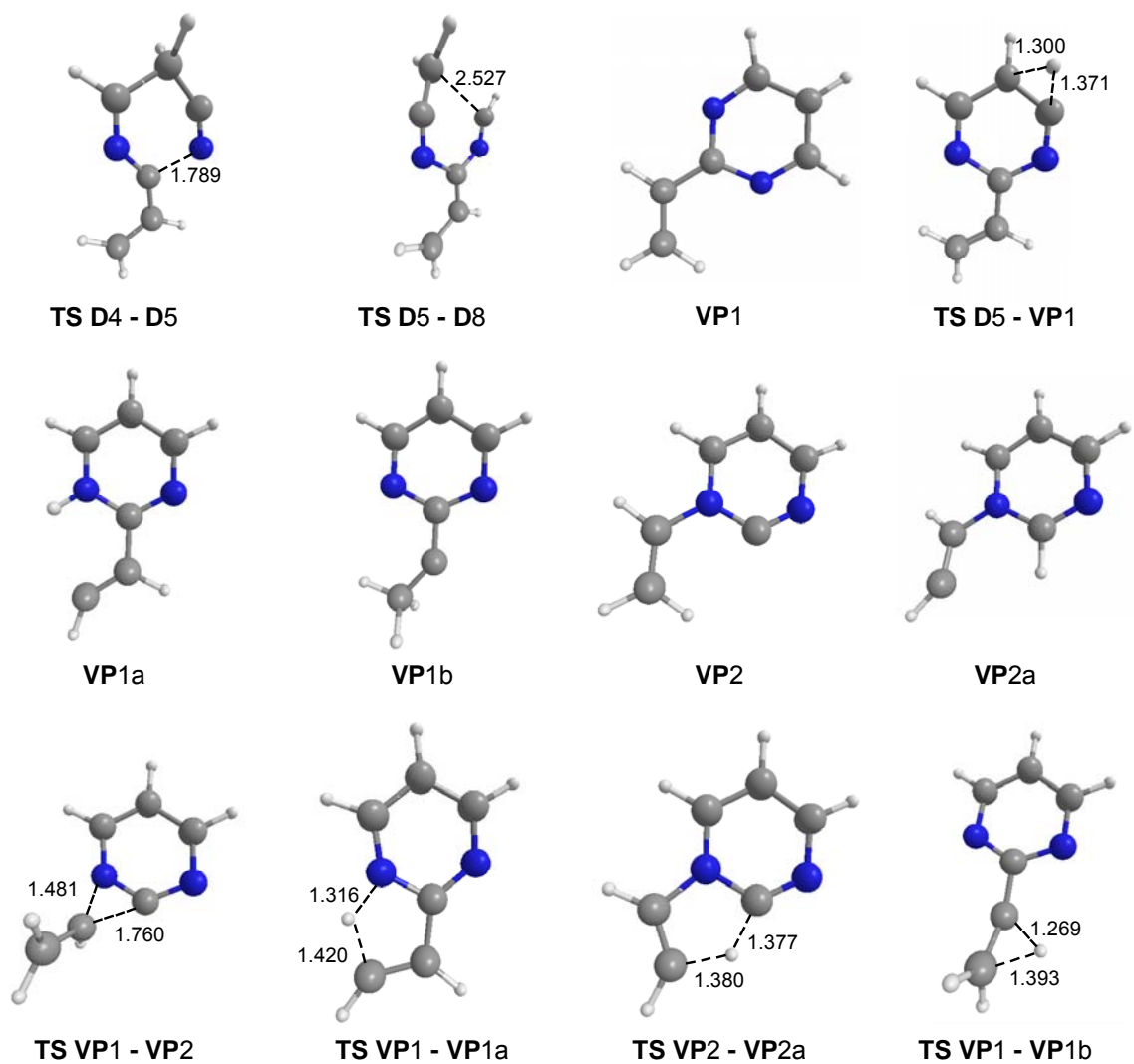


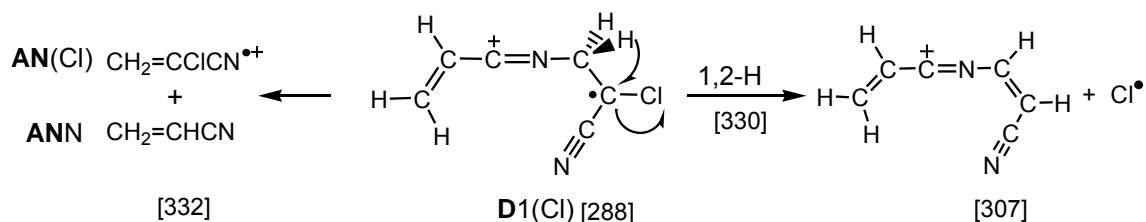
Figure 3.7 (Continued)

small reverse activation energy of 2 kcal mol⁻¹. Note that the TS **D5** → **VP1** at 327 kcal mol⁻¹ was found to be about 5 kcal mol⁻¹ lower in energy than the TS for this dissociation. The energetically most favourable path for the HCN loss involves ring-opening of **D5** (TS at 309 kcal mol⁻¹) to generate ion **D8** (structure shown in Fig. 3.7) at 308 kcal mol⁻¹. This

ion can lose HCN without a reverse barrier yielding the linear m/z 79 ion depicted in Figure 3.6. The energy requirement of this reaction is the same as that for the pyrimidine formation.

3.2.7 The mixed dimer ion of acrylonitrile and 2-chloroacrylonitrile

Further support for the mechanistic proposal of Figure 3.6 comes from a brief analysis of the dissociation behaviour of the dimer ion of acrylonitrile and 2-chloroacrylonitrile. The ionization energy of the chloro compound is lower than that of the parent nitrile (11.58 vs. 11.91 eV [11c]). Therefore, the chloro analogue of ion **D1** depicted in the Scheme below, **D1(Cl)**, is expected to be the principal species in this system of ions. The metastable dimer ions show only two reactions: (i) formation of $C_6H_5N_2^+$ ions (m/z 105) by loss of Cl^\bullet and (ii) formation of 2-chloroacrylonitrile ions (m/z 87) by loss of acrylonitrile. Loss of Cl^\bullet dominates the MI spectrum: the m/z 105 : m/z 87 peak intensity ratio is 4:1. However, this ratio reverses to 1:4 in the CID spectrum of the dimer ions and m/z 87 is now the base peak. To probe the structure of the m/z 105 product ions we obtained their CID mass spectrum and found it to be identical with that of the m/z 105 ions generated by loss of H^\bullet from ions **D1** in Figure 3.4d. These observations indicate that the Cl^\bullet loss is not a direct bond cleavage but rather occurs upon a 1,2-H shift in ions **D1(Cl)**, as depicted in Scheme 3.4.



Scheme 3.4

The product enthalpies for the two dissociation reactions presented in the Scheme (CBS-QB3 results Table 3.1) indicate that the two reactions can only compete if the 1,2-H shift barrier preceding the Cl' loss is sufficiently high. This is indeed the case: our B3LYP/CBSB7 calculations predict the barrier to lie at 330 kcal mol⁻¹ which allows the two processes to compete. However, once ions **D1(Cl)** have undergone the 1,2-H shift, immediate dissociation by loss of Cl' ensues because the reaction is strongly exothermic. This is not the case for the loss of H' from **D1**, which is slightly endothermic, see Figure 3.6. This would explain why ions **D1(Cl)** do not further rearrange to lose HCN and C₂H₂ whereas ions **D1** do.

Finally, we note that metastable ions **D1(Cl)** do not dissociate, via the chloro analogue of **HBRC-1**, into CH₂=CHC≡NH⁺ + [•]CH=C(Cl)C≡N although the energy requirement for this reaction, 329 kcal mol⁻¹, is 3 kcal mol⁻¹ lower than that for the back dissociation (Table 3.1). This is not really surprising considering that in this system too the self-protonation reaction is expected to involve reverse activation energy.

3.3 Summary

Our combined computational and experimental study shows that the interaction of an acrylonitrile ion with its neutral counterpart leads to hydrogen-bridged ion-dipole complexes which may undergo self-protonation (but not self-catalysis) or else isomerize into the very stable covalently bound species **D1** of Figure 3.6. **D1** ions act as the starting point configuration for the reactions that lead to the losses of H', HCN and C₂H₂.

The latter process involves a crucial cyclization step that ultimately yields ionized pyrimidine in admixture with its 2-ylide isomer. This process may be relevant in the context of the quest for the prebiotic pyrimidine molecule in astrochemistry. Neutralization of the isomeric ions by charge exchange with molecular targets in the keV translational energy regime yields pyrimidine and its 2-ylide as stable neutral species [3]. The 2-ylide does not convert into the more stable pyrimidine by an intramolecular 1,2-H shift [3] but this isomerization may readily occur by intermolecular interaction, e.g. with

H₃O⁺ on an icy surface. Such a surface could also promote electron-ion recombination followed by isomerization as has been proposed for the formation of acetic acid in space in a recent SIFT study [7b, 26].

The intriguing question of whether the ion-molecule reaction of acrylonitrile with HCN generates ionized pyrimidine via an analogous mechanism will be discussed in Chapter 6.

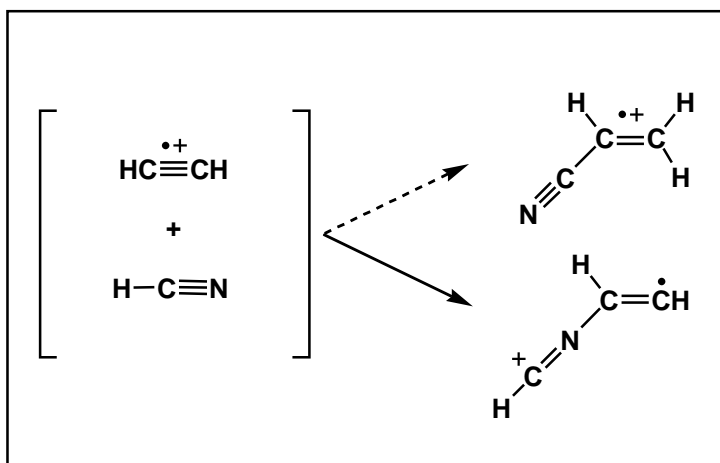
References

- [1] (a) M.A. Trikoupi, P.J.A. Ruttink, P.C. Burgers, J.K. Terlouw, *Int. J. Mass Spectrom.* 217 (2002) 97; (b) M.A. Trikoupi, P.J.A. Ruttink, P.C. Burgers, J.K. Terlouw, *Eur. J. Mass Spectrom.* 10 (2004) 801.
- [2] For selected recent references see : (a) G. van der Rest, P. Mourgues, H.E. Audier, *Int. J. Mass Spectrom.* 231 (2004) 83; (b) C.Y. Wong, P.J.A. Ruttink, P.C. Burgers, J.K. Terlouw, *Chem. Phys. Lett.* 390, (2004) 176; (*ibid*) 387 (2004) 204; (c) X. Wang, J.L. Holmes, *Can. J. Chem.* 83 (2005) 1903 ; (d) P.C. Burgers, P.J.A. Ruttink, *Int. J. Mass Spectrom.* 242 (2005) 49; (d) For an early review see : D.K. Böhme, *Int. J. Mass Spectrom.* 115 (1992) 95.
- [3] D. J. Lavorato, T.K. Dargel, W. Koch, G.A. McGibbon, H. Schwarz, J.K. Terlouw, *Int. J. Mass Spec.* 210/211 (2001) 43.
- [4] E. Herbst, *Chem. Soc. Rev.* 30 (2001) 168.
- [5] (a) F.F. Gardner, G. Winnewisser, *Astrophys. J.* 195 (1975) L127 ; H.E. Matthews, T.J. Sears, *The Astrophysical Journal* 272 (1983) 149 ; (c) F. Raulin, *Adv. Space Res.* 7 (1987) 71; (d) M. C. Pietrogrande, P. Coll, R. Sternberg, C. Szopa, R. Navarro-Gonzales, C. Vidal-Madjar, F. Dondi, *J. Chromatogr. A* 939 (2001) 69.
- [6] P.M. Woods, T.J. Millar, A.A. Zijlstra, E. Herbst, *Astrophys. J.* 574 (2002) L167.
- [7] (a) S. Petrie, D.K. Böhme, *Topics in Current Chemistry* 225 (2003) 37; (b) S. Petrie, D.K. Böhme, *Mass Spectrom. Rev.* 2006 (in press).
- [8] C.F. Chyba, P. J. Thomas, L. Brookshaw, C. Sagan, *Science* 249 (1990) 366.
- [9] Y.-J. Kuan, S.B. Charnley, H.-C. Huang, Z. Kisiel, P. Ehrenfreund, W.-L. Tseng, C.-H. Yan, *Advances in Space Research* 33 (2004) 31
- [10] (a) M.N. Simon, M. Simon, *Astrophys. J.* 184 (1973) 757 ; (b) Y.-J. Kuan, C.-H. Yan, S.B. Charnley, Z. Kisiel, P. Ehrenfreund, H.-C. Huang, *Royal Astro. Soc.* 345 (2003) 650; (c) Z. Peeters, O. Botta, S.B. Charnley, Z. Kisiel, Y.-J. Kuan, P. Ehrenfreund, *Astron. Astrophys.* 433 (2005) 583.
- [11] (a) *Handbook of Chemistry and Physics*. 87th Ed. Edited by David R. Lide. CRC Press, Boca Raton. 2006; (b) E.P.L. Hunter, S.G. Lias, *J. Phys. Chem. Ref. Data* 27 (1998) (3); (c) NIST Chemistry WebBook, July 2006, National Institute of Standards and Technology, Gaithersburg MD, 20899 (<http://webbook.nist.gov>); (d) Yu-Ran Luo. *Handbook of Dissociation Energies in Organic Compounds*. CRC Press, Boca Raton, 2003; (e) S.G. Lias, J.E. Bartmess, J.F. Liebman, J.L. Holmes, R.O. Levin, W.G. Maillard, *J. Phys. Chem. Ref. Data*, 17 (Suppl. 1) (1988).
- [12] T. Bally, G.N. Sastry, *J. Phys. Chem. A*, 101 (1997) 7923.
- [13] J.W. Gauld, L. Radom, *J. Am. Chem. Soc.*, 119 (1997) 9831.
- [14] P.C. Burgers, J.K. Terlouw in: N.M.M. Nibbering (Ed.), *Encyclopedia of Mass Spectrometry*, vol. 4, Elsevier, Amsterdam, 2005, p. 173.
- [15] M. Ichihashi, Y. Sadanaga, T. Kondow, *J. Chem. Phys. A* 102 (1998) 8287.
- [16] M. Meot-Ner, L.W. Sieck, *J. Am. Chem. Soc.* 113 (1991) 4448.

- [17] T. Baer and W.L. Hase in : Unimolecular Reaction Dynamics, Theory and Experiments, Oxford University Press, New York, 1996.
- [18] T. Baer, J.A. Booze in: W.L. Hase (Ed.), Advances in Classical Trajectory Methods, vol. 2, JAI Press Inc., Hampton Hill, 1994, p. 1-42.
- [25] D. J. Lavorato, J.K. Terlouw, G. A. McGibbon, T.K. Dargel, W. Koch, H. Schwarz, Int. J. Mass Spec. 179/180 (1998) 7.
- [26] G. Orlova, V. Blagojevic, D.K. Böhme, J. Phys. Chem. A (2006) in press.

Chapter 4

Does the ion-molecule reaction between $\text{HC}\equiv\text{CH}^{\bullet+}$ and HCN lead to $\text{CH}_2=\text{CH}-\text{C}\equiv\text{N}^{\bullet+}$? A computational and experimental study of the reverse process



The title ion-molecule reaction has been proposed to play an important role in interstellar chemistry if it yields acrylonitrile ions $\text{CH}_2=\text{CH}-\text{C}\equiv\text{N}^{\bullet+}$. This question was probed by examining the formation of $\text{HC}\equiv\text{CH}^{\bullet+}$ and HCN from low-energy ions $\text{CH}_2=\text{CH}-\text{C}\equiv\text{N}^{\bullet+}$ and related isomers, using tandem mass spectrometry based experiments (D and ^{13}C labelling) in conjunction with model chemistry calculations (CBS-QB3/APNO). We conclude that the title reaction is a barrierless multistep rearrangement that may not effectively compete with the straightforward formation of stable distonic ions $\text{HC}=\text{CH}-\text{N}=\text{CH}^+$ from $\text{HC}\equiv\text{CH}^{\bullet+}$ (ion)- HCN (dipole) encounter complexes.

The work described here has been published previously in an article under the same title : K.J. Jobst, S.A. Hasan, J.K. Terlouw, Chem. Phys. Lett. 450 (2008) 243 – 247.

4.1 Introduction

In SIFT experiments, the ion-molecule reaction of $\text{HC}\equiv\text{CH}^{*+}$ and HCN efficiently generates $\text{C}_3\text{H}_3\text{N}^{*+}$ ions [1,2]. Their structure has not been established, but it is argued in ref. 3 : “that, if under interstellar conditions, the corresponding radiative association between $\text{C}_2\text{H}_2^{*+}$ and HCN is fast and leads to the most stable $\text{C}_3\text{H}_3\text{N}^{*+}$ isomer $\text{CH}_2=\text{CH}-\text{C}\equiv\text{N}^{*+}$, then this reaction should be included in cloud chemistry models”.

This scenario underlines the accepted role of ion-molecule reactions in interstellar chemistry [4] and the use of mass spectrometry based techniques in studies of these reactions in a laboratory environment [5-7]. Even so, experimentalists face the ongoing challenge of simulating the low temperature and pressure conditions inherent in inter- and circum-stellar space.

One important question concerns the efficiency of radiative stabilization on which an accurate extrapolation of laboratory observations to genuine interstellar processes hinges [8-10]. In this context, we note that the radiative stabilization rate constant of encounter complexes of $\text{HC}\equiv\text{CH}^{*+}$ and HCN is not known but that the system satisfies the criteria for efficient radiative stabilization proposed by Herbst et al. [8].

Another non-trivial question concerns the structure (atom connectivity) of the stabilized $\text{C}_3\text{H}_3\text{N}^{*+}$ ions. The conjecture of ref. 3 that these ions are acrylonitrile ions $\text{CH}_2=\text{CH}-\text{C}\equiv\text{N}^{*+}$ (**AN**) seems reasonable: electron ionization studies of the nitrile have shown that low-energy ions **AN** dissociate into $\text{HC}\equiv\text{CH}^{*+}$ and HCN [11,12], albeit that H^+ loss is a major competitor. However, our recent study on the acrylonitrile dimer ion [12] also indicates that ions **AN** may have several isomers of comparable stability and dissociation characteristics, which could play a significant role in the association reaction.

In this communication we use a combined experimental and theoretical approach [7,13]: (i) to deduce the dissociation mechanisms of low energy ions **AN**; (ii) to characterize and identify its principal isomers; (iii) to propose $\text{C}_3\text{H}_3\text{N}^{*+}$ association product ion structure(s) founded upon our analysis of the reverse processes.

4.2 Results and discussion

4.2.1 The dissociation chemistry of ionized acrylonitrile

Low energy acrylonitrile ions (AN) lose HCN but also H[•]. Peaks at m/z 26 and m/z 52 are observed in the MI spectrum of Figure 4.1a, in a 1 : 20 ratio with associated kinetic energy releases (KERs) of 4 and 220 meV ($T_{0.5}$ values). These processes are also prominent when the ions are energized by collision, see the CID mass spectrum of Figure 4.1b. Appearance energy (AE) measurements of 13.13 eV and 13.82 eV for the formation of m/z 26 and m/z 52 ions have been reported [11]. The former value is consistent with the formation of $C_2H_2^{\bullet+} + HCN$ at the thermochemical threshold. The latter value signifies that loss of H[•] requires 16 kcal mol⁻¹ more energy than that of HCN. This is at odds with the calculations of Figure 4.2 and also the observed competition of the two reactions among metastable ions AN : two processes whose energy requirement differs by more than 10 kcal mol⁻¹, cannot compete in the metastable timeframe [13]. We therefore contend that the AE for loss of H[•] needs to be reexamined and that the energy requirement for both processes lies very close to the thermochemical threshold for formation of $C_2H_2^{\bullet+} + HCN$. Our model chemistry calculations, see Start A of Figure 4.2, indicate that two consecutive 1,2-H shifts, AN → AN-3 → AN-5, yield $C_2H_2^{\bullet+} + HCN$ at the thermochemical threshold. The relatively small kinetic energy release, $T_{0.5} = 4$ meV, associated with this process points to the involvement of ion-dipole complexes (IDC) as intermediates in the final step of the reaction [13,14]. These complexes are, on the basis of a simple ion-dipole interaction model, estimated to be stabilized by ~20 kcal mol⁻¹, relative to the combined enthalpies of the individual components, $C_2H_2^{\bullet+} + HCN$. Our calculations indicate that the IDCs are not minima on the potential energy surface but rearrange without a barrier into the remarkably stable distonic ion AN-4. A calculation with the N-C distance of the IDC [HCN---CH=CH]^{•+} fixed at 3 Å, yields a stabilization energy of 15 kcal mol⁻¹. Thus IDCs mediate the loss of HCN from AN-4 and also the reverse process, the association reaction $C_2H_2^{\bullet+} + HCN \rightarrow IDCs \rightarrow AN-4$.

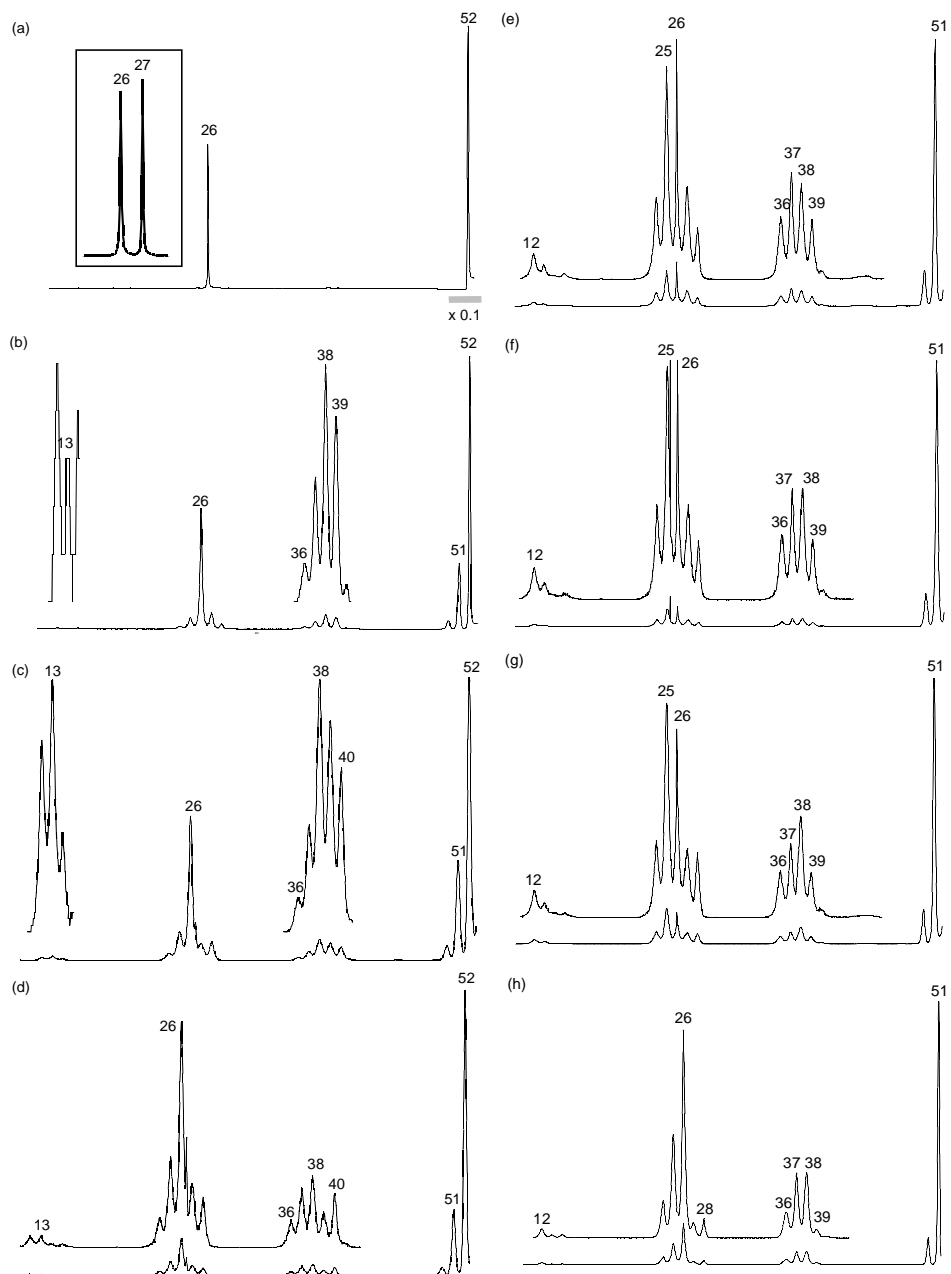


Figure 4.1 (a) MI and (b) CID spectra of m/z 53 acrylonitrile ions AN; the inset displays the partial MI spectrum of $\text{CH}_2=\text{CH}-^{13}\text{C}\equiv\text{N}$ (c) CID spectrum of AN-4, generated by HCN loss from pyrazine ylids; (d) CID spectrum of AN-2, generated by HCN loss from metastable pyridazine ylid-ions; (e-f) CID spectra of m/z 52 ions $\text{HC}=\text{C}=\text{C}=\text{NH}^+$ generated from metastable ions AN and AN-4 respectively; (g) CID spectrum of ions $\text{HC}\equiv\text{C}-\text{N}=\text{CH}^+$ generated from collisionally energized ions AN-4; (h) CID spectrum of ions $\text{CH}_2=\text{C}-\text{C}\equiv\text{N}^+$ generated by dissociative ionization of 2-bromoacrylonitrile.

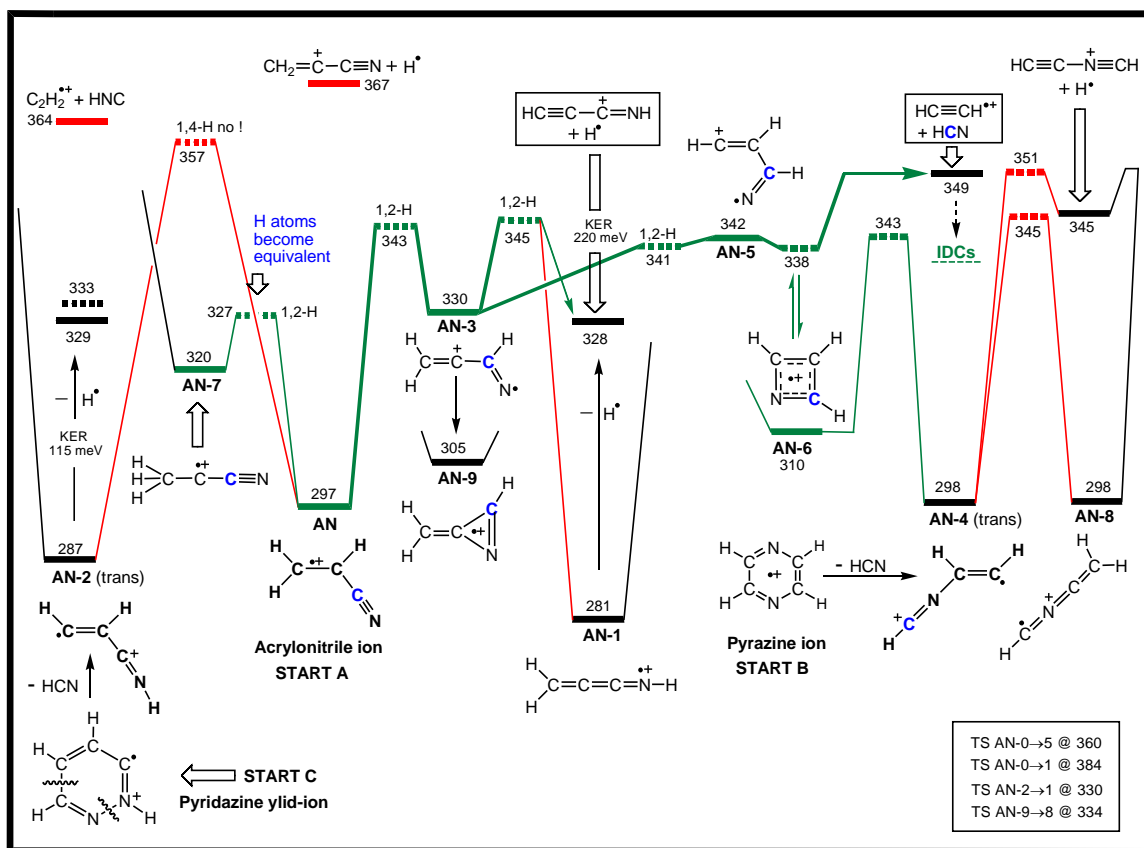


Figure 4.2 Dissociation pathways leading to the loss of HCN and H[•] from acrylonitrile ions (Start A) and two of its principal isomers AN-2 (Start B) and AN-4 (Start C). Energy diagram (kcal mol⁻¹) based on CBS-APNO calculations.

The H[•] loss also proceeds via two consecutive 1,2-H shifts, AN → AN-3 → AN-1, to yield the C₃H₂N⁺ isomer of lowest energy HC≡C-C=NH⁺. The enthalpies of the three lowest energy C₃H₂N⁺ isomers are given in Table 4.1. In contrast to the HCN loss, the final step of the H[•] loss reaction has a reverse barrier that lies 17 kcal mol⁻¹ above the thermochemical threshold. That the resulting product ions are generated with excess internal energies is in line with the substantial KER, T_{0.5} = 220 meV, associated with the reaction.

Table 4.1 Enthalpies of formation (kcal mol⁻¹) and total energies (Hartree) derived from CBS-QB3 and CBS-APNO calculations [a]

Isomer	CBS-QB3 E(total) [0K]	QB3 $\Delta_f H_{298}^0$	APNO $\Delta_f H_{298}^0$	Transition State	CBS-QB3 E(total) [0K]	QB3 $\Delta_f H_{298}^0$	APNO $\Delta_f H_{298}^0$
AN	-170.133508	298	297	AN → AN-1	-169.994327	385	384
AN-1	-170.160585	281	281	AN → AN-2	-170.036983	358	357
AN-2 (trans)	-170.149958	288	287	AN → AN-3	-170.060908	344	343
AN-2 (cis)	-170.148378	289	288	AN → AN-5	-170.037224	361	360
AN-3	-170.082454	330	330	AN → AN-7	-170.084198	329	327
AN-4 (trans)	-170.131721	299	298	AN-1 → AN-2	-170.082185	330	330
AN-4 (cis)	-170.129752	300	299	AN-1 → AN-3	-170.058624	345	345
AN-5	-170.066956	340	342	AN-3 → AN-5	-170.071795	337	341
AN-6	-170.112683	311	310	AN-4 → AN-6	-170.061040	343	343
AN-7	-170.096029	321	320	AN-4 → AN-8	-170.052675	349	345
AN-8	-170.134246	297	298	AN-5 → AN-6	-170.068021	339	338
AN-9	-170.134246	307	305	AN-8 → AN-9	-170.074585	335	334
AN-10	-170.119324	311	309	AN-2 → AN-10	-170.076360	337	335
HC=C=C=NH ⁺	-169.58629	277	276				
HC≡C-N=CH ⁺	-169.55720	295	293	AN2 → <i>m/z</i> 52	-170.07686	334	333
CH ₂ =C-C≡N ⁺	-169.52354	316	315	AN4 → <i>m/z</i> 52	-170.04713	352	351

[a] The CBS-QB3 and APNO values for $\Sigma \Delta_f H_{298}^0$ [C₂H₂⁺⁺ + HCN] are 350 and 349 kcal mol⁻¹ respectively; the experimental value taken from Ref. 17 is 350 kcal mol⁻¹. For AN Ref. 17 gives 296 kcal mol⁻¹.

A direct conversion of ions **AN** into **AN-1** and **AN-5**, which serve as the reacting configurations for the two dissociations, is not feasible. The associated 1,3-H shifts are very energy demanding because they require substantial changes in orbital hybridization.

4.2.2 Analysis of CH₂=CD-C≡N⁺, CD₂=CH-C≡N⁺, and CH₂=CH-¹³C≡N⁺

The isotopologues CH₂=CD-C≡N⁺ and CD₂=CH-C≡N⁺ lose HCN and DCN in ratios (1.7 and 0.5 respectively) that approach the statistical limit for loss of positional identity. Facile 1,2-H shifts between **AN** and **AN-7** via a low-lying transition state as predicted by Figure 4.2, and a small secondary intramolecular kinetic isotope effect [15] of 0.85, provide a rationale for the observed ratios. A similar scenario may obtain for the losses of H[•] and D[•] where the observed ratios (3.6 and 0.6 respectively) signify a preference for loss

of H^\bullet . This could be ascribed to a primary intramolecular kinetic isotope effect in the final step of the reaction, bond cleavage of transient ions **AN-1**, see Fig. 4.2.

(The ratios for (H + D) vs (HCN + DCN) loss from $\text{CH}_2=\text{CH}-\text{C}\equiv\text{N}^{\bullet+}$, $\text{CH}_2=\text{CD}-\text{C}\equiv\text{N}^{\bullet+}$ and $\text{CD}_2=\text{CH}-\text{C}\equiv\text{N}^{\bullet+}$ (19, 10 and 4) show that there is an intermolecular kinetic isotope effect as well.)

The isotopologue $\text{CH}_2=\text{CH}-^{13}\text{C}\equiv\text{N}^{\bullet+}$ loses HCN and H^{13}CN with equal probability, see inset of Fig. 4.1a. This observation supports the proposal of Fig. 4.2 that ions **AN-5** communicate with the 4-membered ring species **AN-6** prior to dissociation. Note that the transition state leading to **AN-6** at $343 \text{ kcal mol}^{-1}$ lies well below the threshold for dissociation into $\text{C}_2\text{H}_2^{\bullet+} + \text{HCN}$.

4.2.3 The dissociation characteristics of related $\text{C}_3\text{H}_3\text{N}^+$ isomers

Loss of HCN from the pyrazine ion and the ylid-ion of pyridazine, see Start B and C in Fig. 4.2, yields $\text{C}_3\text{H}_3\text{N}^+$ ions whose high energy CID mass spectra are shown in Figs. 4.1c and 4.1d respectively. The spectra show a structure diagnostic peak at m/z 40 (loss of CH) which is negligible in that of **AN**, supporting our proposal that ions **AN-4** ($\text{HC}=\text{CH}-\text{N}=\text{CH}^{\bullet+}$) and **AN-2** ($\text{HC}=\text{CH}-\text{C}=\text{NH}^{\bullet+}$) are generated in the above reactions. We note that the m/z 26 peak is more prominent in the spectrum of **AN-4** than that of **AN-2**, reflecting the higher stability of HCN relative to HNC.

The energy diagram of Fig. 4.2 also indicates that (meta)stable ions **AN-2** do not communicate with either **AN** or **AN-1** because the connecting H-shifts are too energy demanding. This is also true for the 1,2-H shift that connects **AN-2** with $\text{HC}\equiv\text{C}-\text{C}(\text{H})=\text{NH}^{\bullet+}$ (**AN-10**), which plays no role in **AN**'s dissociation chemistry. Instead, ions **AN-2** undergo loss of H^\bullet , which dominates the MI and CID mass spectra. Also, the KER for H^\bullet loss is significantly lower than that from **AN** or **AN-4**: $T_{0.5} = 115$ vs 220 meV .

Fig. 4.2 further indicates that ions **AN-4** can communicate with **AN**, but only at internal energies close to the threshold for dissociation. Indeed, metastable ions **AN-4** lose H^\bullet and HCN in a 12 : 1 ratio with the same KERs as measured for **AN**. We also note that the CID

mass spectra of the m/z 52 ions generated by loss of H^\bullet from **AN** and **AN-4**, are closely similar, compare Figures 4.1e/f. These observations indicate that **AN** and **AN-4** yield the same product ion via a common rate-determining transition state.

In line with the critical computational analysis of Takagi et al. [16], **AN-4** loses H^\bullet via the pathway **AN-4** \rightarrow **AN-6** \rightarrow **AN-5** \rightarrow **AN-3** \rightarrow **AN-1** \rightarrow $HC\equiv C-C=NH^+ + H^\bullet$. A direct bond cleavage leading to $HC\equiv C-N\equiv CH^+$ is unlikely: this reaction has a reverse barrier, which is 4 kcal mol⁻¹ higher in energy than the proposed rearrangement reaction. Upon collisional excitation, the $HC\equiv C-N\equiv CH^+$ ion may well be (co)generated: see Fig. 4.1g whose m/z 37 peak (characteristic of NH loss from $HC\equiv C-C=NH^+$) is lower than that of Figures 4.1e/f.

The isomer $CH_2=C-C\equiv N^+$ was also considered as a product ion for loss of H^\bullet , but theory predicts it to be too high in energy to play a role. Indeed, $CH_2=C-C\equiv N^+$ ions generated by Br^\bullet loss from $CH_2=CBr-C\equiv N^+$, display a distinct CID mass spectrum, see Figure 4.1h, in which loss of CH (m/z 39) is almost absent.

4.3 Conclusions

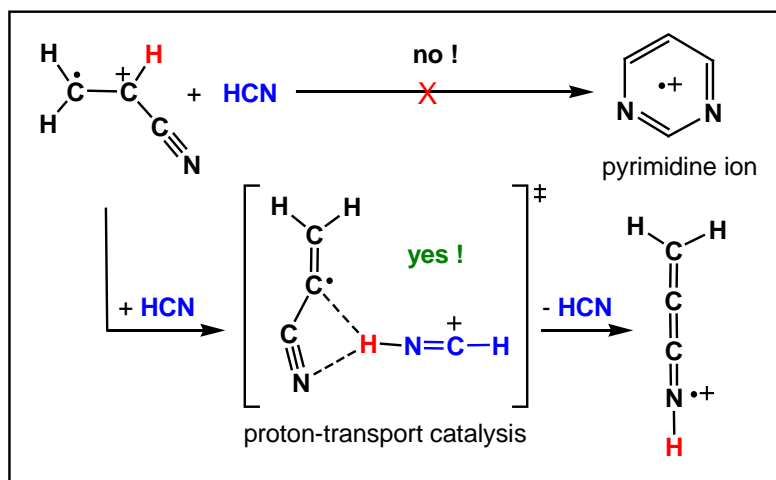
Ionized acrylonitrile (**AN**) dissociates into $HC\equiv CH^{*+}$ and HCN at the thermochemical threshold, via a complex rearrangement whose final step involves the participation of ion-dipole complexes. The association of $HC\equiv CH^{*+}$ and HCN into **AN** therefore involves a barrierless albeit circuitous route. The association reaction could also yield **AN**'s distonic isomer $HC=CH-N=CH^{*+}$ (**AN-4**), by a one step bond forming reaction in ($HC\equiv CH^{*+}$)ion-(HCN)dipole encounter complexes. This newly characterized ion also occupies a deep potential well, thereby satisfying the criteria for an efficient radiative stabilization [8] in encounter complexes between $C_2H_2^{*+} + HCN$. This scenario implies that distonic ions **AN-4** rather than ions **AN** could be preferentially formed in radiative (and termolecular) association processes of ionized acetylene and HCN.

References

- [1] H.I. Schiff, D.K. Bohme, *Astrophys. J.*, 232 (1979) 640.
- [2] J.S. Knight, C.G. Freeman, M.J. McEwan, S.C. Smith, N.G. Adams, D. Smith, *Mon. Not. R. Astr. Soc.* 219 (1986) 89.
- [3] S. Petrie, C.G. Freeman, M.J. McEwan. *Mon. Not. R. Astr. Soc.* 257 (1992) 438.
- [4] D.K. Bohme, S. Petrie, *Mass Spectrom. Rev.*, 26 (2007) 258.
- [5] S. Petrie, D.K. Bohme, *Top. Curr. Chem.* 225 (2003) 37.
- [6] D. Gerlich, M. Smith, *Phys. Scr.* 73 (2006) C25.
- [7] A. Horn, H. Møllendal, O. Sekiguchi, E. Uggerud, H. Roberts, E. Herbst, A.A. Viggiano, T.D. Fridgen, *Astrophys. J.*, 611 (2004) 605.
- [8] E. Herbst, M.J. McEwan, *Astron. Astrophys.* 229 (1990) 201.
- [9] S.J. Klippenstein, Y. Yang, V. Ryzhov, R.C. Dunbar, *J. Chem. Phys.* 104 (1996) 4502.
- [10] V. Ryzhov, R.C. Dunbar, *Int. J. Mass Spectrom.*, 167/168 (1997) 627.
- [11] J. Momigny, J. Urbain, H. Wankenne, *Bull. Soc. Roy. Sci. Liege*, 34 (1965) 337.
- [12] H.K. Ervasti, K. J. Jobst, P.C. Burgers, P.J.A. Ruttink, J.K. Terlouw, *Int. J. Mass Spectrom.* 262 (2007) 88.
- [13] J.L. Holmes, C. Aubry, P.M. Mayer. *Assigning Structures to Ions in Mass Spectrometry*. CRC Press, Boca Raton, 2007.
- [14] J.L. Holmes, J.K. Terlouw, in : N.M.M. Nibbering (Ed.), *Encyclopedia of Mass Spectrometry*, vol. 4, Elsevier, Amsterdam, 2005, p. 287.
- [15] C. Dass, in: N.M.M. Nibbering (Ed.), *Encyclopedia of Mass Spectrometry*, vol. 4, Elsevier, Amsterdam, 2005, p. 39.
- [16] N. Takagi, K. Fukuzawa, Y. Osamura, H.F. Schaefer III. *The Astrophysical Journal.* 525 (1999) 791.
- [17] S.G. Lias, J.E. Bartmess, J.F. Liebman, J.L. Holmes, R.O. Levin, W.G. Maillard, *J. Phys. Chem. Ref. Data* 17 (Suppl. 1) (1988).

Chapter 5

The reaction of the acrylonitrile ion $\text{CH}_2=\text{CH}-\text{C}\equiv\text{N}^{\bullet+}$ with HCN :
Proton-transport catalysis vs formation of ionized pyrimidine



The CBS-QB3 model chemistry predicts that the title ion-molecule reaction, of potential interest in astrochemistry, yields a stable head-to-tail dimer, $[\text{HC}=\text{N}-\text{CH}_2\text{C}(\text{H})\text{C}\equiv\text{N}]^{\bullet+}$ (**D1**). Cyclization of **D1** into ionized pyrimidine seems possible, but the initiating 1,2-H shift is close in energy to back-dissociation into $\text{CH}_2=\text{C}(\text{H})\text{CN}^{\bullet+}$ (**AN**) + HCN. Less energy demanding is formation of the H-bridged isomers $[\text{CH}_2=\text{C}(\text{CN})\text{H}--\text{N}\equiv\text{CH}]^{\bullet+}$ and $[\text{HC}\equiv\text{N}--\text{HC}(\text{H})=\text{C}(\text{H})\text{CN}]^{\bullet+}$, whose HCN component may catalyze isomerization of **AN** into $\text{CH}_2=\text{C}=\text{C}=\text{NH}^{\bullet+}$ (**AN1**) and $\text{CH}=\text{C}(\text{H})\text{C}=\text{NH}^{\bullet+}$ (**AN2**) respectively. Tandem mass spectrometry based experiments using $^{15}\text{N}/^{13}\text{C}$ labelling show that cyclization of **D1** does not occur and that **AN1** is the predominant reaction product instead.

The work described here has been published previously in an article under the same title :
K.J. Jobst, S.A. Hasan, J.K. Terlouw, Chem. Phys. Lett. 482 (2009) 211 – 216.

5.1 Introduction

Ion-molecule interactions in the rarefied gas-phase have proven to be a good way to rationalize various reactions of relevance to astrochemistry that are not possible between neutral molecules [1,2]. Such interactions can lead to (de-)protonation [3], isomerization by Proton-Transport Catalysis (PTC) [4-7], and the formation of new product molecules via covalently bonded reaction intermediates.

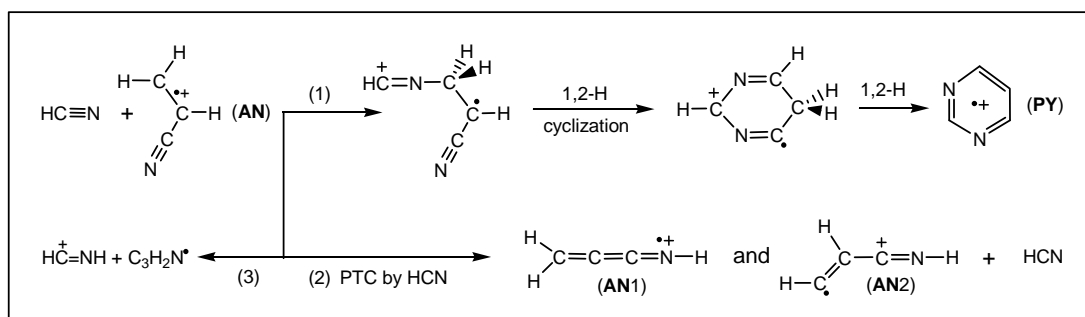
A case in point is our previous study on the reaction of the acrylonitrile ion $\text{CH}_2=\text{CHC}\equiv\text{N}^{+\bullet}$ (AN) with its neutral counterpart [8], a confirmed species in interstellar dust clouds [2]. The resulting dimer ion dissociates by proton transfer, but it can also rearrange to yield the pyrimidine ion (PY) by loss of C_2H_2 . Selected Ion Flow Tube (SIFT) experiments by Petrie et al. [9] and Milligan et al. [10] indicate that the dimer formation takes place at close to the collision rate, which implies that its dissociation into PY could be relevant to astrochemistry. The prebiotic pyrimidine molecule could also be formed from neutral acrylonitrile and HCN but so far there is no experimental or computational to support this suggestion [11].

An *a priori* more attractive possibility for the gas-phase synthesis of (ionized) pyrimidine involves the reaction of the acrylonitrile *ion* (AN) with HCN. This reaction has also been studied in Ref. 9., which reports that it results mainly in adduct formation with varying degrees of H loss. The reaction is evidently exothermic in view of the number of product channels, yet it occurs at only 6 % of the collision rate. The authors argue that such a behaviour indicates that the adduct $\text{C}_4\text{H}_4\text{N}_2^{+\bullet}$ does not correspond to a deep well in the AN/HCN potential energy surface, a deduction which would remove the pyrimidine ion and its cyclic isomers from contention as possible product ions.

The contention that AN/HCN adduct ions would not occupy a deep potential well, whereas the AN/ $\text{CH}_2=\text{CHC}\equiv\text{N}$ complexes studied in Ref. 8 do, prompted us to use computational chemistry and complementary experiments to probe the dissociation chemistry of AN/HCN complexes generated by the ion-molecule reaction of $\text{CH}_2=\text{CHC}\equiv\text{N}^{+\bullet}$ with HCN.

The gas-phase synthesis of the pyrimidine ion from AN and HCN explored in this study is the analogue of the mechanism proposed in Ref. 8 for the reaction of AN with its neutral counterpart. As depicted by Reaction 1 of Scheme 5.1, AN forms a covalently bound head-to-tail dimer with HCN and then proceeds to ring closure and a 1,2-H shift to form the pyrimidine ion.

We have also examined potentially competing reactions, *viz.* the HCN catalyzed isomerization of AN and protonation of HCN by AN, shown as Reactions 2 and 3 of Scheme 5.1.



Scheme 5.1

All three reactions appear to be energetically possible but RRKM-based reaction-rate constant calculations [12] indicate that Reaction 1 cannot effectively compete with the HCN catalyzed isomerization(s) of Reaction 2. Indeed, our experiments with the isotopically labeled compounds H¹³CN and AN(¹⁵N) indicate that the adduct ions do not cyclize into the pyrimidine ion. Instead, it will be shown that HCN catalyzes the transformation of CH₂=CHC≡N⁺ (AN) into CH₂=C=C=N⁺ (AN1).

5.2 Results and discussion

5.2.1 Formation of the pyrimidine ion from the ion-molecule reaction AN + HCN

In our discussion of pyrimidine ion (PY) formation from AN + HCN, the potential energy diagram of Fig. 5.1 will serve as a guide. The right-hand side of the Figure (START A),

which describes the dissociation of **PY** by loss of HCN, will be examined first because it has been studied in considerable detail [14,15].

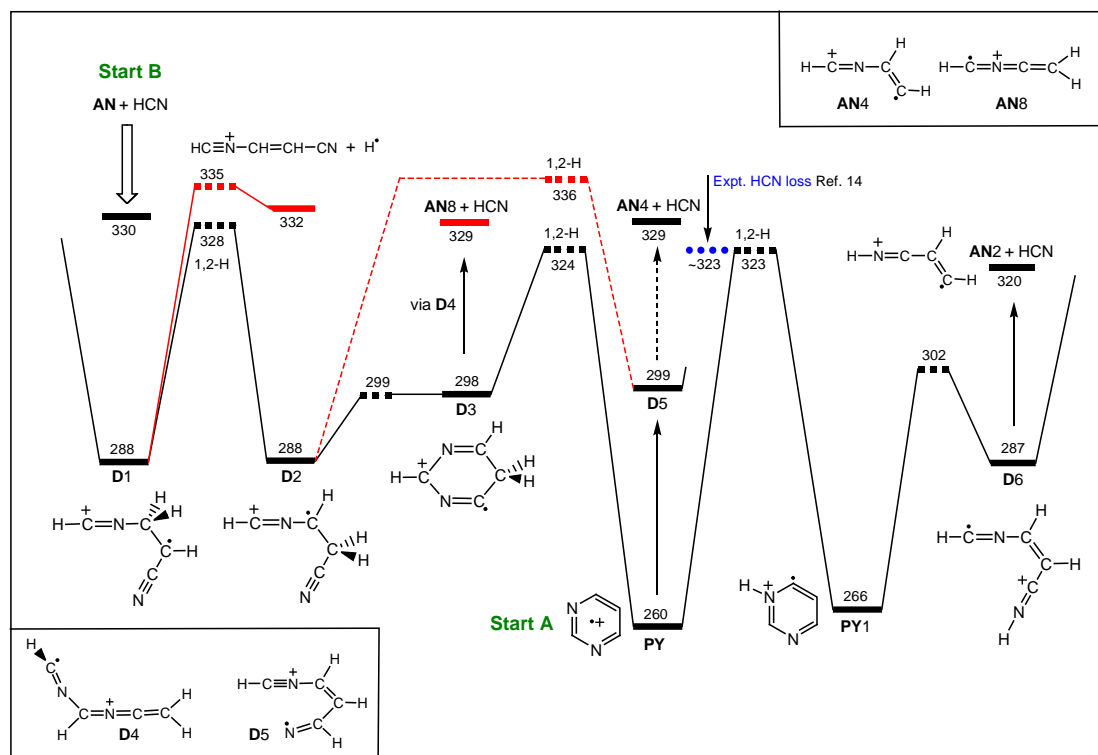


Figure 5.1 The mechanistic proposal for the formation of ionized pyrimidine in the ion-molecule reaction of HCN and ionized acrylonitrile (AN).

The PEPICO study of Ref. 14 shows that $\text{PY} \rightarrow \text{C}_3\text{H}_3\text{N}^{++} + \text{HCN}$ is the reaction of lowest energy requirement with a threshold at $\sim 323 \text{ kcal mol}^{-1}$. A subsequent detailed study [15] of **PY** and several of its 1,2-H shift isomers including **PY1** of Fig. 5.1, concludes that the $\text{C}_3\text{H}_3\text{N}^{++}$ product ion is not AN, but perhaps the keteneimine isomer $\text{CH}_2=\text{C}=\text{C}=\text{NH}^{++}$ (**AN1**). This conclusion was based on a comparative analysis of the high-energy CID mass spectra of the $\text{C}_3\text{H}_3\text{N}^{++}$ ions generated from **PY** and **PY1** with that of AN. Indeed, the spectrum of AN, see Fig. 5.2c, is clearly different from the similar but not identical spectra of **PY** and **PY1**, see Figs. 5.2a/b. Our recent theoretical and experimental study of AN and its principal isomers AN1 – AN8 [16] sheds more light on the structure assignment of the

spectra of Fig. 5.2a and 5.2b. The spectrum of Fig. 5.3b appears to be superimposable upon that of the reference spectrum of $\text{HC}=\text{C}(\text{H})-\text{C}=\text{NH}^{++}$ (**AN2**), while that of Fig. 5.2a appears to be compatible with the formation of **AN2** in admixture with $\text{HC}=\text{C}(\text{H})-\text{N}=\text{CH}^{++}$ (**AN4**).

The reference spectrum of **AN4** [16] is close to that of **AN2** but its m/z 26 peak is more pronounced, in line with the energetically more favourable loss of HCN vis-à-vis that of HNC from **AN2**. The study of Ref. 16 also discusses **AN1**, which occupies a deep potential well and represents the global minimum on the $\text{C}_3\text{H}_3\text{N}^{++}$ PES. Upon CID, **AN1** is expected to dissociate primarily by loss of H^{\bullet} , like its distonic isomer **AN2**. A reference spectrum of pure ions **AN1** is not available, but the m/z 40 peak for loss of CH in the structure diagnostic cluster of ions at m/z 36 – 40 is expected to be insignificant in the spectrum of **AN1** [16]. This expectation is supported by the CID spectra (not shown) of the collision induced loss of H^{\bullet} from $\text{CH}_2=\text{C}(\text{H})\text{C}=\text{NH}^+$ and loss of D^{\bullet} from $\text{CH}_2=\text{C}(\text{D})\text{C}=\text{ND}^+$.

The proposed formation of **AN2** and **AN4** from **PY** is corroborated by the computations of Fig. 5.1. Dissociation into **AN2** + HCN occurs via a three-step reaction, whose energy requirement equals the threshold of Ref. 14. The first step involves a 1,2-H shift in **PY**, whose TS lies at $323 \text{ kcal mol}^{-1}$, to generate **PY1**. A relatively facile ring opening thereof leads to ion **D6**, which can then dissociate into **AN2** + HCN. Fig. 5.1 shows that the proposed co-generation of **AN4** from low-energy (metastable) ions **PY** is also feasible : the ring-opening $\text{PY} \rightarrow \text{D5}$ has a relatively low energy requirement and the subsequent direct bond cleavage $\text{D5} \rightarrow \text{AN4} + \text{HCN}$ is a mere 6 kcal mol^{-1} higher in energy than the **AN2** formation. That metastable ions **PY1** generate **AN2** as the sole $\text{C}_3\text{H}_3\text{N}^{++}$ reaction product is because the isomerization $\text{PY1} \rightarrow \text{PY}$ is more energy demanding than the direct dissociation $\text{PY1} \rightarrow \text{D6} \rightarrow \text{AN2} + \text{HCN}$. This scenario is consistent with the observation of Ref. 15 that the kinetic energy release [13] associated with the HCN loss from **PY1** is lower than that from **PY** (13 vs 32 meV). Finally we note that it is unlikely that the circuitous dissociation route $\text{PY} \rightarrow \text{D3} \rightarrow \text{D4} \rightarrow \text{CH}_2=\text{C}=\text{N}=\text{CH}^{++}$ (**AN8**) can compete with the direct bond cleavage $\text{PY} \rightarrow \text{D5} \rightarrow \text{AN4}$.

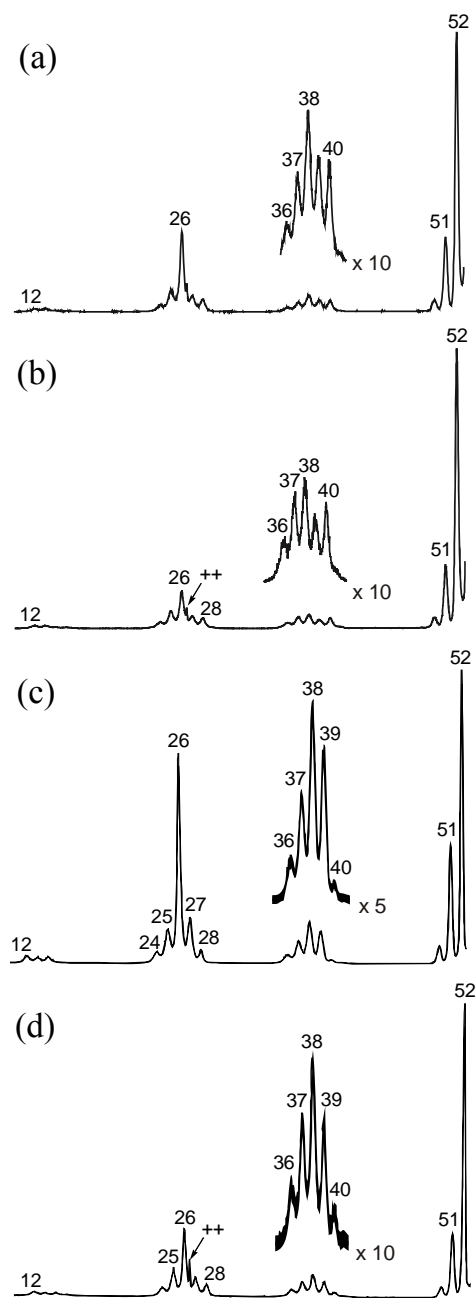


Figure 5.2 CID mass spectra of the C_3H_3N ions generated from : (a) low-energy (metastable) pyrimidine (PY) and (b) pyrimidine-4-ylid (PY1) ions; (c) ionized acrylonitrile (AN) and (d) the ion-molecule reaction AN + HCN.

We now turn to the computational analysis of the formation of **PY** from **AN** + **HCN** as depicted in Fig. 5.1 (START B). Theory predicts that the associative ion-molecule reaction leads to the stable covalently bound adduct ion **D1**, whose high stabilization energy is at par with that of the **AN** dimer [8]. **D1** can isomerize into ion **D2**, via a 1,2-H shift that lies just below the combined enthalpies of **AN** + **HCN**, but the subsequent 1,2-H shift that would yield the ring-opened pyrimidine ion **D5** is associated with a prohibitively high barrier. Instead, ions **D2** may undergo a facile ring closure to form ion **D3**, in which a 1,2 H shift at $324 \text{ kcal mol}^{-1}$ completes the transformation of **D2** into **PY**. Thus the theory of Fig. 5.1 suggests that the gas-phase synthesis of **PY** via the route **D1** \rightarrow **D2** \rightarrow **D3** \rightarrow **PY** is energetically possible because the energy requirements of the direct bond cleavage dissociations available to **D1**, back-dissociation into **AN** + **HCN** and loss of H^{\bullet} as depicted in Fig. 5.1, are slightly higher. Also, loss of **HCN** from **D3** may not favourably compete with the transformation **D3** \rightarrow **PY**.

This prompted us to perform chemical ionization experiments with a mixture of $\text{CH}_2=\text{C}(\text{H})\text{CN}$ and **HCN** using CO_2 as the bath gas. Fig. 5.3a shows a typical CI mass spectrum, which displays a great many peaks, including acrylonitrile dimer ions at m/z 106 and, less prominently, the desired acrylonitrile/**HCN** ions at m/z 80. The MI mass spectrum of the m/z 80 ions only shows a peak at m/z 53, which also dominates the CID spectrum. Thus, loss of **HCN** is the prevailing dissociation but, see Fig. 5.1, this only allows us to differentiate between **D1** and **PY** (or a mixture thereof) if the structure(s) of the resulting m/z 53 ions can be established by a double collision experiment. Unfortunately, insufficient signal intensity prevented this analysis. Instead, we replaced the **HCN** of the above CI experiment by H^{13}CN , considering that the resulting m/z 81 ions, see inset of Fig. 5.3a, should display loss of both **HCN** (via **D5**) and H^{13}CN (via **D6**) in their MI and CID spectra if the **D1**(H^{13}CN) ions have undergone cyclization into **PY**. This appears not to be the case, as witnessed by the spectra of Fig. 5.3c. These spectra display a specific loss of H^{13}CN , indicating that the cyclization does *not* occur.

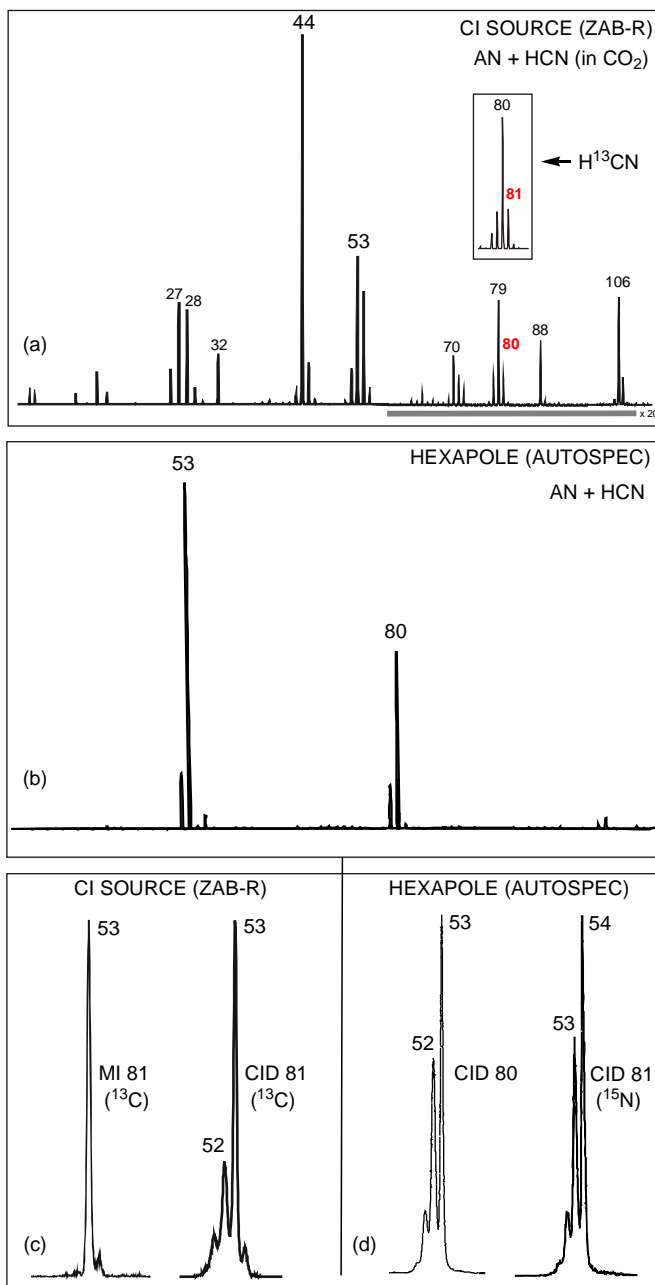


Figure 5.3 (a) Chemical ionization mass spectrum of a 1:3:10 molar mixture of $\text{CH}_2=\text{C}(\text{H})\text{CN}$, HCN and CO_2 [Total source pressure was $7-10 \times 10^{-5}$ Torr]; (b) Mass spectrum of the products of the ion-molecule reaction $\text{AN} + \text{HCN}$ performed in the hexapole reaction chamber of the Autospec; (c) MI and partial CID spectra of m/z 81 adduct ions $\text{AN}/\text{H}^{13}\text{CN}$; (d) Partial CID spectra of adduct ions AN/HCN and $\text{AN}(\text{N}^{15})/\text{HCN}$.

Given the complexity of the ion-molecule chemistry of the above CI experiment, which is further aggravated by the CO₂ catalyzed isomerization [17] of ionized HCN into HNC⁺, we have also performed experiments of *mass-selected* AN ions with HCN in a hexapole reaction chamber, as described in the Experimental. Fig. 5.3b shows that in this set-up, the reaction of AN and HCN yields *m/z* 80 ions almost exclusively : the minor peaks at *m/z* 52 and 79 result from the collision induced H[•] loss from *m/z* 53 and the subsequent ion-molecule reaction $C_3H_2N^+ (m/z\ 52) + HCN \rightarrow C_4H_3N_2^+ (m/z\ 79)$.

Figure 5.3d shows the partial CID spectrum of the *m/z* 80 ions vis-à-vis that of the *m/z* 81 ions obtained by replacing the acrylonitrile with its ¹⁵N-labelled analogue. It is seen that the labelled dimer ion specifically loses HCN, which provides definitive evidence that the reaction of AN with HCN does not yield pyrimidine ions **PY**. In the next Section it will be shown that the reaction leads to the isomerization of AN into AN1 instead.

5.2.2 Protonation and Proton Transport Catalysis in the AN/HCN dimer ions

As indicated in Fig. 5.4, energy-rich dimer ions **D1** can readily adopt the configuration of the hydrogen-bridged radical cations [18] **HBRC1** and **HBRC2**. Proton-transfer in **HBRC1** yields HC=NH⁺ + **ANR1**, whose energy level lies below that of AN + HCN. **HBRC2** would yield HC=NH⁺ + **ANR2**, but this process is too energy demanding to compete with the back-dissociation of the dimer ion **D1**.

The MI spectrum of the dimer ion **D1** displays no *m/z* 28 peak for HC=NH⁺, and its intensity is only marginal in the CID spectrum (not shown). This raises the question whether the incipient HC=NH⁺ ions in the HBRC's can donate a proton back to the incipient radical to generate an AN isomer of lower enthalpy.

The proton-transport catalysis criterion [3-6] predicts HCN to be an efficient catalyst for the isomerization of AN in the ion-molecule encounter complex **HBRC1**, because its proton affinity, 171 kcal mol⁻¹ [19], lies in between that of the **ANR1** radical CH₂=C[•]-CN at C[•] and at N, 167 and 185 kcal mol⁻¹ respectively [8]. Indeed, the energy diagram of Fig. 5.4 indicates that the HCN component of **HBRC1** may rather easily abstract the C-H hydrogen

of AN and transfer it to the N atom to form **HBRC3**, which loses HCN to yield **AN1**. In the same vein, PTC within **HBRC2** leads to **HBRC4**, which dissociates into **AN2** + HCN.

Experimental evidence that PTC indeed occurs in the interaction of AN with HCN in the hexapole reaction chamber of our tandem mass spectrometer is presented in Fig. 5.2d. It is seen that this CID spectrum of m/z 53 ions AN which have interacted with HCN is quite different from that obtained of AN ions transmitted through the empty hexapole, Fig. 5.2c. *Prima facie*, it looks as if AN has been transformed into AN2 : the spectra of Figures 5.2b and d are very similar. However, the m/z 40 tell-tale peak for loss of CH from AN2 is conspicuously low in Fig. 5.2d, indicating that its elusive isomer AN1 discussed in the previous section, is the predominant reaction product.

The picture that emerges from this theoretical and experimental study of the AN/HCN dimer ions is that pyrimidine formation via cyclization as well as protonation is energetically possible but does not compete with the more favoured HCN catalyzed isomerization of AN.

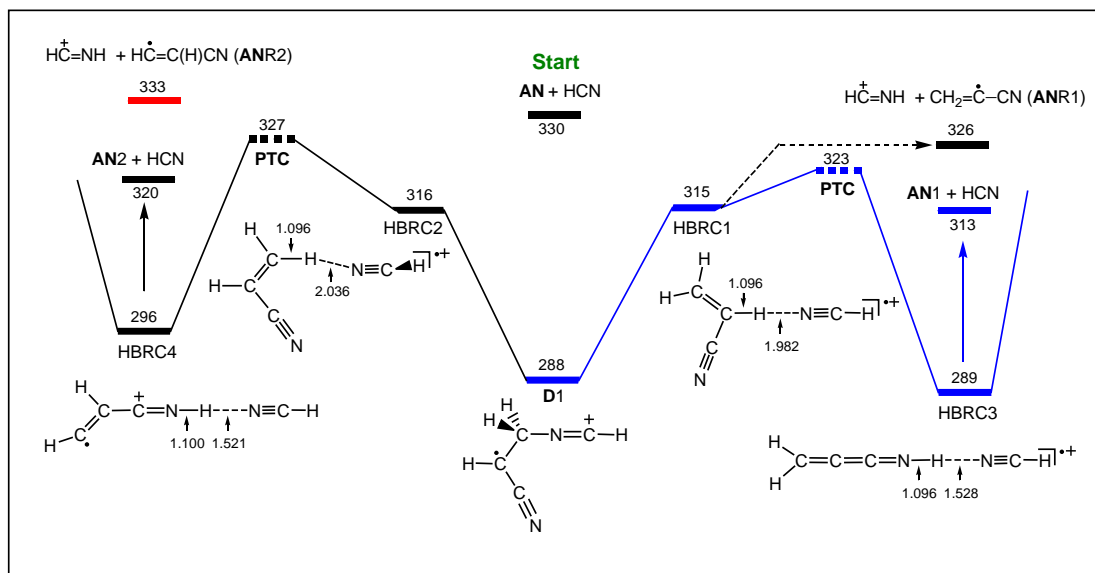


Figure 5.4 Proton-transport catalysis (PTC) of the acrylonitrile ion (AN) with HCN as the catalyst. The numbers refer to CBS-QB3 derived 298 K enthalpies in kcal mol⁻¹.

References

- [1] S. Petrie, D.K. Böhme, *Mass Spectrom. Rev.* 26(2) (2007) 258.
- [2] L.E. Snyder, *PNAS* 103 (2006) 12243.
- [3] E. Uggerud, *Mass Spectrometry Reviews* 11 (1992) 389.
- [4] For an early review see : D.K. Böhme, *Int. J. Mass Spectrom.* 115 (1992) 95.
- [5] R. Lee, P.J.A. Ruttink, P.C. Burgers, J.K. Terlouw, *Int. J. Mass Spectrom.* 255-256 (2006) 244 and references cited therein.
- [6] K.J. Jobst, M.R. Hanifa, J.K. Terlouw, *Chem. Phys. Lett.* 462 (2008) 152.
- [7] K.J. Jobst, P. Gerbaux, G. Dimopoulos-Italiano, P.J.A. Ruttink, J.K. Terlouw, *Chem. Phys. Lett.* 478 (2009) 144.
- [8] H.K. Ervasti, K.J. Jobst, P.C. Burgers, P.J.A. Ruttink, J.K. Terlouw, *Int. J. Mass Spectrom.* 262 (2007) 88.
- [9] S. Petrie, T. J. Chirnside, C. G. Freeman, M. J. McEwan, *Int. J. Mass Spectrom. Ion Processes* 107 (1991) 319.
- [10] D. B. Milligan, P.F. Wilson, M. J. McEwan, V. G. Anicich, *Int. J. Mass Spectrom.* 185/7 (1999) 663.
- [11] Z. Peeters, O. Botta, S.B. Charnley, Z. Kisiel, Y.-J. Kuan, P. Ehrenfreund, *Astron. Astrophys.* 433 (2005) 583.
- [12] H.K. Ervasti, Ph.D. Dissertation, University of Utrecht, The Netherlands, 2008 (Chapter 6).
- [13] J.L. Holmes, C. Aubry, P.M. Mayer. *Assigning Structures to Ions in Mass Spectrometry*, CRC Press, Boca Raton, 2007.
- [14] R. Buff, J. Dannacher, *Int. J. Mass Spectrom. Ion Processes* 62 (1984) 1.
- [15] D. J. Lavorato, T.K. Dargel, W. Koch, G.A. McGibbon, H. Schwarz, J.K. Terlouw, *Int. J. Mass Spec.* 210/211 (2001) 43.
- [16] K.J. Jobst, S.A. Hasan, J.K. Terlouw, *Chem. Phys. Lett.* 450 (2008) 243.
- [17] S. Petrie, C.G. Freeman, M. Meot-Ner (Mautner), M.J. McEwan, E.E. Ferguson, *J. Am. Chem. Soc.* 112 (1990) 7121.
- [18] P.C. Burgers, J.K. Terlouw in: N.M.M. Nibbering (Ed.), *Encyclopedia of Mass Spectrometry*, vol. 4, Elsevier, Amsterdam, 2005, p. 173.
- [19] S.G. Lias, J.E. Bartmess, J.F. Liebman, J.L. Holmes, R.O. Levin, W.G. Maillard, *J. Phys. Chem. Ref. Data* 17 (Suppl. 1) (1988).

Appendix to Chapter 5

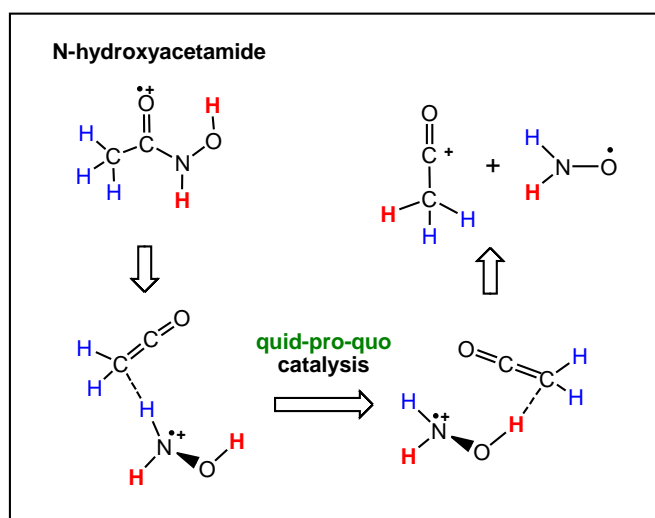
Table 5.1 CBS-QB3 derived enthalpies (kcal mol⁻¹) and total energies (Hartree) of stable ions and transition states involved in the ion-molecule reaction of the acrylonitrile ion and HCN.

Ion	Structure	CBS-QB3 E(total) [0K]	QB3 $\Delta_f H_{298}^0$	Transition State	CBS-QB3 E(total) [0K]	QB3 $\Delta_f H_{298}^0$
D1	Figure 5.1	-263.49108	288	TS D1 → H loss	-263.41648	335
D1-H	Figure 5.1 H loss	-262.92228	280	TS D1 → 2	-263.42636	328
D2	Figure 5.1	-263.48996	288	TS D2 → 3	-263.47093	299
D3	Figure 5.1	-263.47297	298	TS D2 → 5	-263.41275	336
D4	Figure 5.1	-263.46756	303	TS D3 → 4	-263.45368	311
D5	Figure 5.1	-263.47266	299	TS D3 → PY	-263.43094	324
D6	Figure 5.1	-263.49249	287	TS D5 → PY	-263.46953	300
PY	Figure 5.1	-263.53204	260	TS PY → PY1	-263.43340	323
PY1	Figure 5.1	-263.52314	266	TS PY1 → D6	-263.46678	302
HBRC1	Figure 5.4	-263.44906	315			
HBRC2	Figure 5.4	-263.44810	316	TS HBRC1 → D1	-263.44788	315
HBRC3	Figure 5.4	-263.49064	289	TS HBRC1 → 2	-263.43521	323
HBRC4	Figure 5.4	-263.47936	296	TS HBRC2 → 4	-263.42936	327

Note : The CBS-QB3 298 K values for H⁺, HCN and HCNH⁺ are 52, 32 and 226 kcal mol⁻¹; The CBS-QB3 derived $\Delta_f H_{298}^0$ values for the C₃H₃N⁺ isomers CH₂=C(H)CN⁺ (**AN**), CH₂=C=C=NH⁺ (**AN1**), HC=C(H)C=NH⁺ (**AN2**), HC=C(H)N=CH⁺ (**AN4**) and CH₂=C=N=CH⁺ (**AN8**), 298, 281, 288, 299 and 297 kcal/mol respectively, were taken from Ref. 16. Those for the radicals CH₂=C[•]-CN (**ANR₁**) and HC[•]=C(H)CN (**ANR₂**), 100 and 108 kcal mol⁻¹ respectively, are from Ref. 8.

Chapter 6

The loss of $\text{NH}_2\text{O}^\bullet$ from the N-hydroxyacetamide radical cation $\text{CH}_3\text{C}(=\text{O})\text{NHOH}^{\bullet+}$: an ion-catalyzed rearrangement



A previous study (Ch. Lifshitz et al. *Rapid Commun. Mass Spectrom.* 1 (1987) 61) shows that *metastable* N-hydroxyacetamide ions $\text{CH}_3\text{C}(=\text{O})\text{NHOH}^{\bullet+}$ (**HA-1**) do not dissociate into $\text{CH}_3\text{C}=\text{O}^+ + \text{NHOH}^\bullet$ by direct bond cleavage but rather yield $\text{CH}_3\text{C}=\text{O}^+ + \text{NH}_2\text{O}^\bullet$. The tandem mass spectrometry based experiments of the present study on the isotopologue $\text{CH}_3\text{C}(=\text{O})\text{NDOD}^{\bullet+}$ reveal that the majority of the metastable ions lose the $\text{NH}_2\text{O}^\bullet$ radical as NHDO^\bullet rather than $\text{ND}_2\text{O}^\bullet$.

A mechanistic analysis using the CBS-QB3 model chemistry shows that the molecular ions **HA-1** rearrange into hydrogen-bridged radical cations $[\text{O}=\text{C}-\text{C}(\text{H})_2-\text{H}\cdots\text{N}(\text{H})\text{OH}]^{\bullet+}$ whose acetyl cation component then catalyses the transformation $\text{NHOH}^\bullet \rightarrow \text{NH}_2\text{O}^\bullet$ prior to dissociation. The high barrier for the unassisted 1,2-H shift in the free radical, 43 kcal mol^{-1} , is reduced to a mere 7 kcal mol^{-1} for the catalyzed transformation which can be viewed as a *quid-pro-quo* reaction involving two proton transfers.

The work described here has been published previously in an article under the same title : K.J. Jobst, P.C. Burgers, P.J.A. Ruttink, J.K. Terlouw, *Int. J. Mass Spectrom.* 254 (2006) 127 – 135.

6.1 Introduction

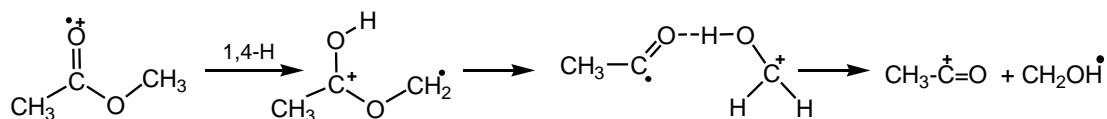
Almost twenty years ago, in a joint project with the late Professor Chava Lifshitz, we reported a study [1], which dealt with the generation and characterization of the prototype nitroxyl radical $\text{NH}_2\text{O}^\bullet$ and its isomer NHOH^\bullet . Using the technique of Neutralization Reionization Mass Spectrometry (NRMS) [2] and related experiments, it was shown that both $\text{NH}_2\text{O}^\bullet$ and NHOH^\bullet are stable radicals in the gas phase separated by a high barrier towards interconversion. The $\text{NH}_2\text{O}^\bullet$ radical has also been identified by far infrared laser, magnetic resonance [3], microwave [4] and UV photoelectron [5] spectroscopy. In contrast, its isomer NHOH^\bullet remains an elusive species, which may inter alia be generated in the reaction of HCO^\bullet with HNO [6]. Experimental enthalpies of formation are not available for either radical. However, the most recent theoretical study [7] yields 298 K enthalpies of formation of 17.5 ± 2 and 23.7 ± 2 kcal mol⁻¹ for $\text{NH}_2\text{O}^\bullet$ and *trans*- NHOH^\bullet and a high interconversion barrier at 70 kcal mol⁻¹; these values are close to those obtained with the computational methods of the present study.

The study of ref. 1 further shows that the *ionic* counterparts of the two radicals are also stable species in the gas-phase. Ions NH_2O^+ and NHOH^+ can conveniently be generated by the dissociative ionization of CH_3ONH_2 and $\text{CH}_3\text{C(=O)NHOH}$ respectively. They can be readily characterized by the unique *m/z* 14-18 peak profiles of their collision induced dissociation (CID) mass spectra. As with the neutral species, the isomerization barrier $\text{NH}_2\text{O}^+ \rightarrow \text{NHOH}^+$ is also high : a subsequent theoretical study at the Gaussian-1 level of theory [8] yields an activation energy of 65.5 kcal mol⁻¹. The more sophisticated model chemistry of this study (see Table 6.1) predicts the same barrier height and 298 K enthalpies of formation of 224 and 242 kcal mol⁻¹ for NH_2O^+ and *trans*- NHOH^+ respectively. Experimental values are only available for the NH_2O^+ isomer : they range from 224 - 225 kcal mol⁻¹ [1] and agree quite well with the theoretical results.

Finally, the study of ref. 1 reports the intriguing experimental observation that *metastable* N-hydroxyacetamide ions $\text{CH}_3\text{C(=O)NHOH}^{+\bullet}$ (**HA-1**) do not dissociate into $\text{CH}_3\text{C=O}^+ + \text{NHOH}^\bullet$ by direct bond cleavage but rather yield $\text{CH}_3\text{C=O}^+ + \text{NH}_2\text{O}^\bullet$. This became clear

when the connectivity of the $[\text{N,H}_2\text{O}]^{\bullet}$ neutral was probed with a CIDI (collision induced dissociative ionization) experiment.

This finding parallels observations on the formation of acetyl cations, $\text{CH}_3\text{-C=O}^+$, from methyl acetate radical cations, $\text{CH}_3\text{C(=O)OCH}_3^{\bullet+}$. For the high-energy source generated ions, the process involves loss of $\text{CH}_3\text{O}^{\bullet}$ by (simple) direct bond cleavage. In contrast, the low-energy *metastable* ions [9] lose the energetically more favourable isomeric $\text{CH}_2\text{OH}^{\bullet}$ radical [10], obviously via a rearrangement. The mechanism of this reaction has been studied in detail using ab initio calculations [11]. As shown in Scheme 6.1, it features a hydrogen-bridged radical cation (HBRC [12]), $\text{CH}_3\text{C=O}\cdots\text{H}\cdots\text{O=CH}_2^{\bullet+}$, as the key intermediate :



Scheme 6.1

In contrast, the mechanism for the loss of $\text{NH}_2\text{O}^{\bullet}$ from *metastable* ions **HA-1** has never been studied. An intriguing possibility is that it involves an (acetyl) ion-catalysed isomerization of the NHOH^{\bullet} radical into its thermodynamically more stable counterpart $\text{NH}_2\text{O}^{\bullet}$. The study of molecular transformations catalysed by ions in the gas-phase is a topic of considerable current interest [13]. This prompted us to probe the mechanism of this reaction by performing additional tandem mass spectrometry based experiments in conjunction with computational chemistry. During the past five years we have successfully used the CBS-QB3 method [14] in mechanistic studies of ionic transformations catalysed by molecules in the gas-phase [15,16]. We therefore decided to use this CBS (complete basis set) variant, which uses density functional geometries and frequencies in the calculations, as the primary computational tool in probing the mechanism for the $\text{NH}_2\text{O}^{\bullet}$ elimination from metastable ions $\text{CH}_3\text{C(=O)NHOH}^{\bullet+}$ (**HA-1**).

Table 6.1 Energetic data for various dissociation products of ionized N-hydroxy-acetamide derived from CBS-QB3 and selected CBS-APNO calculations [a].

Species	m/z	CBS-QB3 E(total) [0 K]	QB3 $\Delta_f H_{298}^0$	APNO $\Delta_f H_{298}^0$	Expt $\Delta_f H_{298}^0$	Ref./ Note
CH₃C=O⁺ + NHOH[*]	43		180.2	181.3	-	
CH ₃ C=O ⁺		-152.68586	158.1	158.7	156	22a
NHOH [*] (trans)		-130.90786	22.1	22.6	-	
NHOH [*] (cis)		-130.89944	27.5	27.9	-	
CH₃C=O⁺ + NH₂O[*]	43		172.4	174.1	-	
NH ₂ O [*]		-130.92056	14.3	15.4	-	
TS NH ₂ O [*] →NHOH [*] (trans)		-130.83876	65.5	65.4	-	
CH₂=C=O⁺⁺ + NH₂OH	42		199.8	199.4	200	
CH ₂ =C=O ⁺⁺		-152.02211	210.3	209.3	210	22a
NH ₂ OH		-131.54158	-11.2	-9.9	-10	22a
NH₂OH⁺⁺ + CH₂=C=O	33		190.5	189.7	200	
NH ₂ OH ⁺⁺		-131.20170	202.2	201.9	211	[b]
CH ₂ =C=O		-152.37579	-11.7	-12.2	-11	22a
NHOH⁺ + CH₃C=O[*]	32		238.9	238.6	-	
NHOH ⁺ (trans)		-130.55794	241.6	242.1	-	
NHOH ⁺ (cis)		-130.54705	248.5	249.0	-	
TS NH ₂ O ⁺ →NHOH ⁺ (trans)		-130.48116	289.8	289.9	-	
CH ₃ C=O [*]		-152.94168	-2.7	-3.5	-2.4	22b
NH₂O⁺ + CH₃C=O[*]	32		220.8	220.8	222.6	
NH ₂ O ⁺		-130.58679	223.5	224.3	225	

[a] $E_{\text{(total)}}$ in Hartrees, all other components, including the ZPE scaled by 0.99, are in kcal mol⁻¹;
 [b] Using IE = 9.6 eV as proposed in the photoionization study of ref. 22c; the unusually large discrepancy between theory and experiment probably originates from large differences in the geometries of the ion and the neutral so that the true adiabatic IE cannot be measured, see also ref. 22d.

6.2 Results and discussion

The MI spectrum of CH₃C(=O)NHOH⁺ (**HA-1**), see Fig. 6.1a, contains only one peak, at m/z 43, which results from the dissociation **HA-1** → CH₃C=O⁺ + [N,H₂,O]^{*}. The CIDI spectrum of the corresponding [N,H₂,O]^{*} neutral is shown in Fig. 6.1d/e. These spectra are very close to those reported in ref. 1 where, based upon additional experimental observations in conjunction with a detailed analysis of the CID spectra of NHOH⁺ and NH₂O⁺, compelling evidence is presented that the (majority of) the neutrals lost in the dissociation of metastable ions **HA-1** have the NH₂O^{*} connectivity.

To gain more insight in the mechanism of the reaction, the (slightly acidic) N-H and O-H hydrogens of CH₃C(=O)NHOH were exchanged with deuterium using methanol-OD. The MI spectrum of the resulting isotopomer **HA-1d₂** (m/z 77) is shown in Fig. 6.1b.

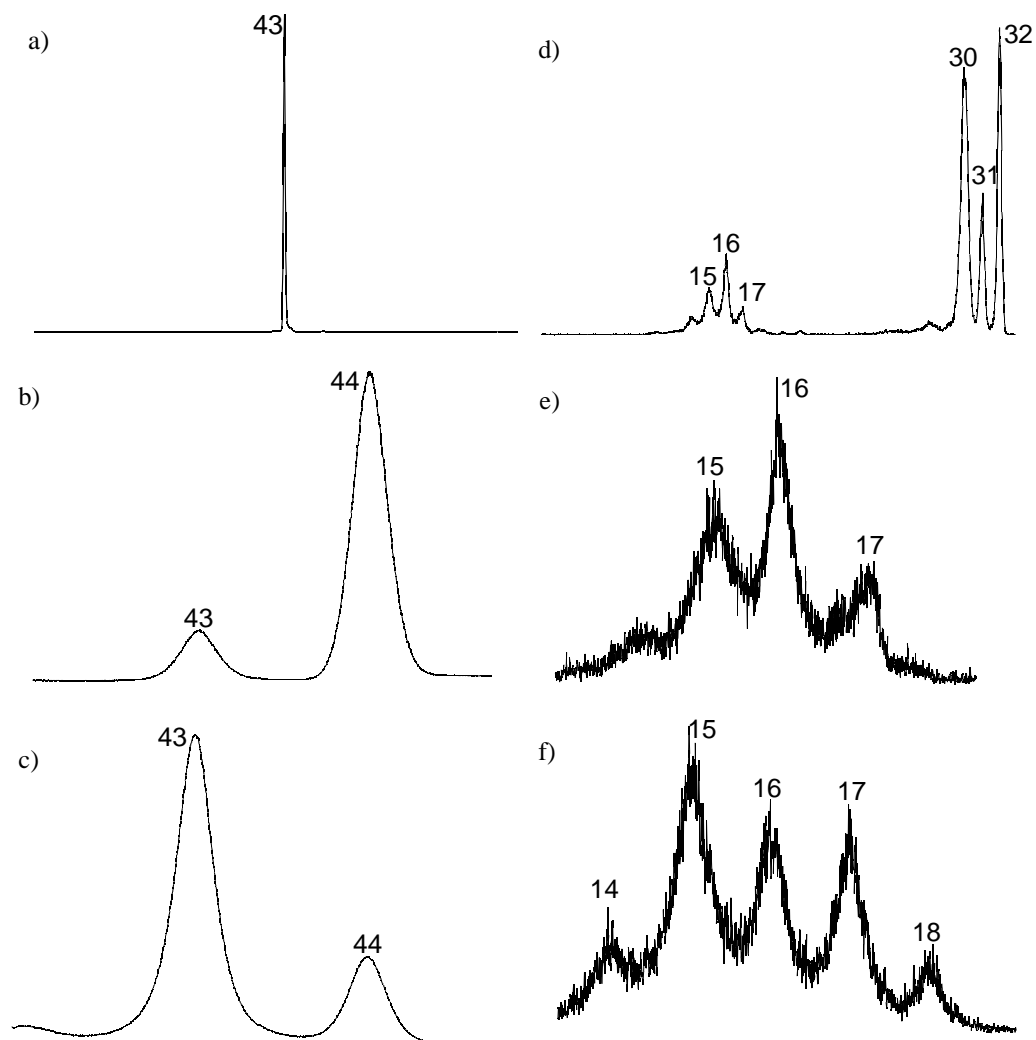


Figure 6.1 (a) MI spectrum of ionized N-hydroxyacetamide, $\text{CH}_3\text{C}(=\text{O})\text{NHOH}^+$ (**HA-1**); (b) Partial (2ffr, 8kV) MI spectrum of $\text{CH}_3\text{C}(=\text{O})\text{NDOD}^+$ (**HA-1d₂**); (c) Partial (2ffr, 8kV, He) CID spectrum of $\text{CH}_3\text{C}(=\text{O})\text{NDOD}^+$ (**HA-1d₂**); (d) (2ffr, 10kV, He) CIDI spectrum of the $m/z = 32$ neutrals generated from metastable ions **HA-1**; (e) The m/z 14 – 18 region in the (2ffr, 10kV, He) CIDI spectrum of the $m/z = 32$ neutrals generated from metastable ions **HA-1**; (f) The m/z 14 – 18 region in the (2ffr, 5kV, He) CID spectrum of m/z 32 reference ions of structure NHOH^+ .

It is seen that the m/z 43 peak is largely shifted to m/z 44, indicating that NHDO^\bullet rather than $\text{ND}_2\text{O}^\bullet$ is preferentially lost. We further note that the intensity of the minor m/z 43 peak in the MI spectrum of Fig. 6.1b is very sensitive to the presence of (residual) collision gas : when the 2fr collision cell was pressurized with He its intensity, see Fig. 6.1c, increased strongly - by a factor of 40 - whereas the m/z 44 peak only increased by a factor of 2. From this result, we conclude that *metastable* ions **HA-1d₂** largely dissociate into $\text{CH}_2\text{DC}=\text{O}^+ + \text{NHDO}^\bullet$, whereas collision induced dissociation of stable ions **HA-1d₂** - which may account for (part of) the m/z 43 peak in the MI spectrum of Fig. 6.1b - leads to the formation of $\text{CH}_3\text{C}=\text{O}^+ + \text{NDOD}^\bullet$, by direct bond cleavage.

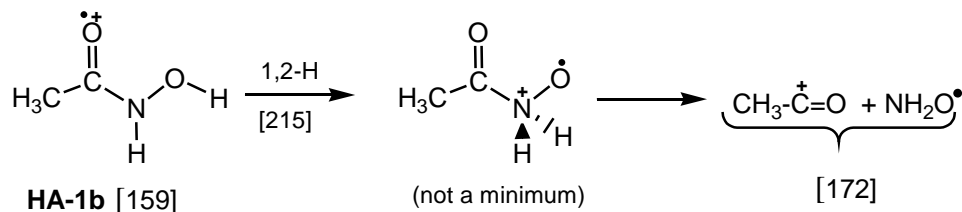
We further note that if part of the m/z 43 peak in the spectrum of Fig. 6.1b is indeed of metastable origin, a second mechanism for the $\text{NH}_2\text{O}^\bullet$ loss may play a (minor) role. Analysis of the shapes [17] of the MI and CID peaks of Fig. 6.1b/c does not provide conclusive evidence for this proposal. The $T_{0.5}$ values of the gaussian shaped metastable peaks at m/z 43 and 44 (18.2 and 17.4 meV) are not significantly different and the same obtains for the corresponding CID peaks, which are only marginally broader ($\sim 5\%$).

Overall, we can assert that during the loss of $\text{NH}_2\text{O}^\bullet$ from *metastable* ions **HA-1**, one of the hydrogen atoms of the NHOH moiety is exchanged with a methylic hydrogen.

In the context of our computational quest of plausible mechanisms for the $\text{NH}_2\text{O}^\bullet$ elimination from metastable ions **HA-1**, an important criterion is that none of the stable intermediates or connecting transition states of a viable proposal should lie significantly above the energy level for the direct bond cleavage **HA-1** \rightarrow $\text{CH}_3\text{C}=\text{O}^+ + \text{NHOH}^\bullet$. Our calculations, see Table 6.1, indicate that $\Sigma \Delta_f H_{298}^0$ ($\text{CH}_3\text{C}=\text{O}^+ + \textit{trans}\text{-NHOH}^\bullet$) lies at 180 kcal mol^{-1} whereas $\Delta_f H_{298}^0$ (**HA-1a**), the lowest energy conformer of **HA-1**, is 150 kcal mol^{-1} . Hence, a 30 kcal mol^{-1} energy window exists in which the rearrangement **HA-1** \rightarrow $\text{CH}_3\text{C}=\text{O}^+ + \text{NH}_2\text{O}^\bullet$ occurs.

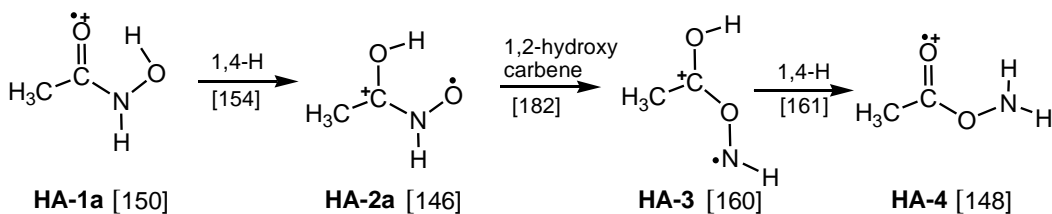
Loss of $\text{NH}_2\text{O}^\bullet$ from **HA-1** clearly does not involve a simple 1,2-H shift in the NHOH moiety of the ion as depicted in Scheme 6.2. The energy requirement for this shift, 56 kcal mol^{-1} , is quite high and considerably larger than that calculated for the dissociation threshold for loss of NHOH^\bullet by direct bond cleavage. In fact, the transformation $\text{NHOH}^\bullet \rightarrow$

$\text{NH}_2\text{O}^\bullet$ in the ion requires even more energy than that in the free radicals, 43 kcal mol^{-1} , see Table 6.1.



Scheme 6.2

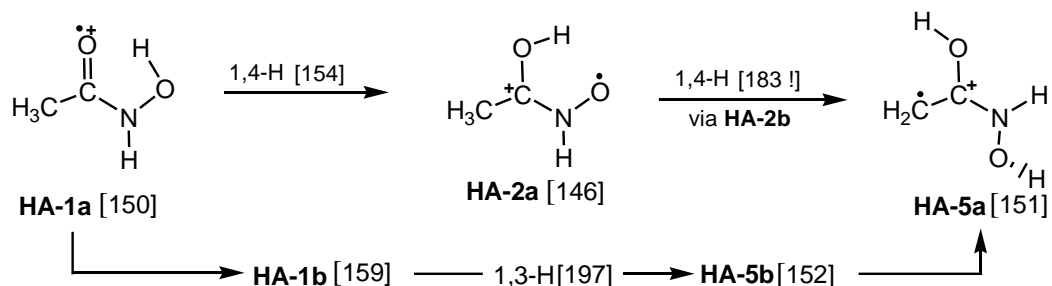
A more plausible route, shown in Scheme 6.3, involves the formation of $\text{CH}_3\text{C}(=\text{O})\text{ONH}_2^{*\bullet}$ (**HA-4**) via a 1,2-hydroxy-carbene shift, a well-documented transformation [10,18] :



Scheme 6.3

A 1,4-H shift in **HA-1** yields the stable distonic isomer **HA-2a**. Next the 1,2-hydroxycarbene shift takes place yielding a second stable distonic isomer, **HA-3**. A subsequent 1,4-H shift completes the rearrangement to **HA-4** which can readily lose $\text{NH}_2\text{O}^\bullet$ by direct bond cleavage. The most energy demanding step of this route is the hydroxycarbene shift : its energy barrier slightly exceeds, by 2 kcal mol^{-1} , the thermochemical threshold for the direct bond cleavage $\text{HA-1} \rightarrow \text{CH}_3\text{C}=\text{O}^\bullet + \text{NHOH}^\bullet$. A conservative estimate of the error in energies derived from the CBS-QB3 method is $\pm 2 \text{ kcal mol}^{-1}$ for local minima and $\pm 4 \text{ kcal mol}^{-1}$ for transition states [15] and thus from an energetic point of view this mechanism could be operative. It may rationalize the minor loss of $\text{ND}_2\text{O}^\bullet$ from $\text{CH}_3\text{C}(=\text{O})\text{NDOD}^{*\bullet}$ (**HA-1d₂**) but cannot easily account for the major pathway which leads to the loss of NHDO^\bullet . We note that H/D exchange reactions that

could lead to a (partial) randomization of the label do not seem to occur. Our calculations provide a rationale : the key intermediate required for this exchange, the enol ion $\text{CH}_2=\text{C}(\text{OH})\text{NHOH}^+$, **HA-5**, cannot readily communicate with its keto counterpart **HA-1**. As shown in Scheme 6.4, the associated barriers lie higher in energy than the dissociation level for $\text{CH}_3\text{C}=\text{O}^+ + \text{NHOH}^*$:



Scheme 6.4

Note that the second 1,4-H transfer in Scheme 6.4 is quite energy demanding (37 kcal mol⁻¹). This has been observed previously [19] for a process involving a 1,4-H *atom* shift to a trigonal CH_2^* group. Starting from **HA-2a** the large barrier is associated with the change in hybridization of the methyl carbon during the 1,4-H shift, but there is a further consideration. It is a well established phenomenon that ionized enol ions lie below the keto form (by about 14 kcal mol⁻¹), but this is not so for **HA-5**, the enol ion of N-hydroxyacetamide. Had ion **HA-5** lain significantly below **HA-2**, then according to Hammond's principle the TS energy of the associated 1,4-H shift might well have been reduced to below the upper limit of 180 kcal mol⁻¹ and H/D mixing would have ensued.

A more promising rearrangement pathway involves hydrogen bridged radical cations (HBRCs) [12] as key intermediates, as depicted in Figure 6.2.

In this proposal, **HBRC-1** is generated from **HA-1** via migration of its NHOH moiety towards the methyl group of the acetyl cation, forming a $\text{C}\cdots\text{H}\cdots\text{N}$ bridged species. The bridging H is closer to the (methyl) carbon because it has the higher proton affinity. However, it can easily move towards the N(H)-OH moiety as a *proton* yielding **HBRC-2**, a hydroxylamine(ion)-ketene(molecule) complex of slightly higher energy. Hardly any additional energy is required for **HBRC-2** to rearrange into **HBRC-3**. This transformation

can be viewed as the movement of the neutral ketene molecule in **HBRC-2** towards the hydroxylic H of the hydroxylamine ion. In this rearrangement, the hydroxylic hydrogen *protonates* the ketene molecule transforming it into an acetyl cation. **HBRC-3** is not a minimum on the PES (the TS at 177 kcal mol⁻¹ connects **HBRC-2** with ion **HA-4**) but rather a transient species that in the calculation collapses into CH₃C(=O)ONH₂⁺⁺ (**HA-4**). However, the incipient **HBRC-3** ions have internal energies in excess of that required for dissociation by direct bond cleavage and thus the transformation **HA-1** → **HBRC-1** → **HBRC-2** → **HBRC-3** → CH₃C=O⁺ + NH₂O[•] adequately describes the course of the reaction.

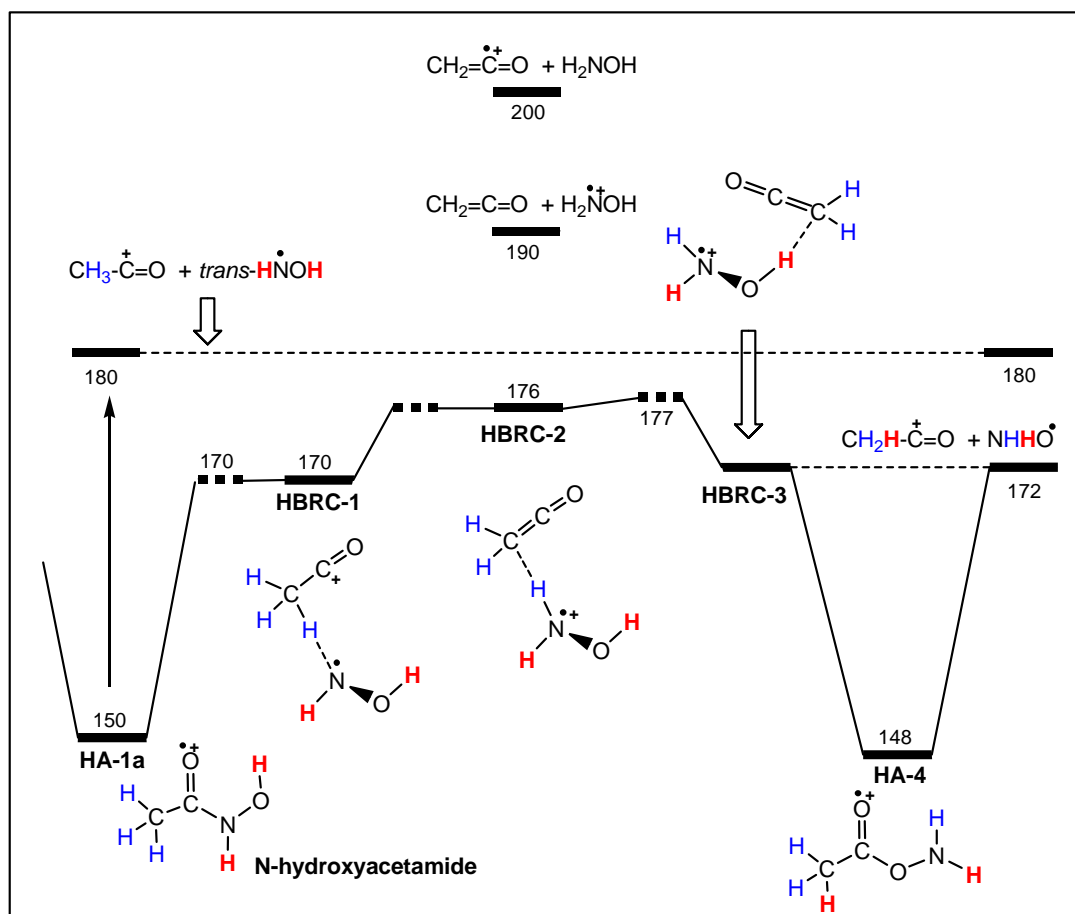
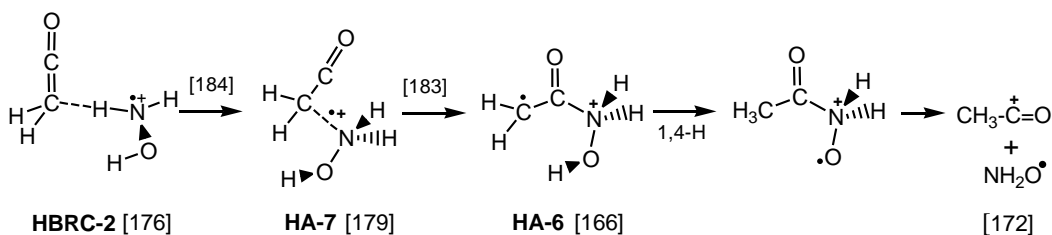


Figure 6.2 Energy-level diagram derived from CBS-QB3 calculations describing the elimination of NH₂O[•] from metastable N-hydroxyacetamide ions **HA-1** via a quid-pro-quo mechanism. The numbers refer to 298K enthalpy values in kcal mol⁻¹. These values are compiled in Table 6.2 (Appendix) and the optimized geometries are displayed in Figure 6.3 (Appendix).

This mechanism satisfies the energetic constraint discussed above and it also readily explains the predominant loss of NHDO^\bullet from metastable ions $\text{CH}_3\text{C}(=\text{O})\text{NDOD}^{*\dagger}$ (**HA-1d₂**). It involves two *proton* transfers : first a methylic hydrogen is abstracted as a proton (**HBRC-1**→ **HBRC-2**) and in the next step (**HBRC-2**→ **HBRC-3**) the hydroxylic hydrogen is donated back as a proton to the methylene carbon atom of the ketene molecule.

This process can be classified as a *quid-pro-quo* reaction. Several recent studies of (radical cat)ion-molecule reactions have reported this type of reaction [20,21] but so far it has not been shown to occur in a dissociative ionization reaction. We note that this mechanistic proposal also provides a prime example of the role of an ion in catalyzing the isomerization of a neutral radical into a more stable hydrogen-shift isomer.

The quid-pro-quo transformation in the proposal of Fig. 6.2 could in principle also be realized via other routes. One intriguing possibility involves rearrangement of **HBRC-2** into distonic ion **HA-6** which could lose $\text{NH}_2\text{O}^\bullet$ following a 1,4-H shift as depicted in Scheme 6.5 :

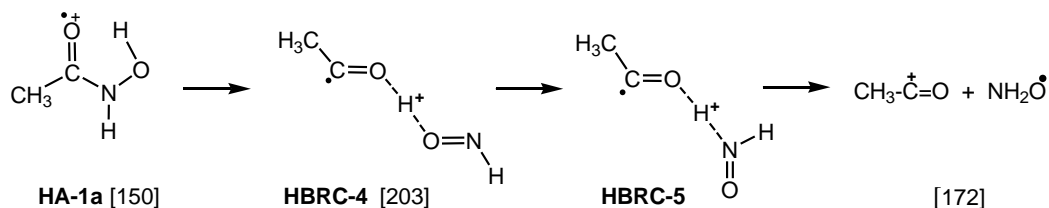


Scheme 6.5

Our calculations indicate that the rearrangement of **HBRC-2** into **HA-6** can take place via intermediate ion **HA-7**, a one-electron bonded species [12] rather than an ion-dipole complex. However, the energy requirement for the route **HBRC-2** → **HA-7** → **HA-6** exceeds that of the direct dissociation **HA-1** → $\text{CH}_3\text{C}=\text{O}^+ + \text{NHOH}^\bullet$ so that this pathway is not a viable alternative for our proposed mechanism.

One further mechanistic proposal deserves comment. In the mechanism for loss of $\text{CH}_2\text{OH}^\bullet$ from metastable methyl acetate ions, see Introduction, $\text{CH}_3\text{C}=\text{O}\cdots\text{H}\cdots\text{O}=\text{CH}_2^{*\dagger}$ is a key intermediate. The analogue of this intermediate in the **HA-1** system is the O-H-O bridged ion **HBRC-4**, shown in Scheme 6.6. This ion could, possibly via proton-transport

catalysis [12,16], rearrange into **HBRC-5** which would then dissociate into the desired products :



Scheme 6.6

However, the first intermediate ion of this proposal, **HBRC-4**, lies so high in energy that this route requires no further consideration.

6.3 Conclusions

Tandem mass spectrometry based collision experiments reveal that low energy N-hydroxyacetamide radical cations, $\text{CH}_3\text{C}(=\text{O})\text{NHOH}^+$ **HA-1**, dissociate to $\text{CH}_3\text{C}=\text{O}^+ + \text{NH}_2\text{O}^\bullet$ and not to the expected HNOH^\bullet radical. The mechanism of this intriguing “hidden” hydrogen rearrangement has been elucidated with the help of the CBS-QB3 model chemistry. The key transformation is comprised of the ion-catalysed rearrangement $\text{HNOH}^\bullet \rightarrow \text{NH}_2\text{O}^\bullet$ where $\text{CH}_3\text{-C}=\text{O}^+$ acts as the catalyst in a quid-pro-quo process. In this reaction the acetyl cation donates a *proton* to the N atom of HNOH^\bullet and then the O-H *proton* of the incipient NH_2OH^+ radical cation is donated back.

In general terms, the quid-pro-quo process between a protonated molecule MH^+ and a (deuterated) substrate radical A-B-D^\bullet can be represented by $:\text{MH}^+ + \text{A-B-D}^\bullet \rightarrow \text{M}\cdots\text{H}^+\cdots\text{A-BD}^\bullet \rightarrow \text{M}\cdots\text{D}^+\cdots\text{B-AH}^\bullet \rightarrow \text{MD}^+ + \text{B-AH}^\bullet$. An important criterion for a smooth reaction is that the PA of M lies between the PA of A-BD^\bullet at A and the PA of B-AH^\bullet at B. This criterion is not met in the system of our study: from the data of Table 6.1 it follows that the PA of ketene ($196 \text{ kcal mol}^{-1}$) is higher than that of both $\text{NH}_2\text{O}^\bullet$ and NHOH^\bullet (179 and $186 \text{ kcal mol}^{-1}$ respectively). As a result the proton abstraction from $\text{CH}_3\text{-C}=\text{O}^+$ is endothermic so that the transformation $\text{NHOH}^\bullet \rightarrow \text{NH}_2\text{O}^\bullet$ still has a (small) barrier of 7 kcal mol^{-1} , see Fig. 6.2. Finally, we note that a minor fraction of the $\text{NH}_2\text{O}^\bullet$ loss may take place via a more “classical” transformation, i.e. the well-known 1,2-hydroxycarbene shift.

References

- [1] Ch. Lifshitz, P.J.A. Ruttink, G. Schaftenaar, J.K. Terlouw, *Rapid Commun. Mass Spectrom.* 1 (1987) 61.
- [2] For a recent review see : F. Turecek, *Top. Curr. Chem. A* 225 (2003) 77.
- [3] P.B. Davies, P. Dransfeld, F. Temps, H.G. Wagner, *J. Chem. Phys.* 81 (1984) 3763.
- [4] H. Mikami, S. Saito, S. Yamamoto, *J. Chem. Phys.*, 94 (1991) 3415.
- [5] J. Baker, V. Butcher, J.M. Dyke, A. Morris, *J. Chem. Soc. Faraday Trans.* 86 (1990) 3843.
- [6] Z.F. Xu, M.C. Lin, *Int. J. Chem. Kinetics*, 36 (2004) 205.
- [7] R. Sumathi, D. Sengupta, M. T. Nguyen, *J. Phys. Chem. A* 102 (1998) 3175.
- [8] F. Grandinetti, J. Hrusak, D. Schröder, H. Schwarz, *J. Phys. Chem.* 96 (1992) 2100.
- [9] J.L. Holmes in: *Encyclopedia of Mass Spectrometry*, vol. 1 (P.B. Armentrout, ed.), Elsevier, Amsterdam, 2004, 91.
- [10] P.C. Burgers and J.K. Terlouw. *In Specialist periodical reports : mass spectrometry*. Vol. 10. Edited by M.E. Rose. The Royal Society of Chemistry, London. 1989. Chapter 2, p. 49.
- [11] N. Heinrich, J. Schmidt, H. Schwarz, Y. Apeloig, *J. Am. Chem. Soc.* 109 (1987) 1317.
- [12] P.C. Burgers and J.K. Terlouw in: *Encyclopedia of Mass Spectrometry*, vol. 4 (N.M.M. Nibbering, ed.), Elsevier, Amsterdam, 2005, 173.
- [13] D.K. Böhme, H. Schwarz, *Angew. Chem. Int. Ed.* 44 (2005) 2.
- [14] (a) J.W. Ochterski, G.A. Petersson, and J.A. Montgomery, Jr. *J. Chem. Phys.* 104, (1996) 2598. (b) J.A. Montgomery, Jr, M.J. Frisch, J.W. Ochterski, and G.A. Petersson. *J. Chem. Phys.* 112, (2000) 6532.
- [15] L.N. Heydorn, Y. Ling, G. de Oliveria, J.M.L. Martin, Ch. Lifshitz, J.K. Terlouw. *Zeitschrift für Physikalische Chemie*, 215 (2001) 141.
- [16] (a) C.Y. Wong, P.J.A. Ruttink, P.C. Burgers, J.K. Terlouw, *Chem. Phys. Lett.* 390, (2004) 176; (ibid) 387, (2004) 204.
- [17] (a) J.L. Holmes, J.K. Terlouw, *Org. Mass Spectrom.* 15 (1980) 383 ; (b) J.L. Holmes in: *Encyclopedia of Mass Spectrometry*, vol. 1 (P.B. Armentrout, ed.), Elsevier, Amsterdam, 2004, 91.
- [18] R. Lee, P.J.A. Ruttink, P.C. Burgers, J.K. Terlouw. *Can. J. Chem.* (2005) in press.
- [19] P.J.A. Ruttink, P.C. Burgers, L.M. Fell, J.K. Terlouw. *J. Phys. Chem. A* 102 (1998) 2976.
- [20] M.A. Trikoupis, P.J.A. Ruttink, P.C. Burgers, J.K. Terlouw. *Eur. J. Mass Spectrom.* 10 (2004) 801 and references cited therein.
- [21] P.C. Burgers, P.J.A. Ruttink. *Int. J. Mass Spectrom.* 242, (2005) 49.
- [22] (a) S.G. Lias, J.E. Bartmess, J.F. Liebman, J.L. Holmes, R.O. Levin, and W.G. Maillard. *J. Phys. Chem. Ref. Data, Suppl.1*, 17 (1988) ; (b) Yu-Ran Luo. *Handbook of dissociation energies in organic compounds*. CRC Press, Boca Raton 2003; (c) R.E. Kutina, G.L. Goodman, G.L. Berkowitz, *J. Chem. Phys.* 77 (1982) 1664 ; (d) P.C. Burgers, Ch. Lifshitz, P.J.A. Ruttink, G. Schaftenaar, J.K. Terlouw, *Org. Mass Spectrom.* 24 (1989) 579.

Appendix to Chapter 6

Table 6.2 Energetic data [a] derived from CBS-QB3 calculations of stable isomers and connecting transition states involved in the loss of $\text{NH}_2\text{O}^\bullet$ from the N-hydroxyacetamide radical cation (**HA-1**).

Ionic species	B3LYP/CBSB7 E(total)	CBS-QB3 E(total) [OK]	ZPE	$\Delta_f H_{298}^0$
HA-1a $\text{CH}_3\text{C}(=\text{O})\text{NHOH}^{*\bullet}$	-284.136268	-283.640009	47.6	150.1
HA-1b conformer of above	-284.122151	-283.626406	46.9	159.1
HA-2a $\text{CH}_3\text{C}(\text{OH})\text{NHO}^{*\bullet}$	-284.148324	-283.646792	48.6	145.6
HA-2b conformer of above	-284.144380	-283.642561	48.4	148.4
HA-3 $\text{CH}_3\text{C}(\text{OH})\text{ONH}^{*\bullet}$	-284.121695	-283.624535	47.6	159.8
HA-3a conformer of above	-284.126329	-283.629495	47.6	156.6
HA-4 $\text{CH}_3\text{C}(=\text{O})\text{ONH}_2^{*\bullet}$	-284.144105	-283.645333	46.8	147.8
HA-5a $\text{CH}_2=\text{C}(\text{OH})\text{NHOH}^{*\bullet}$	-284.135389	-283.638448	48.0	151.0
HA-5b conformer of above	-284.133062	-283.637363	47.8	151.8
HA-6 $\text{CH}_2\text{C}(=\text{O})\text{NH}_2\text{OH}^{*\bullet}$	-284.110470	-283.614910	48.1	165.9
HA-7 $\text{O}=\text{C}=\text{C}(\text{H}_2)\text{NH}_2\text{OH}^{*\bullet}$	-284.104738	-283.596194	46.5	178.5
HBRC-1	-284.107804	-283.609736	45.2	170.1
HBRC-2	-284.101810	-283.600772	44.3	175.8
HBRC-3	collapses to HA-4			
HBRC-4	-284.051387	-283.557534	43.5	202.8
TS HA-1a→2a	-284.128069	-283.633569	45.6	153.8
TS HA-1b→5b	-284.057507	-283.564903	44.7	197.0
TS HA-2a→3	-284.079590	-283.588701	46.6	181.9
TS HA-2b→5a	-284.082397	-283.586945	45.3	182.7
TS HA-6→7	-284.092226	-283.589281	45.7	182.5
TS HA-1a→HBRC-1 [b]	-284.105535	-283.610176	45.4	169.5
TS HBRC-1→2 [b]	-284.101470	-283.601980	42.8	174.7
TS HBRC-2→HA-4	-284.099095	-283.598089	45.3	176.9
TS HBRC-2→HA-7	-284.096193	-283.587935	44.7	183.9
TS HA-3→4	-284.115422	-283.622998	45.1	160.5

[a] $E_{\text{(total)}}$ in Hartrees, all other components, including the ZPE scaled by 0.99, are in kcal mol^{-1} ; [b] The CBS-QB3 energy of the TS is calculated to be slightly lower than that of the least stable of the connecting isomers. This may happen since transition states are more sensitive to correlation effects than minima and the ZPE also tends to favour transition states.

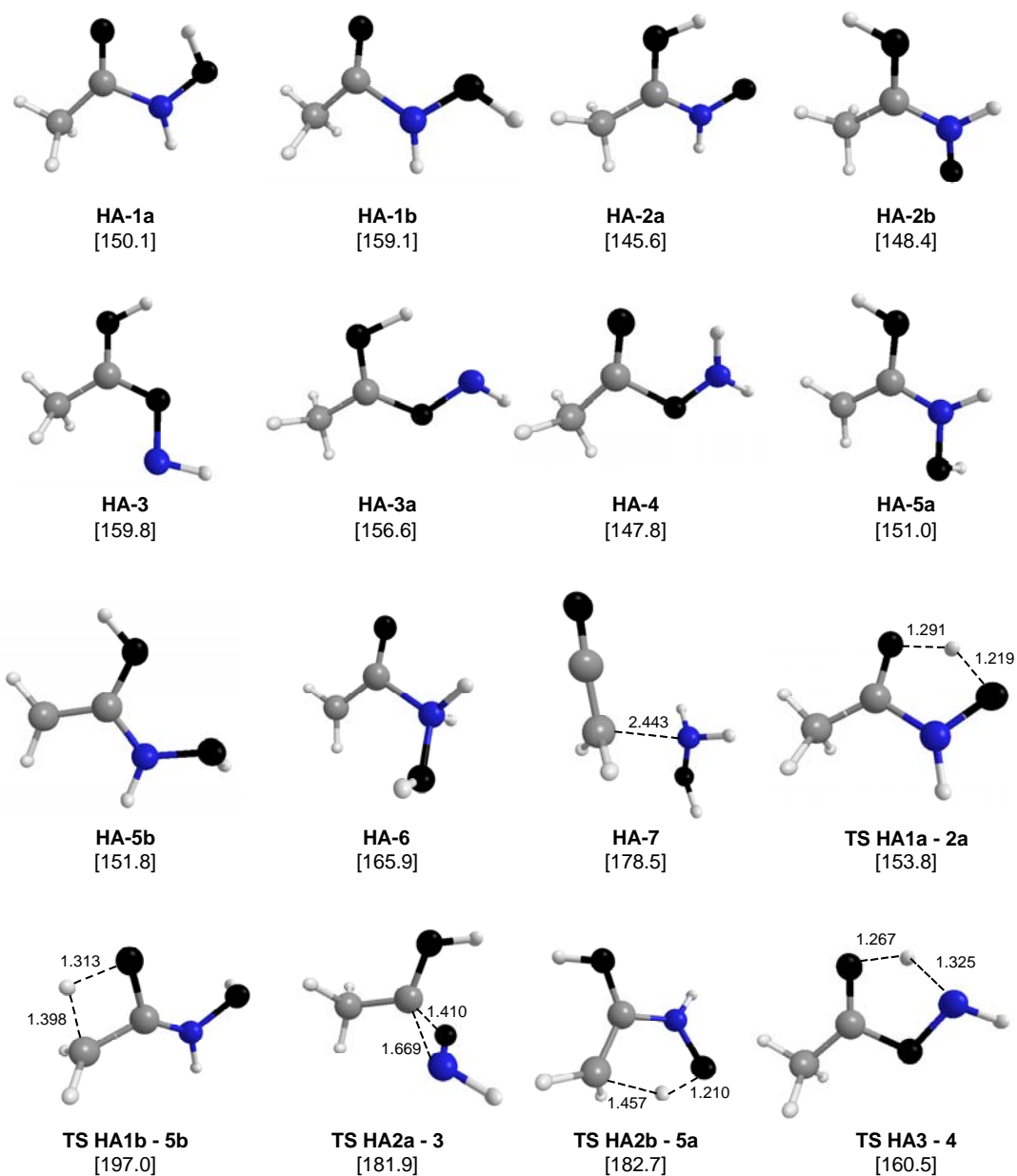


Figure 6.3 Selected optimised geometries (CBSB7 basis set) for stable intermediates and transition states involved in the elimination of NH_2O^+ from ionized N-hydroxyacetamide (**HA-1**).

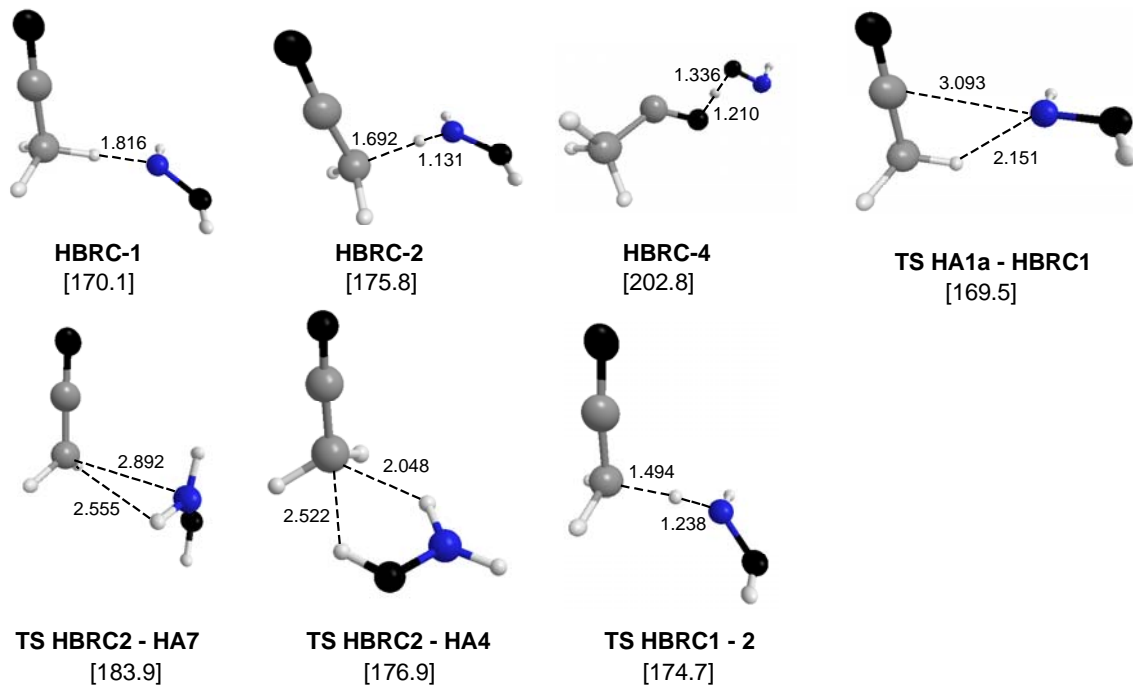
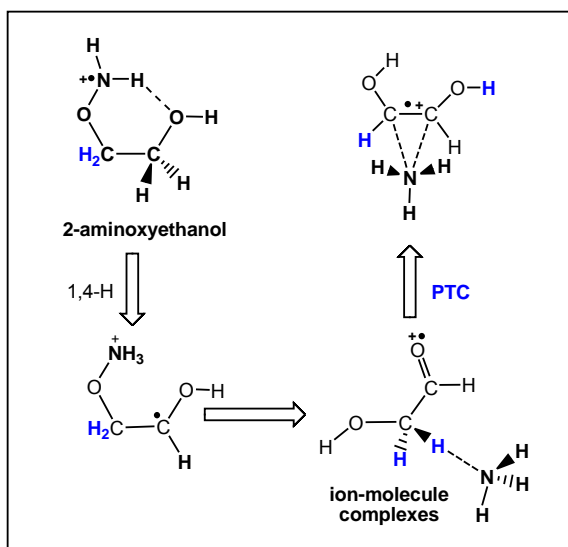


Figure 6.3 (continued)

Chapter 7

The remarkable dissociation chemistry of 2-aminoxyethanol ions $\text{NH}_2\text{OCH}_2\text{CH}_2\text{OH}^{\bullet+}$ studied by experiment and theory



Low-energy 2-aminoxyethanol molecular ions $\text{NH}_2\text{OCH}_2\text{CH}_2\text{OH}^{\bullet+}$ exhibit a surprisingly rich gas-phase ion chemistry. They spontaneously undergo five major dissociations in the μs timeframe, yielding ions of m/z 61, 60, 46, 32 and 18. Our tandem mass spectrometry experiments indicate that these reactions correspond to the generation of $\text{HOCH}_2\text{CH}(\text{OH})^+$ (protonated glycolaldehyde), $\text{HOCH}_2\text{C}(=\text{O})\text{H}^{\bullet+}$ (ionized glycolaldehyde), $\text{HC}(\text{OH})\text{NH}_2^+$ (protonated formamide), $\text{CH}_2\text{OH}_2^{\bullet+}$ (the methylene oxonium ion) and NH_4^+ .

A mechanistic analysis of these processes using the CBS-QB3 model chemistry shows that the molecular ions undergo a 1,4-H shift followed by a facile isomerization into the ion-molecule complex $[\text{HOCH}_2\text{C}(=\text{O})\text{H}^{\bullet+}] \cdots [\text{NH}_3]$ which acts as the reacting configuration for the five exothermic dissociation processes. Analysis of the D-labelled isotopomer $\text{ND}_2\text{OCH}_2\text{CH}_2\text{OD}^{\bullet+}$, in conjunction with our computational results, shows that proton-transport catalysis (PTC) may be responsible for the partial conversion of the m/z 60 glycol-aldehyde ions into the more stable 1,2-dihydroxyethene isomer $\text{HOC}(\text{H})=\text{C}(\text{H})\text{OH}^{\bullet+}$.

The work described here has been published previously in an article under the same title : K.J. Jobst, P.J.A. Ruttink, J.K. Terlouw, *Int. J. Mass Spectrom.* 269 (2008) 165 – 176.

7.1 Introduction

Since the first detection of trihalomethanes in drinking water, the qualitative and quantitative characterization of so-called Disinfection By-Products (DBPs) has become a subject of considerable interest. DBPs are commonly derived from the combination of natural organic matter with disinfection agents like chlorine, chlorine dioxide, ozone and chloramines [1]. Several DBPs have thus far been identified, including trihalomethanes, haloacetic acids, haloacetonitriles, chloral hydrate and cyanogen chloride. It is estimated that these account for approximately 40% of DBPs whereas the remainder are unknown.

In 2001, two unexpected disinfection by-products were reported : the halogenated aminoxyalcohols 1-aminoxy-1-chlorobutan-2-ol and 1-aminoxy-2-bromobutan-2-ol [2]. The structure proposal was based upon a detailed mass spectrometric study involving electron ionization (EI), chemical ionization (CI) and high resolution data but it remains speculative because little is known about the EI characteristics of aminoxyalcohols.

This prompted us to examine the EI and CI characteristics of 2-aminoxyethanol ($\text{NH}_2\text{OCH}_2\text{CH}_2\text{OH}$) as a model compound. In this study we have used tandem mass spectrometry based experiments in conjunction with model chemistry calculations to probe the rich dissociation chemistry of the metastable molecular ions $\text{NH}_2\text{OCH}_2\text{CH}_2\text{OH}^{+\bullet}$ (**AE-1**). These ions dissociate via six competing pathways whereas the related 1,2-ethane diol ion $\text{HOCH}_2\text{CH}_2\text{OH}^{+\bullet}$ only loses HCO^\bullet in the metastable timeframe [3,4] via a mechanism that features proton transport catalysis (PTC) [5] in hydrogen-bridged radical cations (HBRCs) [6] as key intermediates. It will be shown that HBRCs also play a key role in the various dissociation reactions of low energy 2-aminoxyethanol radical cations.

7.2 Results and discussion

7.2.1 Identification of the dissociation products of metastable 2-aminoxyethanol ions

The 70 eV mass spectrum of 2-aminoxyethanol is shown in Fig. 7.1a. A weak molecular ion signal is observed at m/z 77. Pseudo-direct bond cleavage in the molecular ion leads to

the base peak at m/z 45 corresponding to CH_3CHOH^+ [3] (direct bond cleavage into $^+\text{CH}_2\text{CHOH}$ is not an option : this ion is not a minimum on the $\text{C}_2\text{H}_5\text{O}^+$ potential energy surface). Losses of NH_2^\bullet and NH_3 lead to the low intensity peaks at m/z 60 and 61. The signals at m/z 31 (CH_2OH^+) and 29 (HCO^+), characteristic of ions having primary hydroxyl functionalities, result from carbon-carbon bond cleavage. The complementary reaction, resulting from $\text{CH}_2\text{OH}^\bullet$ loss, rationalizes the weak signal at m/z 46. By analogy with ionized 1,2-ethanediol [4], a double hydrogen transfer reaction could take place to generate protonated methanol at m/z 33. However, a high-resolution GC-MS experiment shows that the m/z 33 ions are $[\text{N},\text{H}_3,\text{O}]^{++}$ ions and that they do not originate from a contaminant.

On the other hand, the metastable ion (MI) spectrum of $\text{NH}_2\text{OCH}_2\text{CH}_2\text{OH}^{++}$ is dominated by a different set of reactions. As shown in Fig. 7.1b, substantial signals at m/z 61, 60, 46, 32 and 18 are observed along with a much less intense m/z 47 peak. The m/z 45 signal, which is the base peak in the 70 eV EI mass spectrum and also the CID mass spectrum (Fig. 7.1c), is absent in the MI spectrum.

Structure assignments of the product ions produced in the above low energy dissociations follow from the analysis of our tandem mass spectrometry results, that is from the high-energy CID mass spectra of ions dissociating in the metastable timeframe [3].

The CID mass spectrum of the m/z 61 product ions is shown in Fig. 7.1e. This spectrum is compatible with that of carbonyl-protonated glycolaldehyde ions $\text{HOCH}_2\text{CH}(\text{OH})^+$ (**1a**): it closely resembles that of the m/z 61 ions generated by loss of HCO^\bullet from ionized glyceraldehyde, $\text{HOCH}_2\text{CH}(\text{OH})\text{CHO}^{++}$. Further support for this assignment comes from a detailed experimental and computational study of protonated glycolaldehyde [7], which, inter alia provides a convincing rationale for the intense water loss peak at m/z 43 ($\text{CH}_3\text{C}=\text{O}^+$) in the CID mass spectrum.

Analysis of the CID spectrum of Fig. 7.1f leads to the proposal that the m/z 60 ions of the MI spectrum represent a 3:1 mixture of ionized glycolaldehyde, $\text{HOCH}_2\text{C}(=\text{O})\text{H}^{++}$ (**2a**), and dihydroxyethene, $\text{HOC}(\text{H})=\text{C}(\text{H})\text{OH}^{++}$ (**2b**).

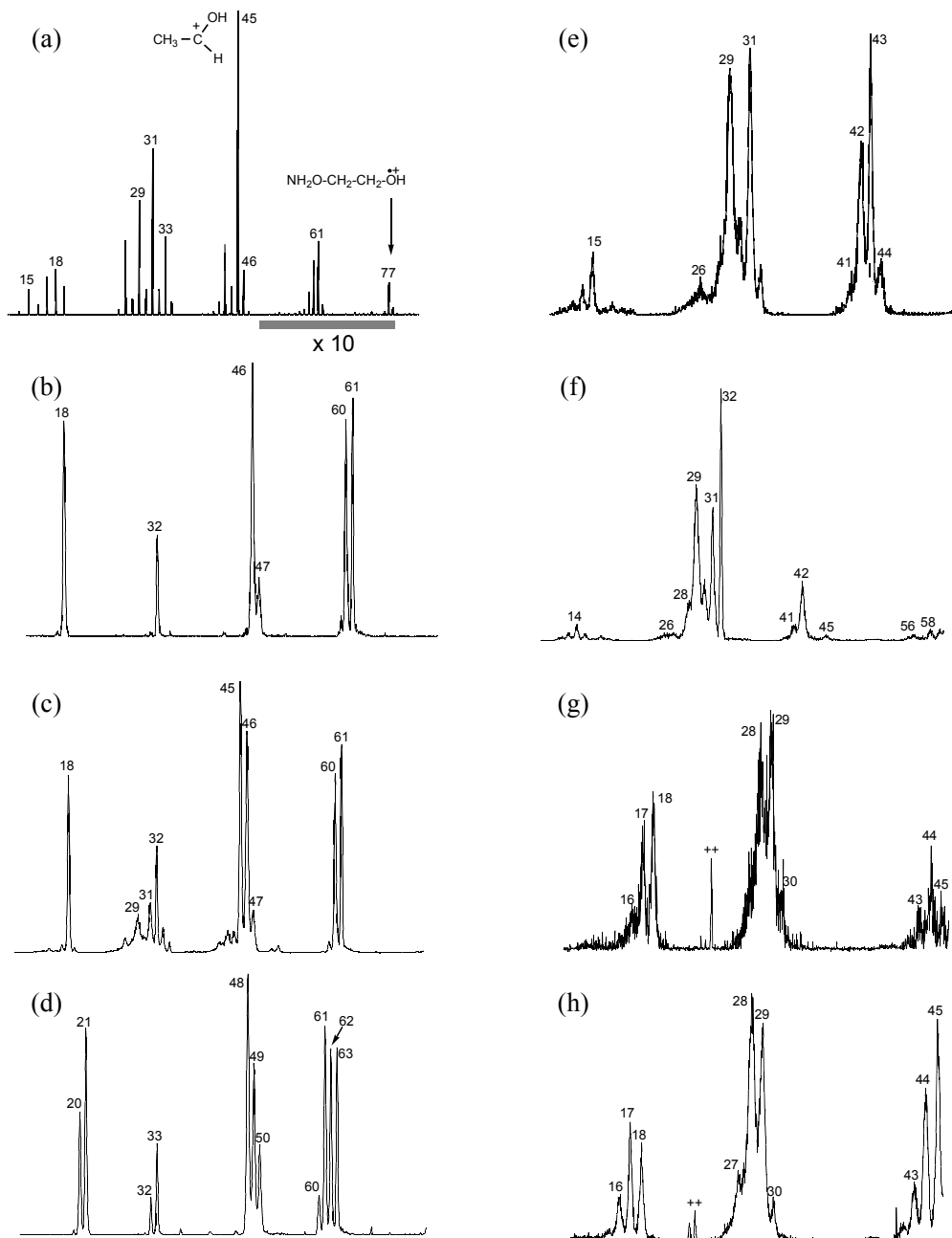
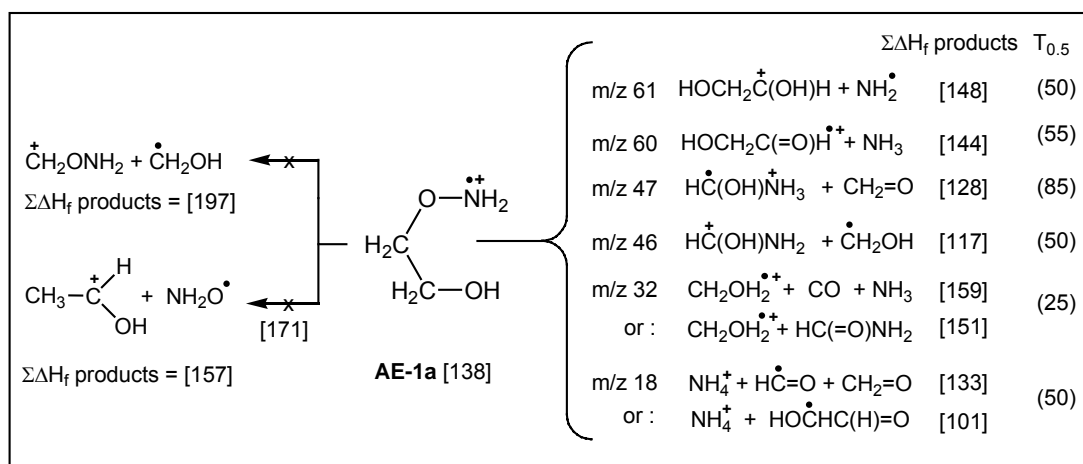


Figure 7.1 (a) 70 eV EI mass spectrum of $\text{NH}_2\text{OCH}_2\text{CH}_2\text{OH}$ (2-aminoxyethanol); the (8kv, 2ffr) MI and (8kv, 2ffr, O_2) CID spectra of the molecular ion are represented by items (b) and (c) respectively, whereas item (d) shows the MI spectrum of $\text{ND}_2\text{OCH}_2\text{CH}_2\text{OD}^+$; items (e) to (h) are (10kV, 3ffr, O_2) CID spectra of respectively m/z 61, 60, 47 and 46 ions generated from metastable ions $\text{NH}_2\text{OCH}_2\text{CH}_2\text{OH}^+$.

This assertion is based upon a careful comparison with the reference spectra available in the literature [3, 8a,d]. The spectrum of Fig. 7.1f is close to that of ionized glycolaldehyde and features a narrow peak at m/z 32 for its decarbonylation into $\text{CH}_2\text{OH}_2^{+\bullet}$ [8b,c]. On the other hand, loss of H_2O does not occur from **2a** and the broadened peak at m/z 42 characterizes the presence of enol ions **2b**.

Figure 7.1g shows the CID mass spectrum of the m/z 47 product ion generated by loss of CH_2O . This spectrum is not compatible with that of ionized N- or O-methylhydroxylamine for which reference spectra are available [9a]. We propose that it corresponds to $\text{HC}(\text{OH})\text{NH}_3^{+\bullet}$ (**3a**), an ylide ion that has not previously been characterized experimentally. The exothermicity of its generation, see Scheme 7.1, makes it an attractive proposal.



Scheme 7.1 Structure assignments and thermochemical energy requirements for the various reactions. See Table 7.1 (Appendix to this Chapter) for full set of data.

The CID mass spectrum of Fig. 7.1h clearly represents [9b] that of m/z 46 ions having the structure of carbonyl-protonated formamide, $\text{HC}(\text{OH})\text{NH}_2^+$ (**4a**). The spectra of the m/z 18 and 32 ions (not shown) are in excellent agreement with those of NH_4^+ and the well-characterized methylene oxonium ion $\text{CH}_2\text{OH}_2^{+\bullet}$ [3].

Scheme 7.1 summarizes the above ion structure assignments and lists the thermochemical energy requirement for the various reactions. Also given are the kinetic energy releases derived from the metastable peaks ($T_{0.5}$ values in meV). Their relatively high values

suggest that the reactions do not take place at the thermochemical threshold [3]. We further note that lack of sensitivity prevented us to use the CIDI technique [3] to probe the identity of the neutral species lost in the generation of the m/z 32 and m/z 18 ions.

7.2.2 *The energy requirement for dissociating metastable 2-aminoxyethanol ions*

The generation of m/z 45 ions CH_3CHOH^+ is the predominant reaction among source-generated ions, but it is absent among the dissociating metastable ions. The reaction likely involves the pseudo direct bond cleavage reaction of Scheme 7.1, which is calculated to lie at $171 \text{ kcal mol}^{-1}$. In the absence of energetic information from appearance energies, we propose as an alternative criterion that the calculated mechanistic proposals for the dissociation chemistry of metastable 2-aminoxyethanol ions are viable only if their energy requirement lies below that of the above pseudo direct bond cleavage reaction at $171 \text{ kcal mol}^{-1}$.

The activation energy for this process, relative to the lowest energy conformer **AE-1a**, is significant (33 kcal mol^{-1} , see Scheme 7.1) and leads one to expect that 2-aminoxyethanol would exhibit a sizeable molecular ion signal in its EI mass spectrum. This is clearly not the case, see Fig. 7.1a, and the following provides a rationale. First we note that neutral 2-aminoxyethanol possesses a great many conformational isomers. Of these, the two “cis” isomers of Figure 7.2 are the most stable because of internal hydrogen-bridges (the “cis/trans” annotation refers to the relative position of the hydroxyl and the aminoxy groups). The lowest energy conformer **AE(N)-2** is internally hydrogen bridged with the hydroxyl hydrogen acting as the bridging hydrogen. The other conformer, **AE(N)-1**, whose bridging hydrogen belongs to the aminoxy functional group, lies $2.3 \text{ kcal mol}^{-1}$ higher in energy. Thus, if one assumes that an equilibrium exists between these conformers prior to ionization, almost all of the incipient ions are formed from neutrals having the structure of **AE(N)-2**. Our calculations indicate that the vertical ionization energy of **AE(N)-2** is 9.27 eV and that the ion is not a minimum on the potential energy surface : it optimizes to ion **AE-1a**. This scenario predicts that EI generates **AE-1a** ions

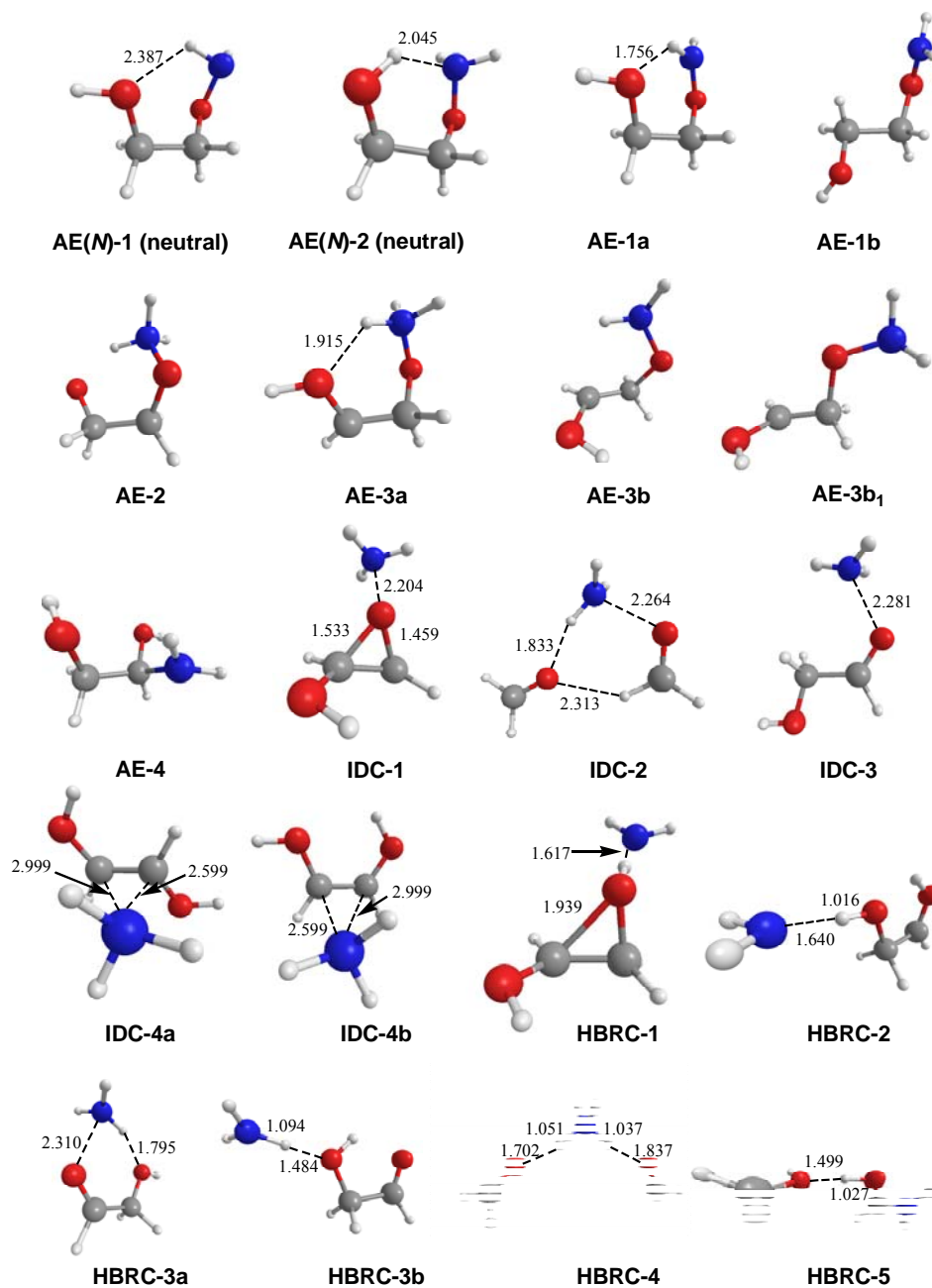


Figure 7.2 Optimized geometries (B3LYP/CBSB7 method) of selected stable intermediates and connecting transition states involved in the dissociation of 2-aminoxyethanol ions **AE1**. The corresponding 298 K enthalpies are compiled in Table 7.2 of the Appendix to this Chapter.

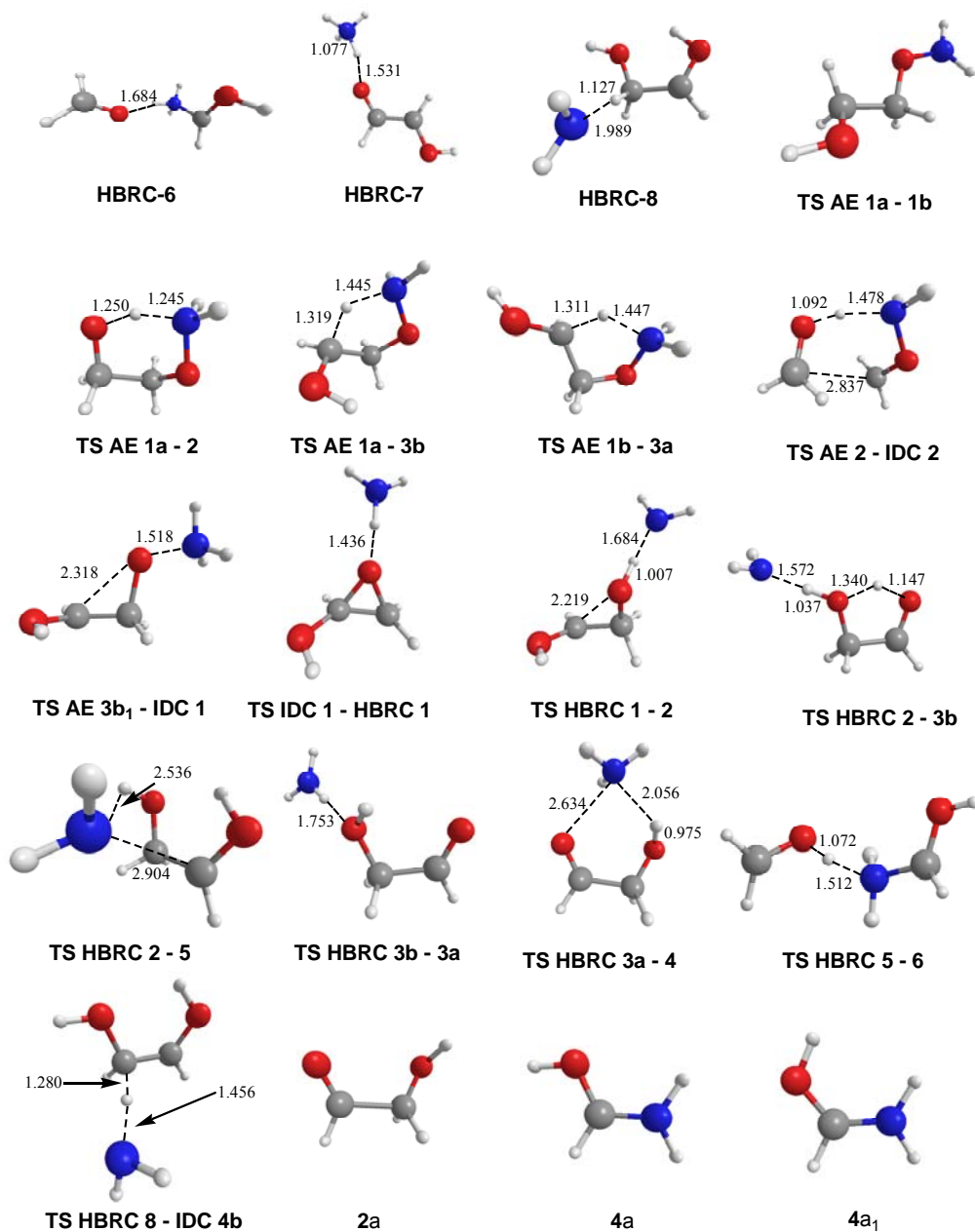
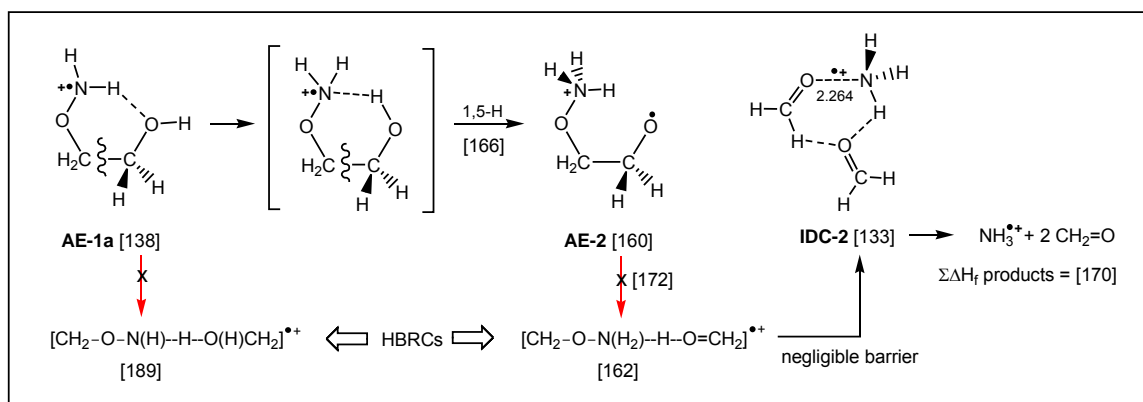


Figure 7.2 (continued).

having 22 kcal mol⁻¹ of excess internal energy. These ions require a mere 11 kcal mol⁻¹ of energy to dissociate into *m/z* 45 ions and this may well explain the low intensity of the molecular ion signal.

7.2.3 The dissociation mechanisms for metastable 2-aminoxyethanol ions : does its dissociation chemistry resemble that of ionized 1,2-ethanediol ?

In this and the following sections, we present the results of our CBS-QB3 computational analysis of the mechanisms by which metastable aminoxyethanol ions dissociate. Previous work [3,4] has shown that metastable 1,2-ethanediol ions dissociate via the hydrogen-bridged intermediate, CH₂O(H)•••H•••O=CH₂⁺⁺. Therefore, we first examined the possibility that the metastable 2-aminoxyethanol ions isomerize into the two hydrogen-bridged analogues shown in Scheme 7.2 :



Scheme 7.2

Their generation may be envisaged to occur via carbon-carbon bond cleavage of ions **AE-1a**. In HBRC [CH₂-O-N(H)•••H•••O(H)CH₂]⁺⁺ the bridging H atom is donated by the NH₂O group, whereas it originates from the OH group in its isomer [CH₂-O-N(H₂)•••H•••O=CH₂]⁺⁺.

The calculated enthalpies of formation for the two species are 189 and 162 kcal mol⁻¹ respectively. This implies that the ion [CH₂-O-N(H)•••H•••O(H)CH₂]⁺⁺ does not play a role in the dissociation chemistry as it lies higher in energy than the 1,2-H shift transition state

that yields the m/z 45 ion. The enthalpy of $[\text{CH}_2\text{-O-N}(\text{H}_2)\cdots\text{H}\cdots\text{O}=\text{CH}_2]^{++}$ is not too high to discount it as a possible intermediate, but our calculations indicate that the process by which it is generated is too energy demanding. As shown in Scheme 7.2, ion **AE-1a** first rearranges by a 1,5-H shift into the distonic ion **AE-2**, which further rearranges into the HBRC by fission of its carbon-carbon bond. The overall energy requirement for this transformation lies at $172 \text{ kcal mol}^{-1}$, slightly above the energy criterion of Section 7.2.1. We further note that ions having the structure $\text{CH}_2\text{ONH}_3^{++}$ are expected to exothermically dissociate by loss of CH_2O [9]. Thus it is not surprising that the calculation indicates that the CH_2ONH_3 component of the HBRC $[\text{CH}_2\text{-O-N}(\text{H}_2)\cdots\text{H}\cdots\text{O}=\text{CH}_2]^{++}$ triggers a facile conversion to the energetically more attractive ter-body complex **IDC-2**. However, incipient **IDC-2** ions generated by the route of Scheme 7.2 have some 40 kcal mol^{-1} of internal energy, more than enough for a rapid dissociation into $\text{NH}_3^{++} + 2 \text{ CH}_2=\text{O}$. It is conceivable that NH_4^+ ions are co-generated in this process but, as shown in next Section, a pathway of much lower energy is available for this reaction.

7.2.4 The dissociation mechanisms for metastable 2-aminoxyethanol ions : losses of NH_2^\bullet , NH_3 , and the generation of NH_4^+

The first step of all of our mechanistic proposals for the dissociation of metastable 2-aminoxyethanol ions **AE-1** is the 1,4-H shift leading to **AE-3b** depicted in Figure 7.3a* . This step appears to be less energy demanding than the 1,5-H shift leading to ion **AE-2** of Scheme 7.2. It reflects the finding that ion **AE-3b** is more stable than ion **AE-2**.

The transformation **AE-1a** \rightarrow **AE-3b** lies at $163 \text{ kcal mol}^{-1}$. However, a more circuitous route involving the rotational conformer **AE-3a**, *viz.* **AE-1a** \rightarrow **AE-1b** \rightarrow **AE-3a** \rightarrow **AE-3b** is 3 kcal mol^{-1} less energy demanding. Ion **AE-3b** can easily generate its rotational conformer **AE-3b₁**, which subsequently rearranges into **IDC-1**. This rearrangement

* (A reviewer has suggested that O-N bond cleavage in **AE-1** followed by a delayed (hidden) 1,3-H shift could account for the NH_2^\bullet loss. Our calculations indicate that this is not a viable option : the $\text{HOCH}_2\text{CH}_2\text{O}^+$ product ion is not a minimum and elongation of the O-N bond leads to the ter-body complex $[\text{CH}_2=\text{O}\cdots\text{NH}_3\cdots\text{O}=\text{CH}_2]^{++}$ with an energy requirement of 48 kcal mol^{-1} . A direct 1,3-H shift to the ONH_2 moiety does not initiate loss of NH_2^\bullet either : this reaction would generate $\text{CH}_2=\text{CH-OH}^{++} + \text{NH}_2\text{OH}$, via a prohibitively high barrier of 50 kcal mol^{-1}).

involves elongation of the nitrogen-oxygen bond in concert with the formation of a bond between the aminoxy oxygen atom and the hydroxyl-substituted carbon atom. The resulting ion, **IDC-1**, can be viewed as an ion-dipole complex between a substituted oxirane ion and NH_3 . An ensuing barrierless H atom transfer yields the protonated oxirane complex **HBRC-1** which can ring open with a negligible barrier into **HBRC-2**.

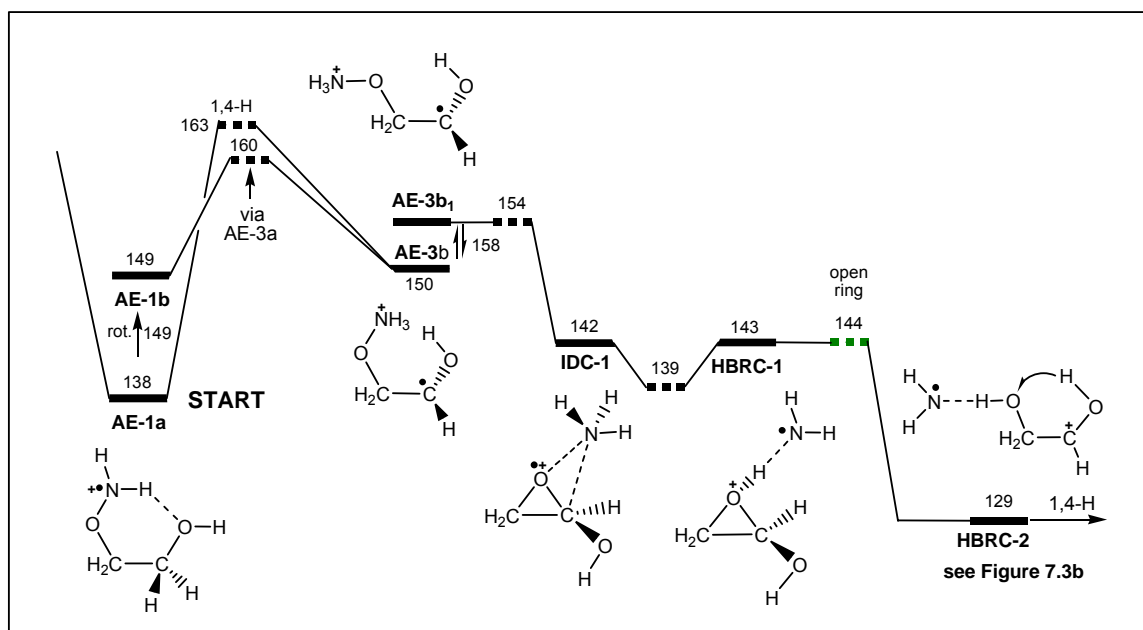


Figure 7.3a Energy diagram depicting the isomerization of ionized 2-aminoxyethanol (**AE-1**) into the hydrogen-bridged radical cation **HBRC-2**. The numbers refer to 298 K enthalpies (in kcal mol^{-1}) derived from CBS-QB3 calculations.

Figure 7.2 shows that the more heavily substituted carbon atom of **HBRC-1** possesses an unusually long bond (1.9 \AA) with the protonated oxirane oxygen atom. A recent computational study [10] suggests that DFT methods underestimate the strength of the C-O bond of such species and further recommends the use of CCSD derived geometries. We therefore performed a geometry optimization of **HBRC-1** using the more sophisticated QCISD/6-311G(d,p) level of theory. At this level of theory **HBRC-1** is not even a minimum

and its optimized geometry is that of **HBRC-2** supporting the proposal that C-O bond cleavage in **HBRC-1** involves no significant barrier.

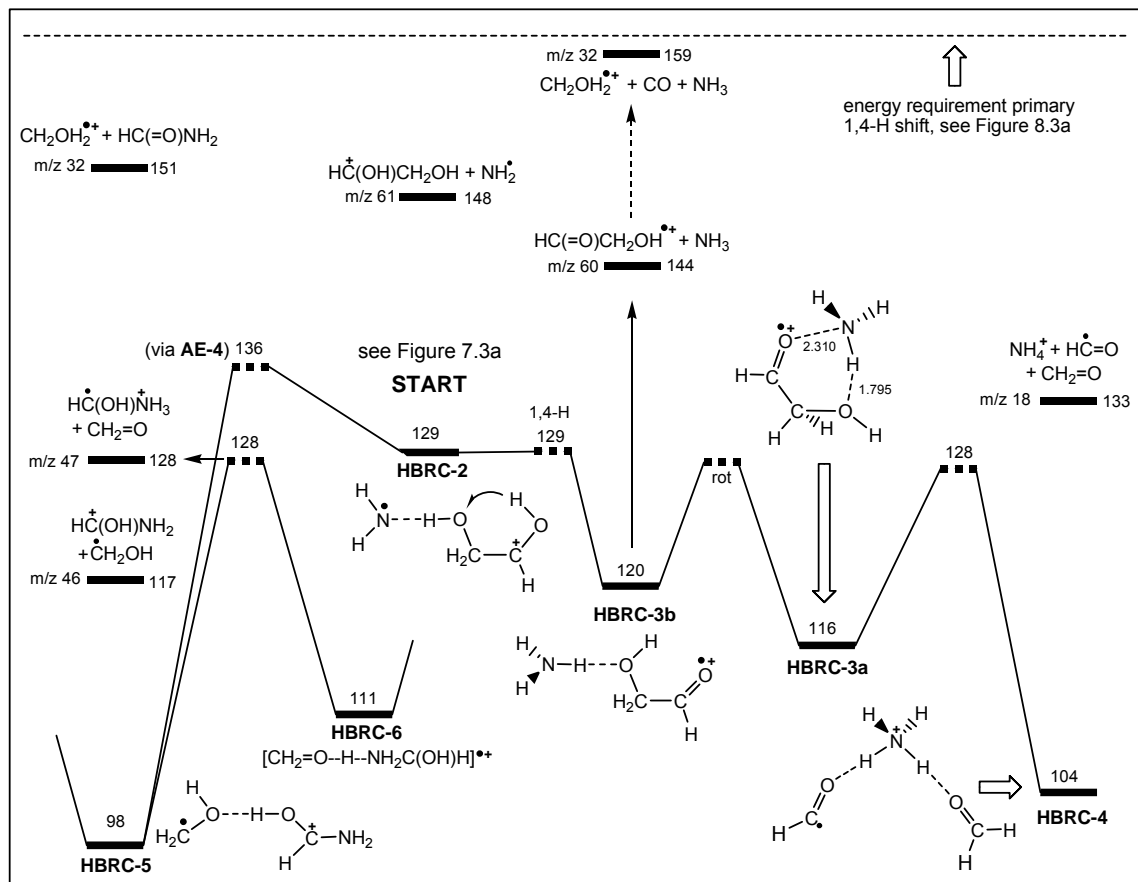
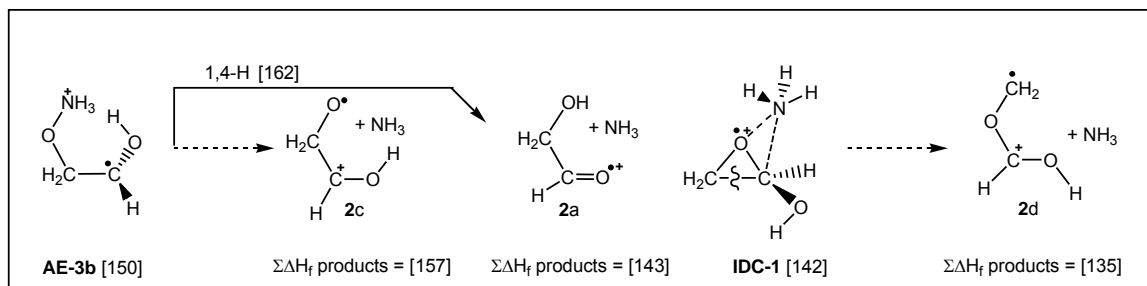


Figure 7.3b Energy diagram depicting the various dissociation mechanisms initiated from **HBRC-2**. The numbers are 298 K enthalpies (in kcal mol⁻¹) derived from CBS-QB3 calculations.

Loss of NH_2^{\bullet} from **HBRC-2** may well account for the abundant production of protonated glycolaldehyde (m/z 61 in Fig. 7.1b). As shown in Figure 7.3b, the other dissociation processes also involve **HBRC-2** as a key intermediate.

A hydrogen transfer to its NH_2^{\bullet} component in concert with a 1,4-H shift in the incipient glycolaldehyde component leads to **HBRC-3b**, which can be viewed as an ionized glycolaldehyde- NH_3 complex. The incipient **HBRC-3b** ions may lose NH_3 to yield ionized

glycolaldehyde, or rearrange further via carbon-carbon bond cleavage into the ter-body complex **HBRC-4**. Ions **HBRC-4** generated from **AE-1** have a very high internal energy content ($> 56 \text{ kcal mol}^{-1}$, see the dashed line in Figure 7.3b) and will therefore rapidly decompose into NH_4^+ by the consecutive loss of $\text{HCO}^\bullet + \text{CH}_2=\text{O}$.



Scheme 7.3

For the loss of NH_3 we have also considered the three pathways depicted in Scheme 7.3.

(i) The incipient ions **AE-3b** generated by a 1,4-H shift at $160 \text{ kcal mol}^{-1}$ can be envisaged to undergo direct bond cleavage into the $\text{C}_2\text{H}_4\text{O}_2^{++}$ isomer **2c** and NH_3 ; the calculated minimum energy requirement for this reaction is $157 \text{ kcal mol}^{-1}$. Our calculations also indicate that upon extension of the nitrogen-oxygen bond in **AE-3b**, a 1,4-H shift may occur in concert yielding ionized glycolaldehyde and NH_3 . However, neither of these routes is expected to effectively compete with the energetically much more attractive pathway of Figures 7.3a/b.

(ii) Ions **IDC-1** of Figure 7.3a may be envisaged to undergo the C–C bond cleavage depicted on the right hand side of Scheme 7.3. This would lead to the formation of the $\text{C}_2\text{H}_4\text{O}_2^{++}$ isomer **2d**, a stable distonic ion whose dissociation chemistry has been studied in detail [8d,e] in conjunction with that of its 1,4-H shift isomer ionized methyl formate [8f]. From an energetic point of view this route cannot be excluded: a potential energy surface scan (at the B3LYP/CBSB7 level of theory) of **IDC-1** involving elongation of the C–C bond indicates that at 1.86 \AA , the reaction goes through a maximum at $157 \text{ kcal mol}^{-1}$.

However, upon further elongation of the bond an exothermic concerted proton transfer occurs leading to $[\text{CH}_2\text{-O-C(H)=O}\cdots\text{H}\cdots\text{NH}_3]^{++}$, an intermediate HBRC of **2d** and NH_3 , which easily rearranges into the ter-body complex **HBRC-4** discussed above, see Figure 7.3b. Thus, the C–C bond cleavage of Scheme 7.3, if it occurs at all, is not expected to yield the distonic ion **2d** but rather **HBRC-4**'s dissociation products $\text{NH}_4^+ + \text{CH}_2=\text{O} + \text{HCO}^\cdot$. Experiment supports this proposal: the CID mass spectrum of Fig. 7.1f does not contain the tell-tale peak at m/z 45 indicative of the presence of the distonic ion **2c** or its isomer ionized methylformate [8d].

As discussed in Section 7.2.1, our experiments indicate that c. 25 % of the $\text{C}_2\text{H}_4\text{O}_2^{++}$ ions generated by loss of NH_3 are not glycolaldehyde ions $\text{HOCH}_2\text{C(=O)H}^{++}$ (**2a**) but rather their more stable enol isomer $\text{HOC(H)=C(H)OH}^{++}$ (**2b**). The enol ions cannot be generated from solitary glycolaldehyde ions: the fairly low energy requirement for the decarbonylation of **2a** into $\text{CH}_2\text{OH}_2^{++}$ (15 kcal mol⁻¹) [8b,c] prohibits isomerization into **2b** by a 1,3-H shift (32 kcal mol⁻¹, this work). However, the co-generation of **2b** can readily be rationalized if a catalyzed transformation of **2a** is invoked.

In proton-transport catalysis (PTC), a base molecule abstracts a proton from its ionic partner, and subsequently back donates the proton to an alternative acceptor site on the ion [5]. In line with the pioneering computational studies of Radom et al. [11], this process is most efficient when the base molecule's proton affinity lies between the proton affinities of the donor and acceptor sites of the associated radical.

We propose that NH_3 acts as the base in the proton-transport catalysis mechanism depicted in the top part of Figure 7.4. The first step involves the barrierless abstraction of the methylene *proton* by the base in the ion-dipole complex **IDC-3**, which can readily be generated from the **HBRC-3a** ions depicted in Figure 7.3b.

The resulting ammoniated complex, **HBRC-7**, is very stable, having an enthalpy of formation of only 82 kcal mol⁻¹. Back-donation of the proton to the oxygen atom yields **IDC-4a**, which can be viewed as an ionized 1,2-dihydroxyethene- NH_3 complex. We note that in this catalyzed transformation, the proton affinity of the base, NH_3 , is higher than

the proton affinity of the acceptor site of the radical, $\text{HC}(-\text{O}^\bullet)=\text{CHOH}$. This is reflected on the difference in threshold energies for the generation of the dissociation products, $\text{NH}_4^+ + \text{HC}(=\text{O})-\dot{\text{C}}(\text{H})\text{OH}^+$ at $101 \text{ kcal mol}^{-1}$ and $\text{HOC}(\text{H})=\text{C}(\text{H})\text{OH}^{+\bullet} + \text{NH}_3$ at $114 \text{ kcal mol}^{-1}$. Since ions **HBRC-7** generated from **AE-1** are energy rich, their dissociation may account for the generation of ions **2b** by PTC and also contribute to the formation of NH_4^+ ions.

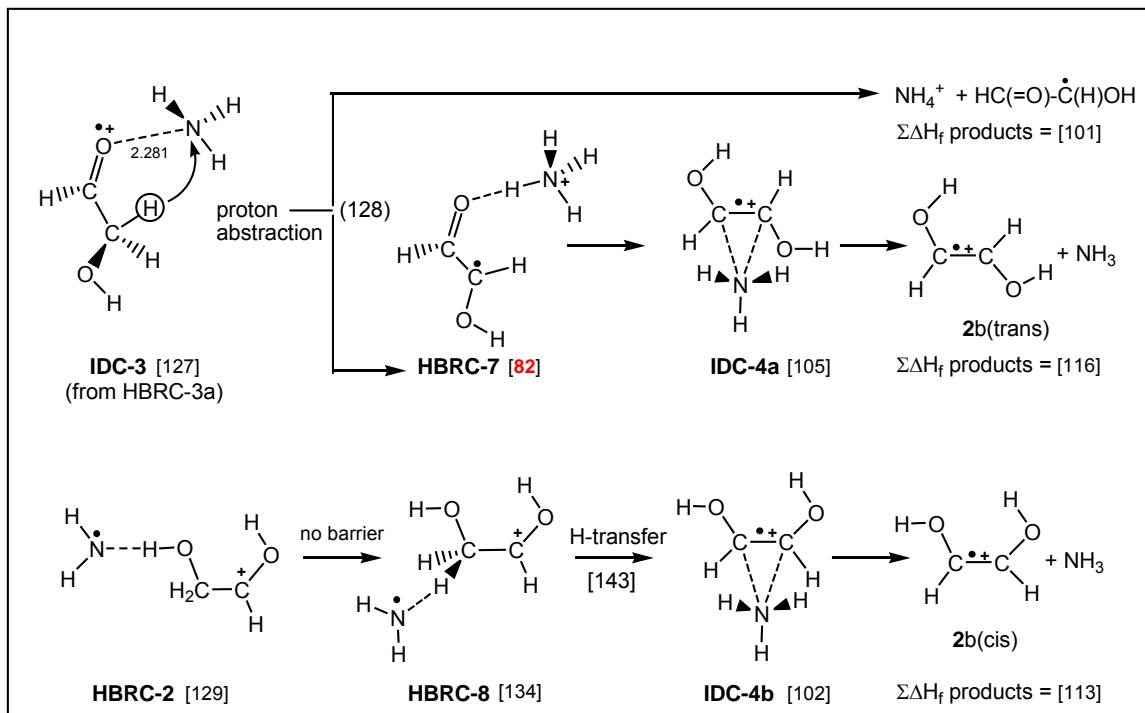


Figure 7.4 Transformation of the glycolaldehyde ion **2a** into the 1,2-dihydroxyethene ions **2b** by proton-transport catalysis. The numbers are 298 K enthalpies (in kcal mol^{-1}) derived from CBS-QB3 calculations.

The bottom part of Figure 7.4 depicts an alternative pathway for the conversion **2a** \rightarrow **2b**. In it the NH_2^\bullet component of **HBRC-2** migrates to the methylene group to form **HBRC-8**. The subsequent abstraction of the methylene hydrogen *atom* leads to the formation of **IDC-4b**, a rotational isomer of the ionized 1,2-dihydroxyethene- NH_3 complex, which dissociates into the *trans* isomer of **2b**. This route is less attractive because its overall energy requirement ($143 \text{ kcal mol}^{-1}$) is considerably higher than that for the proton-transport catalysis discussed above.

7.2.5 The dissociation mechanisms for metastable 2-aminoxyethanol ions : losses of CH_2O , $\text{CH}_2\text{OH}^\bullet$ and the generation of $\text{CH}_2\text{OH}_2^{*+}$

As shown in Figure 7.3b, the m/z 32, 46, and 47 ions also originate from rearrangement processes initiated in the **HBRC-2** ion. The NH_2^\bullet radical can migrate to the aldehyde carbon atom via a connecting transition state at $136 \text{ kcal mol}^{-1}$. The resulting covalently bound structure, **AE-4**, is not very stable and easily rearranges into the hydrogen bridged ions **HBRC-5/6**. Loss of the $\text{CH}_2\text{OH}^\bullet$ component of **HBRC-5** yields the observed protonated formamide, whereas **HBRC-6** readily generates the m/z 47 ion $\text{HC}(\text{OH})\text{NH}_3^{*+}$ by loss of its $\text{CH}_2=\text{O}$ component.

Proton abstraction by the $\text{CH}_2\text{OH}^\bullet$ moiety of **HBRC-5** would yield the $\text{CH}_2\text{OH}_2^{*+}$ ion at m/z 32. However, this process is 34 kcal mol^{-1} higher in energy than the simple bond cleavage of the **HBRC-5** complex into $\text{CH}_2\text{OH}^\bullet + \text{HC}(\text{OH})\text{NH}_2^+$. This makes it unlikely that **HBRC-5** acts as a major precursor for the generation of $\text{CH}_2\text{OH}_2^{*+}$. A more plausible route, see Figure 7.3b, involves the decarbonylation of the energy rich fraction of the incipient glycolaldehyde ions generated from **HBRC-3a/b**. This decarbonylation has been studied before by experiment and theory [8b,c] and appears to occur at the thermochemical threshold. This threshold lies at $159 \text{ kcal mol}^{-1}$, slightly below the energy requirement for the primary 1,4-H shift in **AE-1**.

7.2.6 Analysis of the deuterium labeled isotopomer, $\text{ND}_2\text{OCH}_2\text{CH}_2\text{OD}^{*+}$

Apart from the energy criterion discussed above, the proposed mechanisms must also satisfy the experimental observations of the D-labeled isotopomer $\text{ND}_2\text{OCH}_2\text{CH}_2\text{OD}$, whose MI spectrum is presented in Figure 7.1d.

The proposals of Figs. 7.3a/b imply that ions **HBRC-2a** are initially generated with a D atom bonded to the carbonyl oxygen and two D atoms and one H atom in the $\text{H}_2\text{N}---\text{H}-\text{O}$ moiety of the complex. The H/D atoms of this moiety may rapidly exchange (via **HBRC-1**

and **IDC-1**) so that the bridging atom becomes either H or D. Exchange reactions involving the CH₂ hydrogen atoms are unlikely: the primary 1,4-H shift leading to **AE-3b** is not expected to be reversible because all pathways leading therefrom are strongly exothermic. This scenario accounts for the observed losses of ND₂H, ND₂[•] and NDH[•] as exemplified by the *m/z* 61-63 cluster of peaks in the MI spectrum. It also accounts for the cluster of peaks at *m/z* 48, 49 and 50: D-labelled HC(OH)NH₂⁺ ions yield the peaks at *m/z* 48 and 49, while the HC(OH)NH₃⁺⁺ ions cleanly shift to *m/z* 50. In support of this interpretation we note that the peak intensity ratio (*m/z* 48 + *m/z* 49) : *m/z* 50 is close to the *m/z* 46 : *m/z* 47 ratio of the MI spectrum of the unlabelled compound.

The MI spectrum of Fig. 7.1d also displays a peak at *m/z* 60. This shows that to some extent the ammonia loss can also occur as ND₃. It suggests that the ND₂[•] component of **HBRC-2** can also abstract, via a suitably oriented conformer, the D atom bonded to the carbonyl oxygen.

The peaks at *m/z* 21 and *m/z* 20 in the MI spectrum correspond to the D-labelled ammonium ions ND₃H⁺ and ND₂H₂⁺ respectively. The ND₃H⁺ ion is the expected product ion from the route proposed in Figure 7.3b, whereas ND₂H₂⁺ could readily originate from the competing abstraction process presented in the top part of Figure 7.4.

As discussed in Section 7.2.4, this route may also lead to proton-transport catalysis yielding ions DOC(H)=C(H)OD⁺⁺ and ions HOC(H)=C(H)OD⁺⁺. These are expected to contribute to the intensities of the *m/z* 61 and *m/z* 62 peaks in the MI spectrum. Since CID mass spectra of mixtures of partially labelled C₂H_{4/5}O₂ ions are very complex, we have not attempted to verify this interpretation by experiment.

The labeling results shed further light on the mechanisms of formation of the CH₂OH₂⁺⁺ ions discussed in the previous Section. Dissociation of **HBRC-5**, by loss of formamide, is expected to yield both CH₂OHD⁺⁺ (*m/z* 33) and CH₂OD₂⁺⁺ (*m/z* 34) but a peak at *m/z* 34 is absent in the MI spectrum of Fig. 7.1d. Moreover this pathway cannot account for the presence of the peak at *m/z* 32 (CH₂OH₂⁺⁺). Our proposed route, involving decarbonylation of part of the incipient glycolaldehyde ions, provides a rationale: decarbonylation may

occur from both m/z 60 ($\text{HOCH}_2\text{C(=O)H}^{*+}$) and m/z 61 ($\text{DOCH}_2\text{C(=O)H}^{*+}$) ions yielding the observed $\text{CH}_2\text{OH}_2^{*+}$ (m/z 32) and $\text{CH}_2\text{OHD}^{*+}$ (m/z 33) ions respectively.

7.3 Summary

In this study we have examined the dissociation chemistry of low-energy 2-aminoxyethanol ions $\text{NH}_2\text{OCH}_2\text{CH}_2\text{OH}^{*+}$ (**AE-1**) using tandem mass spectrometry in conjunction with deuterium labelling and computational chemistry.

In the μs time-frame, these ions spontaneously dissociate into the following ions: protonated glycolaldehyde (m/z 61, $\text{HOCH}_2\text{CH(OH)}^+$), ionized glycolaldehyde in admixture with its enol (m/z 60, $\text{HOCH}_2\text{C(=O)H}^{*+}$ and $\text{HOC(H)=C(H)OH}^{*+}$), protonated formamide (m/z 46, HC(OH)NH_2^+), the methylene oxonium ion (m/z 32, $\text{CH}_2\text{OH}_2^{*+}$) and the ammonium cation (m/z 18, NH_4^+). The minor m/z 47 peak in the MI spectrum represents the generation of the distonic ion HC(OH)NH_3^{*+} .

A mechanistic analysis based upon CBS-QB3 model chemistry calculations indicates that the distonic ion $\text{NH}_3\text{OCH}_2\text{CHOH}^{*+}$ (**AE-3**) is a common intermediate in all dissociation pathways of **AE-1**. **AE-3** is generated from **AE-1** by a 1,4-H shift of moderate energy requirement. Once generated, ions **AE-3** readily isomerize into various interconverting hydrogen-bridged radical cations of which ionized glycolaldehyde- NH_3 complexes are key species. These complexes also account for the partial conversion of glycolaldehyde ions into their more stable enol counterpart by proton-transport catalysis.

References

- [1] (a) S.D. Richardson, *Trends in Anal. Chem.* 22 (2003) 666; (b) S.D. Richardson, *Anal. Chem.* 74 (2002) 2719.
- [2] V.Y. Taguchi, *Rapid Commun. Mass Spectrom.* 15 (2001) 455.
- [3] J.L. Holmes, C. Aubry, P.M. Mayer. *Assigning Structures to Ions in Mass Spectrometry.* CRC Press, Boca Raton, 2007.
- [4] P.J.A. Ruttink, P.C. Burgers, L.M. Fell, J.K. Terlouw, *J. Phys. Chem A* 102 (1998) 176.
- [5] (a) D.K. Bohme, *Int. J. Mass Spectrom. Ion Processes*, 115 (1992) 95 ; (b) C.Y. Wong, P.J.A. Ruttink, P.C. Burgers, J.K. Terlouw, *Chem. Phys. Lett.* 387 (2004) 204 and references cited therein.
- [6] P.C. Burgers, J.K. Terlouw, in N.M.M. Nibbering (Ed.), *Encyclopedia of Mass Spectrometry*, vol. 4, Elsevier, Amsterdam, 2005, p. 173.
- [7] G. Bouchoux, F. Penaud-Berruyer, W. Bertrand, *Eur. J. Mass Spectrom.* 7 (2001) 351.
- [8] (a) J.K. Terlouw, C.G. de Koster, W. Heerma, J.L. Holmes, P.C. Burgers, *Org. Mass Spectrom.* 18 (1983) 222 ; (b) R. Postma, P.J.A. Ruttink, J.H. van Lenthe, J.K. Terlouw, *Chem. Phys. Lett.* 156 (1989) 245; (c) H.K. Ervasti, P.J.A. Ruttink, manuscript in preparation; (d) R. Flammang, M. Plisnier, G. Leroy, M. Sana, M.T. Nguyen, L.G. Vanquicken-borne, *Chem. Phys. Lett.* 186 (1991) 393 ; (e) B.J. Smith, M.T. Nguyen, L. Radom, *J. Am. Chem. Soc.*, 114 (1992) 1151 ; (f) N. Heinrich, Th. Drewello, P.C. Burgers, J.C. Morrow, J. Schmidt, W. Kulik, J.K. Terlouw, H. Schwarz, *J. Am. Chem. Soc.* 114 (1992) 3776.
- [9] (a) P.C. Burgers, C. Lifshitz, P.J.A. Ruttink, G. Schaftenaar, J.K. Terlouw, *Org. Mass Spectrom.* 24 (1989) 579 ; (b) G. Schaftenaar, R. Postma, P.J.A. Ruttink, P.C. Burgers, G.A. McGibbon, J.K. Terlouw, *Int. J. Mass Spectrom. Ion Processes* 100 (1990) 521.
- [10] P.R. Carlier, N. Deora, T. Crawford, *J. Org. Chem.* 71 (2006) 1592.
- [11] J.W. Gauld, L. Radom, *J. Am. Chem. Soc.* 119 (1997) 9831.
- [12] (a) S.G. Lias, J.E. Bartmess, J.F. Liebman, J.L. Holmes, R.O. Levin, W.G. Maillard, *J. Phys. Chem. Ref. Data*, 17 (Suppl. 1) (1988) ; (b) Yu-Ran Luo. *Handbook of Dissociation Energies in Organic Compounds*, CRC Press, Boca Raton 2003; (c) NIST Chemistry WebBook, NIST Standard Reference Data Base Number 69, National Institute of Standards and Technology. Gaithersburg, MD, August 2007.

Appendix to Chapter 7

Table 7.1 Energetic data for various dissociation products of ionized 2-aminoxyethanol derived from CBS-QB3 and selected CBS-APNO calculations [a].

Species		CBS-QB3	QB3	QB3	APNO	Expt	Ref./
	<i>m/z</i>	<i>E</i> (total) [0 K]	$\Delta_f H^0_0$	$\Delta_f H^0_{298}$	$\Delta_f H^0_{298}$	$\Delta_f H^0_{298}$	note
HOCH ₂ CH(OH) ⁺ + NH ₂ [•]	1a	61		152	148	147	-
HOCH ₂ CH(OH) ⁺	1a	-229.01653	106.6	102.6	102.4	-	[b]
HC(=O)CH ₂ OH ₂ ⁺	1b	-229.00695	112.6	108.3	107.9	-	[b]
NH ₂ [•]		-55.79117	45.7	45.1	44.9	45	[c]
HOCH ₂ C(=O)H ⁺ + NH ₃	2a	60		149	144	143	-
HOC(H)=C(H)OH ⁺ + NH ₃	2b	60		119	114	113	112
HOCH ₂ C(=O)H ⁺	2a	-228.35314	157.6	154.8	154.0	-	[d]
HOC(H)=C(H)OH ⁺ (cis)	2b	-228.40028	128.0	124.6	124.0	123	[e]
HOC(H)=C(H)OH ⁺ (trans)		-228.39561	130.9	127.7	126.9	-	[f]
OCH ₂ C(H)OH ⁺	2c	-228.33339	170.0	166.6	166.5	-	[g]
CH ₂ OC(H)OH ⁺	2d	-228.36750	148.6	145.4	145.0	-	-
NH ₃		-56.46019	-8.8	-10.5	-10.8	-11	[c]
TS AE-3b → <i>m/z</i> 60 (2a)		-284.81374	168.2	162.2	-	-	-
HC(OH)NH ₃ ⁺ + CH ₂ O	3a	47		133	128	128	-
HC(OH)NH ₃ ⁺	3a	-170.49411	159.5	155.4	154.7	-	-
CH ₂ O		-114.34411	-26.4	-27.3	-26.6	-26	[c]
HC(OH)NH ₂ ⁺ + CH ₂ OH [•]	4a	46		122	117	116	121
HC(OH)NH ₂ ⁺	4a	-169.96749	124.7	121.1	120.9	125	[d,i]
	4a₁	-169.96227	128.0	124.4	124.1	-	[d]
CH ₂ ONH ₂ ⁺	4b	-169.83951	205.0	201.7	202.6	-	-
CH ₂ OH [•]		-114.88817	-2.5	-4.2	-5.2	-4	[j]
CH ₃ C(H)OH ⁺ + NH ₂ O [•]		45		161	157	157	-
TS AE-1 → CH ₃ C(H)OH ⁺		45	-284.77013	175.9	170.6	-	-
CH ₃ C(H)OH ⁺		-153.87252	145.7	142.2	141.1	139	[h]
NH ₂ O [•]		-130.92056	15.8	14.3	15.4	-	-
CH ₂ OH ₂ ⁺⁺ + CO + NH ₃		32		162	159	158	158
CH ₂ OH ₂ ⁺⁺ + HC(=O)NH ₂		32		155	151	150	151
CH ₂ OH ₂ ⁺⁺		-115.14931	198.9	196.5	195.3	195	[h]
CO		-113.18197	-27.7	-26.9	-26.4	-26.5	[c]
HC(=O)NH ₂		-169.65355	-43.6	-46.0	-45.3	-44	[c]
NH ₄ ⁺ + HCO [•] + CH ₂ O		18		137	133	134	136
NH ₄ ⁺ + HC(=O)CHOH [•]		18		107	101	101	-
NH ₄ ⁺		-56.78320	153.8	151.1	150.6	151	[c]
HCO [•]		-113.70496	9.4	9.5	9.6	10	[j]
HC(=O)CHOH [•]		-228.09740	-47.2	-49.7	-49.6	-	-

[a] $E_{\text{(total)}}$ in Hartrees, all other components, including the ZPE scaled by 0.99, are in kcal mol⁻¹; [b] calculation refers to the most stable conformer as reported in ref. 7 [c] ref. 12a; [d] calculation refers to the conformer shown in Fig. 7.2; [e] from ref. 12a but using IE = 8.62 eV, not 9.62 eV (misprint); [f] calculation refers to the conformer of Fig. 7.4; [g] calculation refers to the conformer of Scheme 7.3; [h] experimental value from ref. 3; [i] experimental value from ref. 3, which uses -44.5 kcal mol⁻¹ as the 298 K enthalpy of formation of formamide from ref. 12c; the CBS-QB3 and CBS-APNO values are -46.0 and -45.3 kcal mol⁻¹ respectively; [j] ref. 12b.

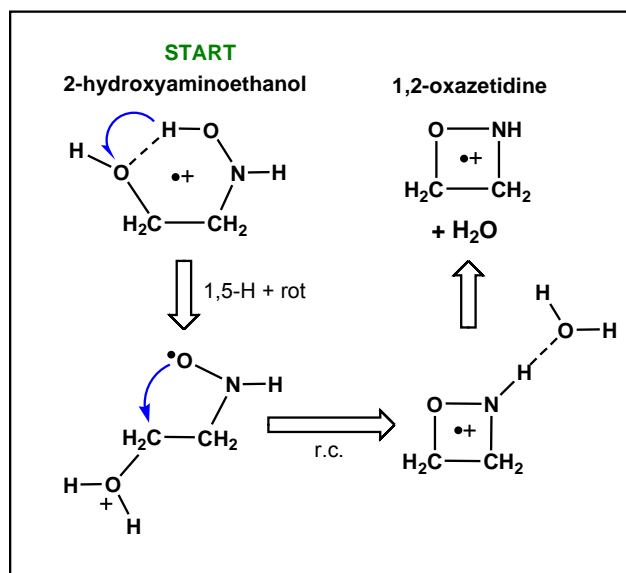
Table 7.2 Energetic data [a] derived from CBS-QB3 calculations of stable isomers and connecting transition states involved in the dissociation chemistry of ionized 2-aminoxethanol (AE-1).

Ionic species		B3LYP/CBSB7 E(total)	CBS-QB3 E(total) [0K]	ZPE	QB3 $\Delta_f H^0_0$	QB3 $\Delta_f H^0_{298}$	$\langle S^2 \rangle$
AE-1a	(Scheme 7.1)	-285.34536	-284.82107	63.3	143.9	137.5	0.77
AE-1b	(Figure 7.3a)	-285.32671	-284.80312	62.7	155.2	149.3	0.77
AE(N)-1	(Figure 7.2)	-285.63142	-285.12150	63.4	-44.6	-50.7	-
AE(N)-2	(Figure 7.2)	-285.63745	-285.12518	63.8	-46.9	-53.3	-
AE-2	(Scheme 7.2)	-285.31049	-284.78503	63.3	166.5	160.0	0.76
AE-3a	(Figure 7.3a)	-285.33139	-284.81028	63.5	150.7	144.6	0.76
AE-3b	(Figure 7.3a)	-285.32185	-284.80118	63.3	156.4	150.4	0.76
AE-3b ₁	(Figure 7.3a)	-285.31859	-284.79577	62.6	159.8	154.1	0.77
AE-4	(Figure 7.3b)	-285.37330	-284.85345	62.8	123.6	117.4	0.77
TS AE 1a → 1b		-285.32327	-284.80272	62.3	155.4	149.2	0.77
TS AE 1a → 2		-285.30154	-284.77520	60.7	172.7	165.8	0.76
TS AE 1a → 3b		-285.30193	-284.78040	61.0	169.4	162.6	0.78
TS AE 1b → 3a		-285.30655	-284.78467	61.0	166.8	160.0	0.79
TS AE 3a → 3b		-285.31706	-284.79807	62.5	158.4	152.0	0.76
TS AE 3b → 3b ₁		-285.31658	-284.78909	62.4	164.0	158.1	0.78
IDC-1	(Figure 7.3a)	-285.34494	-284.81562	61.1	147.3	142.0	0.77
IDC-2	(Scheme 7.2)	-285.36316	-284.83185	58.0	137.2	132.8	0.77
TS AE 2 → IDC 2		-285.29012	-284.76615	59.3	178.4	172.3	0.76
TS AE 3b ₁ → IDC 1		-285.31837	-284.79414	62.0	160.8	154.9	0.77
HBRC-1	(Figure 7.3a)	-285.33748	-284.81701	59.9	146.5	141.2	0.76
HBRC-2	(Figure 7.3a)	-285.35486	-284.83549	59.2	134.9	129.0	0.76
HBRC-3a	(Figure 7.3b)	-285.38561	-284.85707	60.5	121.3	116.0	0.76
HBRC-3b	(Figure 7.3b)	-285.36620	-284.84980	58.4	125.9	120.3	0.76
HBRC-4	(Figure 7.3b)	-285.39749	-284.87845	58.1	107.9	104.3	0.76
HBRC-5	(Figure 7.3b)	-285.41128	-284.88688	60.9	102.6	97.5	0.76
HBRC-6	(Figure 7.3b)	-285.38726	-284.86617	61.3	115.6	110.7	0.76
[CH ₂ -O-N(H)••H••O(H)CH ₂] ⁺⁺		-285.27300	-284.74215	59.2	193.4	189.0	0.76
[CH ₂ -O-N(H ₂)••H••O=CH ₂] ⁺⁺		-285.30503	-284.78464	59.9	166.8	161.9	0.76
TS IDC 1 → HBRC 1		-285.33458	-284.82069	58.4	144.2	138.5	0.76
TS HBRC 1 → 2		-285.33208	-284.81267	59.6	149.2	143.7	0.76
TS HBRC 2 → 3b		-285.35363	-284.83649	57.4	134.2	128.5	0.76
TS HBRC 2 → 5		-285.34207	-284.82498	59.7	141.5	135.8	0.76
TS HBRC 3b → 3a		-285.36530	-284.83883	59.0	132.8	127.5	0.76
TS HBRC 3a → 4		-285.37314	-284.83722	59.8	133.8	128.3	0.81
TS HBRC 5 → 6		-285.36445	-284.83851	58.4	133.0	127.5	0.76
IDC-3	(Figure 7.4)	-285.37067	-284.83880	59.8	132.8	127.4	0.77
IDC-4a	(Figure 7.4)	-285.40272	-284.87498	61.8	110.1	105.0	0.76
IDC-4b	(Figure 7.4)	-285.40844	-284.87961	62.1	107.2	102.0	0.76
HBRC-7	(Figure 7.4)	-285.43833	-284.91141	62.0	87.2	81.6	0.81
HBRC-8	(Figure 7.4)	-285.34267	-284.82347	59.0	142.4	137.5	0.76
TS HBRC 8 → IDC 4b		-285.33502	-284.82347	56.9	148.5	143.1	0.76

[a] $E_{(\text{total})}$ in Hartrees, all other components, including the ZPE scaled by 0.99, are in kcal mol⁻¹

Chapter 8

A mechanistic study of the prominent loss of H₂O from ionized 2-hydroxyaminoethanol



Tandem mass spectrometry experiments on the HCl salt of 2-hydroxyaminoethanol reveal that low-energy ions HOCH₂CH₂NHOH⁺ dissociate by loss of H₂O with remarkable efficiency (*c.* 10%). Analysis of its high energy collision-induced dissociation (CID) mass spectrum leaves little doubt that the resulting *m/z* 59 ion is the cyclic 1,2-oxazetidine ion, whose elusive neutral counterpart has not yet been identified by experiment.

A mechanistic analysis using the CBS-QB3 model chemistry indicates that the dissociation chemistry of HOCH₂CH₂NHOH⁺ is entirely different from that of the structurally related ions HOCH₂CH₂ONH₂⁺ and HOCH₂CH₂OH⁺. It involves a 1,5-H transfer in one of its stable conformers that leads to a hydrogen-bridged radical cation of the 1,2-oxazetidine ion and a water molecule. In support of this proposal the isotopologues DOCH₂CH₂NDOD.DCl and HOCH₂CD₂NHOH.HCl, upon ionization (almost) exclusively lose D₂O and H₂O respectively.

The work described here has been published previously in an article under the same title : K.J. Jobst, S. Joguee, R.D. Bowen, J.K. Terlouw, *Int. J. Mass Spectrom.* (2010) in press.

8.1 Introduction

Some ten years ago, two unexpected disinfection by-products in chlorinated drinking water samples were tentatively identified as halogenated aminoxyalcohols [1] on the basis of various mass spectrometric experiments. This proposal was rather speculative (and as established recently, erroneous [2]) because hardly any information was available about the dissociation characteristics of ionized aminoxyalcohols. This prompted our combined experimental and theoretical study of ionized 2-aminoxyethanol, $\text{HOCH}_2\text{CH}_2\text{ONH}_2$, as a model compound [3]. Its low energy (metastable) molecular ions display a surprisingly rich chemistry involving five major dissociation pathways. The model chemistry calculations indicate that a 1,4-H shift in the molecular ion generates the ion-molecule complex $[\text{HOCH}_2(\text{C}=\text{O})\text{H}^+]\cdots[\text{NH}_3]$, which acts as the common reacting configuration. This is in contrast to the related 1,2-ethanediol ion $\text{HOCH}_2\text{CH}_2\text{OH}^+$ whose dissociation chemistry is triggered by C-C bond cleavage [4]. However, proton transport catalysis (PTC) features as an important component of both mechanisms [5]. The present study deals with 2-aminoxyethanol's isomer $\text{HOCH}_2\text{CH}_2\text{NHOH}$, 2-hydroxyaminoethanol. This compound is not commercially available and all our efforts to isolate and purify it in a synthetic procedure involving the reduction of 2-nitroethanol (see Experimental) were unsuccessful. However, its (very hygroscopic) HCl salt is sufficiently stable at room temperature to be used instead for our tandem mass spectrometric measurements.

These experiments revealed that metastable ions $\text{HOCH}_2\text{CH}_2\text{NHOH}^+$ (**HE-1**) show a remarkably abundant (~10 % of the main beam of ions) loss of H_2O to form m/z 59 ions $\text{C}_2\text{H}_5\text{NO}^+$ as the only reaction. Further, the labelled isotopologue $\text{DOCH}_2\text{CH}_2\text{NDOD}^+$ (almost) exclusively loses D_2O , whereas upon collisional activation only one important competing dissociation occurs, *viz.* the direct bond cleavage to give $^+\text{CH}_2\text{NDOD} + \cdot\text{CH}_2\text{OD}$. Unfortunately, the structure of the product ion cannot readily be assigned on the basis of a comparison of its collision induced dissociation (CID) mass spectrum with reference spectra. A critical evaluation of the $\text{C}_2\text{H}_5\text{NO}^+$ system of ions has not been included in the

book of Ref. 6a and none of the reported CID mass spectra [7,8] matches the spectrum obtained.

These intriguing and challenging observations inspired us to initiate a quest for plausible mechanisms for the H₂O elimination from *metastable* ions **HE**-1, using the model chemistry approach of our study of the loss of water from ionized ethyl acetate [9]. An important precondition of this approach imposed by the experimental data is that none of the stable intermediates, connecting transition states or products of a viable calculated mechanism should lie significantly higher in energy than the thermochemical threshold for direct bond cleavage to ⁺CH₂NHOH (*m/z* 46) + [•]CH₂OH.

Although the involvement of hydrogen-bridged radical cations (HBRCs) [10] remains a common thread, the first step of our proposed mechanism for dissociation of **HE**-1 is entirely different from that of either HOCH₂CH₂ONH₂^{•+} [3] or HOCH₂CH₂OH^{•+} [4]. It involves a unique 1,5-H transfer that leads to the formation of an ion-dipole complex comprising the four membered ring species ionized 1,2-oxazetidine [11] and a water molecule. This ion easily rearranges to a more stable HBRC but is otherwise resistant towards further isomerization and eventually loses water to yield the 1,2-oxazetidine ion (*m/z* 59), whose neutral counterpart is predicted to be stable by theory but it has never been characterized in the condensed phase [11].

8.2 Results and discussion

8.2.1 Identification of the *m/z* 59 ions generated from metastable ions HOCH₂CH₂NHOH^{•+}

Before considering various mechanistic proposals for the water loss from metastable ions HOCH₂CH₂NHOH^{•+}, we will first focus on the structure assignment of the C₂H₅NO^{•+} product ion. In lieu of a critical review [6a] of this system of ions, we have compiled the selection of isomers shown in Figure 8.1 with their computed enthalpies of formation. As pointed out in the Introduction, the energy required for the water loss must not exceed that for the direct bond cleavage to CH₂NHOH⁺ (*m/z* 46) + CH₂OH[•], which is an important reaction in the EI and CID mass spectra shown in Figs. 8.2 and 8.3b. This criterion

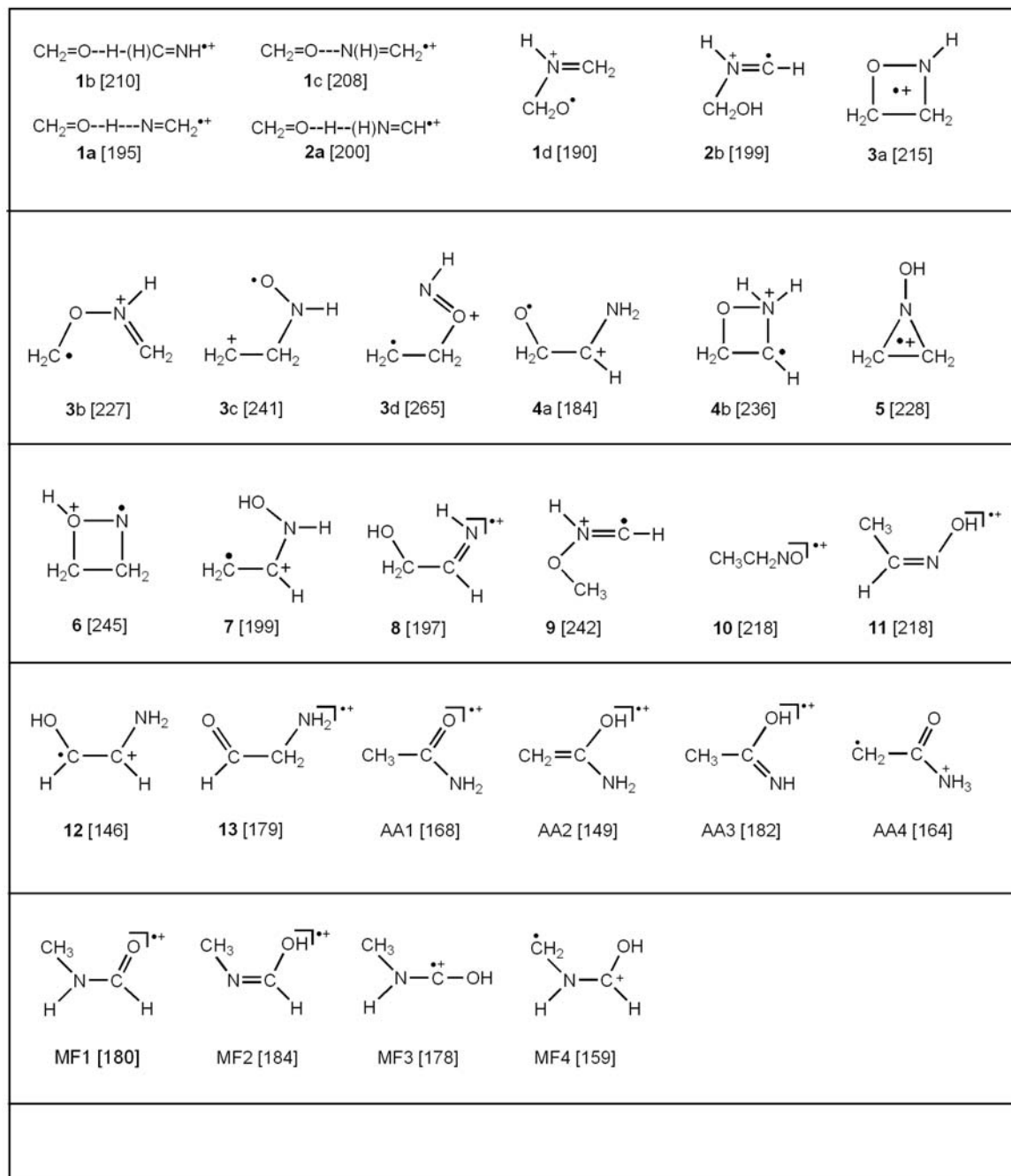


Figure 8.1 Structures of m/z 59 $\text{C}_2\text{H}_5\text{NO}^{+\cdot}$ product ions and their enthalpies of formation (298 K values in kcal mol^{-1} derived from CBS-QB3 calculations, see Table 8.1 in the Appendix to this Chapter).

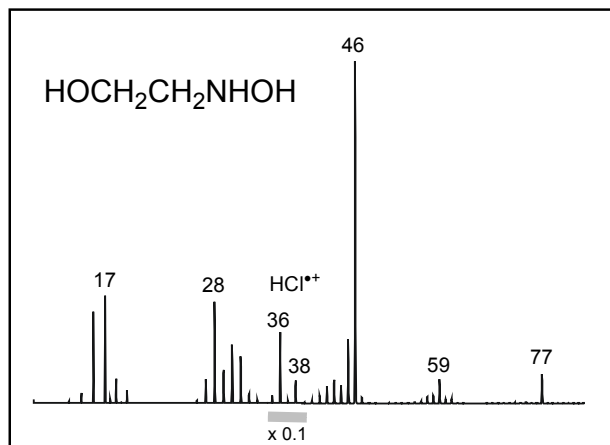


Figure 8.2 70 eV EI mass spectrum of 2-hydroxyaminoethanol hydrochloride.

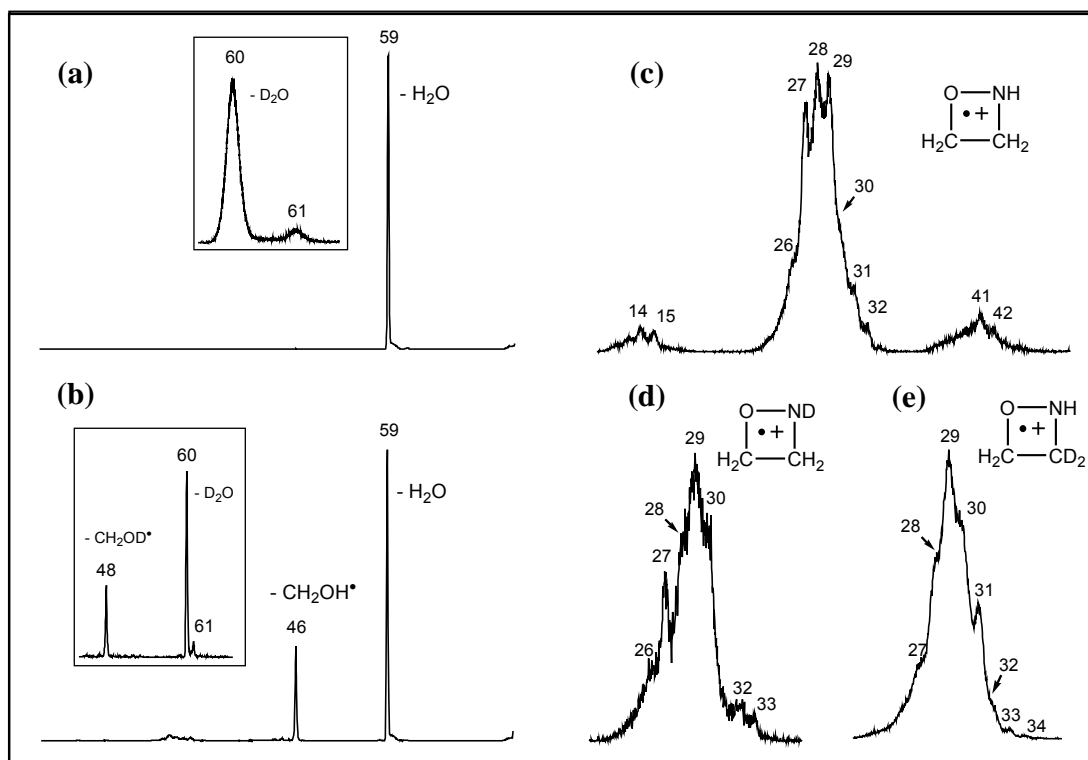


Figure 8.3 MI and CID spectra of molecular ions HOCH₂CH₂NHOH⁺, items (a) and (b) respectively. The insets refer to the corresponding spectra of the isotopologue DOCH₂CH₂NDOD⁺. Item (c) is the CID spectrum of the *m/z* 59 ions generated from metastable ions HOCH₂CH₂NHOH⁺ while items (d) and (e) represent the corresponding partial spectra of the *m/z* 60 and 61 ions from DOCH₂CH₂NDOD⁺ and HOCH₂CD₂NHOH⁺, respectively. Spectra (c) and (d) contain a partially resolved peak for loss of H[•] with an intensity of ~ 30 % of the base peak.

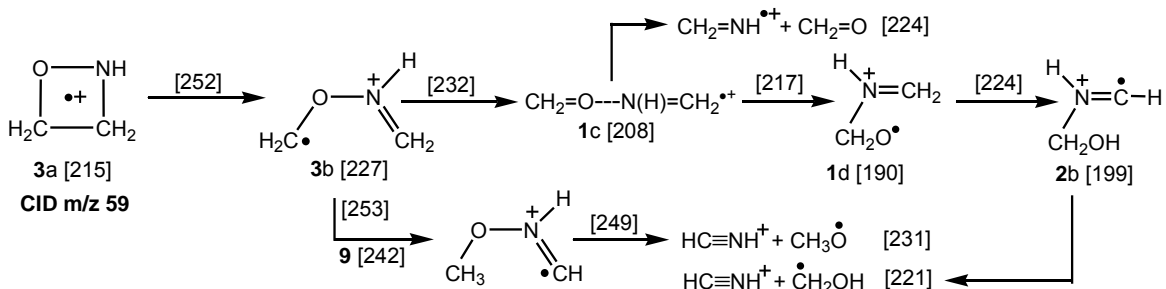
dictates an upper limit of $229 \text{ kcal mol}^{-1}$ for the enthalpy of formation of the $\text{C}_2\text{H}_5\text{NO}^+$ ions that comprise the single intense peak at m/z 59 in the MI mass spectrum of Fig. 8.3a. The previously studied ions **MF1**–**4** and **AA1**–**4** of Figure 8.1 satisfy this criterion, but the prominent structure diagnostic peaks of their CID mass spectra [7,8] are not compatible with the spectrum of Fig. 8.3c : ions **AA1**–**4** predominantly lose NH_3 , NH_2^\bullet and CH_3^\bullet to generate ions of m/z 42 – 44, whereas ions **MF1**, **MF2** and **MF3** produce intense peaks at m/z 30, 42 and 44 for loss of HCO^\bullet , OH^\bullet and CH_3^\bullet respectively. The CID mass spectrum of the distonic ion **MF4** resembles that of **MF1** but it displays a unique intense charge stripping peak at m/z 29.5. In this context we note that ions **10** – **13** of Fig. 8.1 (whose CID mass spectra are not available) are unlikely candidates as well. Simple thermochemical considerations lead to the expectation that ions **10** and **11** will show a prominent loss of CH_3^\bullet upon collisional activation. Acetaldoxime ions **11** may also readily lose H_2O as witnessed by the prominent m/z 41 peak in its reported EI mass spectrum [6d] and this may also be true for the enol ion **12**, which probably represents the global minimum of the $\text{C}_2\text{H}_5\text{NO}^+$ system of ions. Alternatively, ion **12** may rearrange into its 1,3-H shift isomer **13**, $\text{H}_2\text{NCH}_2\text{C}(\text{H})=\text{O}^+$, and then readily dissociate into CH_2NH_2^+ (m/z 30) + HCO^\bullet , rather than HCO^+ (m/z 29) + $\text{CH}_2\text{NH}_2^\bullet$, which requires $\sim 45 \text{ kcal mol}^{-1}$ more energy [6a,c].

The CID mass spectrum of Fig. 8.3c displays a prominent pair of ill resolved broad peaks at m/z 29 and m/z 28. These peaks likely represent ions CH_3N^+ ($\text{CH}_2=\text{NH}^+$ or HCNH_2^+ [6a]) and CH_2N^+ ($\text{HC}=\text{NH}^+$), rather than C_2H_5^+ / C_2H_4^+ . In line with this proposal, the m/z 29 peak shifts to m/z 30 in the CID mass spectrum of the $\text{C}_2\text{H}_4\text{DNO}^+$ ions, see Fig. 8.3d, generated from the isotopologue $\text{DOCH}_2\text{CH}_2\text{NDOD}^+$. Since the D_2O loss is (almost) specific, it is a sound assumption that the methylene hydrogens do not readily exchange with the D-atoms by unimolecular processes. Thus, it is impossible that a D-atom would become incorporated at a carbon atom in C_2H_5^+ . We further note that the large width of the peaks ($T_{0.5}$ is $\sim 600 \text{ meV}$) indicates that the dissociation of the m/z 59 ions to m/z 29 and m/z 28 ions is associated with a substantial reverse energy barrier.

Another feature of Fig. 8.3c is the cluster of unresolved peaks at m/z 24 – 27, corresponding to ions C_2^{*+} , C_2H^+ , $C_2H_2^{*+}$ and $C_2H_3^+$, which attests to the C-C atom connectivity of the $C_2H_5NO^{*+}$ ions. Confirmation of this deduction is found in the observation that these peaks do not shift in the CID spectrum of Figure 8.3d.

In summary, the structure of the $C_2H_5NO^{*+}$ ion must have the following characteristics : (i) its heat of formation ($\Delta_f H^{298}$) must not exceed $229 \text{ kcal mol}^{-1}$; (ii) the ion must have a structure motif ($CH_2=NH$ or $H-C-NH_2$) that accounts for the generation of m/z 29 and m/z 28 ions upon collisional activation with a substantial kinetic energy release; (iii) the ion has a C-C atom connectivity.

Based on these characteristics, only ions **3a**, **4a**, **7** and **8** of Figure 8.1 retain their candidacy as potential product ions. However, it is unlikely that we are dealing with ions **7** or **8**, considering that their CID mass spectra are expected to show a significant m/z 41 peak for loss of H_2O : in these ions, the thermochemically favourable generation of $CH_2=C=NH^{*+} + H_2O$ ($\Sigma\Delta H_f = 189 \text{ kcal mol}^{-1}$) can be realized by a simple 1,3-H shift.



To decide between the remaining possibilities, namely the cyclic ion **3a** and the distonic ion **4a**, we have explored their dissociation characteristics. Theory indicates that ring-opening of ion **3a** to **3b** requires less energy than that to **3c** or **3d**, see Fig. 8.1, but even the C-C bond cleavage is associated with a substantial reverse barrier. As shown below (Scheme 8.1), the computed dissociation sequence $3a \rightarrow 3b \rightarrow 1c \rightarrow CH_2=NH^{*+}$ (m/z 29) and the competing rearrangements $3b \rightarrow 1c \rightarrow 1d \rightarrow 2b \rightarrow HC=NH^+$ (m/z 28) and $3b \rightarrow 9 \rightarrow$

$\text{HC}=\text{NH}^+$ (m/z 28) may account for the pair of broad peaks at m/z 29 and m/z 28 in the CID mass spectrum of Fig. 8.3c.

In contrast, theory predicts that the dissociation $\mathbf{4a} \rightarrow \text{H}-\text{C}-\text{NH}_2^{\bullet+}$ (m/z 29) + $\text{CH}_2=\text{O}$ is a barrierless reaction, which does not account for the experimental observations. In addition, a simple 1,4-H shift in ion $\mathbf{4a}$ would produce ion $\mathbf{8}$ and lead, as argued above, to a significant loss of water, which is not observed.

Thus we propose that the CID mass spectrum of Fig. 8.3c represents the cyclic ion $\mathbf{3a}$, ionized 1,2-oxazetidine, whose elusive neutral counterpart has not (yet) been identified by experiment [11].

8.2.2 Does the loss of H_2O from $\text{HOCH}_2\text{CH}_2\text{NHOH}^{\bullet+}$ involve cleavage of the C-C bond ?

In our mechanistic analysis of the water loss from ionized 2-hydroxyaminoethanol ($\mathbf{HE1}$), we will first consider the selection of conformers $\mathbf{HE1a} - \mathbf{e}$ and their neutral counterparts $\mathbf{HEN1a} - \mathbf{e}$ shown in Figure 8.4.

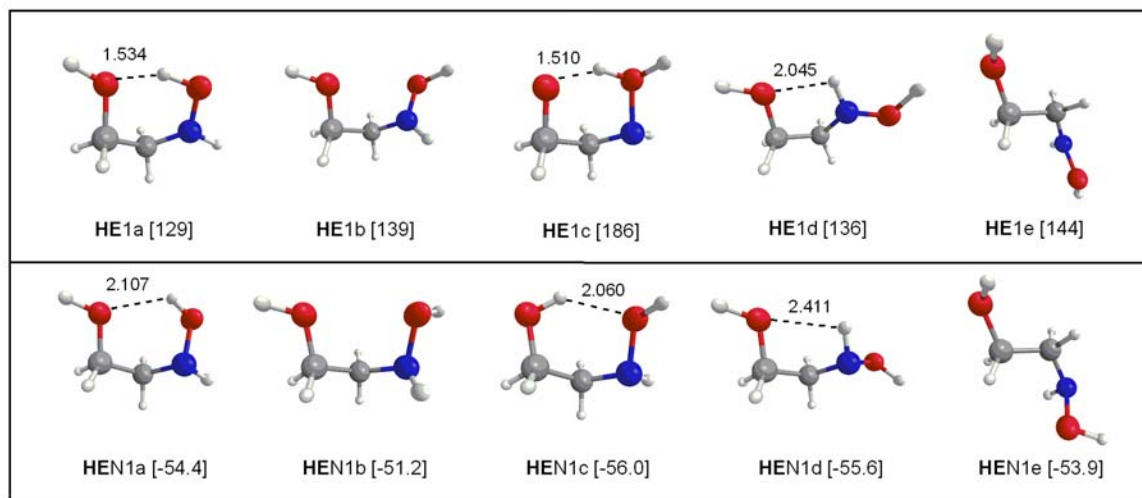


Figure 8.4 Optimized geometries of various conformers of ionized 2-hydroxyaminoethanol ($\mathbf{HE1a} - \mathbf{e}$) and their neutral counterparts ($\mathbf{HEN1a} - \mathbf{e}$). Optimized geometries of the intermediates and connecting transition states involved in the H_2O loss from $\mathbf{HE1}$ are shown in Figure 8.8 in the Appendix to this Chapter.

Surprisingly, the most stable ionic conformer, **HE1a**, is not the most stable neutral conformer : the internally hydrogen bridged conformer **HEN1c** is more stable by 1.6 kcal mol⁻¹. However, ionization of **HEN1c** does not yield a minimum while its related 1,5-H shift isomer **HE1c** lies an astounding 57 kcal mol⁻¹ higher in energy than **HE1a**. A plausible explanation for these remarkable results is that ionization takes place at the hydroxylamine moiety : the localized positive charge would repel the bridging hydrogen and thus raise the energy. Indeed, a charge distribution analysis supports this view and the transformation of the N-pyramidal geometry of neutrals **N1a – e** into the planar geometry of ions **HE1a – e** indicates the removal of a nitrogen lone pair electron.

The difference in the geometries of the ions and neutrals is also borne out by the substantial difference in vertical and adiabatic ionization energies : the calculations predict that vertical ionization of neutrals **N1a**, **N1b**, **N1c**, **N1d** and **N1e**, as it occurs during electron ionization, would yield excited ions at 158, 166, 172, 167 and 164 kcal mol⁻¹.

As becomes clear from Fig. 8.5, ions generated from **N1c** have sufficient energy to dissociate to CH₂NHOH⁺ (*m/z* 46) + CH₂OH[•], which may well explain the moderate intensity of the *m/z* 77 molecular ion relative to the *m/z* 46 peak in the EI mass spectrum of Fig. 8.2. On the other hand, neutrals **N1a**, **N1b**, **N1d** and **N1e** yield ions with onset energies that are quite high but insufficient to promote dissociation to the *m/z* 46 ion. This result is consistent with the remarkably high population of metastable ions, as witnessed by the *c.* 10 % abundance of the *m/z* 59 peak for loss of H₂O relative to the main beam in the MI mass spectrum. Interestingly, the metastable ions can still undergo C-C bond cleavage, albeit to generate the stable hydrogen-bridged radical cation **HBRC2** of Fig. 8.5. Although the formation of **HBRC2** appears to be a *cul-de-sac* rearrangement, these findings raise the intriguing question of whether another C-C bond cleavage initiates the loss of water from metastable ions **HE1**.

Figure 8.5 indicates that ion **HE1a** readily interconverts with its conformer **HE1b** via a rotational TS at 145 kcal mol⁻¹. The next step involves an energy demanding transfer of the hydroxylic hydrogen to the hydroxylamine group in concert with cleavage of the C-C

bond. The resulting ion, **HBRC1**, is not a minimum and rearranges to a ter-body complex [12], ion **TBC1a**, by elongation of the N-O bond. The long N-O bond (2.116 Å) is characteristic of a two-center three electron bond [13]. Loss of H₂O from **TBC1a** would yield the stable hydrogen-bridged radical cation ion **1a** as the *m/z* 59 product ion. However, theory predicts that **TBC1a** smoothly rearranges to the remarkably stable isomer **TBC1b**. These ions may subsequently generate *m/z* 47 and 49 ions with the same energy requirement as that for the loss of water. Signals at *m/z* 47 or 49 are not detectable in the MI mass spectrum of **HE1**, so we conclude that the water loss is not initiated by C-C bond cleavage.

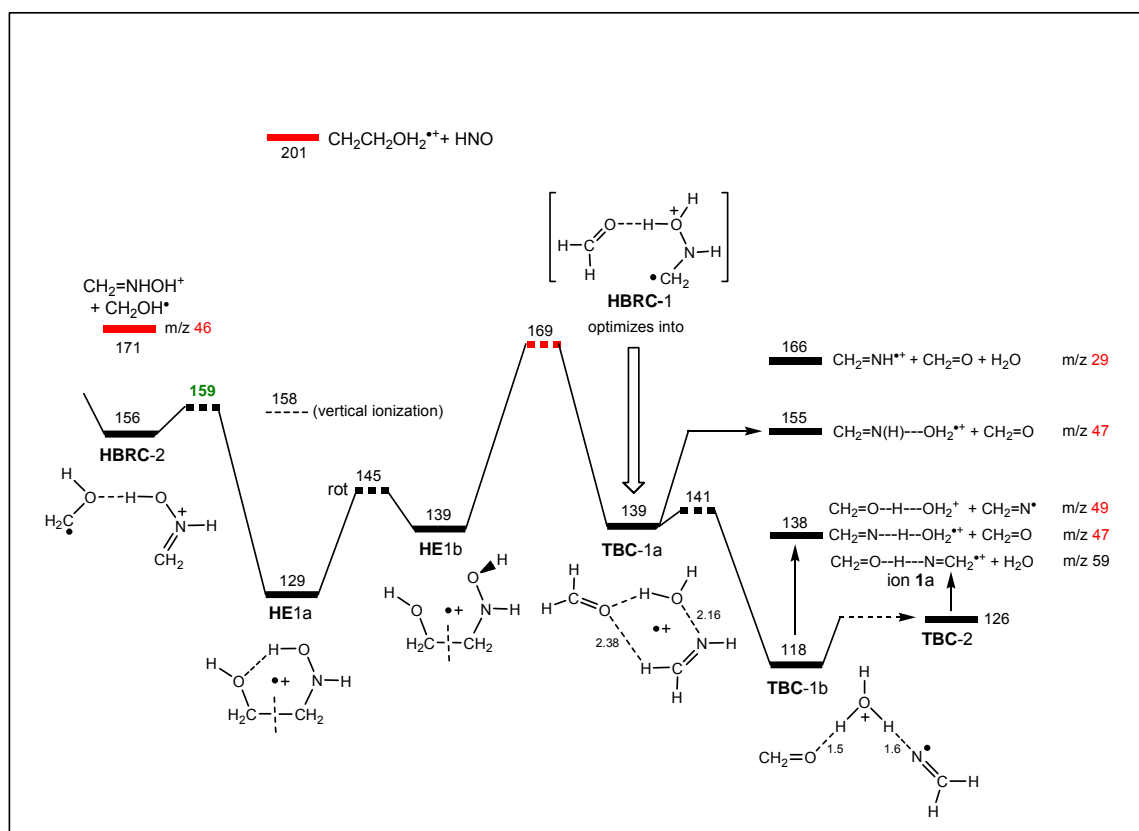


Figure 8.5 Energy diagram depicting the C-C bond cleavage of the hydroxyaminethanol ion **HE1a**. The numbers are CBS-QB3 derived 298 K enthalpies (in kcal mol⁻¹).

8.2.3 The proposed mechanism for the loss of H₂O from metastable ions **HE1**.

As shown in the previous Section, ion **HE1a** is the most stable conformer of ionized 2-hydroxyaminoethanol because of the favourable O-H-O interaction. Cleavage of the C-C bond of **HE1a**, while preserving the integrity of the hydrogen bridge, yields the remarkably stable ion **HBRC2**. In this Section, we will show that the key step in the water loss mechanism involves transfer of the bridging hydrogen of **HE1a** while the integrity of the C-C bond is preserved.

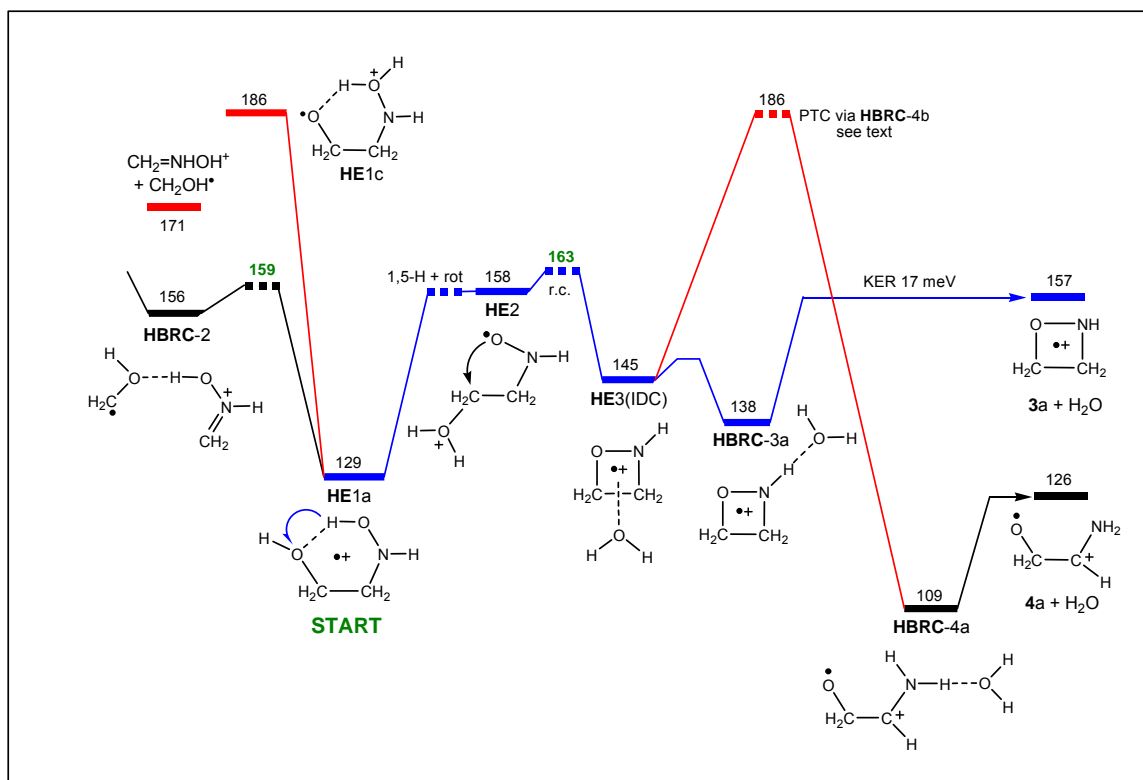
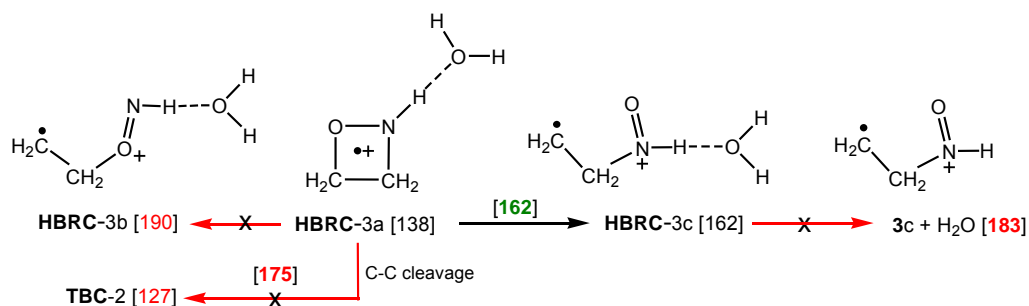


Figure 8.6 Energy diagram depicting the proposed mechanism for loss of water from 2-hydroxyaminoethanol ions **HE1a**. The numbers are CBS-QB3 derived 298 K enthalpies (in kcal mol⁻¹).

Figure 8.6 indicates that the isomerization **HE1a** → **HE2** is a continuously endothermic process involving transfer of the bridging hydrogen in concert with rotation of the C-C bond. Ion **HE2** is a reasonably stable species, which lies at 158 kcal mol⁻¹ and needs only

5 kcal mol⁻¹ of internal energy to ring-close to the ion-dipole complex **HE3** (IDC). Subsequent loss of water from **HE3** yields the cyclic species **3a**, ionized 1,2-oxazetidene. The calculations also show that **HE3** readily isomerizes into the more stable hydrogen-bridged radical cation **HBRC3a**. The significant stabilization enjoyed by **HBRC3a** with respect to water loss raises the intriguing question of whether further isomerization within the ion-molecule complex takes place.

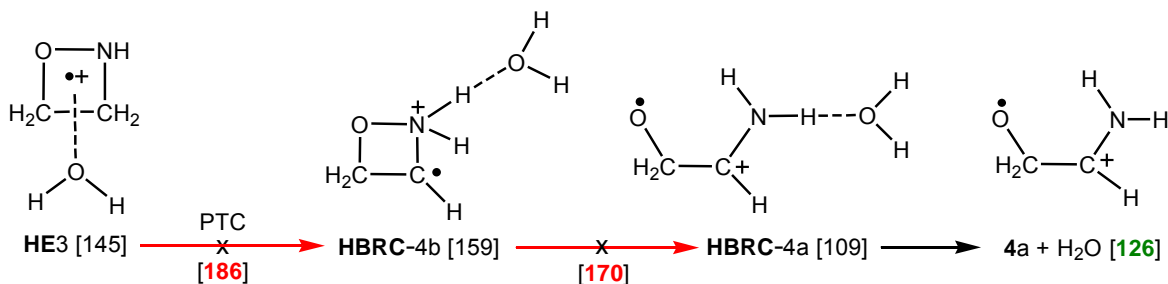
Scheme 8.2 indicates that fission of the C-C and C-N bonds is too energy demanding, but that the TS for ring-opening to **HBRC3c** lies slightly below the critical energy of the reaction **HE1a** → **HBRC3a**. This implies that a small fraction of the metastable **HE1** ions could communicate with ions **HBRC3c**, but the reaction is circuitous because of the high energy required for their subsequent dissociation to **3c** + H₂O.



Scheme 8.2

Another interesting question is whether the water molecule of **HE3** catalyzes the isomerization of **3a** to the energy rich ion **4a** by a process termed proton-transport catalysis (PTC) [5]. The proposed two-step reaction mechanism is depicted in Scheme 8.3. The first step involving PTC requires that the water molecule abstracts a methylene proton from **HE3** and transfers it to the nitrogen to generate **HBRC4b**. In the second step, **HBRC4b** ring-opens to **HBRC4a**. However, theory predicts that the PTC reaction does not occur because the associated TS lies 29 kcal mol⁻¹ above the dissociation threshold **3a** + H₂O. This result is not surprising considering the fact that the proton affinity of H₂O (165 kcal mol⁻¹) is considerably lower than that required to abstract the methylene proton (220

kcal mol⁻¹). These findings leave little doubt that incipient ions **HE3** and **HBRC3a** have no alternative but to dissociate into **3a** + H₂O.



Scheme 8.3

Thus, the mechanistic proposal of Fig. 8.6 agrees well with the experimental findings discussed in Section 8.2.1 in terms of the structure of the C₂H₅NO⁺ ions and the energy requirement of the reaction. The reverse barrier of the dissociation (6 kcal mol⁻¹, Fig. 8.6) is associated with a kinetic energy release (KER) of only 0.5 kcal mol⁻¹ (17 meV). If a covalent bond were cleaved, the KER would be expected to be significantly larger. However, as with the celebrated case of the H₂O loss from metastable *n*-propanol ions [4], the precursor to dissociation (**HE3**) is an ion-dipole complex and for such ions only a minor fraction of the excess internal energy is partitioned among translational degrees of freedom.

Finally, the predominant loss of D₂O from DOCH₂CH₂NDOD^{•+}, see inset of Fig. 8.3a, is readily explained by the proposed mechanism, as is the fate of the label : evidence that the N-H of ion **3a** is labelled is provided by the shift of the *m/z* 28 and 29 peaks in Fig. 8.3c to *m/z* 29 and 30 in Fig. 8.3d. Likewise, the isotopologue HOCH₂CD₂NHOH^{•+} specifically loses H₂O to yield *m/z* 61 ions whose CID mass spectrum displays prominent peaks at *m/z* 29 (DC=NH⁺) and *m/z* 31 (CD₂=NH^{•+}), see Fig. 8.3e.

Thus, we propose that 1,2-oxazetidine ions **3a** are generated via the mechanism proposed in Figure 8.6.

8.2.4 Alternative pathways for the loss of H₂O from HOCH₂CH₂NHOH^{•+}

To back up the above proposal we have performed a great many exploratory calculations of other pathways for the loss of water from metastable ions **HE1**. The most relevant of these are summarized in Figure 8.7.

An *a priori* alternative route to the formation of 1,2-oxazetidine ions **3a** involves the O-H-N bridged conformer **HE1d**, which communicates with **HE1a** via a double rotation. A 1,4-H shift in **HE1d** yields **HE5a** and **HE5b**, energetically equivalent rotamers of a distonic ion. Of these, **HE5b** may ring-close to **HBRC6**. The H₂O molecule therein acts as an efficient catalyst for the reaction **HBRC6** → **HBRC3b** → **3a** + H₂O, but the energy barrier for the prerequisite ring-closure is too great (179 kcal mol⁻¹). Considering the overall energy requirement (170 kcal mol⁻¹), ring-closure of **HE5a** to the three-membered species **HBRC5** may also be discounted.

Figure 8.7 also displays two routes involving a 1,3-H shift of a methylene H of the CH₂NH moiety of **HE1**. These are **HE1a** → **HE1d** → **HBRC7** → **7a** + H₂O and **HE1a** → **HE8** → **8** + H₂O. The TS for the 1,3-H shift associated with the first pathway (177 kcal mol⁻¹) is prohibitively high and the same undoubtedly obtains for the conversion **HE1a** → **HE8**, whose TS we could not locate. The observation that HOCH₂CD₂NHOH^{•+} loses H₂O only, shows that these two 1,3-H shifts do not occur.

The third 1,3-H shift depicted in Fig. 8.7, **HE1a** → **HE7**, involves a methylene H of the CH₂OH moiety of **HE1**. This 1,3-H shift has a high barrier at 175 kcal mol⁻¹ whereas the corresponding 1,4-H shift **HE1a** → **HE4** lies at 173 kcal mol⁻¹. The direct bond cleavage **HE1** → CH₂NHOH⁺ (*m/z* 46) lies at 171 kcal mol⁻¹, so that these processes are not expected to play an important role in the dissociation chemistry of the metastable ions **HE1**. However, the conversion **HE1** → **HE4** could account for the minor loss of HDO (~ 5 %) observed in the MI and CID mass spectra of DOCH₂CH₂NDOD^{•+}, see Fig. 8.3a/b. As shown in Scheme 8.4, ions **HE4** need only 4 kcal mol⁻¹ of internal energy to lose HDO to generate N-D labelled ions **MF4**. A collision experiment on the *m/z* 61 ions could confirm

the putative structure of ions **MF4**, but unfortunately the signal intensity was not sufficient to obtain a meaningful CID mass spectrum.

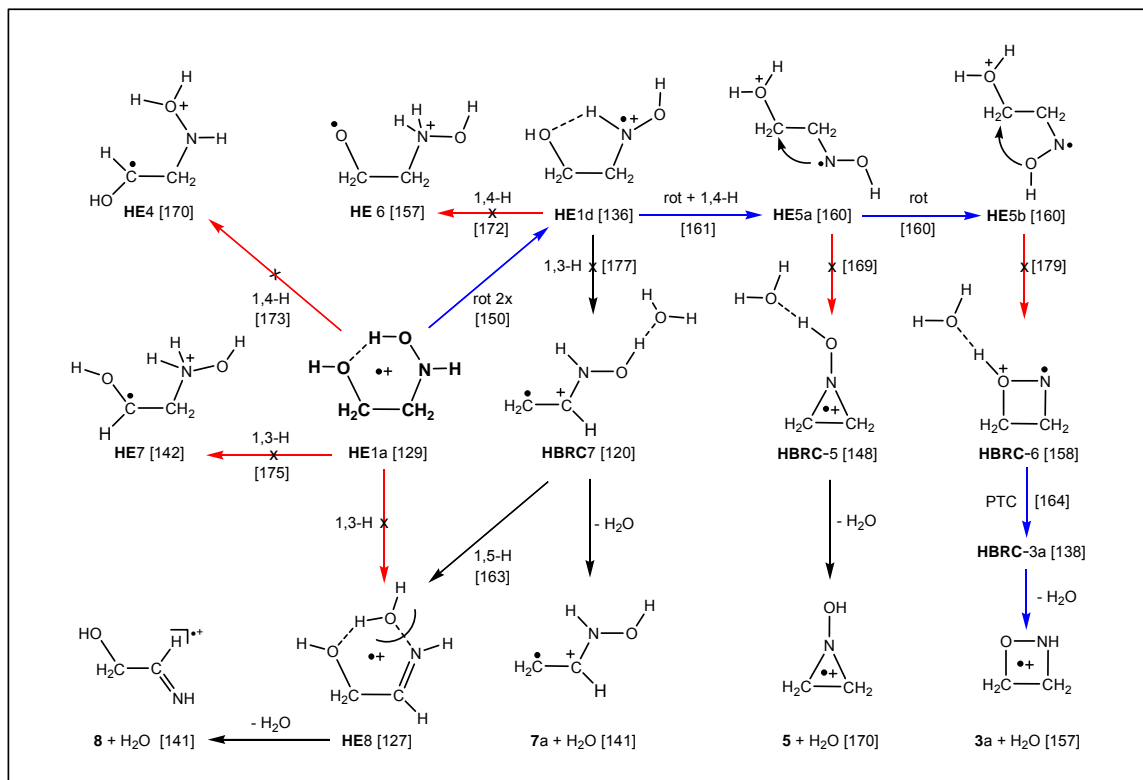
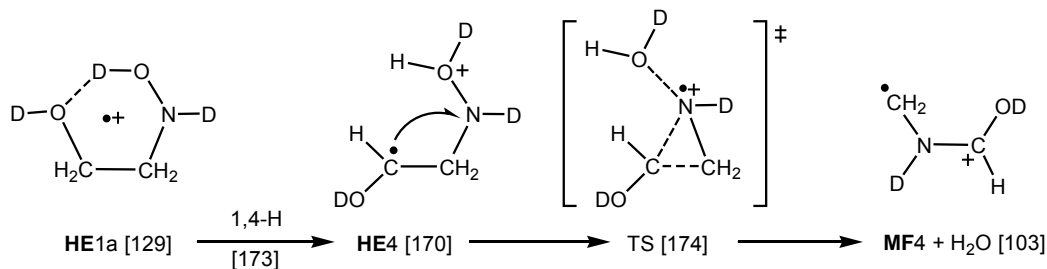


Figure 8.7 Alternative mechanisms for the loss of water from 2-hydroxyaminoethanol ions **HE1a**. The numbers in square brackets are CBS-QB3 derived 298 K enthalpies (in kcal mol⁻¹).



Scheme 8.4

It is conceivable that the above 1,3-H and 1,4-H shifts play a role in the water loss from **HE1** ions that dissociate in the ion source. Their CID mass spectra (not shown) display a prominent cluster of peaks at m/z 24 – 34, whose intensity distribution is close to that of the metastable ions of Fig. 8.3c. The spectra also display a peak of comparable intensity at m/z 41, which could be attributed to the loss of H₂O from the C₂H₅NO^{•+} isomers **7** or **8**. This proposal remains highly speculative because the relative intensity of the m/z 41 peak in the CID spectra appeared to vary by more than a factor of two during the evaporation of the samples, indicating that part of the source-generated m/z 59 ions originates from thermal decomposition products.

8.3 Summary

The results of our combined experimental and computational study leave little doubt that the loss of H₂O from metastable 2-hydroxyaminoethanol ions **HE1** generates 1,2-oxazetidene ions **3a**. As discussed in Section 8.2.1, ion **3a** is readily compatible with the features of the CID mass spectrum of Fig. 8.3c : the ion is characterized by a C-C atom connectivity and a CH₂=NH structure motif represented by the cluster of peaks at m/z 24 – 29. Further, our calculations indicate that the generation of m/z 28 and 29 ions from **3a** is associated with a high reverse barrier in line with the observed kinetic energy release.

A mechanistic analysis using the CBS-QB3 model chemistry indicates that the dissociation of ions **HE1** involves neither C-C bond cleavage (Section 8.2.2) nor 1,3-H or 1,4-H shift reactions (Section 8.2.4). Instead, see Section 8.2.3, theory predicts that the reaction is initiated by a 1,5-H transfer that leads to the formation of ionized 1,2-oxazetidene. The surprising efficiency of this reaction is readily explained by the substantial difference in adiabatic and vertical ionization energies : ions **HE1** are generated with minimum internal energies close to the calculated critical energy of the proposed mechanism. Finally, the results of experiments with the isotopologues DOCH₂CH₂NDOD^{•+} and HOCH₂CD₂NHOH^{•+} fit nicely with the above proposal.

References

- [1] V.Y. Taguchi, *Rapid Commun. Mass Spectrom.* 15 (2001) 455.
- [2] K.J. Jobst, M.A. Trikoupis, V.Y. Taguchi, J.K. Terlouw, manuscript in preparation
- [3] K.J. Jobst, P.J.A. Ruttink, J.K. Terlouw, *Int. J. Mass Spectrom.* 269 (2008) 165.
- [4] (a) P.J.A. Ruttink, P.C. Burgers, L.M. Fell, J.K. Terlouw, *J. Phys. Chem A* 102 (1998) 176; (b) J.L. Holmes, J.K. Terlouw, in N.M.M. Nibbering (Ed.), *Encyclopedia of Mass Spectrometry*, vol. 4, Elsevier, Amsterdam, 2005, p. 287.
- [5] R. Lee, P.J.A. Ruttink, P.C. Burgers, J.K. Terlouw, *Int. J. Mass Spectrom.* 255 (2006) 244 and references cited therein.
- [6] (a) J.L. Holmes, C. Aubry, P.M. Mayer. *Assigning Structures to Ions in Mass Spectrometry*. CRC Press, Boca Raton, 2007; (b) S.G. Lias, J.E. Bartmess, J.F. Liebman, J.L. Holmes, R.O. Levin, W.G. Maillard, *J. Phys. Chem. Ref. Data*, 17 (Suppl. 1) (1988) ; (c) Yu-Ran Luo. *Handbook of Dissociation Energies in Organic Compounds*, CRC Press, Boca Raton 2003; (d) NIST Chemistry WebBook, NIST Standard Reference Data Base Number 69, National Institute of Standards and Technology. Gaithersburg, MD, August 2007.
- [7] G.A. McGibbon, P.C. Burgers, J.K. Terlouw, *Int. J. Mass Spectrom.* 136 (1994) 191.
- [8] M.A. Trikoupis, P.C. Burgers, P.J.A. Ruttink, J.K. Terlouw, *Int. J. Mass Spectrom.* 217 (2002) 97.
- [9] R. Lee, P.J.A. Ruttink, P.C. Burgers, J.K. Terlouw, *Can. J. Chem.* 83 (2005) 1847.
- [10] P.C. Burgers, J.K. Terlouw, in N.M.M. Nibbering (Ed.), *Encyclopedia of Mass Spectrometry*, vol. 4, Elsevier, Amsterdam, 2005, p. 173.
- [11] (a) D.H. Magers, S.R. Davis, *J. Mol. Struct. (Theochem)* 487 (1999) 205; (b) A.L. Schwan, J. Warkentin in *Comprehensive Heterocyclic Chemistry II*, vol. 1b (Eds.: A.R. Katritzky, C.W. Rees, E.F.V. Scriven), Pergamon Press, Oxford, 1996, p. 969.
- [12] (a) G. van der Rest, L.B. Jensen, S. Abdel Azeim, P. Morgues, H.E. Audier, *J. Am. Soc. Mass Spectrom.* 15 (2004) 966; (b) G. van der Rest, J. Chamot-Rooke, P. Morgues, T.B. McMahon, H.E. Audier, *J. Am. Soc. Mass Spectrom.* 15 (2004) 966.
- [13] (a) P.M.W. Gill, L. Radom, *J. Am. Chem. Soc.* 110 (1988) 4931; (b) S. Humbel, I. Côte, N. Hoffmann, *J. Bouquant, J. Am. Chem. Soc.* 121 (1999) 5507.

Appendix to Chapter 8

Table 8.1 Energetic data derived from CBS-QB3 calculations [a] used to probe the dissociation chemistry of ionized 2-hydroxyaminoethanol.

Species and mass	CBS-QB3 E(total) [0 K]	QB3 $\Delta_f H^0_{298}$	Species and mass	CBS-QB3 E(total) [0 K]	QB3 $\Delta_f H^0_{298}$
Fig. 8.1 ion 1a 59	-208.48964	195.1	Fig. 8.1 ion 10 59	-208.45234	217.7
Fig. 8.1 ion 1b 59	-208.46601	210.0	Fig. 8.1 ion 11 59	-208.45250	217.5
Fig. 8.1 ion 1c 59	-208.46966	207.5	Fig. 8.1 ion 12 59	-208.56543	146.2
Fig. 8.1 ion 1d 59	-208.49580	189.9	Fig. 8.1 ion 13 59	-208.50780	179.0
Fig. 8.1 ion 2a 59	-208.48141	200.2			
Fig. 8.1 ion 2b 59	-208.48213	198.8	TS 3a → 3b	-208.39717	251.5
Fig. 8.1 ion 3a 59	-208.45631	214.6	TS 3b → 9	-208.39550	252.7
Fig. 8.1 ion 3b 59	-208.43716	227.0	TS 9 → m/z 28	-208.40230	249.1
Fig. 8.1 ion 3c 59	-208.41518	240.8	TS 3b → 1c	-208.42975	231.7
Fig. 8.1 ion 3d 59	-208.37704	264.6	TS 1c → 1d	-208.45341	217.1
Fig. 8.1 ion 4a 59	-208.50553	183.8	TS 1d → 2b	-208.44142	223.8
Fig. 8.1 ion 4b 59	-208.42220	235.9			
Fig. 8.1 ion 5 59	-208.43420	228.4	Fig. 8.1 ion MF-1 59	-208.51247	179.8
Fig. 8.1 ion 6 59	-208.40726	245.2	Fig. 8.1 ion MF-2 59	-208.50594	184.3
Fig. 8.1 ion 7 59	-208.48277	198.5	Fig. 8.1 ion MF-3 59	-208.51584	177.8
Fig. 8.1 ion 8 59	-208.48568	196.6	Fig. 8.1 ion MF-4 59	-208.54478	159.2
Fig. 8.1 ion 9 59	-208.41263	242.3	Fig. 8.1 neutral DP-1 58	-208.10729	69.1
			Fig. 8.1 neutral DP-2 58	-208.17041	29.9
			Fig. 8.1 neutral DP-3 58	-208.17183	28.9
CH ₂ =O 30	-114.34417	- 27.0	CH ₂ =O--H---OH ₂ ⁺ 49	-190.99545	81.5
CH ₂ OH [*] 29	-114.88817	- 5.2	CH ₂ =N--H--OH ₂ ⁺⁺ 47	-170.48072	165.1
CH ₃ O [*] 29	-114.87541	3.9	CH ₂ =N(H)--OH ₂ ⁺⁺ 47	-170.45287	182.4
CH ₂ =NH ⁺ 29	-94.10039	250.7	CH ₂ =NHOH ⁺ 46	-169.87875	177.3
H-C-NH ₂ ⁺⁺ 29	-194.10578	247.2	CH ₂ -CH ₂ -OH ₂ ⁺⁺ 45	-154.39990	176.8
HC≡NH ⁺ 28	-93.55430	226.4	CH ₂ =C=NH ⁺ 41	-132.16308	247.0
CH ₂ =N [*] 28	-93.82791	57.2	HNO 31	-130.32328	24.8
H ₂ O 18	-76.33750	- 57.0			

[a] E(total) in Hartrees, 298K enthalpies in kcal mol⁻¹.

Table 8.2 Energetic data [a] derived from CBS-QB3 calculations of stable isomers and connecting transition states involved in the H₂O loss from 2-hydroxyaminoethanol ions **HE-1**.

Ionic species		B3LYP/CBSB7 E(total)	CBS-QB3 E(total) [OK]	ZPE	QB3 $\Delta_f H^0$	QB3 $\Delta_f H^0_{298}$	$\langle S^2 \rangle$
HE-1a	(Figure 8.4)	-285.35978	-284.83556	63.5	135.4	128.9	0.77
HE-1b	(Figure 8.4)	-285.34046	-284.82105	62.8	144.5	138.6	0.77
HE-1c	(Figure 8.5)	-285.27125	-284.74447	63.3	192.6	185.9	0.76
HE-1d	(Figure 8.6)	-285.34622	-284.82530	63.0	141.9	135.7	0.77
HE-2	(Figure 8.5)	-285.31495	-284.79097	62.9	163.4	157.5	0.77
HE-3	(Figure 8.5)	-285.32520	-284.81197	60.8	150.2	145.2	0.77
HE-4	(Figure 8.6)	-285.29201	-284.77017	62.3	176.5	170.1	0.76
HE-5a	(Figure 8.6)	-285.30766	-284.78676	62.7	166.0	160.3	0.76
HE-5b	(Figure 8.6)	-285.30814	-284.78634	62.8	166.3	160.4	0.76
HE-6	(Figure 8.6)	-285.31428	-284.79130	63.6	163.2	156.8	0.76
HE-7	(Figure 8.6)	-285.33672	-284.81645	63.4	147.4	141.6	0.76
HE-8	(Figure 8.6)	-285.36753	-284.83922	61.3	133.1	127.4	0.87
HBRC-2a	(Figure 8.4)	-285.31604	-284.79503	60.5	160.8	155.7	0.77
HBRC-2b	(text)	-285.31818	-284.79725	60.5	159.5	154.4	0.76
HBRC-3a	(Figure 8.5)	-285.34062	-284.82301	61.0	143.3	137.8	0.77
HBRC-3b	(text)	-285.30697	-284.78556	58.3	166.8	161.8	1.13
HBRC-3c	(text)	-285.26569	-284.74042	57.8	195.1	190.4	0.99
HBRC-4a	(Figure 8.5)	-285.39141	-284.86930	60.6	114.2	109.0	0.76
HBRC-4b	(Figure 8.5)	-285.30393	-284.78940	60.7	164.4	159.0	0.76
HBRC-5	(Figure 8.6)	-285.32809	-284.80603	60.8	153.9	148.2	0.77
HBRC-6	(Figure 8.6)	-285.30847	-284.79012	59.6	163.9	158.1	0.76
HBRC-7	(Figure 8.6)	-285.37620	-284.85243	60.8	124.8	119.5	0.94
TBC-1a	(Figure 8.4)	-285.34977	-284.82238	58.3	143.7	139.1	0.90
TBC-1b	(Figure 8.4)	-285.37368	-284.85626	56.2	122.4	118.2	0.90
TBC-2	(Figure 8.4)	-285.35603	-284.84186	56.2	131.5	127.2	0.89
TS HE-1a → b		-285.33319	-284.80938	62.1	151.8	145.4	0.77
TS HE-1a → d		-285.32657	-284.80329	61.6	155.7	149.6	0.77
TS HE-1a → 4		-285.28650	-284.76499	60.3	179.7	172.9	0.77
TS HE-1d → 6		-285.29041	-284.76705	59.6	178.4	171.7	0.76
TS HE-1a → 7		-285.28343	-284.76208	60.2	181.5	175.1	0.80
TS HE-1d → 5a		-285.30618	-284.78445	62.6	167.5	161.1	0.76
TS HE-1a → 2		-285.31237	-284.78854	63.0	164.9	158.4	0.77
TS HE-1a → HBRC-2a		-285.31077	-284.78824	60.8	165.1	159.2	0.81
TS HE-1b → TBC-1a		-285.29602	-284.77247	58.3	175.0	169.4	0.78
TS HE-1a → HBRC-7		-285.28034	-284.75959	59.3	183.1	176.8	0.77
TS HE-2 → 3		-285.30661	-284.78320	61.1	168.3	162.6	0.77
TS HE-3 → HBRC-3a		-285.32392	-284.80972	60.8	151.6	146.0	0.77
TS HE-3 → HBRC-3c		-285.30027	-284.78463	58.0	167.4	162.2	0.76
TS HE-3 → HBRC-4b		-285.26048	-284.74542	59.6	192.0	186.0	0.76
TS HE-4 → MF4		-285.28889	-284.76517	60.7	179.6	173.5	0.76
TS HE-5a → 5b		-285.30711	-284.78546	62.6	166.9	160.5	0.76
TS HE-5a → HBRC-5		-285.29363	-284.77261	60.1	174.9	169.3	0.78
TS HE-5b → HBRC-6		-285.27585	-284.75750	59.9	184.4	178.7	0.76
TS HBRC-4b → a		-285.28454	-284.77067	59.9	176.1	170.4	1.20
TS HBRC-6 → 3a		-285.29607	-284.78075	60.8	169.8	164.0	0.77
TS TBC-1a → 1b		-285.33691	-284.81986	55.9	145.3	141.0	0.87

[a] $E_{(\text{total})}$ in Hartrees, all other components, including the ZPE scaled by 0.99, are in kcal mol⁻¹

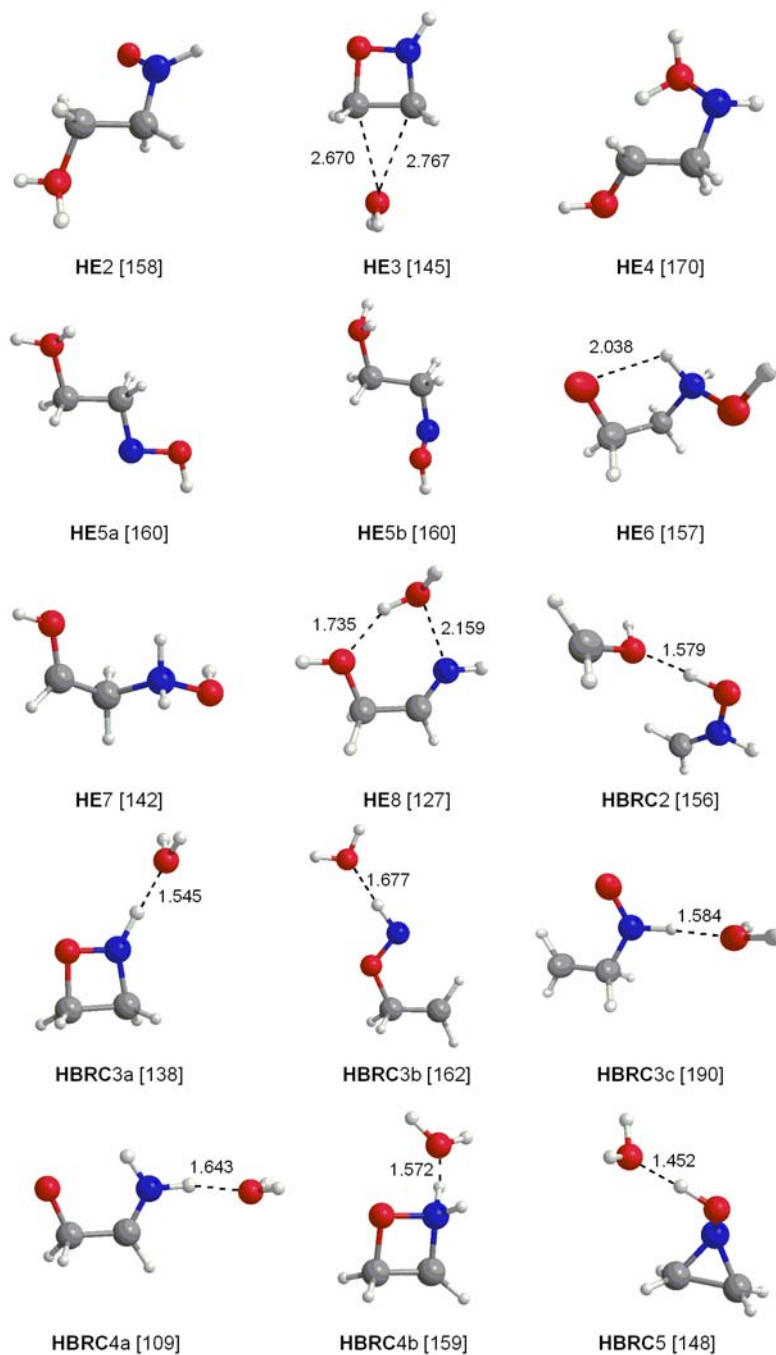


Figure 8.8 Optimized geometries (B3LYP/CBSB7) of minima and transition states involved in the water loss from ionized 2-hydroxy-aminoethanol (**HE-1**). The numbers are 298 K enthalpies derived from CBS-QB3 calculations, see Table 8.2 in the Appendix of this Chapter.

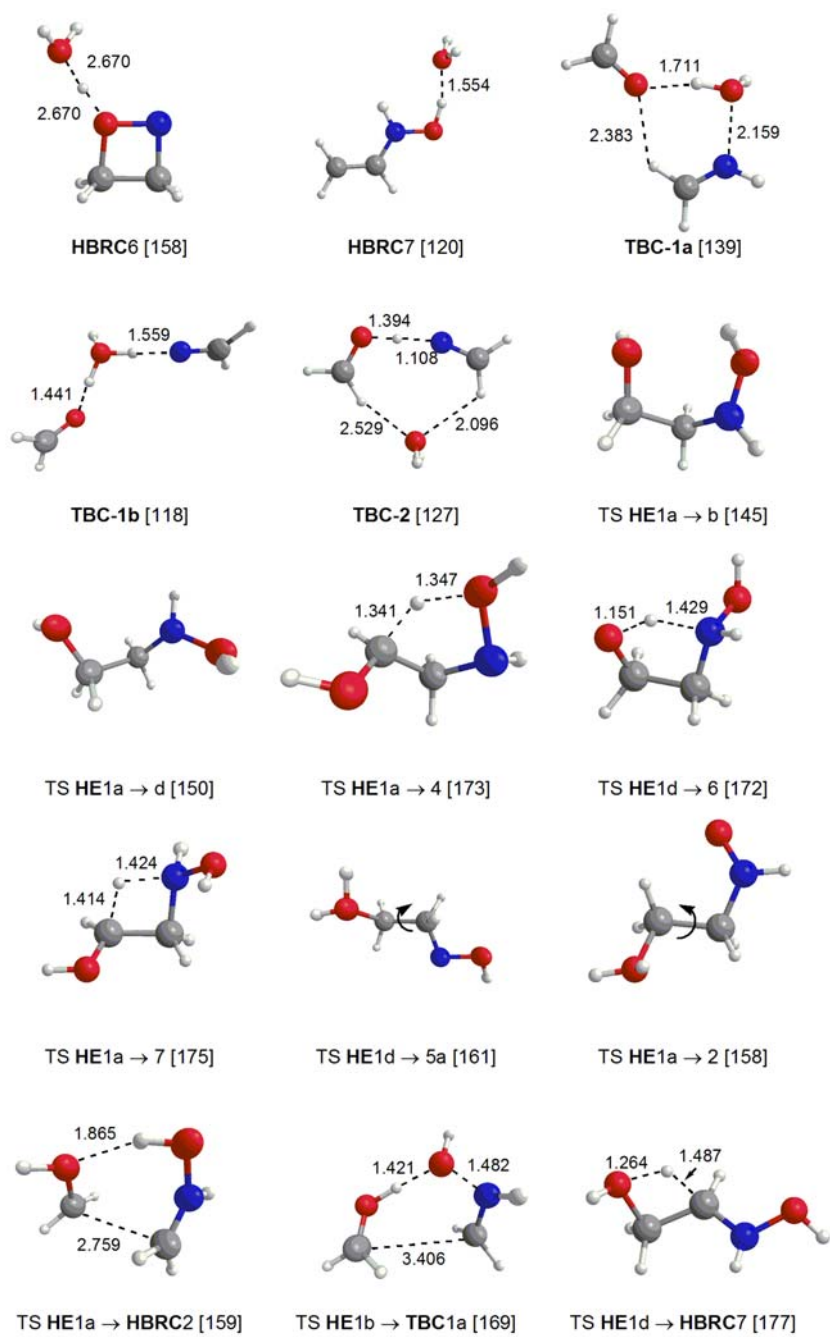


Figure 8.8 (continued).

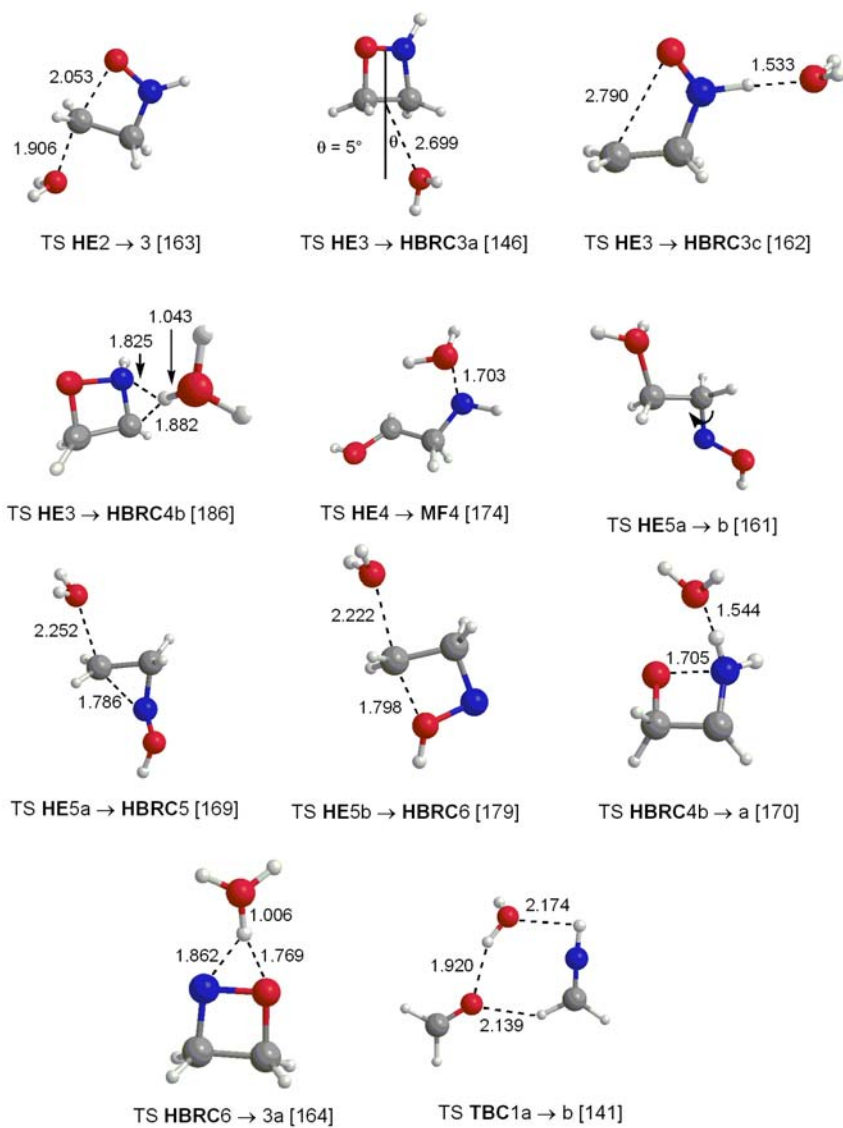
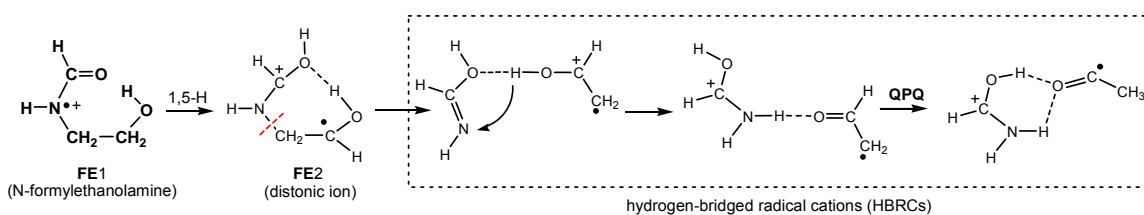


Figure 8.8 (continued).

Chapter 9

The dissociation chemistry of low-energy N-formyl-ethanolamine ions : HBRCs as key intermediates



Tandem mass spectrometry experiments show that N-formylethanolamine molecular ions $\text{HOCH}_2\text{CH}_2\text{NHC(H)=O}^{\bullet+}$ (**FE1**) lose $\text{C}_2\text{H}_3\text{O}^\bullet$, CH_2O and H_2O to yield m/z 46 ions HC(OH)NH_2^+ , m/z 59 ions $^\bullet\text{CH}_2\text{N(H)CHOH}^+$, and m/z 71 N-vinylformamide ions $\text{CH}_2=\text{C(H)N(H)CHO}^{\bullet+}$.

A detailed mechanistic study using the CBS-QB3 model chemistry reveals that the readily generated 1,5-H shift isomer $\text{HOCHCH}_2\text{N(H)C(H)OH}^{\bullet+}$ (**FE2**) and hydrogen-bridged radical cations (HBRCs) act as key intermediates in a ‘McLafferty + 1’ type rearrangement that yields the m/z 46 ions. The co-generated $\text{C}_2\text{H}_3\text{O}^\bullet$ neutrals are predicted to be vinyloxy radicals $\text{CH}_2=\text{CHO}^\bullet$ in admixture with $\text{CH}_3\text{C}=\text{O}^\bullet$ generated by quid-pro-quo (QPQ) catalysis.

A competing C–C bond cleavage in **FE1** leads to HBRC $[\text{CH}_2\text{N(H)C(H)=O}^{\bullet+}\cdots\text{H}\cdots\text{O}=\text{CH}_2]^{\bullet+}$, which serves as the direct precursor for CH_2O loss.

In addition, ion **FE2** also communicates with a myriad of ion-molecule complexes of vinyl alcohol and formimidic acid whose components may recombine to form distic ion **FE3**, $\text{HOCH(CH}_2\text{)N(H)C(H)OH}^{\bullet+}$, which loses H_2O after undergoing a 1,5-H shift. Further support for these proposals comes from experiments with D- and ^{18}O -labelled isotopologues.

Previously reported proposals for the H_2O and CO losses from protonated N-formylethanolamine are briefly re-examined.

The work described here has been published previously in an article under the same title : K.J. Jobst, R.D. Bowen, J.K. Terlouw, *Int. J. Mass Spectrom.* (2011) in press.

9.1 Introduction

The well-known McLafferty rearrangement is arguably the most important hydrogen-shift rearrangement in the structure analysis of organic compounds by electron ionization (EI) mass spectrometry [1]. The reaction was discovered in the early 1950s [1c], but its detailed mechanism has been a subject of animated debate for almost 40 years. The issue of whether the γ -H transfer and α - β bond cleavage reactions occur in a *concerted* or a *step-wise* manner was not finally settled until the isotopic labelling study of Derrick and Bowie [2] left little doubt that the 1,5-H shift yields a distonic ion [3] as a stable intermediate.

Early investigators recognized that integrating theory and experiment would be an ideal approach to study reaction mechanisms, but this only became feasible in the late 1980s following spectacular advances in computer technology and software. The pioneering computational studies [4] of the prototypal McLafferty rearrangement in ionized n-butanal (using simple Hartree-Fock calculations) therefore appeared at a relatively late stage in the debate over the mechanism. Nevertheless, these studies provided crucial mechanistic information, *viz.*, the structures and energies of the key intermediates and transition-states, which cannot readily be ascertained by experiment. More recently, the Schwarz group has published a trilogy of papers [5] dealing with the dissociation of ionized valeramide. By bringing to bear sophisticated DFT (density functional theory) based calculations, the authors provide an elegant (mechanistic) rationale of a stepwise McLafferty rearrangement and three other competing dissociations, in excellent agreement with the experimental observations.

The presently available CBS [6a], Gaussian [6b] and Weizmann [6c] model chemistries often make it possible to study mechanisms with chemical accuracy (± 1 kcal mol⁻¹ [6d]). In our research we have exploited these powerful tools to study dissociation mechanisms of low-energy radical cations for which experiment alone can at best provide tentative proposals [7]. This approach has led to the growing realization that rearrangements of

solitary radical cations containing heteroatoms often involve hydrogen-bridged radical cations (HBRCs) [8], a subclass of ion-molecule complexes [1a], as key intermediates. HBRCs are often more stable than the incipient molecular ions and at elevated energies they may catalyze further H-transfers leading to energetically more favourable product ions or neutrals. Proton-transport catalysis (PTC) [9a], where, in a complex, a neutral molecule induces an ion to isomerize via a HBRC, is a prime example. An interesting variant is the catalyzed transformation of a neutral species by an ion [9b].

In the present study, we use the CBS-QB3 model chemistry [6d] to probe the dissociation of $\text{HOCH}_2\text{CH}_2\text{NHC(H)=O}^+$ (**FE1**), ionized N-formylethanolamine. This challenging ion, whose three heteroatoms make it prone to extensive hydrogen-shift rearrangements via HBRCs, has not been previously studied by either experiment or theory. It undergoes three competing fragmentations that feature in both the conventional EI and the MI (metastable ion) mass spectra : loss of $\text{C}_2\text{H}_3\text{O}^\bullet$, CH_2O and H_2O .

The $\text{C}_2\text{H}_3\text{O}^\bullet$ loss from **FE1** points to a ‘McLafferty + 1’ rearrangement in which a second H-transfer occurs following the α - β bond cleavage to produce oxygen-protonated formamide, HC(OH)NH_2^+ . There is compelling evidence for the involvement of ion-molecule complexes in this type of rearrangement [10] and in the present system these are expected to adopt the configuration of HBRCs. This opens the possibility that PTC also plays a role in this rearrangement. Indeed, theory predicts that the neutrals of this reaction are vinyloxy radicals $\text{CH}_2=\text{CHO}^\bullet$ in admixture with $\text{CH}_3\text{C}=\text{O}^\bullet$ generated by catalysis.

The competing loss of CH_2O from **FE1** could involve a 1,6-H shift to yield the distonic ion $^\bullet\text{CH}_2\text{N(H)CHOH}^+$ but, here too, a very stable HBRC appears to act as a key intermediate.

Perhaps not surprisingly [7], the loss of H_2O appears to be a fairly complex multi-step reaction. It yields ionized N-vinylformamide, $\text{CH}_2=\text{C(H)N(H)CHO}^+$, in admixture with its more stable cyclic distonic isomer. The time-honoured approach of isotopic labelling [11] was also used to study this reaction. Analysis of various D- and ^{18}O -labelled isotopologues supports our mechanistic proposal but it also challenged theory to evaluate a bewildering array of potential exchange reactions in the key intermediates.

9.2 Results and discussion

9.2.1 The EI mass spectrum of N-formylethanolamine and the MI and CID mass spectra of the (pseudo) molecular ions

The mass spectrum of N-formylethanolamine (**NFE**), see Fig. 9.1, displays a weak molecular ion signal relative to the peaks at m/z 71, 59 and 46. These fragment ions correspond to the losses of H_2O , $\text{CH}_2=\text{O}$ and $\text{C}_2\text{H}_3\text{O}^\bullet$ and they are also observed in the MI mass spectrum of Fig. 9.2a. Fig. 9.1 also displays prominent peaks at m/z 58 and 30, which likely results from the direct bond cleavage reaction $\text{HC}(=\text{O})\text{NHCH}_2\text{CH}_2\text{OH}^{+\bullet}$ (**FE1**) \rightarrow $\text{HC}(=\text{O})\text{NH}=\text{CH}_2^+$ (m/z 58) + $\text{CH}_2\text{OH}^\bullet$ and a subsequent partial decarbonylation of the m/z 58 ions into CH_2NH_2^+ (m/z 30). These ions are absent in the MI spectrum but they reappear in the CID spectrum of Fig. 9.2b. Therefore, an important precondition imposed by experiment on theory is that enthalpies of stable intermediates, connecting transition states and dissociation thresholds of proposed dissociation mechanisms of the *metastable* ions should not exceed $157 \text{ kcal mol}^{-1}$, the calculated $\Sigma\Delta_f\text{H}$ value of the direct bond cleavage products $\text{HC}(=\text{O})\text{NHCH}_2^+ + \text{CH}_2\text{OH}^\bullet$.

The conspicuous peak at m/z 90 in Fig. 9.1 represents $[\text{M}+\text{H}]^+$ ions resulting from the remarkably efficient self-protonation of **NFE** by chemical ionization : raising the source pressure from *c.* 3×10^{-7} to 1×10^{-6} Torr, by gently heating the sample, causes the m/z 90 : 89 peak intensity ratio to increase to $\sim 10:1$! In line with this, our calculations show that the various proton transfer reactions between **FE1** and its neutral **NFE** are exothermic : the proton affinity (PA) of **NFE** is $214 \text{ kcal mol}^{-1}$ but those of $\text{O}=\text{C}^\bullet\text{-NHCH}_2\text{CH}_2\text{OH}$, $\text{HC}(=\text{O})\text{NHC}^\bullet\text{HCH}_2\text{OH}$, $\text{HC}(=\text{O})\text{NH-CH}_2\text{C}^\bullet\text{HOH}$, $\text{HC}(=\text{O})\text{NHCH}_2\text{CH}_2\text{O}^\bullet$ and $\text{HC}(=\text{O})\text{N}^\bullet\text{CH}_2\text{-CH}_2\text{OH}$ are only 190, 187, 187, 203 and $204 \text{ kcal mol}^{-1}$ respectively.

The MI and CID mass spectra of protonated N-formylethanolamine (**PFE**), see Figs. 9.2c/d, are dominated by peaks at m/z 62 and 72, corresponding to the losses of CO and H_2O . The associated reaction mechanisms have been briefly addressed by Tip *et. al* [26] in their study of N-formylethanolamine as a matrix for the Fast Atom Bombardment analysis

of non-polar compounds, including saccharides. One point that was not addressed concerns the notable peaks at m/z 71, 59 and 46 in the CID spectrum of Fig. 9.2d. That these peaks do not originate from the naturally occurring ^{13}C -isotopologue of **FE1** follows from the fact that the CID spectrum of Fig. 9.2d does not change with the m/z 90 : 89 peak ratio. Their presence suggests that **PFE** may lose a H^\bullet radical to produce an m/z 89 ion having dissociation characteristics akin to those of **FE1**.

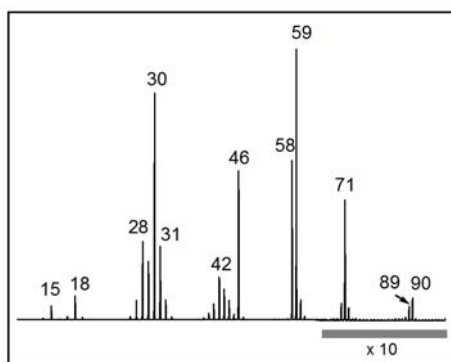


Figure 9.1 EI mass spectrum of N-formylethanolamine $\text{HOCH}_2\text{CH}_2\text{NHCHO}$

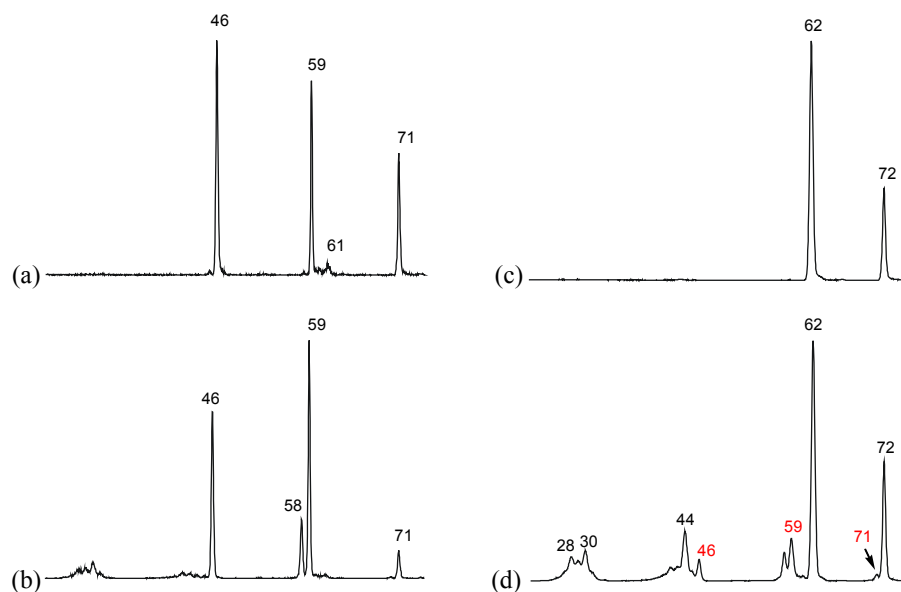


Figure 9.2 (a) MI and (b) CID mass spectra of the N-formylethanolamine radical cation (**FE1**); (c) MI and (d) CID mass spectra of protonated N-formylethanolamine (**PFE**); note : a weak peak (*c.* 5%) at m/z 89 in Fig. 9.2d is not shown.

The next Section (9.2.2) deals with the structures of the m/z 71, 59 and 46 product ions generated from (metastable) ions **FE1**. Sections 9.2.3 – 9.2.5 present a conformational and mechanistic analysis of the dissociation chemistry of ions **FE1** and D- and ^{18}O -labelled isotopologues. Section 9.2.6 re-examines the previously reported dissociation mechanisms [14] of *protonated* N-formylethanolamine.

9.2.2 Identification of the product ions generated in the dissociation of ions **FE1**

A comparison of the CID mass spectra of the m/z 59 and 46 product ions, see Figs. 9.3a/b with reference spectra [12,13] leaves little doubt that the distonic ion $\text{HC(OH)NH=CH}_2^{*+}$ (m/z 59) and oxygen-protonated formamide HC(OH)NH_2^+ (m/z 46) are generated.

Using the values from Table 9.2 (Appendix), we find that the sum of the enthalpies of $\text{HC(OH)NH=CH}_2^{*+}$ and $\text{CH}_2=\text{O}$ ($\Sigma\Delta_f\text{H} = 132 \text{ kcal mol}^{-1}$) is well below the upper limit of $157 \text{ kcal mol}^{-1}$ imposed by experiment. Using this energy criterion, we can safely conclude that formaldehyde is lost rather than its elusive hydroxycarbene HCOH [14], which lies considerably higher in energy.

In contrast, the structure of the mass 43 neutral is not so easily ascertained because the enthalpies of $\text{CH}_3\text{C}=\text{O}^\bullet$ and $\text{CH}_2=\text{CHO}^\bullet$ are close, see Table 9.1. Moreover, the combined enthalpies $\Sigma\Delta_f\text{H} [\text{HC(OH)NH}_2^+ + \text{CH}_3\text{C}=\text{O}^\bullet] = 124 \text{ kcal mol}^{-1}$ and $\Sigma\Delta_f\text{H} [\text{HC(OH)NH}_2^+ + \text{CH}_2=\text{CH-O}^\bullet] = 129 \text{ kcal mol}^{-1}$ both satisfy the energy criterion discussed in Section 9.2.1. A recent computational study [15a] predicts that the isomers $\text{CH}_2=\text{C-OH}^\bullet$ and $\text{CH}=\text{CH-OH}^\bullet$ lie 29 and 33 kcal mol^{-1} higher than the acetyl radical global minimum and thus can be excluded from our analysis. Unfortunately, a CIDI experiment [16] to probe the structure of the $\text{C}_2\text{H}_3\text{O}^\bullet$ radical could not be realized due to insufficient signal intensity. The intriguing possibility that both $\text{CH}_3\text{CO}^\bullet$ and $\text{CH}_2=\text{CHO}^\bullet$ isomers are co-generated is discussed in Section 9.2.4.

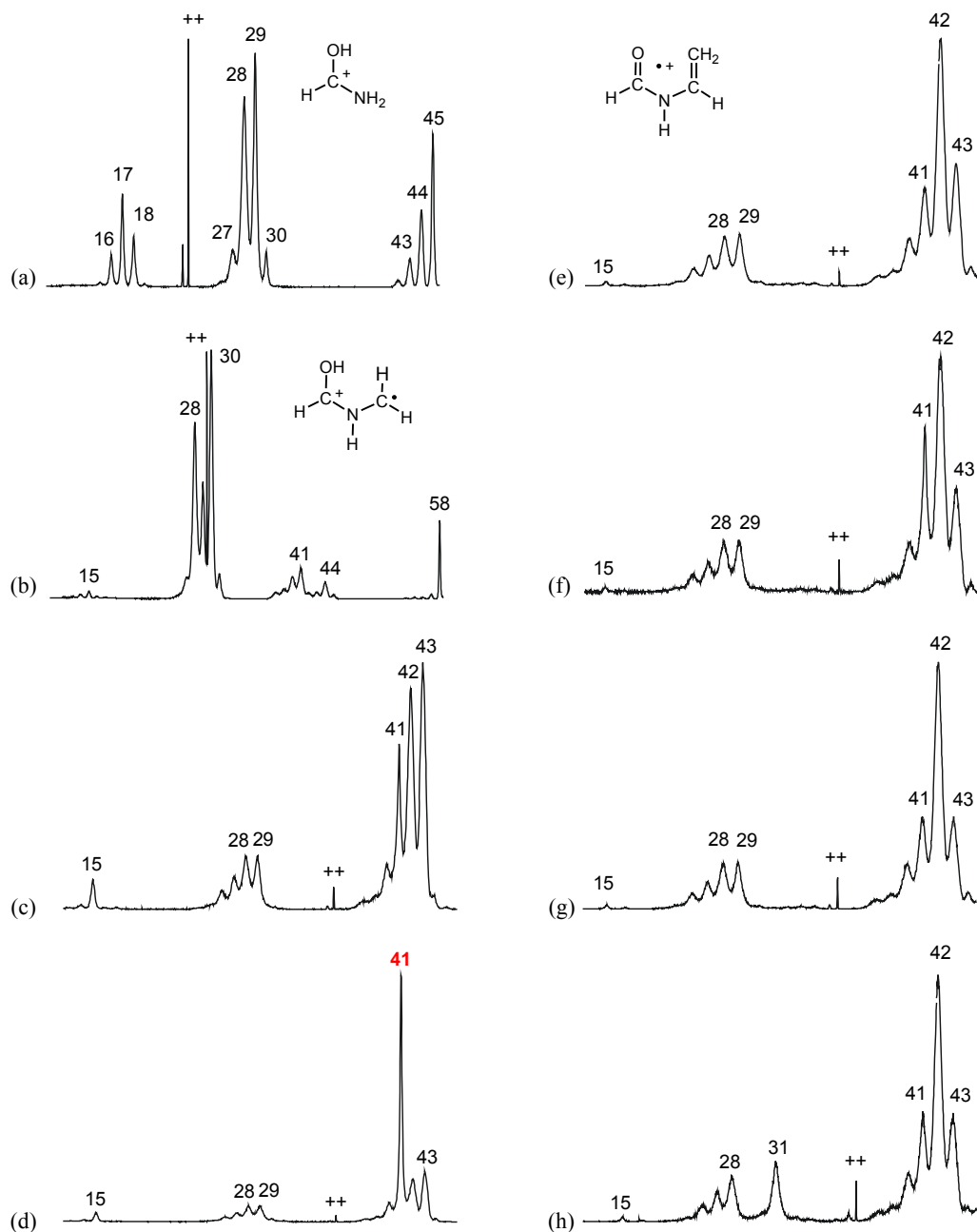


Figure 9.3 Left column: (a), (b) and (c) are CID mass spectra of the source generated m/z 46, m/z 59 and m/z 71 ions from N-formylethanolamine; (d) CID spectrum of the m/z 71 ions generated by thermal decomposition; Right column : CID spectra with the collision chamber at -1 kV of m/z 71 ions generated from (e) N-vinyl-formamide; (f) N-formyl-ethanolamine and (g) N-formyl-O-methylethanolamine $\text{CH}_3\text{OCH}_2\text{CH}_2\text{NHCHO}$; (h) CID spectrum of the m/z 73 ions generated from ^{18}O -labelled N-formylethanolamine $\text{HOCH}_2\text{CH}_2\text{NHCHO}^{18}$.

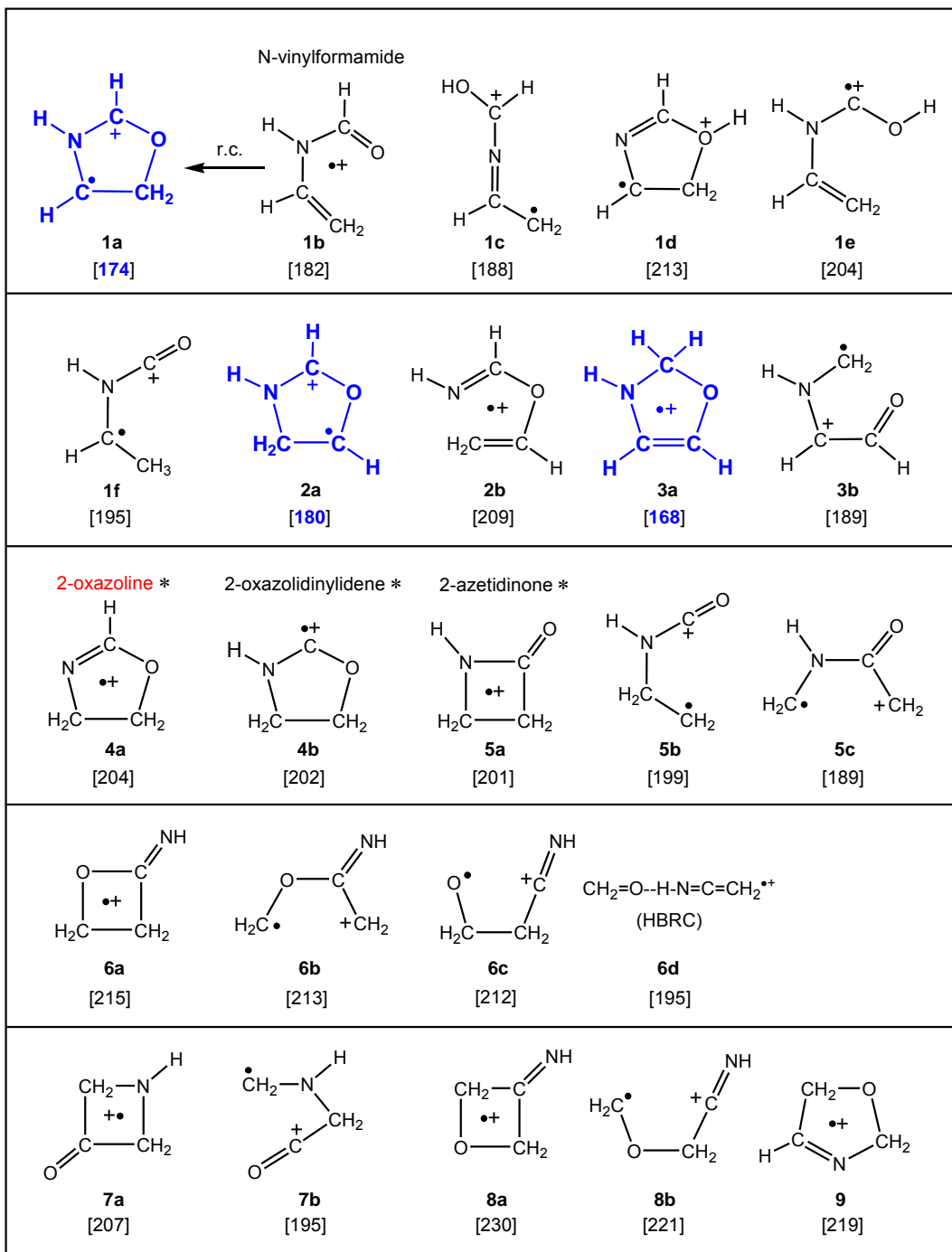


Figure 9.4 $\text{C}_3\text{H}_5\text{NO}^{+\bullet}$ (m/z 71) ion structures and their 298 K enthalpies of formation in kcal mol^{-1} derived from CBS-QB3 calculations; * For these ions, the CID mass spectra have been reported [18a].

Establishing the structure of the m/z 71 product ion structure is not straightforward because there is a dearth of information on the $C_3H_5NO^{*+}$ system of ions [17] and very few CID mass spectra have been reported [18a]. Figure 9.4 shows potential m/z 71 product ion structures and their associated CBS-QB3 derived 298 K enthalpies. These will be used as a guide in the analysis of the CID mass spectrum of Figure 9.3c.

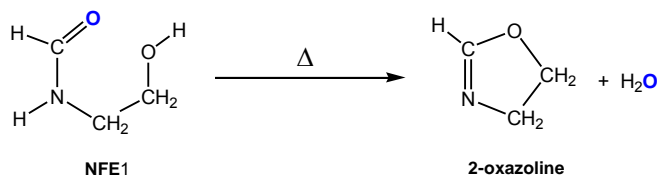
As pointed out in Section 9.2.1, the combined enthalpy of $C_3H_5NO^{*+} + H_2O$ must not exceed $157 \text{ kcal mol}^{-1}$. Using $\Delta_f H (H_2O) = -58 \text{ kcal mol}^{-1}$, an upper limit of $215 \text{ kcal mol}^{-1}$ is obtained for $\Delta_f H (C_3H_5NO^{*+})$ so that ions **8a**, **8b** and **9** can be ruled out as viable candidates.

The most attractive of the remaining structures is the very stable N-vinylformamide ion **1b**. Its CID spectrum appears to be close to that of Fig. 9.3c, but it does not display the prominent, narrow m/z 41 peak and its m/z 43 peak is considerably more intense.

We are confident, however, on the basis of the arguments presented below, that a mixture of ions **1b** and its cyclic distonic isomer **1a** (see Fig. 9.4), is generated in the H_2O loss.

First, the discrepancy in the relative intensity of the m/z 43 peaks appears to be due to the fact that they represent both collision-induced and spontaneous dissociations. When the unimolecular component (whose intensity strongly depends on the precursor ions' internal energy) is removed by applying an external voltage (-1 kV) to the collision cell [19], the spectra of Fig. 9.3e and 9.3f are obtained. It is gratifying to observe that the m/z 42 : 43 peak ratios are now virtually the same. In fact, the more intense m/z 41 peak of Fig. 9.3f, which may consist of a narrow and a broad component, and the more prominent charge-stripping peak (++) are the only distinguishing features.

Second, we propose that the narrow part of the m/z 41 peak of Fig. 9.3f results from thermal decomposition because its intensity appeared to vary during the evaporation of the sample. Indeed, the CID spectrum of the m/z 71 ions obtained from a sample that had been subjected to prolonged heating (at 100°C for 8 h), see Fig. 9.3d, is dominated by a narrow m/z 41 peak. A plausible thermal decomposition product, see Scheme 9.1, is 2-oxazoline (**4a**), whose CID spectrum [18b] is very close that of Fig. 9.3d.

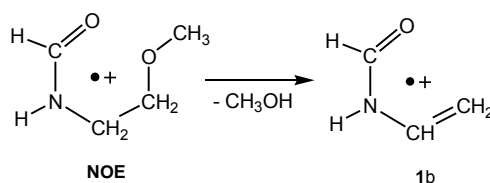


Scheme 9.1

In this context, we note that experiments with HOCH₂CH₂NHCH¹⁸O indicate that the thermal decomposition involves a specific loss of H₂¹⁸O : the CID spectrum of the resulting *m/z* 71 ions (not shown) displays an intense, narrow peak at *m/z* 41 whereas the CID spectrum of the *m/z* 73 ions shown in Figure 9.3h, does not.

This leads us to conclude that the *m/z* 73 ions are generated by the specific loss of H₂¹⁶O from the ¹⁸O-labelled radical cations **FE1**. Indeed, a comparison of Figs 9.3e and 9.3h provides strong evidence that ions **1b** are generated because the *m/z* 41 – 43 peak clusters are almost identical and the shift of *m/z* 29 to 31 confirms the HCO structure motif.

Complementary evidence that ions **1b** are generated comes from an analysis of N-formyl-O-methylethanolamine (**NOE**). As shown in Scheme 9.2, ion **NOE** readily loses the methoxy oxygen atom (in the form of CH₃OH) to generate ions of *m/z* 71.



Scheme 9.2

The CID spectrum of the *m/z* 71 ions, see Fig. 9.3g, is virtually the same as those of Figs. 9.3e/f, indicating that ions **FE1** and **NOE** dissociate into **1b** via analogous mechanisms. Note that the analogous thermal decomposition of Scheme 9.1 cannot occur in **NOE** and indeed the spectrum of Fig. 9.3g, which shows no trace of a narrow component in the *m/z* 41 peak.

A subtle difference between the CID spectra of ion **1b** (Fig. 9.3e) and the **FE1** derived ions

(Fig. 9.3f) is the enhanced charge-stripping peak at m/z 35.5 in Figure 9.3f.

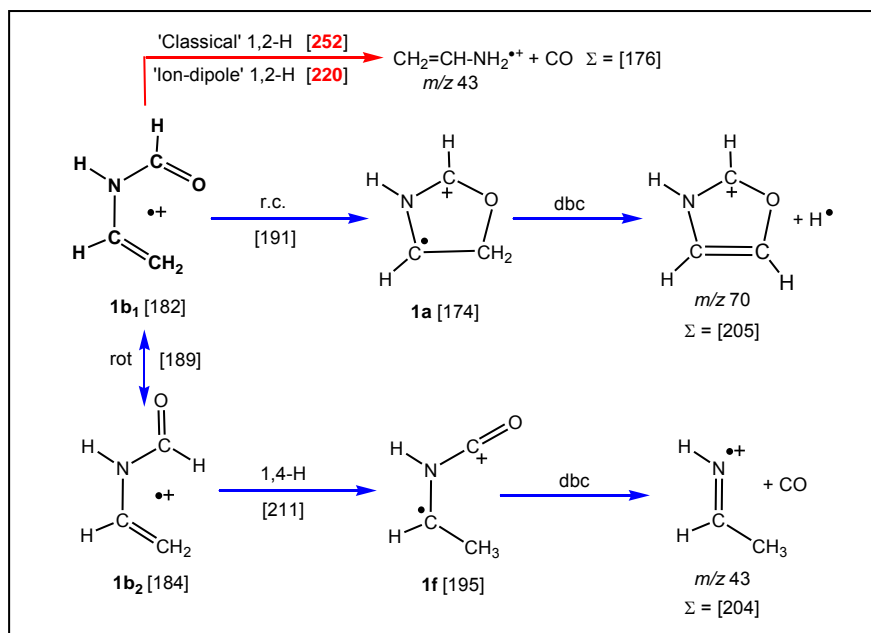
This prompted us to consider the co-generation of the cyclic counterpart of ion **1b**, the remarkably stable distonic ion **1a** of Figure 9.4. Distonic ions are often more prone to charge-stripping, especially with O₂ as collision gas, and in line with this, our calculated vertical IE of **1a** (13.6 eV) is considerably lower than that of **1b** (16.3 eV).

Nevertheless, the proposal that the spectrum of Fig. 9.3f is compatible with a mixture of ions **1a** and **1b** hinges on the question whether the two isomers have closely similar CID characteristics. The CID spectrum of pure ions **1a** is not accessible, but the following computational analysis indicates that this indeed the case.

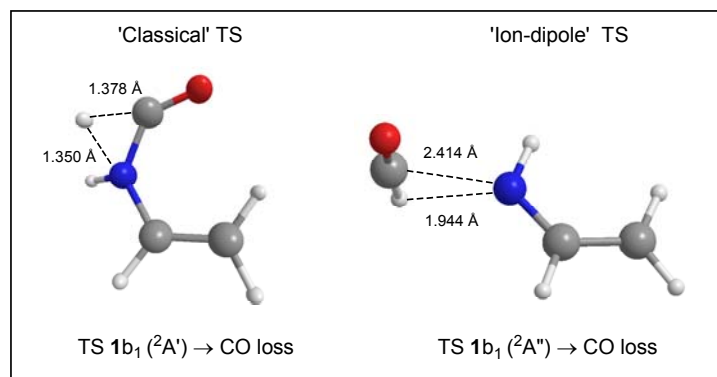
Scheme 9.3 summarizes our computational results on metastable ions **1b**, which generate both m/z 43 and m/z 70 ions. We propose that the H[•] loss does not occur from ion **1b** directly, but rather from its cyclic distonic isomer **1a** : the transformation **1b** → **1a** involves a facile ring-closure via a TS (at 191 kcal mol⁻¹) that lies well below the dissociation threshold at 205 kcal mol⁻¹. In contrast, direct H[•] loss reactions from ion **1b** into CH₂=CH–NH–C=O⁺, ⁺CH₂–CH=N–CH=O or CH₂=C–NH–CH=O⁺ have ΣΔ_fH values of 236, 234 and 245 kcal mol⁻¹ and are thus far more energy demanding !

The competing formation of the m/z 43 ion involves loss of CO : the identity of the neutral was established by a CID experiment on the isotopologue HC(=O¹⁸)CH=CH₂. A previous theoretical study [20] indicates that ionized formamide undergoes decarbonylation via an ion-dipole complex accessible from the first excited state, rather than a classical 1,2-H shift. Although the energy difference between the first two bands of the PE spectrum of N-vinylformamide^a is larger than that of formamide (1.0 vs. 0.2 eV), it seemed worth considering whether ions **1b** also decarbonylate via an excited state. Scheme 9.4 shows the optimized geometries of the classical 1,2-H shift and ion-dipole type transition states. Both are quite energy demanding with enthalpies of 252 and 220 kcal mol⁻¹ respectively.

^a The HeI photoelectron spectrum of N-vinylformamide was obtained using a home-built instrument in the laboratory of Dr. N.H. Werstiuk.



Scheme 9.3 Mechanistic proposals for the loss of CO and H[•] from N-vinylformamide ions **1b**. The numbers are CBS-QB3 derived 298 K enthalpies in kcal mol⁻¹.



Scheme 9.4 Optimized geometries of the transition states for the loss of CO from the A' and A'' states of the N-vinylformamide ion **1b**.

A more attractive decarbonylation route involves the 1,4-H shift connecting ions **1b₂** and **1f** of Scheme 9.3. Loss of CO therefrom yields the *m/z* 43 acetimine ion $\text{CH}_3\text{C}(=\text{NH})\text{H}^+$.

An important result from the above computational analysis is that the TS connecting ions **1a** and **1b** lies ~ 15 – 20 kcal mol⁻¹ below the dissociation thresholds for the losses of H[•] and CO. This implies that a significant fraction of the stable ions **1a/b** may interconvert and that, apart from the charge-stripping peak, their CID mass spectra may not be significantly different. Thus, the CID spectrum of Fig. 9.3b may well represent a mixture of **1a** and **1b**.

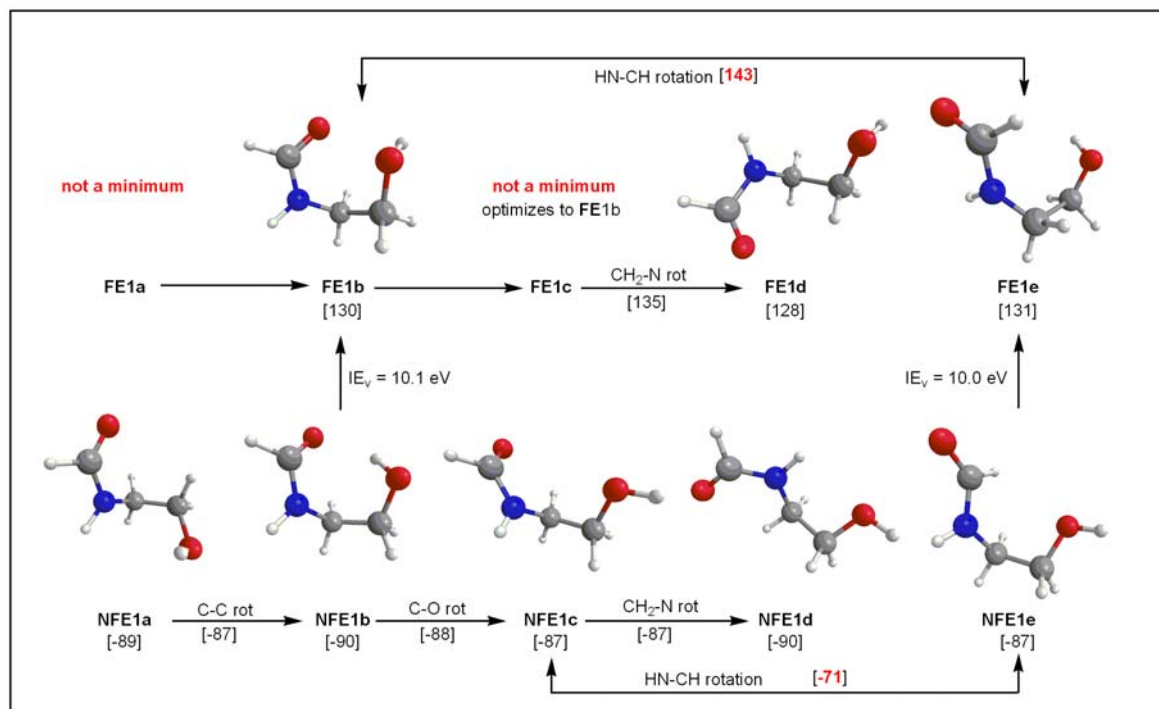
9.2.3 Conformational analysis of neutral and ionized *N*-formylethanolamine

Before addressing the proposed mechanisms, we will first consider the various conformers of neutral and ionized *N*-formylethanolamine. This is relevant in view of the *E/Z*-isomerism of the amide functionality [21], whose barrier may greatly exceed that of a McLafferty-type 1,5-H shift.

The calculations of Scheme 9.5 (bottom) indicate that the O-H-O and N-H-O bridged **NFE** conformers **1b** and **1d** are only a few kcal mol⁻¹ more stable than the non-bridging neutrals **1a**, **1c** and **1e**. The barriers connecting **1a**, **1b**, **1c** and **1d** are marginal, but rotation of the C-N amide bond **NFE1c**→**1e**, and the associated disturbance of the π -system [21], requires 16 kcal mol⁻¹! This would imply that **1b** and **1d** are the principal species among the freely equilibrating *Z*-conformers and that the less stable *E*-conformer **NFE1e** may also be present in the sample.

The corresponding ionic conformers are shown in the top part of Scheme 9.5. Ion **FE1a** is not a minimum but instead it rearranges to the distonic ion **FE2** via a 1,5-H shift. This reaction will be discussed in the next section. Ion **FE1c** is not a minimum either: it rotamerizes to **FE1b**.

Prima facie, it is surprising that the O-H-O bridge is broken upon ionization of **NFE1b**. However, a charge-distribution analysis indicates that the amide moiety is ionized, which would repel the bridging proton.

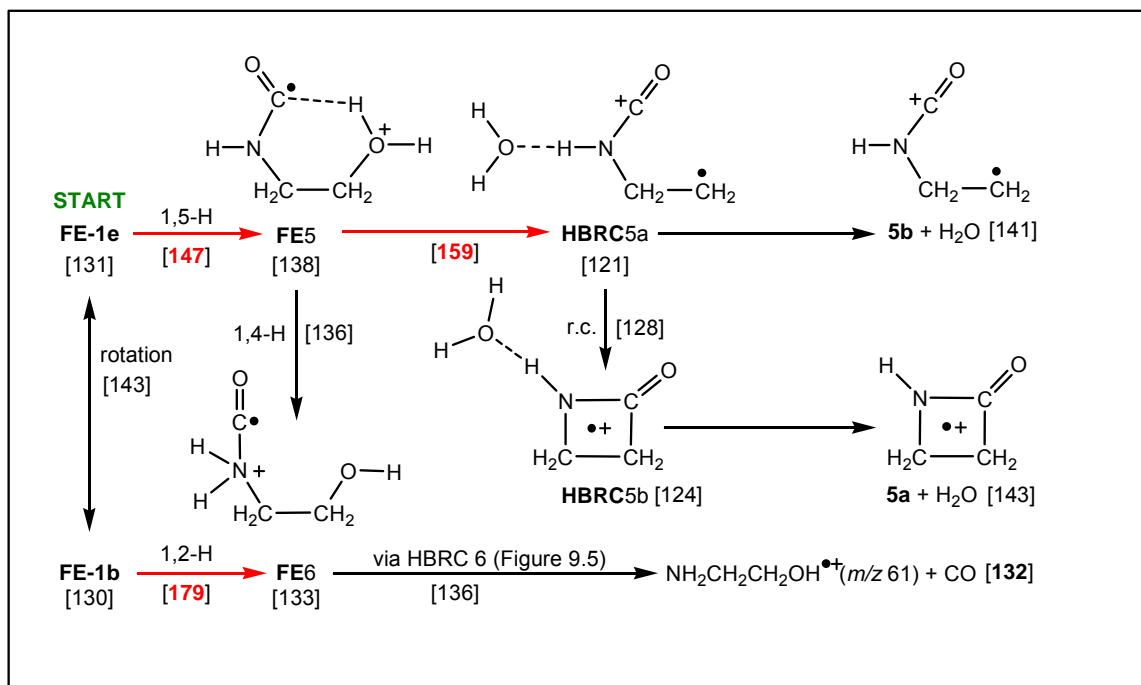


Scheme 9.5 Conformers of neutral (NFE) and ionized (FE) N-formylethanolamine. Numbers in brackets are CBS-QB3 derived 298 K enthalpies of formation in kcal mol⁻¹. IE_v is the calculated vertical ionization energy.

Ions **FE1b** and **FE1d** are separated by a negligible barrier but, as with the neutrals, the rotation of the amide bond **FE1b**→**1e** is energy demanding. This raises the possibility that the dissociation chemistry of **FE1e** differs from that of conformers **FE1b/d**.

Scheme 9.6 explores the *a priori* plausible H₂O loss from conformer **FE1e**. A 1,5-H shift in **FE1e** would produce distonic ion **FE5**, which may further rearrange into **HBRC5a** by cleaving the C-OH₂⁺ bond. The subsequent loss of H₂O from **HBRC5a**, or its ring-closed isomer **HBRC5b**, would produce ions **5a** and **5b** respectively. However, the C-OH₂⁺ bond cleavage is surprisingly high, which makes this an unrealistic proposal.

Experiment supports this conclusion because the CID spectrum of ion **5a**, the 2-azetidinone ion, is dominated by *m/z* 28 [18a] and the same is undoubtedly true for **5b**.



Scheme 9.6 Potential mechanisms for the H₂O loss from the ionized N-formylethanolamine conformer **FE1e**, in conjunction with the non-observed decarbonylation. The numbers refer to 298 K enthalpies (in kcal mol⁻¹) derived from CBS-QB3 calculations.

Scheme 9.6 also predicts that the decarbonylation route **FE5**→**FE6**→NH₂CH₂CH₂OH^{•+} (*m/z* 61) + CO lies well below the critical energy for the 1,5-H shift **FE1e**→**FE5**. However, the MI spectrum of Fig. 9.2a shows that decarbonylation does **not** occur. The spectrum does contain a minor peak at *m/z* 61 but its non-integral position on the energy scale (*m/z* 61.3) betrays its identity as an interference peak [22] originating from the protonated precursor molecule.

That the decarbonylation does not occur is because the prerequisite 1,5-H shift requires some 4 kcal mol⁻¹ more energy than the rotation of **FE1e** to **FE1b/d**. In the next Section it is shown that conformer **FE1b** initiates the losses of H₂O, CH₂O and C₂H₃O[•].

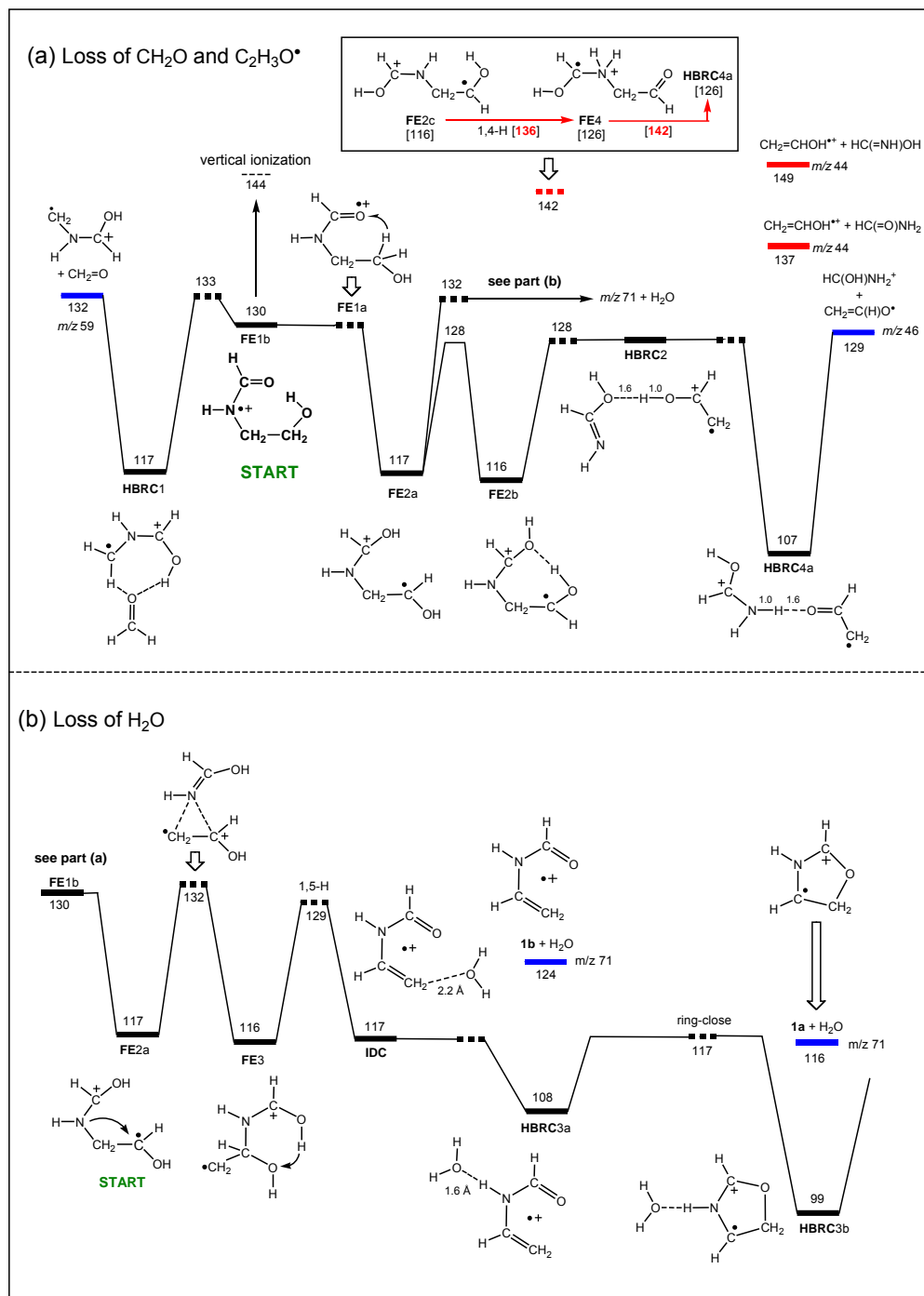
9.2.4 *The proposed mechanisms for the losses of CH₂O, C₂H₃O[•] and H₂O from ionized N-formylethanolamine*

The energy diagrams of Scheme 9.7 summarize our proposed mechanisms starting from conformer **FE1b**.

The calculations predict that vertical ionization of **NFE1b** yields vibrationally excited ions **FE1b** at an energy level (144 kcal mol⁻¹) that lies well above the low TS (133 kcal mol⁻¹) for the dissociation route **FE1b** → **HBRC1** → CH₂N(H)CHOH⁺ (*m/z* 59) + CH₂O, of Scheme 9.7a. This scenario is consistent with the fact that the molecular ion in the EI mass spectrum of Fig. 9.1 is very weak relative to the *m/z* 59 base peak. Likewise, the deep potential well of **HBRC1** would explain the high relative intensity of the *m/z* 59 peak in the MI spectrum, c. 10% of the precursor ion beam. Since the *m/z* 46 and 71 peaks of this spectrum have comparable intensities, the key transition states of their proposed generation should not significantly exceed the TS for the CH₂O loss at 133 kcal mol⁻¹. It will be seen that this is indeed the case.

The loss of a C₂H₃O[•] radical from ion **FE1** formally results from the consecutive transfer of two hydrogens in a process coined the “McLafferty + 1” rearrangement [1]. In the first step of the mechanism, **FE1b** rotamerizes to **FE1a**, which spontaneously undergoes a γ -H shift to produce the distonic ion **FE2a**. A reasonable proposal for the second H-transfer involves the classical 1,4-H shift **FE2c** → **FE4**, shown in the inset of Scheme 9.7a. However, its minimum energy requirement (12 kcal mol⁻¹) is so much higher than that of the CH₂O loss (3 kcal mol⁻¹) that competition becomes unlikely.

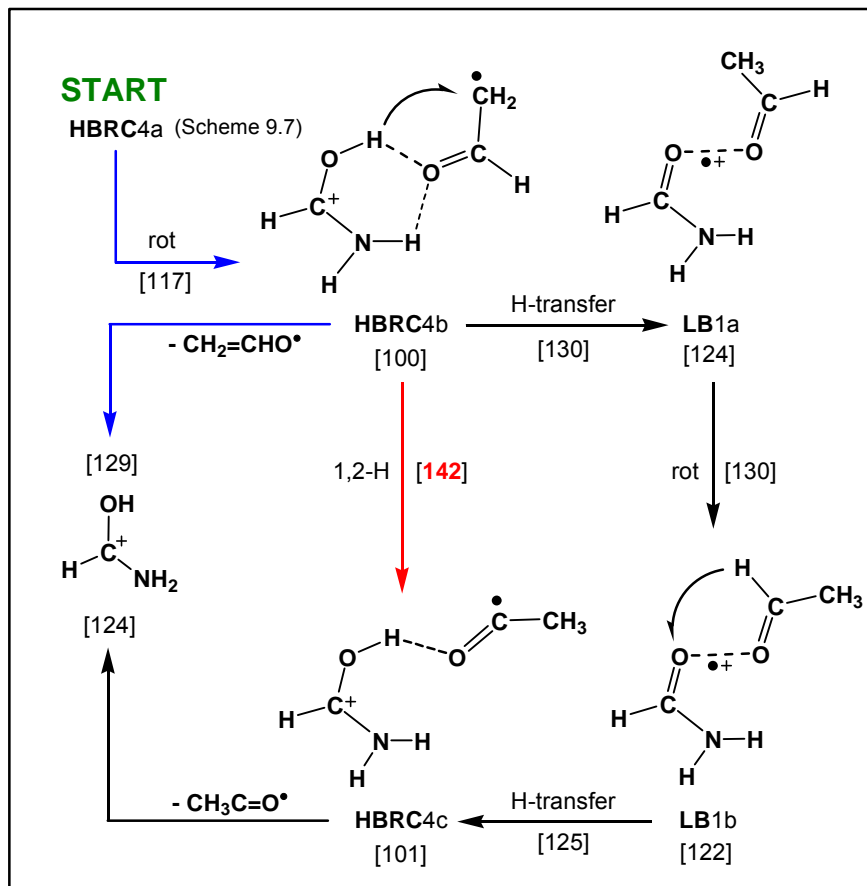
Inspired by the proposal that ion-molecule complexes can play an important role in the McLafferty + 1 mechanism [10], we have explored the possibility that HBRCs are generated from **FE2a**. Indeed, the calculations of Scheme 9.7a show that conformer **FE2b** may cleave at the C-N bond to yield the remarkably stable ion **HBRC2**. Transfer of a proton from the vinyl alcohol moiety of **HBRC2** to the amide nitrogen leads to the even more stable N-H-O bridged species **HBRC4a**, which may dissociate into HC(OH)NH₂⁺ (*m/z* 46) + CH₂=CHO[•].



Scheme 9.7 Mechanistic proposals for the losses of CH_2O and $\text{CH}_2=\text{CHO}^\bullet$ (top), and H_2O (bottom) from N-formylethanamine ions FE1. The numbers refer to 298 K enthalpies derived from CBS-QB3 calculations.

We note that the computed transition-state energies involved in this HBRC mediated reaction lie below the enthalpy of FE1 so that the reaction is barrierless !

The above proposal implies that the vinyloxy radical $\text{CH}_2=\text{CHO}^\bullet$ is lost in the dissociation, but an intriguing question is whether the more stable isomer $\text{CH}_3\text{CO}^\bullet$ is also generated, as is the case with the 1-methoxy-2-propanol ion [23]. As mentioned above, it was not possible to probe this by experiment and so we have turned to the calculations of Scheme 9.8, which uses **HBRC4a** of Scheme 9.7 as the starting point, to shed light on this question.



Scheme 9.8 The proposed quid-pro-quo catalysis mechanism that leads to the loss of $\text{CH}_3\text{C}=\text{O}^\bullet$ from ionized N-formylethanolamine. The numbers refer to 298 K enthalpies (in kcal mol^{-1}) derived from CBS-QB3 calculations.

Scheme 9.8 indicates that the 1,2-H shift in the $\text{CH}_2=\text{CHO}^\bullet$ component of **HBRC4b** that leads to **HBRC4c** is not feasible because its TS lies 13 kcal mol^{-1} above the dissociation threshold $\text{HC(OH)NH}_2^+ + \text{CH}_2=\text{CHO}^\bullet$. However, the 1,2-H shift barrier may be lowered significantly if protonated formamide acts as a catalyst. In this scenario, the protonated formamide component of **HBRC4b** transfers a hydrogen to the methylene carbon of $\text{CH}_2=\text{CHO}^\bullet$, to produce ion **LB1a**, a two center, 3-electron bonded complex [24] comprising formamide and acetaldehyde. The subsequent transformation **LB1a** \rightarrow **LB1b** may be viewed as a simple rotation of the $\text{CH}_3\text{C(H)=O}$ component. This orients the aldehydic hydrogen so that it may be transferred back to the formamide moiety to generate **HBRC4c**, which decomposes into $\text{CH}_3\text{C=O}^\bullet$ and HC(OH)NH_2^+ , the ‘regenerated’ catalyst.

This route reduces the barrier for the transformation $\text{CH}_2=\text{CHO}^\bullet \rightarrow \text{CH}_3\text{C=O}^\bullet$ from 42 to 30 kcal mol^{-1} so that it now lies within 1 kcal mol^{-1} of the dissociation threshold $\text{HC(OH)NH}_2^+ + \text{CH}_2=\text{CHO}^\bullet$. As a result, a fraction of the $\text{C}_2\text{H}_3\text{O}^\bullet$ radicals lost may be $\text{CH}_3\text{C=O}^\bullet$.

Overall, the mechanism is characterized by the catalyst donating a proton to one site of the substrate, and subsequently abstracting a proton from a different site. This variant of proton-transport catalysis has been coined as quid-pro-quo catalysis [9b].

Returning to Scheme 9.7, it is seen in part (b) that the H_2O loss mechanism is initiated from distonic ion **FE2a**. Lengthening of its N-C bond leads to an ion-molecule complex of a vinyl alcohol ion and formimidic acid, which, at an energy level of $132 \text{ kcal mol}^{-1}$, may recombine to form distonic ion **FE3**. In essence, the reaction **FE2** \rightarrow **FE3** involves transfer of the formimidic acid component of **FE2** to the adjacent carbon in the vinyl alcohol moiety. A 1,5-H shift in **FE3**, followed by elongation of the incipient C-OH₂ bond, results in the formation of ion-dipole complex **IDC** at $117 \text{ kcal mol}^{-1}$. Ion **IDC** may either dissociate into the N-vinylformamide ion **1b** + H_2O , or adopt the configuration of **HBRC3a** at $108 \text{ kcal mol}^{-1}$.

As discussed in Section 9.2.1, solitary ions **1b** may cyclize to the more stable distonic

ions **1a** and the same reaction may also occur in **HBRC3a** to produce **HBRC3b**, with the water molecule acting as a spectator. Since the associated TS lies well below the dissociation threshold **1b** + H₂O, a mixture of ions **1a** and **1b** may be generated. This is consistent with the analysis of the CID spectrum of the *m/z* 71 ions in Section 9.2.2.

Finally, we note that the mechanisms of Scheme 9.7 have no reverse barriers, in line with the observed modest T_{0.5} values of 23, 18 and 36 meV for the formation of the *m/z* 46, 59 and 71 ions.

9.2.5 The dissociation behaviour of D- and O¹⁸-isotopologues of N-formylethanolamine

To seek further support for the proposals of Scheme 9.7, we have examined the MI mass spectra of the D- and ¹⁸O-labelled molecular ions of Table 9.3. For the sake of clarity, the Table expresses the normalized MI peak intensities as neutral losses.

First we note that the proposals of Scheme 9.7 for the losses of CH₂O and C₂H₃O• are entirely compatible with the labelling data of Table 9.3 as are the CID spectra of the labelled product ions (not shown). It is (also) obvious that D isotope effects are operating in these losses but, given the complexity of the system, these were not further analyzed.

Table 9.3 The neutral losses in the MI spectra of various isotopologues of N-formylethanolamine.

Ion	Neutral Lost								
	C ₂ H ₃ O•	C ₂ D ₃ O•	CH ₂ O	C D ₂ O	H ₂ O	H D O	H ₂ O	H D O	D ₂ O
HOCH ₂ CH ₂ NHCHO ⁺⁺	100	-	77	-	45	-	-	-	-
HOCH ₂ CH ₂ NH C D O ⁺⁺	100	-	92	-	38	13	-	-	-
D OCH ₂ CH ₂ N D CHO ⁺⁺	100	-	53	-	5	40	-	-	10
HO C D ₂ C D ₂ NHCHO ⁺⁺	-	100	-	47	13	23	-	-	-
HOCH ₂ CH ₂ NH C O ⁺⁺	100	-	80	-	40	-	10	-	-
HOCH ₂ CH ₂ NH C D O ⁺⁺	100	-	83	-	30	4	6	5	-

The ¹⁸O and D isotopes are printed in bold face; intensities relative to the most intense loss = 100%

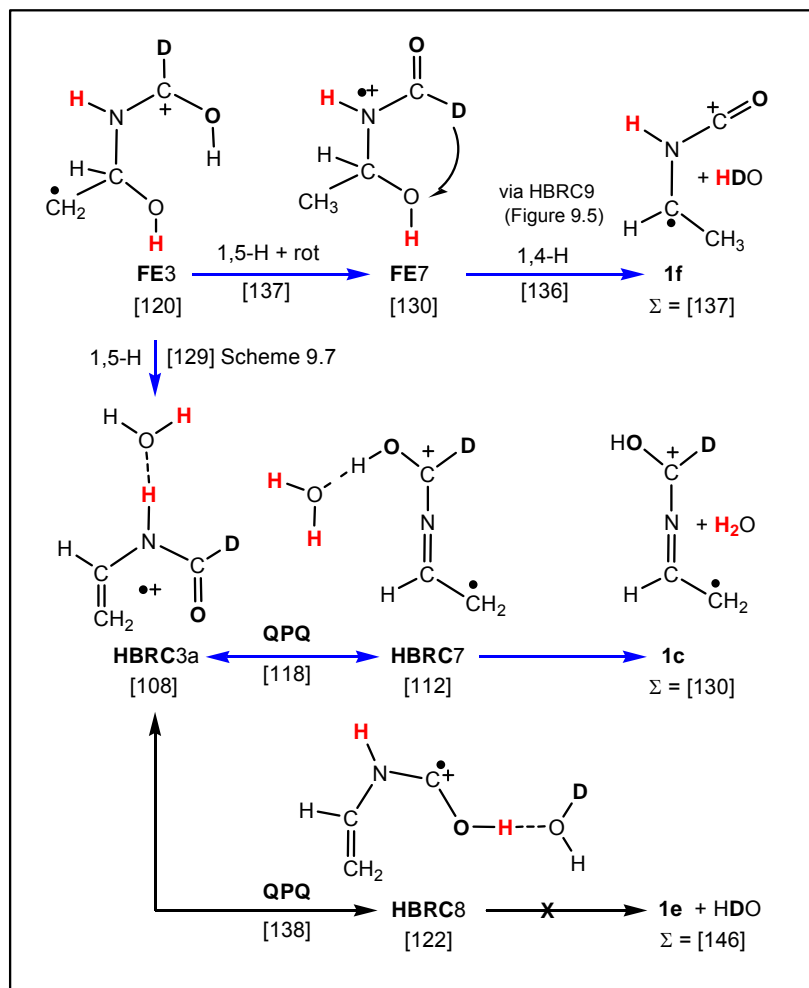
In contrast, the data pertaining to the water loss suggest that a partial exchange of the H and O atoms occurs or that this reaction involves additional (minor) dissociation pathways.

The aldehydic hydrogen does not participate in the proposal of Scheme 9.7b and indeed ions $\text{HOCH}_2\text{CH}_2\text{NHCDO}^{++}$ predominantly lose H_2O . However, $\sim 25\%$ of the ions lose HDO and mechanisms that could account for this observation are presented in Scheme 9.9.

One option is that ion **FE3** of Scheme 9.7b undergoes a competing 1,5-H shift of the same TS-energy : the route **FE3** \rightarrow **FE7** \rightarrow **1f** + HDO of Scheme 9.9. This proposal is not attractive, considering that the CID spectrum of the 3-methylaziridinone ion [18b], the cyclic isomer of distonic ion **1f**, is characterized by an intense CH_3 loss and that this loss is absent in the CID spectrum of Fig. 9.3c.

An intriguing alternative is the H/D exchange reaction depicted at the bottom of Scheme 9.9. Here, the H_2O molecule of **HBRC3a** abstracts the aldehydic *deuteron* and then donates a *proton* back to the carbonyl oxygen atom, yielding **HBRC8** in a QPQ type reaction. Loss of HDO from **HBRC8** is likely too energy demanding but TS **HBRC3a** \rightarrow **8** may be sufficiently low ($138 \text{ kcal mol}^{-1}$) to account for a partial exchange of the H_2O hydrogens and the aldehydic deuterium of ions **HBRC3a** by a back-and-forth QPQ reaction with **HBRC8**.

The minor loss of D_2O from $\text{DOCH}_2\text{CH}_2\text{NDCHO}^{++}$ may also arise from a QPQ type reaction: Scheme 9.9 shows that TS **HBRC3a** \rightarrow **7** lies so low in energy, at $118 \text{ kcal mol}^{-1}$, that the hydronium hydrogens of **HBRC3a** are expected to exchange prior to dissociation. Loss of D_2O may also occur from **HBRC7** to generate **1c**, a tautomer of the N-vinylformamide ion. The minor H_2O loss from $\text{DOCH}_2\text{CH}_2\text{NDCHO}^{++}$ may similarly be explained by the QPQ transformation **HBRC3a** \rightarrow **8** mentioned above. Finally, by invoking the above exchange reactions, the losses of HDO and H_2O from $\text{HOCD}_2\text{CD}_2\text{NHCHO}^{++}$ can also be rationalized.

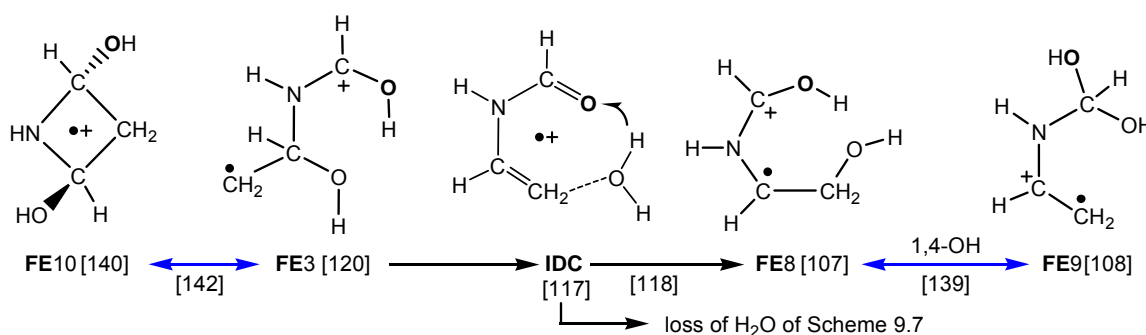


Scheme 9.9 Potential pathways for the minor HDO loss from the N-formylethanolamine isotopologue HOCH₂CH₂NHCDO. Numbers in brackets are CBS-QB3 derived 298 K enthalpies in kcal mol⁻¹.

Table 9.3 shows, in agreement with the mechanism of Scheme 9.7b, that most of the ions HOCH₂CH₂NHCH¹⁸O⁺⁺ lose their hydroxyl oxygen as H₂O¹⁶. However, ~ 25% of the ions loses the labelled amide oxygen. We further note that ions HOCH₂CH₂NHCD¹⁸O⁺⁺ lose H₂O, HDO, H₂¹⁸O and HD¹⁸O, which indicates that the loss of the ¹⁸O- and D-labels involves different (exchange) mechanisms.

A likely rationale for the partial loss of the ¹⁸O-label is that a key intermediate of Scheme

9.7 communicates with an isomer whose oxygen atoms are equivalent. This scenario was probed by many exploratory calculations which yielded the two pathways depicted in Scheme 9.10 as plausible candidates. The first one involves ion **FE9** generated by the route **IDC** → **FE8** → **FE9**. In this reaction, the water molecule of **IDC** attacks the terminal methylene group and synchronously transfers one of its hydrogens to the carbonyl oxygen atom. The resulting ion **FE8** may then undergo a 1,4-OH shift to generate ion **FE9**. The second option is slightly more energy demanding and involves cyclization of ion **FE3** to the symmetric ion **FE10**.



Scheme 9.10

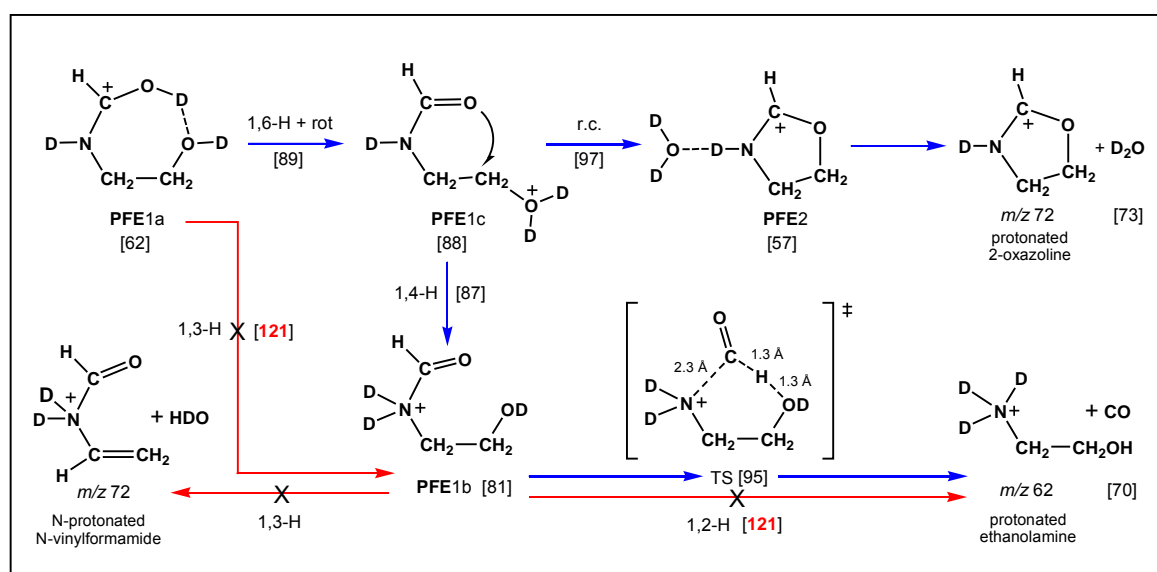
The energy of the TS of these exchange routes lies below that of the incipient molecular ions **FE1** of Scheme 9.7 (144 kcal mol⁻¹), but well above the dissociation threshold **1** + H₂O. This may be the reason why only a fraction of the O¹⁸-labelled ions loses the positional identity of the oxygen atoms prior to dissociation. In the same vein, the proposed H/D exchange reactions of the D-labelled ions do not lead to a statistical distribution of the label [25].

9.2.6 The losses of H₂O and CO from protonated *N*-formylethanolamine

N-formylethanolamine may be protonated at three different sites : at the amide oxygen, the amide nitrogen, or the hydroxyl oxygen. The resulting ions, **PFE1a-c**, are shown in Scheme 9.11. As expected, the carbonyl protonated ion **PFE1a** is calculated to have a

much greater stability than the other tautomers.

Tip et al. [26] propose that the prominent loss of H₂O (see Fig. 9.2 c/d) is initiated by a 1,3-H shift in N-protonated ions **PFE1b**, yielding N-protonated N-vinylformamide. This, however, is at odds with our observation that D-labelled ions DOCH₂CH₂NDCHOD⁺ specifically lose D₂O. Moreover, the proposed 1,3-H shift is undoubtedly quite energy demanding, much like the 1,3-H shift connecting **PFE1a** and **PFE1b** in Scheme 9.11.



Scheme 9.11 Mechanistic proposals for the losses of H₂O and CO from protonated N-formylethanolamine (**PFE1a**). Numbers in brackets are CBS-QB3 derived 298 K enthalpies in kcal mol⁻¹.

Instead, we propose that the water loss involves a concerted cyclization and direct bond cleavage in **PFE1c**. The resulting proton-bridged ion **PFE2** may then lose water (as D₂O) to produce protonated 2-oxazoline. An analogous mechanism has been proposed for the loss of H₂O from serine residues in protonated peptides and proteins [27].

A direct 1,2-H shift in **PFE1b** [26] cannot account for the competing loss of CO because it requires 24 kcal mol⁻¹ more energy than our proposed H₂O loss mechanism. However, a search of the potential energy surface yielded the remarkable structure “TS [95]” of

Scheme 9.11, whose energy lies 2 kcal mol⁻¹ below the rate-determining TS for the water loss. In this decarbonylation, the N-C bond of “TS [95]” elongates as the aldehydic H is transferred to the hydroxyl group. The resulting transient complex, comprising the O-protonated species H₂OCH₂CH₂NH₂⁺ and CO, then rearranges via a 1,4-H shift to produce HOCH₂CH₂NH₃⁺ + CO.

As suggested in Section 9.2.1, the notable peaks at *m/z* 71, 59 and 46 in the CID spectrum of PFE ions generated by self-protonation (Fig. 9.2d) arise from **PFE** ions that have lost a H[•] radical to produce *m/z* 89 ions having dissociation characteristics akin to that of ionized N-formylethanolamine. We have not computationally examined the myriad of NFEA isomers that can be envisaged to be generated upon H[•] loss. An attractive possibility is that distonic ion **FE2** of Scheme 9.7, a key intermediate in the dissociation of ion **FE1**, is generated.

9.3 Summary

The fruitful interplay of theory and experiment of this study reveals that distonic ions and hydrogen-bridged radical cations (HBRCs) play a key role in the fascinating dissociation chemistry of the N-formylethanolamine radical cation, HOCH₂CH₂NHC(H)=O^{•+} (**FE1**).

As discussed in Section 9.2.2, the primary fragmentations involving the loss of CH₂O and C₂H₃O[•] yield the distonic ion [•]CH₂N(H)CHOH⁺ and O-protonated formamide HC(OH)NH₂⁺ respectively. The competing H₂O loss yields a mixture of N-vinylformamide ions **1b** and its cyclized distonic isomer **1a**: the CID spectrum is very close to a reference spectrum of **1b**, but its enhanced charge-stripping peak betrays that ions **1a** are also present.

Rotation of the amide bond of the conformers of neutral and ionized N-formylethanolamine involves a sizeable energy barrier. In Section 9.2.3 and Scheme 9.6, theory provides a rationale for the experimental finding that the ions do *not* decarbonylate which implies that the *E*- and *Z*-conformers have the same dissociation characteristics.

The mechanistic analysis of Section 9.2.4 and Scheme 9.7 indicates that :

(i) cleavage of the C–C bond in the incipient molecular ions **FE1** generates **HBRC1**,

$[\text{CH}_2\text{N}(\text{H})\text{C}(\text{H})=\text{O}--\text{H}---\text{O}=\text{CH}_2]^{\bullet+}$, which serves as the direct precursor to CH_2O loss.

(ii) a competing 1,5-H shift, the first step of a McLafferty rearrangement, generates distonic ion **FE2**, $\text{HOCHCH}_2\text{N}(\text{H})\text{C}(\text{H})\text{OH}^{\bullet+}$, which serves as the precursor for the loss of both $\text{C}_2\text{H}_3\text{O}^\bullet$ and H_2O .

(iii) loss of $\text{C}_2\text{H}_3\text{O}^\bullet$ from **FE2** involves a “McLafferty + 1” type reaction in which HBRCs act as key intermediates : **FE2** \rightarrow **HBRC2** \rightarrow **HBRC4a** \rightarrow $\text{HC}(\text{OH})\text{NH}_2^+ + \text{CH}_2=\text{CHO}^\bullet$. Prior to dissociation, a fraction of ions **HBRC4a** may undergo the quid-pro-quo (QPQ) catalysis of Scheme 9.8, which would co-generate the more stable acetyl radical $\text{CH}_3\text{C}=\text{O}^\bullet$.

(iv) loss of H_2O from **FE2** involves communication with ion-molecule complexes of vinyl alcohol and formimidic acid, whose components may recombine to form distonic ion **FE3**, $\text{HOCH}(\text{CH}_2)\text{N}(\text{H})\text{C}(\text{H})\text{OH}^{\bullet+}$. This ion loses H_2O via the 1,5-H shift reaction **FE3** \rightarrow **HBRC3a** \rightarrow ion **1b** + H_2O . The facile cyclization of **HBRC3a** to **HBRC3c** may account for the co-generation of ion **1a**.

The behaviour of the various D- and ^{18}O -labelled isotopologues examined in Section 9.2.5 is basically in accord with the above mechanisms. The MI spectra of the labelled ions indicate that in the loss of water, the positional identity of the D and O atoms is not completely retained. A rationale provided by theory for this finding involves the participation of the QPQ type reactions of Scheme 9.9 for H/D exchange. Scheme 9.10 presents two side reactions of ion **IDC**, a key intermediate in the H_2O loss of Scheme 9.7, that lead to unreactive isomers whose O atoms are equivalent. These reactions could account for the partial equilibration of the O-atoms.

Finally, a re-examination of the dissociation of protonated N-formylethanolamine proposes that the losses of H_2O and CO generate protonated 2-oxazoline and N-protonated ethanol-amine respectively via the mechanisms of Scheme 9.11.

References

- [1] (a) I. Howe, D.H. Williams, R.D. Bowen, *Mass Spectrometry : Principles and Applications*. 2nd Ed. McGraw-Hill International Book Company, New York, 1981. (b) F.W. McLafferty, F. Tureček. *Interpretation of Mass Spectra*. 4th Ed. University Science Books, Mill Valley, 1993. p. 81 ; (c) R.M. Smith. *Understanding Mass Spectra : A Basic Approach*. 2nd Ed. John Wiley & Sons, Hoboken, 2004. p. 234; (d) F. Tureček, in N.M.M. Nibbering (Ed.), *Encyclopedia of Mass Spectrometry*, vol. 4, Elsevier, Amsterdam, 2005, p. 396
- [2] M.B. Stringer, D.J. Underwood, J.H. Bowie, C.E. Allison, K.F. Donchi, P.J. Derrick, *Org. Mass Spectrom.* 27 (1992) 270.
- [3] D. Kuck, in N.M.M. Nibbering (Ed.), *Encyclopedia of Mass Spectrometry*, vol. 4, Elsevier, Amsterdam, 2005, p. 110 – 111.
- [4] (a) G. Bouchoux, Y. Hoppilliard, *Int. J. Mass Spectrom.* 90 (1989) 197; (b) C.E. Hudson, L.L. Griffin, D.J. McAdoo, *Org. Mass Spectrom.* 24 (1989) 866; (c) A.E. Dorigo, M.A. McCarrick, R.J. Loncharich, K.N. Houk, *J. Am. Chem. Soc.* 112 (1990) 7508.
- [5] (a) J. Loos, D. Schröder, W. Zummack, H. Schwarz, R. Thissen, O. Dutuit, *Int. J. Mass Spectrom.* 214 (2002) 105; (b) M. Semialjac, J. Loos, D. Schröder, H. Schwarz, *Int. J. Mass Spectrom.* 214 (2002) 129. (c) D. Schröder, J. Loos, M. Semialjac, T. Weiske, H. Schwarz, G. Hohne, R. Thissen, O. Dutuit, *Int. J. Mass Spectrom.* 214 (2002) 155.
- [6] (a) J.A. Montgomery, Jr., M.J. Frisch, J.W. Ochterski, G.A. Petersson, *J. Chem. Phys.* 112 (2000) 6532; (b) L.A. Curtiss, P.C. Redfern, K. Raghavachari, *J. Chem. Phys.* 126 (2007) 084108; (c) J.M.L. Martin, S. Parthiban, in J. Cioslowski and A. Szarecka (Ed.), *Quantum Mechanical Prediction of Thermochemical Data, Understanding Chemical Reactivity Series*, Vol. 22, Kluwer Academic Publishers, Dordrecht, 2005, p. 31 - 65; (d) L.N. Heydorn, Y. Ling, G. de Oliveria, J.M.L. Martin, Ch. Lifshitz, J.K. Terlouw, *Zeitschrift für Physikalische Chemie* 215 (2001) 141.
- [7] (a) R. Lee, P.J.A. Ruttink, P.C. Burgers, J.K. Terlouw, *Can. J. Chem.* 83 (2005) 1847; (b) K.J. Jobst, T.R. Khan, J.K. Terlouw, *Int. J. Mass Spectrom.* 42 (2007) 1024.
- [8] P.C. Burgers, J.K. Terlouw, in N.M.M. Nibbering (Ed.), *Encyclopedia of Mass Spectrometry*, vol. 4, Elsevier, Amsterdam, 2005, p. 173
- [9] (a) R. Lee, P.J.A. Ruttink, P.C. Burgers, J.K. Terlouw, *Int. J. Mass Spectrom.* 255 (2006) 244 and references cited therein; (b) K.J. Jobst, P.C. Burgers, P.J.A. Ruttink, J.K. Terlouw, *Int. J. Mass Spectrom.* 254 (2006) 127.
- [10] (a) D.J. McAdoo, C.E. Hudson, M. Skyiepal, E. Broido, L.L. Griffin, *J. Am. Chem. Soc.* 109 (1987) 7648; (b) J. Loos, D. Schröder, H. Schwarz, *J. Org. Chem.* 70 (2005) 1073.
- [11] J.L. Holmes, K.J. Jobst, J.K. Terlouw, *J. Labelled Compd. Radiopharm.* 50 (2007) 1088
- [12] G. Schaftenaar, R. Postma, P.J.A. Ruttink, P.C. Burgers, G.A. McGibbon, J.K. Terlouw, *Int. J. Mass Spectrom. Ion Process.* 100 (1990) 521.
- [13] G.A. McGibbon, P.C. Burgers, J.K. Terlouw, *Int. J. Mass Spectrom.* 136 (1994) 191.
- [14] P.R. Schreiner, H.P. Reisenauer, F.C. Pickard IV, A.C. Simmonett, W.D. Allen, E. Matyus, A.G. Csaszar, *Nature* 453 (2008) 906.
- [15] (a) G. da Silva, C-H Kim, J.W. Bozzelli, *J. Phys. Chem. A*, 110 (2006) 7925; (b) E.A. Fogleman, H. Koizumi, J.P. Kercher, B. Sztáray, T. Baer, 108 (2004) 5288. (c) G. Bouchoux, J. Chamot-Rooke, D. Leblanc, P. Morgues, M. Sablier, *Chem. Phys. Chem.* 2 (2001) 235.
- [16] B.L.M. van Baar, P.C. Burgers, J.L. Holmes, J.K. Terlouw, *Org. Mass Spectrom.*, 23 (1988) 355; note that the CIDI mass spectra of CH_3CO^+ (Fig. 2a) and CH_2CHO^+ (Fig. 2b) are transposed.
- [17] J.L. Holmes, C. Aubry, P.M. Mayer. *Assigning Structures to Ions in Mass Spectrometry*. CRC Press, Boca Raton, 2007.
- [18] (a) T. Wong, J. Warkentin, J.K. Terlouw, *Int. J. Mass Spectrom. Ion Proc.* 115 (1992) 33; (b) M.M. Cordero, J.J. Houser, C. Wesdemiotis, *Anal. Chem.* 65 (1993) 1594.

- [19] J.K. Terlouw, P.C. Burgers, J.L. Holmes, *Org. Mass Spectrom.*, 14 (1979) 387.
- [20] P.J.A. Ruttink, P.C. Burgers, J.K. Terlouw, *Int. J. Mass Spectrom. Ion Proc.* 145 (1995) 35.
- [21] (a) D.M. Pawar, A.A. Khalil, D.R. Hooks, K. Collins, T. Elliot, J. Stafford, L. Smith, E.A. Noe, *J. Am. Chem. Soc.* 120 (1998) 2108; (b) J.P. Terhorst, W.L. Jorgensen, *J. Chem. Theory Comput.* 6 (2010) 2762.
- [22] W. Heerma, M.M. Sarneel, J.K. Terlouw, *Org. Mass Spectrom.* 16 (1981) 326.
- [23] S. Nakajima, T. Asakawa, O. Sekiguchi, S. Tajima, N.M.M. Nibbering, *Eur. J. Mass Spectrom.* 7 (2001) 47.
- [24] (a) P.M.W. Gill, L. Radom, *J. Am. Chem. Soc.* 110 (1988) 4931; (b) S. Humbel, I. Côte, N. Hoffmann, J. Bouquant, *J. Am. Chem. Soc.* 121 (1999) 5507.
- [25] R.G. Cooks, J.H. Beynon, R.M. Caprioli, G.R. Lester. *Metastable Ions*. Elsevier Scientific Publishing Company, New York, 1973, p. 257.
- [26] L. Tip, C. Versluis, J.W. Dallinga, W. Heerma, *Anal. Chim. Acta* 241 (1990) 219.
- [27] B. Paizs, S. Suhai, *Mass Spectrom. Rev.* 24 (2005) 508.

Appendix to Chapter 9

Table 9.1 Energetic data derived from CBS-QB3 calculations [a] used to probe the structure and reactivity of dissociation products of ionized N-formylethanolamine (Figure 9.3 and Schemes 9.3/9.4).

Species and mass	CBS-QB3 E(total) [0 K]	QB3 $\Delta_f H^0_{298}$	Species and mass	CBS-QB3 E(total) [0 K]	QB3 $\Delta_f H^0_{298}$
Fig. 9.4 ion 1a 71	-246.57683	174.2	Fig. 9.4 ion 6a 71	-246.51284	214.7
Fig. 9.4 ion 1b ₁ 71	-246.56491	182.3	Fig. 9.4 ion 6b 71	-246.51551	213.4
Sch. 9.4 ion 1b ₂ 71	-246.56198	184.2	Fig. 9.4 ion 6c 71	-246.51742	212.3
Fig. 9.4 ion 1c 71	-246.55627	188.0	Fig. 9.4 ion 6d 71	-246.54710	194.7
Fig. 9.4 ion 1d 71	-246.51574	212.8	Fig. 9.4 ion 7a 71	-246.52469	207.3
Fig. 9.4 ion 1e 71	-246.53003	204.4	Fig. 9.4 ion 7b 71	-246.54593	194.5
Fig. 9.4 ion 1f 71	-246.54533	195.3	Fig. 9.4 ion 8a 71	-246.46343	245.5
Fig. 9.4 ion 2a 71	-246.56802	179.9	Fig. 9.4 ion 8b 71	-246.50370	221.2
Fig. 9.4 ion 2b 71	-246.52221	209.1	Fig. 9.4 ion 9 71	-246.50699	218.0
Fig. 9.4 ion 3a 71	-246.58663	167.9	TS 1a → m/z 70	-246.52039	209.6
Fig. 9.4 ion 3b 71	-246.55412	189.0	TS 1b ₁ → 1b ₂	-246.55441	188.6
Fig. 9.4 ion 4a 71	-246.52992	203.6	TS 1b ₁ → 1a	-246.54987	191.0
Fig. 9.4 ion 4b 71	-246.53251	202.1	TS 1b ₁ → m/z 43	-246.45400	251.8
Fig. 9.4 ion 5a 71	-246.53566	200.6	TS 1b ₁ → m/z 43 [b]	-246.50773	218.9
Fig. 9.4 ion 5b 71	-246.53980	198.7	TS 1b ₂ → 1f	-246.51782	211.4
Fig. 9.4 ion 5c 71	-246.55398	189.3	TS 1f → m/z 43	-246.53291	203.2
Sch. 9.3 ion 1a-H 70	-246.02895	153.2	HC(=NH)CH ₃ ⁺	-133.35001	230.9
CH ₂ N(H)CHOH ⁺ 59	-208.54478	159.2	CH ₃ C=O [c]	-152.94205	-2.1
HC(OH)NH ₂ ⁺ 46	-169.96226	124.7	CH ₂ =CHO* [c]	-152.93284	3.4
HC(=O)NH ₂ 45	-169.65356	-45.7	CH ₂ =O 30	-114.34417	-27.0
HC(=NH)OH 45	-169.63475	-34.2	CO 28	-113.18201	-26.6
CH ₂ =CHOH ⁺ 44	-153.22216	186.2	H ₂ O 18	-76.33750	-57.0

[a] E(total) in Hartrees, 298K enthalpies in kcal mol⁻¹; [b] "ion dipole" TS of Scheme 9.4 [c] the tabulated values are in close agreement with the experimental values of -2.3 and 3.1 kcal mol⁻¹ found in Refs 15b/c.

Table 9.2a Energetic data [a] from CBS-QB3 calculations of stable isomers involved in the dissociation chemistry of N-formylethanolamine ions **FE1**.

Species		B3LYP/CBSB7 E(total)	CBS-QB3 E(total) [0K]	ZPE	QB3 $\Delta_f H^0_0$	QB3 $\Delta_f H^0_{298}$	$\langle S^2 \rangle$
NFE1a	(Scheme 9.5)	-323.82528	-323.24071	67.0	-83.4	-89.4	-
NFE1b	(Scheme 9.5)	-323.82706	-323.24156	67.3	-83.9	-90.1	-
NFE1c	(Scheme 9.5)	-323.82142	-323.23703	66.8	-81.1	-87.0	-
NFE1d	(Scheme 9.5)	-323.82683	-323.24147	67.1	-83.9	-89.9	-
NFE1e	(Scheme 9.5)	-323.82232	-323.23745	66.7	-81.4	-87.2	-
FE1b	(Scheme 9.5)	-323.50004	-322.89040	66.9	136.4	130.1	0.77
FE1d	(Scheme 9.5)	-323.49489	-322.89483	66.0	133.6	127.7	0.94
FE1e	(Scheme 9.5)	-323.48986	-322.88961	65.8	136.9	131.1	0.96
FE2a	(Scheme 9.7a/b)	-323.50756	-322.91103	67.1	123.5	117.2	0.76
FE2b	(Scheme 9.7a)	-323.50953	-322.91367	66.8	121.8	115.9	0.76
FE2c	(Scheme 9.7a)	-323.50920	-322.91312	66.7	122.1	116.3	0.76
FE3	(Scheme 9.7b)	-323.50794	-322.91411	65.9	121.5	115.7	0.76
FE4	(Scheme 9.7a)	-323.49180	-322.89800	66.9	131.6	125.6	0.76
FE5	(Scheme 9.6)	-323.47327	-322.87645	66.7	145.2	139.0	0.76
FE6	(Scheme 9.6)	-323.48281	-322.88688	67.1	138.6	132.7	0.78
FE7	(Scheme 9.9)	-323.49109	-322.89120	65.3	135.9	130.0	0.76
FE8	(Scheme 9.10)	-323.52560	-322.92649	67.0	113.8	107.4	0.80
FE9	(Scheme 9.10)	-323.51812	-322.92581	66.3	114.2	108.2	0.84
FE10	(Scheme 9.10)	-323.46636	-322.87536	65.2	145.8	139.8	0.77
IDC	(Scheme 9.7b)	-323.51318	-322.91348	65.0	121.9	116.6	0.77
LB1a	(Scheme 9.8)	-323.51981	-322.90252	64.3	128.8	123.6	0.77
LB1b	(Scheme 9.8)	-323.52181	-322.90477	64.4	127.4	122.2	0.77
HBRC1	(Scheme 9.7a)	-323.51259	-322.91384	64.0	121.7	116.5	0.82
HBRC2	(Scheme 9.7a)	-323.49539	-322.89580	64.4	133.0	127.6	0.77
HBRC3a	(Scheme 9.7b)	-323.52366	-322.92885	63.7	112.3	107.5	0.86
HBRC3b	(Scheme 9.7b)	-323.53146	-322.94155	64.8	104.3	98.9	0.84
HBRC4a	(Scheme 9.7a)	-323.52832	-322.92920	64.4	112.1	107.0	0.86
HBRC4b	(Scheme 9.8)	-323.54258	-322.93982	65.0	105.4	100.0	0.82
HBRC4c	(Scheme 9.8)	-323.53891	-322.93843	64.9	106.3	101.3	0.76
HBRC5a	(Scheme 9.6)	-323.49940	-322.90789	61.8	125.4	121.2	0.76
HBRC5b	(Scheme 9.6)	-323.49096	-322.90211	62.4	129.1	124.0	0.91
HBRC6	(Scheme 9.6)	-323.49910	-322.90335	64.1	128.3	123.6	0.78
HBRC7	(Scheme 9.9)	-323.51895	-322.92015	63.4	117.7	112.9	0.90
HBRC8	(Scheme 9.9)	-323.49969	-322.90551	63.2	126.9	121.9	0.87
HBRC9	(Scheme 9.9)	-323.50921	-322.91527	61.8	120.8	116.4	0.78

[a] $E_{\text{(total)}}$ in Hartrees, all other components, including the ZPE scaled by 0.99, are in kcal mol⁻¹

Table 9.2b Energetic data [a] from CBS-QB3 calculations of the connecting transition states involved in the dissociation chemistry of N-formylethanolamine ions **FE1**.

Species		B3LYP/CBSB7 E(total)	CBS-QB3 E(total) [0K]	ZPE	QB3 $\Delta_r H^0_0$	QB3 $\Delta_r H^0_{298}$	$\langle S^2 \rangle$
TS NFE1a → b	(Scheme 9.5)	-323.82081	-323.23558	67.4	-80.2	-86.8	-
TS NFE1b → c	(Scheme 9.5)	-323.82041	-323.23648	66.5	-80.8	-87.0	-
TS NFE1c → d	(Scheme 9.5)	-323.82136	-323.23738	66.7	-81.3	-87.7	-
TS NFE1c → e	(Scheme 9.5)	-323.79310	-323.21054	66.5	-64.5	-71.0	-
TS FE1b → d	(Scheme 9.5)	-323.47975	-322.88220	65.5	141.6	135.2	0.76
TS FE1b → e	(Scheme 9.5)	-323.47121	-322.87311	64.8	147.3	141.3	0.78
TS FE1b → 2a	(Scheme 9.7a)	-323.48963	-322.89026	65.8	136.5	130.3	0.78
TS FE1b → 6	(Scheme 9.6)	-323.40192	-322.81344	63.0	184.7	178.7	0.79
TS FE1b → 7	(Scheme 9.10)	-323.46028	-322.86744	62.5	150.8	144.6	0.80
TS FE1b → 9	(Scheme 9.10)	-323.45826	-322.86223	63.0	154.1	147.5	0.76
TS FE1b → HBRC1	(Scheme 9.7a)	-323.48772	-322.88549	64.3	139.5	133.4	0.77
TS FE1e → 5	(Scheme 9.6)	-323.46057	-322.86376	66.4	153.1	147.0	0.76
TS FE2a → b	(Scheme 9.7a)	-323.48601	-322.89432	65.7	133.9	127.9	0.76
TS FE2a → 3	(Scheme 9.7b)	-323.48746	-322.88894	64.8	137.3	131.5	0.77
TS FE2a → 10	(Scheme 9.10)	-323.46304	-322.87033	63.0	149.0	142.7	0.76
TS FE2b → c	(Scheme 9.7a)	-323.50061	-322.90787	65.9	125.4	119.4	0.76
TS FE2b → HBRC2	(Scheme 9.7a)	-323.49387	-322.89520	64.2	133.4	127.6	0.77
TS FE2c → 4	(Scheme 9.7a)	-323.47197	-322.88049	64.1	142.6	136.3	0.76
TS FE3 → 7	(Scheme 9.9)	-323.48386	-322.89105	63.2	136.0	129.4	0.79
TS FE3 → 10	(Scheme 9.10)	-323.46103	-322.87167	65.4	148.2	141.6	0.79
TS FE3 → IDC	(Scheme 9.7b)	-323.48684	-322.89275	64.4	134.9	128.6	0.76
TS FE4 → HBRC4	(Scheme 9.7a)	-323.47133	-322.87227	64.5	147.8	141.8	0.93
TS FE5 → 6	(Scheme 9.6)	-323.47395	-322.88016	65.1	142.8	136.4	0.77
TS FE5 → HBRC5a	(Scheme 9.6)	-323.45533	-322.84521	63.3	164.8	159.3	0.76
TS FE6 → HBRC6	(Scheme 9.6)	-323.48119	-322.88215	65.5	141.6	135.7	0.76
TS FE7 → HBRC9	(Scheme 9.9)	-323.47504	-322.88060	63.9	142.6	136.2	0.78
TS FE8 → 9	(Scheme 9.10)	-323.46838	-322.87663	65.9	145.0	138.6	0.76
TS IDC → HBRC3a	(Scheme 9.7b)	-323.50905	-322.91927	63.6	118.3	113.1	0.82
TS IDC → FE8	(Scheme 9.10)	-323.51190	-322.91028	66.0	123.9	117.6	0.77
TS LB1a → 1b	(Scheme 9.8)	-323.50549	-322.89145	63.4	135.7	130.3	0.78
TS LB1b → HBRC4c	(Scheme 9.8)	-323.51333	-322.89953	63.0	130.7	125.3	0.78
TS HBRC2 → 4	(Scheme 9.7a)	-323.49204	-322.89453	64.1	133.8	128.3	0.77
TS HBRC3a → b	(Scheme 9.7b)	-323.50544	-322.91285	63.8	122.3	116.8	0.78
TS HBRC3a → 7	(Scheme 9.9)	-323.50662	-322.90980	63.1	124.2	118.2	0.91
TS HBRC3a → 8	(Scheme 9.9)	-323.47406	-322.87975	64.0	143.1	137.7	0.82
TS HBRC4a → b	(Scheme 9.8)	-323.51051	-322.91368	63.3	121.8	116.5	0.85
TS HBRC4b → LB1a	(Scheme 9.8)	-323.49055	-322.89100	60.2	136.0	130.3	0.79
TS HBRC4b → c	(Scheme 9.8)	-323.47228	-322.87312	62.3	147.3	141.9	0.77
TS HBRC5a → b	(Scheme 9.6)	-323.48681	-322.89611	62.6	132.8	127.7	0.83

[a] $E_{(\text{total})}$ in Hartrees, all other components, including the ZPE scaled by 0.99, are in kcal mol⁻¹

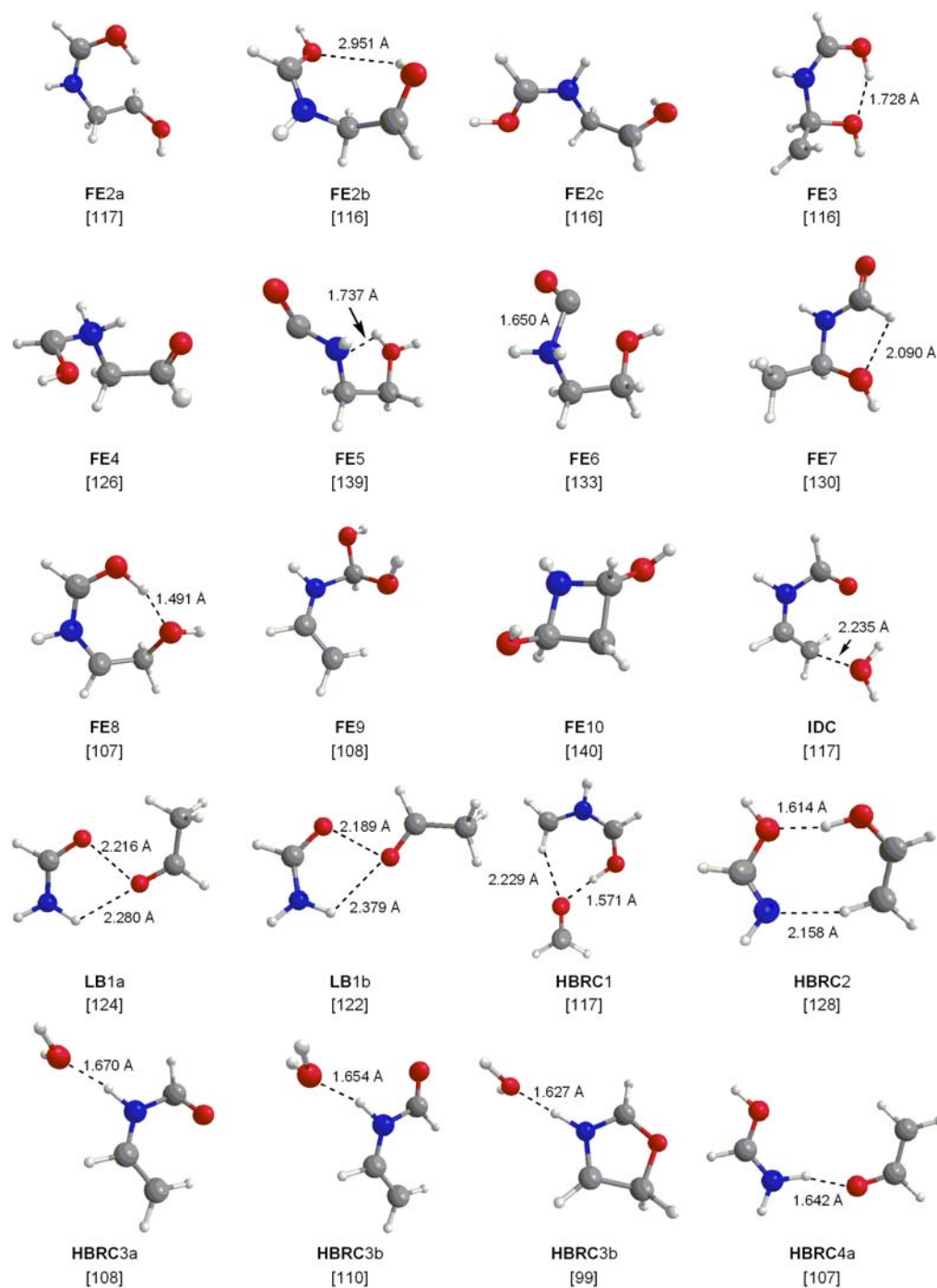


Figure 9.5 Optimized geometries of selected minima and transition states involved in the dissociation chemistry of ionized N-formylethanolamine. Numbers in brackets are CBS-QB3 derived 298 K enthalpies in kcal mol⁻¹.

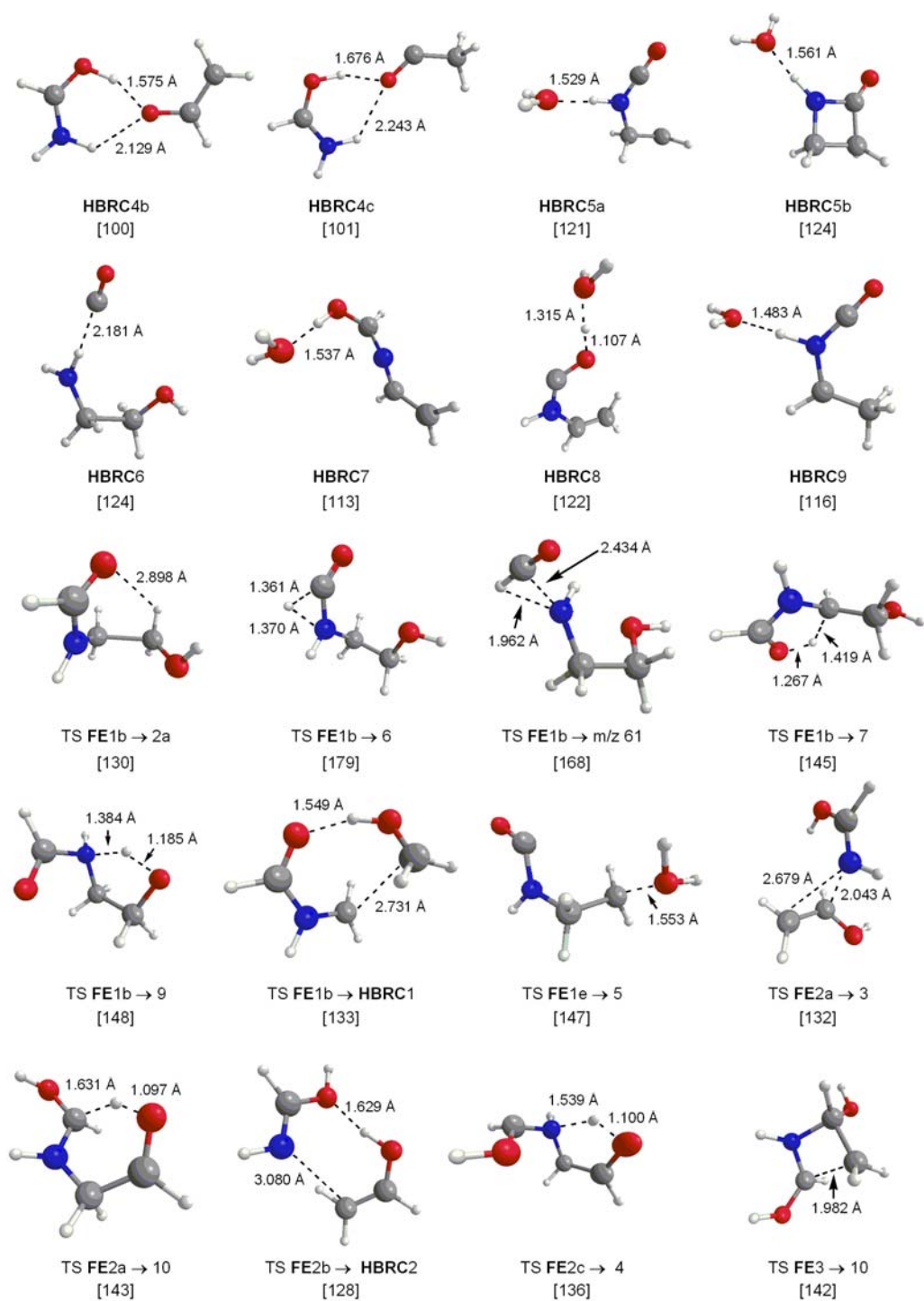


Figure 9.5 continued

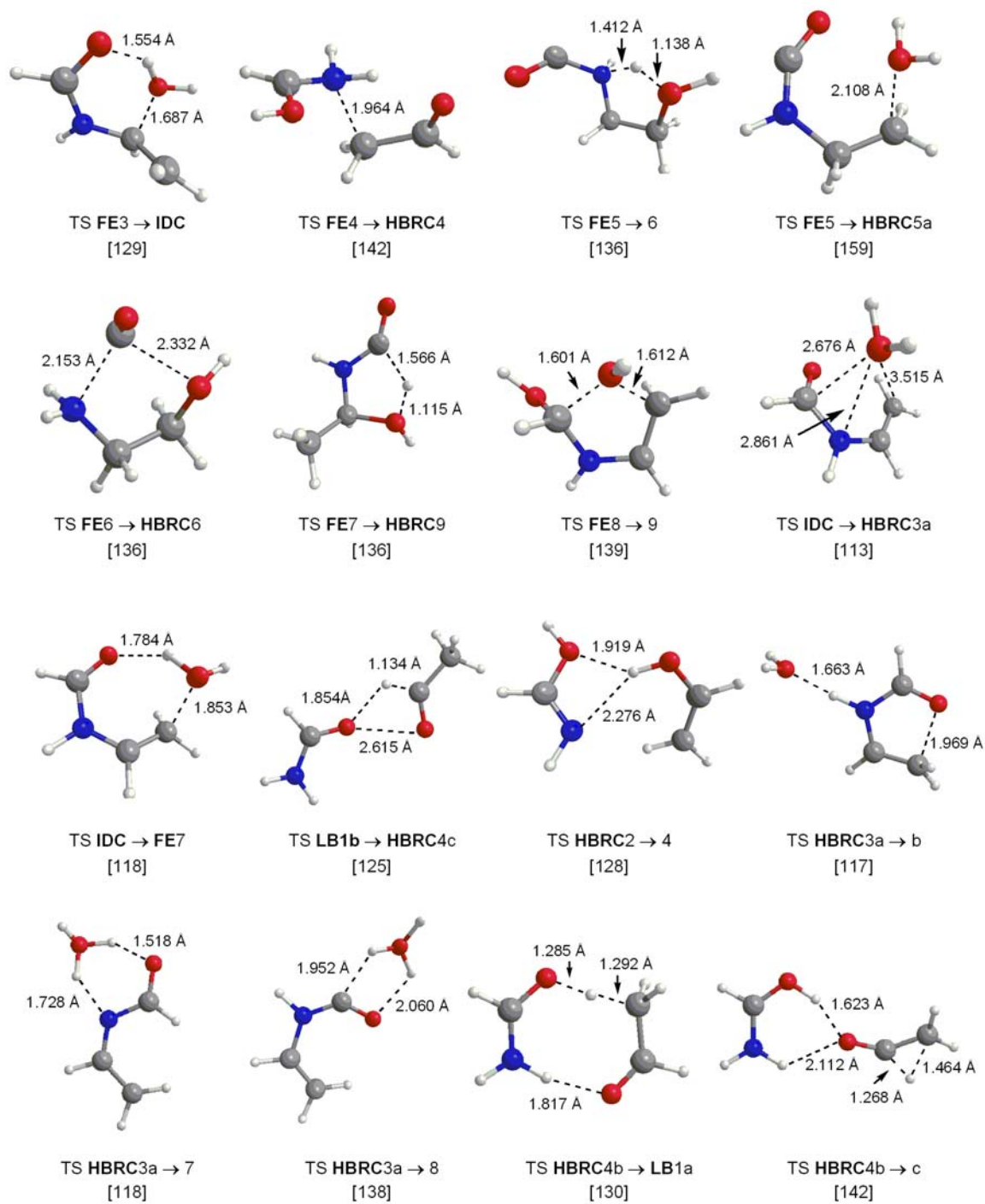
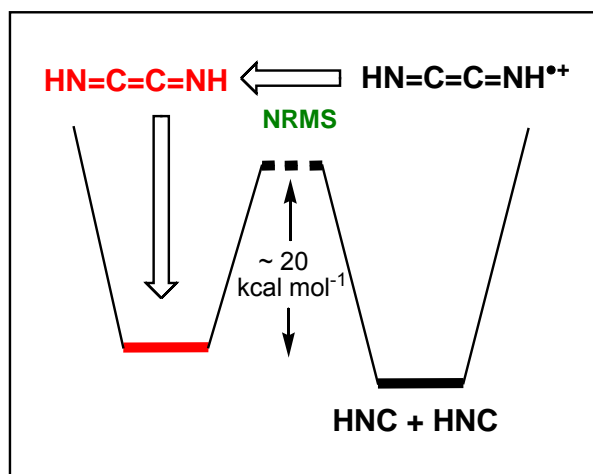


Figure 9.5 continued

Chapter 10

The covalently bound HNC dimer ion $\text{HN}=\text{C}=\text{C}=\text{NH}^{\bullet+}$ has a kinetically stable neutral counterpart



Neutralization-Reionization Mass Spectrometry (NRMS) and computational chemistry (CBS-QB3/APNO methods) have been used to show that $\text{HN}=\text{C}=\text{C}=\text{NH}$ (ethenediimine) and its isomer $\text{H}_2\text{N}-\text{C}-\text{C}\equiv\text{N}$ (aminocyanocarbene) are generated as kinetically stable molecules in the rarefied gas-phase by one electron reduction of their ionic precursors. One route to the very stable ion $\text{HN}=\text{C}=\text{C}=\text{NH}^{\bullet+}$ involves loss of $\text{HC}\equiv\text{N}$ from the hydrogen bridged radical cation $[\text{HN}\equiv\text{C}\cdots\text{H}_2\text{N}-\text{C}-\text{C}\equiv\text{N}]^{\bullet+}$ via a remarkable *quid-pro-quo* catalysis in which both the ion and the neutral undergo isomerization.

The work described here has been published previously in an article under the same title : K.J. Jobst, M.R. Hanifa, J.K. Terlouw, Chem. Phys. Lett. 462 (2008) 152 – 157.

10.1 Introduction

Gaseous HCN and HNC molecules as well as their radical cations are thought to be ubiquitous in both cold, dark molecular clouds and comets [1]. Their covalently bound (ionized) dimers [2] and other $C_2H_2N_2$ isomers are therefore of considerable interest as potential interstellar and also prebiotic species [3].

So far, two $C_2H_2N_2$ isomers have been generated and thoroughly characterized by various spectroscopic methods as stable molecules in the gas-phase: $CH_2=N-C\equiv N$ (N-cyanomethan-amine) and $HN=C(H)C\equiv N$ (iminoacetonitrile or C-cyanomethanimine) [3-5]. In an earlier study [6] it had been proposed that the thermal or photolytic decomposition of alkali metal salts of 1-cyanoformamide tosylhydrazone yields a third $C_2H_2N_2$ isomer, $NH_2-C-C\equiv N$ (aminocyanocarbene). However, the exhaustive studies of refs. 3-5 leave little doubt that the above reaction yields the iminoacetonitrile isomer instead.

On the other hand, a recent detailed computational study [7] reports quite a high barrier (56 kcal mol^{-1}) for the carbene's *intramolecular* isomerization (via a 1,2-insertion reaction) into the more stable iminoacetonitrile isomer. This indicates that the carbene should be an observable species in the rarefied gas-phase of the mass spectrometer where *intermolecular* reactions are absent.

We therefore decided to probe the stability of the carbene by Neutralization-Reionization Mass Spectrometry (NRMS) [8] of its ionic counterpart generated by the dissociative ionization of a suitable precursor molecule. The same stratagem we applied in our search for the elusive heterocumulene $HN=C=C=NH$ (ethenediimine) [9], whose ionic counterpart is a prominent fragment ion in the EI mass spectra of various oxy-purines [9-12].

It will be shown that $HN=C=C=NH$ and $NH_2-C-C\equiv N$ are both (kinetically) stable $C_2H_2N_2$ molecules in the microsecond timeframe of the NRMS experiment.

10.2 Results and discussion

10.2.1 Analysis of the CID mass spectra of $\text{HN}=\text{C}=\text{C}=\text{NH}^{*\dagger}$ and $\text{NH}_2\text{-C-C}\equiv\text{N}^{*\dagger}$

The EI mass spectrum of xanthine [10] shows a prominent peak at m/z 54. These m/z 54 ions have been proposed [10-12] to be ethenediimine ions $\text{HN}=\text{C}=\text{C}=\text{NH}^{*\dagger}$ (**1**), generated by the consecutive loss of HNCO , CO and HCN as depicted in Figure 10.1. It is conceivable that a less transparent dissociation pathway, initiated from a tautomer of either the neutral or the ionized precursor, could be operative. However, a survey of the potential energy surface using the two model chemistries, see Table 10.1, indicates that **1** (which has two conformers **1a** and **1b**, connected by a negligible energy barrier) represents the most stable $\text{C}_2\text{H}_2\text{N}_2^{*\dagger}$ isomer. Thus, from a thermochemical standpoint, route (a) in Figure 10.1 is the most plausible. The CID mass spectrum of ion **1** generated from ionized xanthine is shown in Fig. 10.2a.

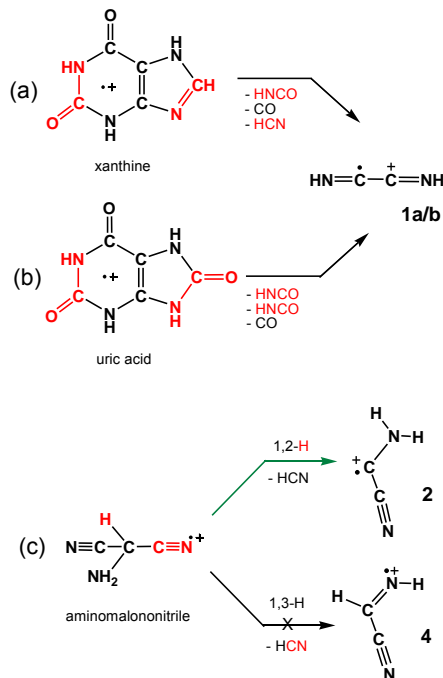


Figure 10.1 Proposed fragmentation pathways of precursor ions which yield the HCN dimer ions **1** and **2**.

Table 10.1 Enthalpies of formation (kcal mol⁻¹) and total energies (Hartree) derived from CBS-QB3 and CBS-APNO calculations [a].

Isomer		CBS-QB3 E(total) [0K]	QB3 $\Delta_f H^0_{298}$	APNO $\Delta_f H^0_{298}$	RE _v [b]	Transition State	CBS-QB3 E(total) [0K]	QB3 $\Delta_f H^0_{298}$	APNO $\Delta_f H^0_{298}$
HN=C=C=NH ⁺	1a	-186.216134	288	286 [c]	7.3	TS 1a → b	-186.215545	288	289
HN=C=C=NH ⁺	1b	-186.214811	289	289	7.2	TS 1a → 3	-186.139175	336	335
H ₂ N-C-C≡N ⁺	2	-186.204802	295	295	8.4	TS 3 → 4a	-186.124516	345	[d]
HN=C-C(H)=N ⁺	3	-186.205889	294	295	7.1	TS 4a → b	-186.181356	310	310
HN=C(H)-C≡N ⁺ (<i>E</i>)	4a	-186.181675	309	310	9.9	TS 4b → 2	-186.115557	351	350
HN=C(H)-C≡N ⁺ (<i>Z</i>)	4b	-186.181132	310	310	9.9	TS 1a → 2	-186.090620	366	365
HN=C=C=NH	N1a	-186.518834	98	98	-	TS 1a → <i>m/z</i> 53	-	[e]	338
HN=C=C=NH	N1b	-186.517408	99	99	-	TS 2 → <i>m/z</i> 53	-186.128390	343	344
H ₂ N-C-C≡N	N2	-186.537042	86	86	-				
N=C(H)C=NH	N3	no minimum	-	-	-	TS N1a → N1b	-186.491778	115	114
HN=C(H)-C≡N (<i>E</i>)	N4a	-186.581318	58	58	-	TS N4a → N4b	-186.540876	84	84
HN=C(H)-C≡N (<i>Z</i>)	N4b	-186.582492	58	58	-	TS N4b → N2	-186.458389	136	136
						TS N1a → N2	-186.419764	159	156
HN=C=C=N ⁺ + H [•]		-	336	336	-				
HN=C=C=N [•] + H [•]		-	153	153	-	TS N1a → 2 HNC	-186.483945	120	119
HCN + HCN		-	63	64	-	TS N1b → 2 HNC	-186.486378	118	118
HCN + HNC		-	78	79	-	TS N4a → HCN + HNC	-186.443606	145	144
HNC + HNC		-	92	93	-	TS N1a → HCN + HNC	-186.439735	147	[d]

[a] The CBS-QB3 and CBS-APNO values for H[•] are 52.1 kcal mol⁻¹; [b] Vertical recombination energies in eV from calculations at the B3LYP/CBSB7 level of theory; [c] CBS-QB3 predicts that the ionic HN=C=C=NH conformer **1a** in Fig. 10.3 is a minimum but CBS-APNO predicts it to be a saddle point. The latter is an “artefact” originating from the use of vibrational frequencies obtained at the HF/6-311G(d,p) level of theory, which yields only one stable conformer for the ion; [d] The desired transition state could not be found; [e] The standard B3LYP/CBSB7 routine does not locate a transition state; the BMK/CBSB7 [19] optimization procedure yields 339 kcal mol⁻¹.

Ionized uric acid, which also shows a prominent *m/z* 54 peak in its mass spectrum [10], is expected to generate ion **1** by consecutive losses of two HNCO molecules and CO, see Figure 10.1. In line with this, the CID mass spectrum of these *m/z* 54 ions is identical to that of Fig. 10.2a. The spectrum is characterized by intense signals at *m/z* 53, 28 and 27, corresponding to losses of H[•], CN[•] and HNC. These peaks are prominent in the CID mass

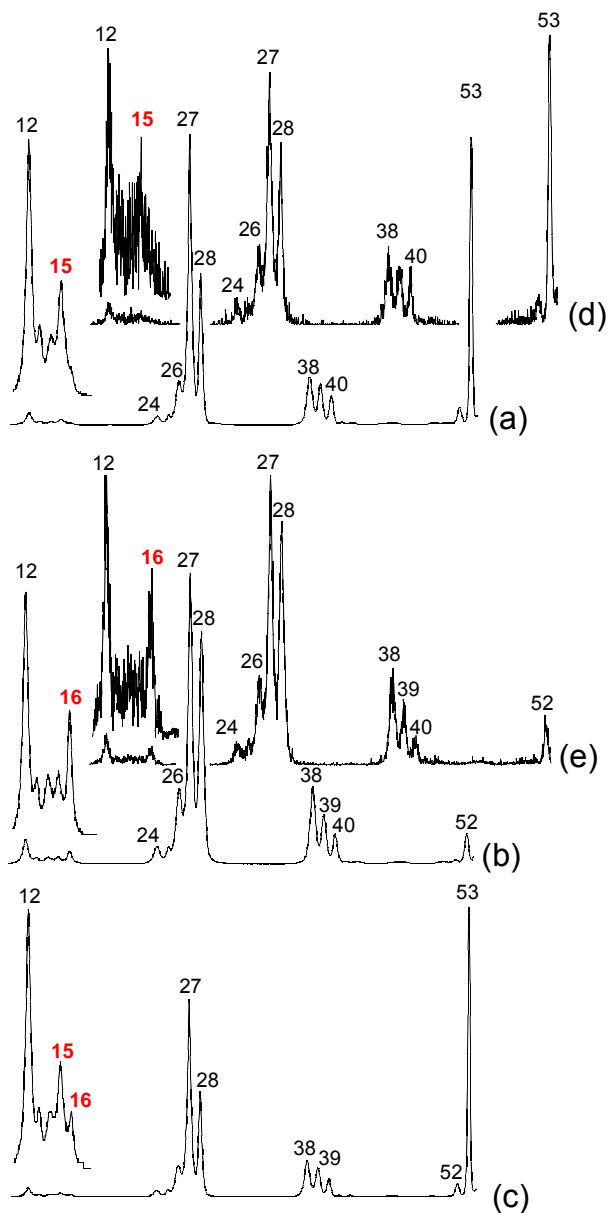


Figure 10.2 (Front) (3ffr, 8kV, O₂) CID mass spectra of *m/z* 54 ions generated by dissociative ionization of (a) xanthine, (b) aminomalonnitrile and (c) diaminomaleonitrile. The *m/z* 53 peak in spectra (b) and (e) is not shown; it is four times as intense as the *m/z* 27 peak. (Back) the corresponding (3ffr, 8kV, O₂) NR-CID mass spectra of the *m/z* 54 ions (d) $\text{HN}=\text{C}=\text{C}=\text{NH}^{*\dagger}$ (1) and (e) $\text{H}_2\text{N}-\text{C}-\text{C}\equiv\text{N}^{*\dagger}$ (2).

spectra of all known $C_2H_2N_2^{*+}$ isomers [4,9] albeit that the relative intensities vary. There are also significant peaks at m/z 40, 39 and 38, corresponding to the losses of N, NH and $NH + H^{\bullet}$. In line with the study of ref. 12 we note that the intensity of the m/z 40 peak is greatly enhanced when O_2 rather than He is used as the collision gas. Finally, there is a weak but structure-diagnostic signal at m/z 15, indicative of the =NH connectivity of ion **1**. The mass spectrum of aminomalononitrile also exhibits a substantial m/z 54 peak. Route (c) of Figure 10.1 depicts the loss of HCN from aminomalononitrile via a 1,2-H shift to generate the aminocyanocarbene ion **2**. One could also envisage that a 1,3-H shift precedes the loss of HCN, which would yield the well characterized [3,4] iminoacetonitrile ion **4**. However, the CID mass spectrum of the m/z 54 ions from aminomalononitrile, see Fig. 10.2b, and the reported literature CID mass spectrum of ion **4** differ considerably. Ion **4** is characterized by a more intense m/z 28 peak (the m/z 27/28 peak intensity ratios for ion **4** in ref. 4 and ion **2** in Fig. 10.2b are 0.85 and 1.10), which corresponds to the direct bond cleavage reaction $\mathbf{4} \rightarrow HC=NH^+ + CN^{\bullet}$. More importantly, the spectrum shows a clear structure-diagnostic peak at m/z 16, indicating that the ions contain the $-NH_2$ connectivity of the proposed carbene structure.

Dissociative ionization of diaminomaleonitrile (DAMN) could also yield ions **2**, by direct C-C bond cleavage: $N\equiv C(NH_2)C=C(NH_2)C\equiv N^{*+} \rightarrow NH_2-C-C\equiv N^{*+}$ (**2**) + $NH_2-C-C\equiv N^{\bullet}$. However, the CID mass spectrum of these ions, see Fig. 10.2c, indicates that we are dealing with a mixture of ions **1** and **2**: their structure diagnostic peaks at m/z 15 and 16 are both present. Further evidence that this is the case comes from the NRMS experiments discussed in Section 10.2.3. A mechanistic proposal which rationalizes these observations is discussed in Section 10.2.4.

10.2.2 Isomerization reactions of ions **1** and **2** and their neutral counterparts *N1* and *N2*

The CID experiments of Section 10.2.1 indicate that ions **1** and **2** do not readily interconvert. Our computational analysis of the various hydrogen shift reactions connecting ions **1** and **2**, see Figure 10.3 (top), provides a rationale.

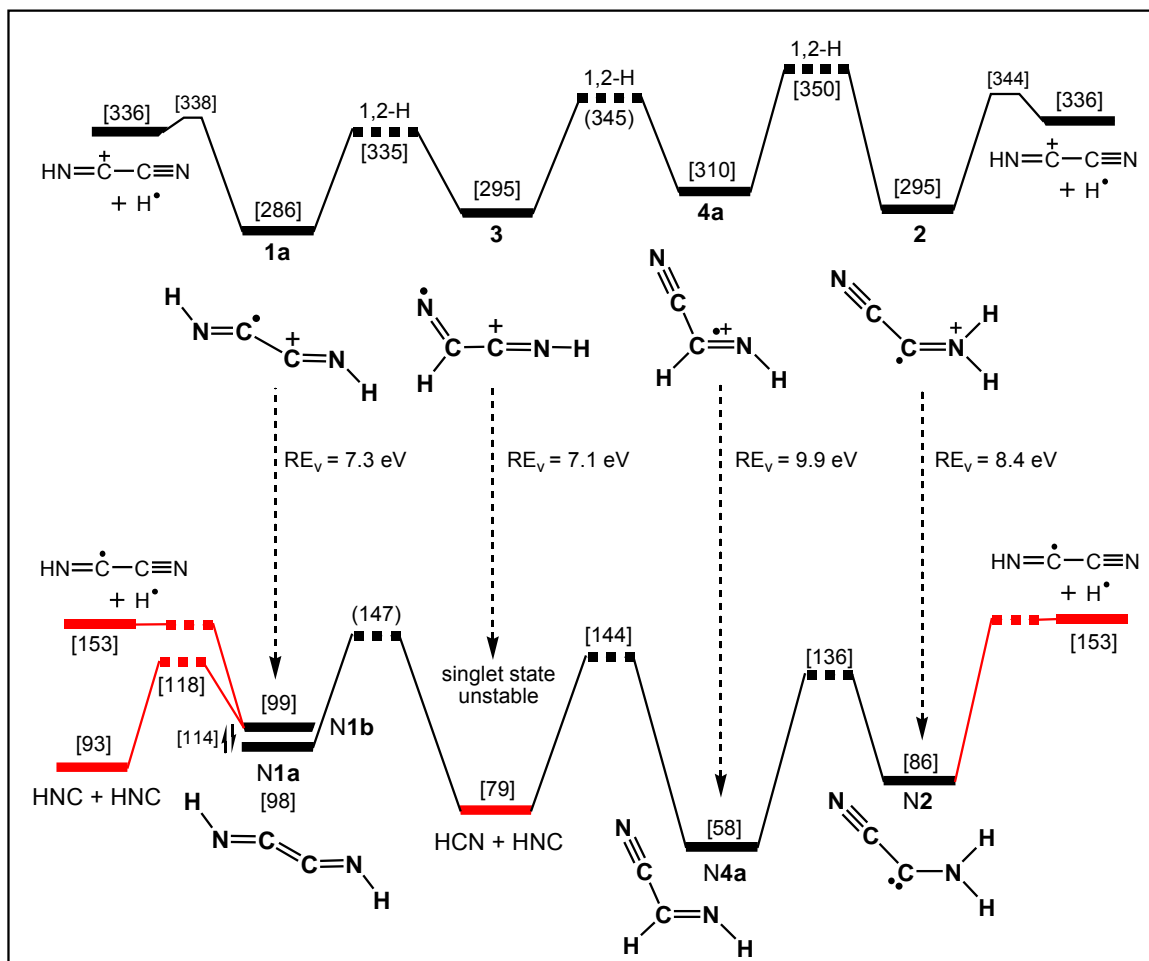


Figure 10.3 Computational results pertaining to the isomerization and dissociation of the $C_2H_2N_2$ ions **1-4** (top) and their neutrals **N1-N4** (bottom). The numbers in square-brackets refer to CBS-APNO derived 298 K enthalpies in kcal mol⁻¹. Vertical recombination energies (RE_v) are given in eV.

The direct transformation **1** \rightarrow **2** via a 1,4-H shift lies at 365 kcal mol⁻¹, well above the dissociation threshold of lowest energy requirement, H^\bullet loss. Similarly, consecutive 1,2-hydrogen shift reactions, involving the nitrene ion $HN=C-C(H)=N^{++}$ (**3**) and $HN=C(H)C\equiv N^{++}$ (**4**) as intermediates, are also prohibited by high barriers. Admittedly, ions **1** and **3** can interconvert, but only at energies close to the dissociation threshold. Thus we conclude that the majority of the non-dissociating m/z 54 ions generated from xanthine and uric acid

retain the ethenediimine structure **1** prior to collision induced dissociation. Likewise, the stable carbene ions **2** generated from aminomalononitrile will only undergo post-collisional isomerization [13] reactions.

Theory, see Figure 10.3 (bottom), predicts that a similar situation obtains for the singlet-state neutral counterparts of ions **1** and **2** (triplet-states were not further considered [14]; that of the carbene lies 29 kcal mol⁻¹ above the singlet [7]). The conformers of the neutral HNC dimer (N**1a/b**) lie ~5 kcal mol⁻¹ above the thermochemical energy level of the monomers. Nevertheless, our calculations indicate that a substantial barrier at 118 kcal mol⁻¹ provides N**1** with significant kinetic stability. Other dissociation (and isomerization) pathways of N**1** require much more energy.

The carbene isomer N**2**, which lies at 86 kcal mol⁻¹, can isomerize via a 1,2-H shift reaction at 136 kcal mol⁻¹ into iminoacetonitrile (N**4**). A further 1,2-H shift in N**4** at 144 kcal mol⁻¹ leads to the neutral counterpart of ion **3** which is not stable and dissociates into HCN + HNC. We note that the energy threshold for H• loss lies at 153 kcal mol⁻¹ and that neutrals having elevated internal energies may well isomerize into N**4**. However, it is not likely that the majority of the N**2** neutrals generated in a NRMS experiment will have sufficient internal energy for isomerization. The charge-transfer is a vertical Frank-Condon process and assuming that resonant charge exchange occurs, a crude estimate of the internal energy (*E*) of the neutrals may be obtained by subtracting their vertical recombination energy (*RE_v*) from their adiabatic ionization energy (*IE_a*). Thus, see Table 10.1, the majority of the N**2** neutrals is generated with ~15 kcal mol⁻¹ of excess internal energy (*IE_a* – *RE_v*) and should not readily isomerize. In the same vein, we expect that N**1** neutrals are generated with 20 kcal mol⁻¹ of internal energy, precisely the amount required for the dedimerization into two HNC molecules. This point will be discussed further in Section 10.2.3.

10.2.3 The NR mass spectra of $\text{HN}=\text{C}=\text{C}=\text{NH}^{\bullet+}$ and $\text{NH}_2-\text{C}-\text{C}\equiv\text{N}^{\bullet+}$

The NR mass spectra of **1** and **2** are shown in Fig. 10.4a/b. Both spectra show intense signals at m/z 54 corresponding to ions that have survived the NR process. It is important to note that the peaks in the NR spectrum originate from (i) re-ionized dissociation products of neutralized m/z 54 ions; (ii) collision-induced dissociation of reionized m/z 54 ions; (iii) reionized neutral fragments of metastable and collision induced dissociations which occur before the ion beam reaches the deflector electrodes. Thus, the fact that the CID and NR spectra of **1** (and likewise for **2**) appear similar derives from the fact that a significant amount of fragmentation occurs from reionized mass 54 neutrals, which do not rearrange during the NR process.

The NR spectrum of **1** is quite remarkable in that it displays two peaks with non integral m/z values, *viz.* m/z 26.6 and 27.4. These we propose represent the ‘horns’ of a dish-shaped peak [13] centered at m/z 27. The substantial kinetic energy release ($T_h \cong 15 \text{ kcal mol}^{-1}$) associated with this peak shows that the corresponding dissociation involves a sizable reverse barrier. Since we do not observe such a broad m/z 27 peak in the CID or MI spectra, the peak must relate to the dissociation of *neutralized* ethenediimine ions, $\text{N1} \rightarrow \text{HNC} + \text{HNC}$, whose dissociation products are subsequently re-ionized. As discussed in Section 10.2.2, our model chemistry calculations predict that (i) the two conformers of ethenediimine, **N1a** and **N1b** lie at 98 and 99 kcal mol^{-1} respectively and are connected by a rotational barrier of 15 kcal mol^{-1} ; (ii) the dissociation $\text{N1a/b} \rightarrow 2 \text{ HNC}$ requires c. 20 kcal mol^{-1} ; (iii) the incipient neutrals generated by vertical neutralization have $\sim 20 \text{ kcal mol}^{-1}$ of internal energy. These findings support the interpretation of the NR results: the kinetic barrier prevents dissociation of the low energy neutrals, while the fraction of incipient neutrals generated with an internal energy at or above the barrier leads to dissociation into two HNC molecules with the release of a large amount of kinetic energy. The NR spectrum of **2**, see Fig. 10.4b, does not display a dish-shaped peak at m/z 27. This is not surprising considering that the “dedimerization” $\text{N2} \rightarrow \text{N4} \rightarrow \text{N3} \rightarrow \text{HCN} + \text{HNC}$

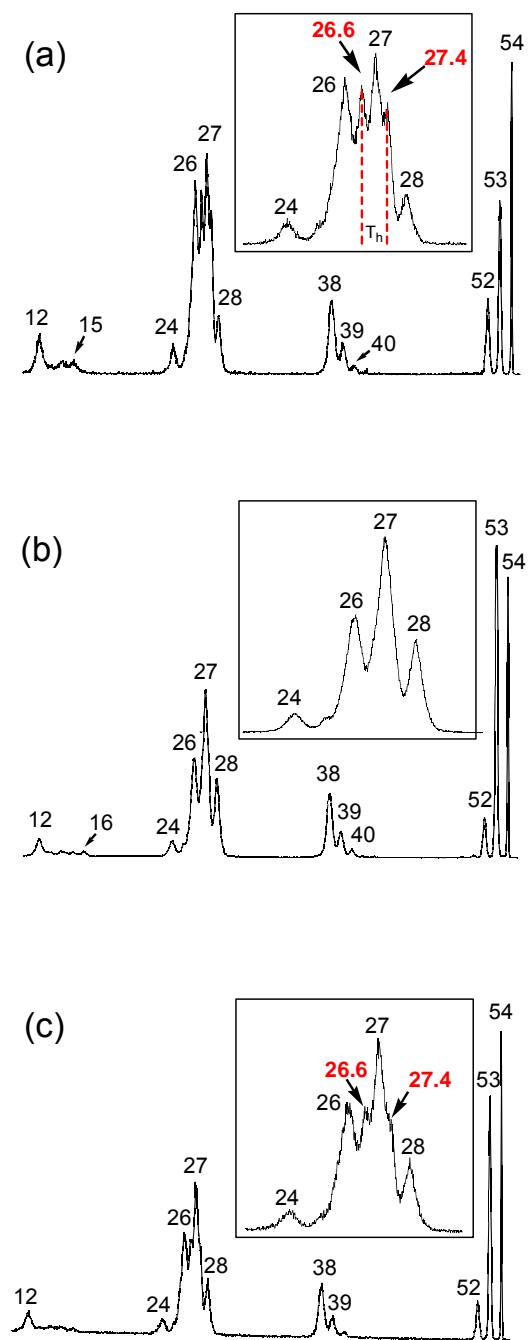


Figure 10.4 (8kv, 2ffr, NDMA, O₂) NR mass spectra of m/z 54 ions generated by dissociative ionization of (a) xanthine, (b) aminomalnonitrile and (c) diaminomaleonitrile. Insets show an expanded view of the m/z 23 – 29 region.

requires 58 kcal mol^{-1} whereas the internal energy of the incipient neutrals is estimated to be only $\sim 15 \text{ kcal mol}^{-1}$.

The NR spectrum of the m/z 54 ions generated from DAMN is shown in Fig 11.4c. We note that the m/z 24–28 region contains signals at m/z 26.6 and 27.4, which characterize the dissociation of N1. However, the relative intensity of these peaks is lower than that in the spectrum of Fig. 10.4a. This further supports our proposal that a mixture of ions **1** and **2** is generated in this dissociation.

10.2.4 The generation of ions **1** and **2** by dissociative ionization of diaminomaleonitrile : an intriguing example of *quid-pro-quo* catalysis

Analysis of the MI and CID mass spectra (not shown) of the DAMN molecular ion and its prominent fragment ion at m/z 81 indicates that the major routes for the formation of the m/z 54 ions are those depicted in Figure 10.5 rather than the direct bond cleavage mentioned in Section 10.2.1.

The first step in the proposal of Figure 10.5 involves loss of HCN from the DAMN molecular ion to yield the m/z 81 product ion DAMN-1. Loss of HNC from this species would yield ion **2**, but a potential energy surface scan indicates that HBRC-**1a**, a hydrogen-bridged radical cation [15], acts as an intermediate in the dissociation. From its rotamer HBRC-**1b**, two additional reaction pathways become available: proton-transport catalysis (PTC) [16,17] and a variant thereof, coined *quid-pro-quo* catalysis (QPQ) [18].

In the PTC reaction, the HNC molecule in HBRC-**1b** abstracts a proton from the carbene's amino group and transports it to the cyano nitrogen atom to yield HBRC-**3**, a complex of ion **1** with an HNC molecule. Essentially the same proton abstraction takes place in QPQ, but now the proton being back-donated by the incipient $\text{HC}=\text{NH}^+$ ion comes from its NH moiety to yield HBRC-**2**, a complex of ion **1** with an HCN molecule. The barriers for these proton transfers are negligible. As shown in Fig. 10.5, HBRC-**2** of the QPQ reaction may readily dissociate into $\text{HN}=\text{C}=\text{C}=\text{NH}^+$ (**1**) + HCN. In contrast, formation of **1** from HBRC-**3**

of the PTC reaction cannot effectively compete with dissociation into $\text{HC}=\text{NH}^+ + \text{HN}=\text{C}=\text{CN}^*$ because HNC rather than (its lower energy isomer) HCN is lost.

The scenario that emerges from the computational results of Figure 10.5 is that the reaction of lowest energy requirement of the m/z 81 ions from DAMN involves formation of m/z 54 ions **1** via a remarkable QPQ reaction in which both the ion and the neutral undergo isomerization. At elevated energies, m/z 54 ions of structure **2** and m/z 28 ions $\text{HC}=\text{NH}^+$ may be co-generated.

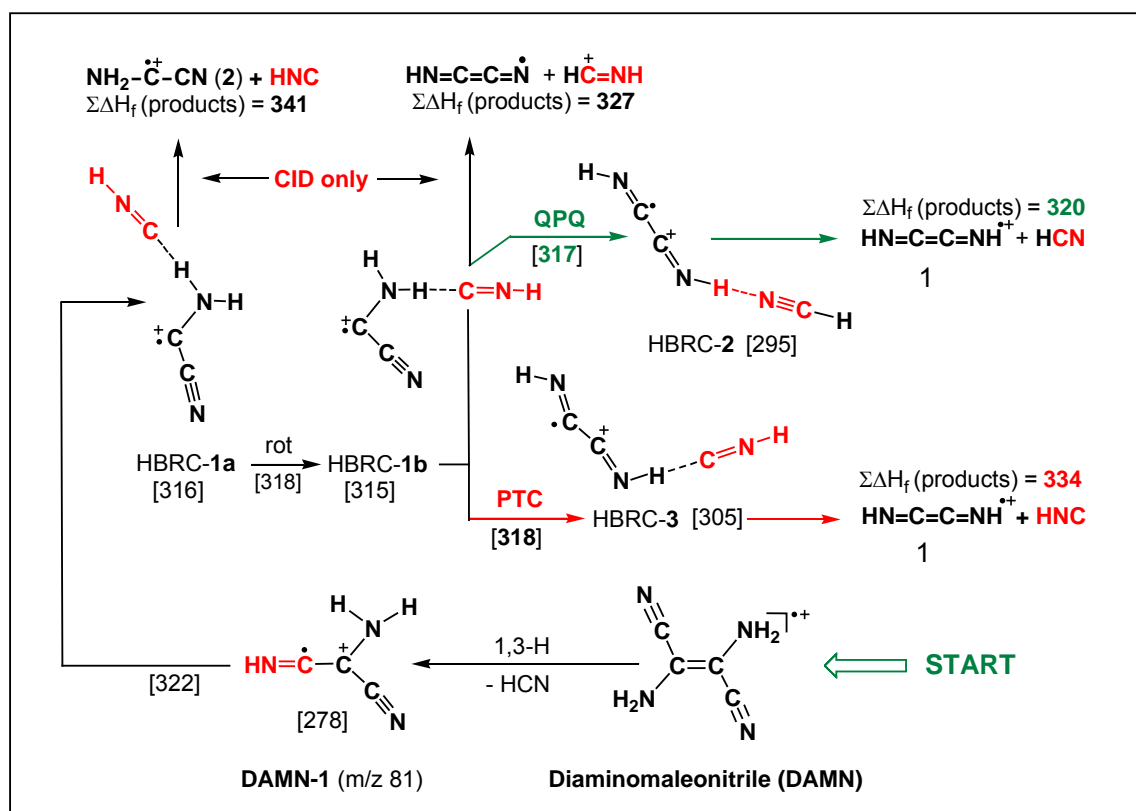


Figure 10.5 Mechanistic proposal rationalizing the generation of ions **1** and **2** from ionized diaminomaleonitrile. The numbers refer to 298 K enthalpies in kcal mol^{-1} calculated by the CBS-QB3 model chemistry.

In line with this proposal we note that low-energy (metastable) m/z 81 ions only dissociate into m/z 54 ions of structure **1**. When more internal energy becomes available, as is the case with m/z 81 ions subjected to collisional activation, ions **1** are generated in admixture with carbene ions **2**. This situation also obtains for m/z 81 ions that decompose into m/z 54 ions in the ion source, as exemplified by the m/z 54 CID and NR spectra of DAMN discussed in Section 10.2.1 and 10.2.3.

10.2.5 Analysis of the NR-CID mass spectra of $\text{HN}=\text{C}=\text{C}=\text{NH}^{\bullet+}$ and $\text{NH}_2\text{-C-C}\equiv\text{N}^{\bullet+}$

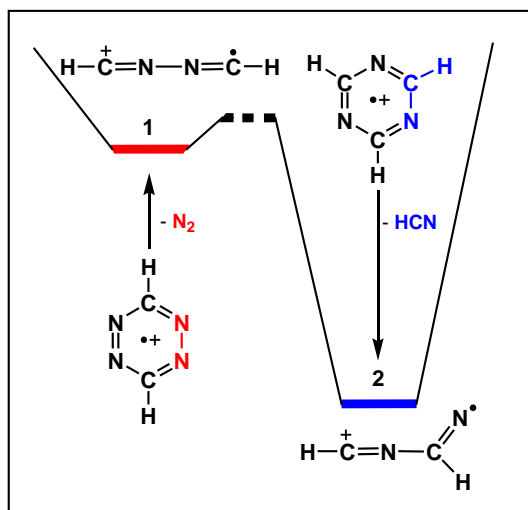
We have shown that the ions **1** and **2** are readily distinguishable on the basis of their CID mass spectra and thus do not interconvert prior to collisional activation. While the intense survivor signals in their associated NR mass spectra suggest that ions **1** and **2** have stable neutral counterparts, one could still argue that the reionized m/z 54 survivor signal is (in part) due to isomeric and/or isobaric impurities. To discount this possibility, we have probed the structure of the m/z 54 survivor ions by collision-induced dissociation. In such an experiment, the non-dissociating neutrals are reionized (yielding the survivor) and then induced to dissociate by collision with O_2 . If the survivor ions have maintained their structural integrity, the NR-CID spectrum obtained should closely resemble the CID spectrum [14]. The NR-CID mass spectra of the surviving ions **1** and **2** are shown in Figs 10.2d/e respectively. One observes that the NR-CID and CID mass spectra are practically superimposable. In particular, the structure diagnostic peaks at m/z 15 (for ion **1**) and m/z 16 (for ion **2**) are clearly present. These results leave little doubt that ethenediimine and aminocyanocarbene are stable neutrals in the rarefied gas-phase.

References

- [1] F. Pichieri, *Chem. Phys. Lett.* 353 (2002) 383 and references cited therein.
- [2] For a recent study of non-covalently bound dimers see : A. Heikkilä, J. Lundell, *J. Phys. Chem. A* 104 (2000) 6637.
- [3] R.A. Evans, P. Lorencak, T-K. Ha, C. Wentrup. *J. Am. Chem. Soc.* 113 (1991) 7261.
- [4] C. Wentrup, P. Lorencak, A. Maquestiau, R. Flammang, *Chem. Phys. Lett.* 137 (1987) 241.
- [5] R.A. Evans, S.M. Lacombe, M.J. Simon, G. Pfister-Guillouzo, C. Wentrup, *J. Phys. Chem.* 96 (1992) 4801.
- [6] R.E. Moser, J.M. Fritsch, T.L. Westman, R.M. Kliss, C.N. Matthews, *J. Am. Chem. Soc.* 89 (1967) 5673.
- [7] F. Freeman, M. Gomarooni, *Int. J. Quant. Chem.* 106 (2006) 2379.
- [8] P.C. Burgers, J.K. Terlouw, in : M.E. Rose (Ed.), *Specialist Periodical Reports: Mass Spectrometry*, vol. 10, The Royal Society of Chemistry, London, 1989, p. 44 (Chapter 2).
- [9] R. Flammang, Y. Van Haverbeke, S. Laurent, M. Barbieux-Flammang, M.W. Wong, C. Wentrup, *J. Phys. Chem.* 98 (1994) 5801.
- [10] C. Lifshitz, E.D. Bergmann, U. Sheinok, *Israel J. Chem.* 6 (1968) 827.
- [11] S.N. Bose, R.J.H. Davies, D.R. Boyd, *Biomed. Mass Spectrom.* 4 (1977) 305.
- [12] R. Flammang, L. Gallez, Y. Van Haverbeke, M.W. Wong, C. Wentrup, *Rapid Commun. Mass Spectrom.* 10 (1996) 232.
- [13] J.L. Holmes, C. Aubry, P.M. Mayer. *Assigning Structures to Ions in Mass Spectrometry*, CRC Press, Boca Raton, 2007.
- [14] G.A. McGibbon, C.A. Kingsmill, J.K. Terlouw, *Chem. Phys. Lett.* 222 (1994) 129.
- [15] P.C. Burgers, J.K. Terlouw, in: N.M.M. Nibbering (Ed.), *Encyclopedia of Mass Spectrometry*, vol. 4, Elsevier, Amsterdam, 2005, p. 173.
- [16] C.Y. Wong, P.J.A. Ruttink, P.C. Burgers, J.K. Terlouw, *Chem. Phys. Lett.* 390 (2004) 176.
- [17] C.Y. Wong, P.J.A. Ruttink, P.C. Burgers, J.K. Terlouw, *Chem. Phys. Lett.* 387 (2004) 204.
- [18] K.J. Jobst, P.C. Burgers, P.J.A. Ruttink, J.K. Terlouw, *Int. J. Mass Spectrom.* 254 (2006) 127.
- [19] A.D. Boese, J.M.L. Martin, *J. Chem. Phys.* 121 (2004) 3405.

Chapter 11

The covalently bound HC≡N dimer ions HC=N–N=CH^{•+} and HC=N–C(=N)H^{•+} are stable species in the gas-phase, but the neutral counterparts are not



Tandem mass spectrometry based experiments and computational chemistry (CBS-QB3/APNO methods) indicate that ionized *s*-tetrazine eliminates N₂ to yield the elusive linear HC≡N dimer ion HC=N–N=CH^{•+} (1). The ion is stable in the rarefied gas-phase but, as it is generated with considerable internal energy, it readily interconverts with HC=N–C(=N)H^{•+} (2), via a 1,2-HCN shift. This more stable HCN dimer ion was generated independently by loss of HCN from ionized *s*-triazine. Whereas the HN≡C dimer ion HN=C=C=NH^{•+} has a (kinetically) stable neutral counterpart, theory and experiment (neutralization-reionization mass spectrometry) agree that the HC≡N dimer ions 1 and 2 do not.

The work described here has been published previously in an article under the same title : K.J. Jobst, M.R. Hanifa, P.J.A. Ruttink, J.K. Terlouw, Chem. Phys. Lett. 473 (2009) 257 - 262.

11.1 Introduction

Neutral and ionized $\text{HC}\equiv\text{N}$ and $\text{HN}\equiv\text{C}$ molecules are ubiquitous in the various regions of interstellar space and the relatively high abundance of the thermodynamically less stable neutral $\text{HN}\equiv\text{C}$ isomer serves as a salutary reminder that reaction kinetics is an important driving force behind the relative abundances of interstellar molecules and ions [1-3].

The characterization of the covalently bound [H,C,N] dimers, the family of $\text{C}_2\text{H}_2\text{N}_2^{++}$ ions and neutrals, is therefore of relevance to astrochemistry and studies of prebiotic syntheses [1]. So far, the $\text{C}_2\text{H}_2\text{N}_2$ species $\text{CH}_2=\text{N}-\text{C}\equiv\text{N}$ (N-cyano-methanimine) and $\text{HN}=\text{CH}-\text{C}\equiv\text{N}$ (C-cyano-methanamine) have been thoroughly characterized, using a variety of spectroscopic techniques and quantum chemical calculations, as stable neutrals and ions in the rarefied gas-phase [4-6].

In addition, we have shown recently [7] that the very stable $\text{HN}\equiv\text{C}$ dimer ion $\text{HN}=\text{C}=\text{C}=\text{NH}^{++}$ and the aminocyanocarbene ion $\text{NH}_2-\text{C}-\text{C}\equiv\text{N}^{++}$ have kinetically stable neutral counterparts.

Nenner et al. [8], in a pioneering TPEPICO study of the dissociation chemistry of the *s*-tetrazine ion, have reported the energetics of the $\text{C}_2\text{H}_2\text{N}_2^{++}$ ion generated by loss of N_2 therefrom. The structure of the ion could not be established, but an intriguing possibility is that it represents the linear $\text{HC}\equiv\text{N}$ dimer ion $\text{HC}=\text{N}-\text{N}=\text{CH}^{++}$ (**1**).

In this study, we report results of tandem mass spectrometry based experiments and model chemistry calculations which indicate that ionized *s*-tetrazine indeed generates the elusive (linear) dimer ion $\text{HC}=\text{N}-\text{N}=\text{CH}^{++}$ (**1**). However, the ion lies in a shallow potential well and can readily isomerize into the more stable dimer $\text{HC}=\text{N}-\text{C}(=\text{N})\text{H}^{++}$ (**2**), an ionized nitrene. An analysis of the $\text{C}_2\text{H}_2\text{N}_2^{++}$ ions generated from *s*-triazine supports this proposal. Neutralization-reionization mass spectrometry (NRMS) [9] confirms the prediction by theory that the two HCN dimer ions have no stable neutral counterpart on the μs time-frame of the experiment.

11.2 Results and discussion

11.2.1 The structure of the $C_2H_2N_2^{2+}$ ions generated from *s*-tetrazine

The peak at m/z 54 in the mass spectrum of *s*-tetrazine, see Figure 11.1a, may well represent the HC≡N dimer ion HC=N–N=CH⁺ (**1**), generated by loss of N₂ as depicted in Figure 11.2. Its collision-induced dissociation (CID) mass spectrum is shown in Figure 11.1b. Examination of reported reference spectra [3,7], shows that we are not dealing with a previously identified C₂H₂N₂²⁺ isomer : the spectrum of Figure 11.1b shows a tell-tale peak at m/z 13 indicative of the –CH connectivity of ion **1**, in contrast with the spectra of CH₂=N–C≡N⁺ (N-cyano-methanamine), HN=C=C=NH⁺ (ethenediimine), and NH₂–C–C≡N⁺ (amino cyanocarbene), which display structure diagnostic peaks at m/z 14, 15 and 16 respectively. Further, the CID spectrum of HN=CH–C≡N⁺ shows a much higher m/z 53 : 28 ratio than that of Figure 11.1b (20:1 vs. 1:2).

That the incipient m/z 54 ions are dimer ions **1**, is firmly supported by the calculated potential energy surface of Figure 11.2. The first step of the proposed mechanism involves C–N bond cleavage in the *s*-tetrazine ion **TET-1** with a transition state (TS) at 358 kcal mol⁻¹. The resulting ring-opened intermediate, **TET-2**, is sufficiently excited to further rearrange, by elongation of the C–N₂ bond, to the hydrogen-bridged radical cation **TET-3**. This ion has only a marginal stabilization energy, c. 1 kcal mol⁻¹, with respect to dissociation into HC=N–N=CH⁺ (**1**) + N₂. In the above scenario, ions **TET-3** are generated with at least ~30 kcal mol⁻¹ of internal energy. A sizeable fraction of this energy (~ 15 kcal mol⁻¹) is released as kinetic energy in the subsequent N₂ loss, as witnessed by the broad dishd m/z 54 peak ($T_{0.5}$ = 600 meV) in the spectrum of metastable ions **TET-1**.

For the appearance energy (AE) of m/z 54, Nenner *et al.* [8] have reported a value of 10.2 eV. This value translates into a dissociation threshold of 349 kcal mol⁻¹ if neutral *s*-tetrazine's CBS-APNO derived enthalpy of 115 kcal mol⁻¹ (**TET-1N** in Table 11.1) is used rather than the estimate of ref. 15 (111 kcal mol⁻¹) or that adopted by ref. 8 (102 kcal mol⁻¹). There is thus a 9 kcal mol⁻¹ discrepancy with our computed threshold of 358 kcal mol⁻¹.

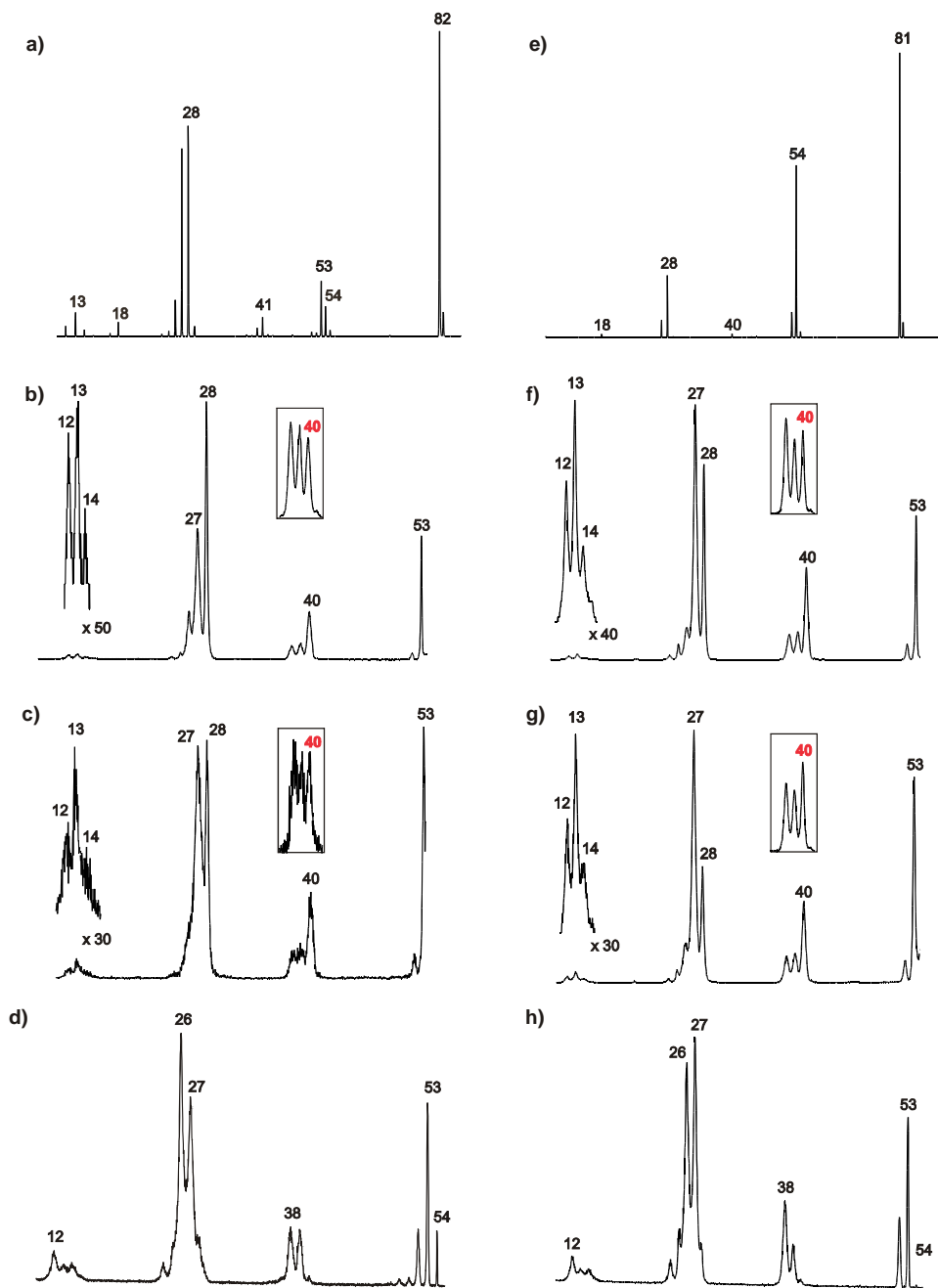


Figure 11.1 (left) Measurements on *s*-tetrazine : (a) 70 eV EI mass spectrum; (b,c) CID mass spectra (O_2) of the m/z 54 ions generated in the ion source and from metastable molecular ions; (d) NR mass spectrum of the m/z 54 ions. (right) Measurements on *s*-triazine : (e) 70 eV EI mass spectrum; (f,g) CID mass spectra (O_2) of the m/z 54 ions generated in the ion source and from metastable molecular ions; (h) NR mass spectrum of the m/z 54 ions.

Partial CID spectra (He) of the m/z 38- 40 region are shown in the insets.

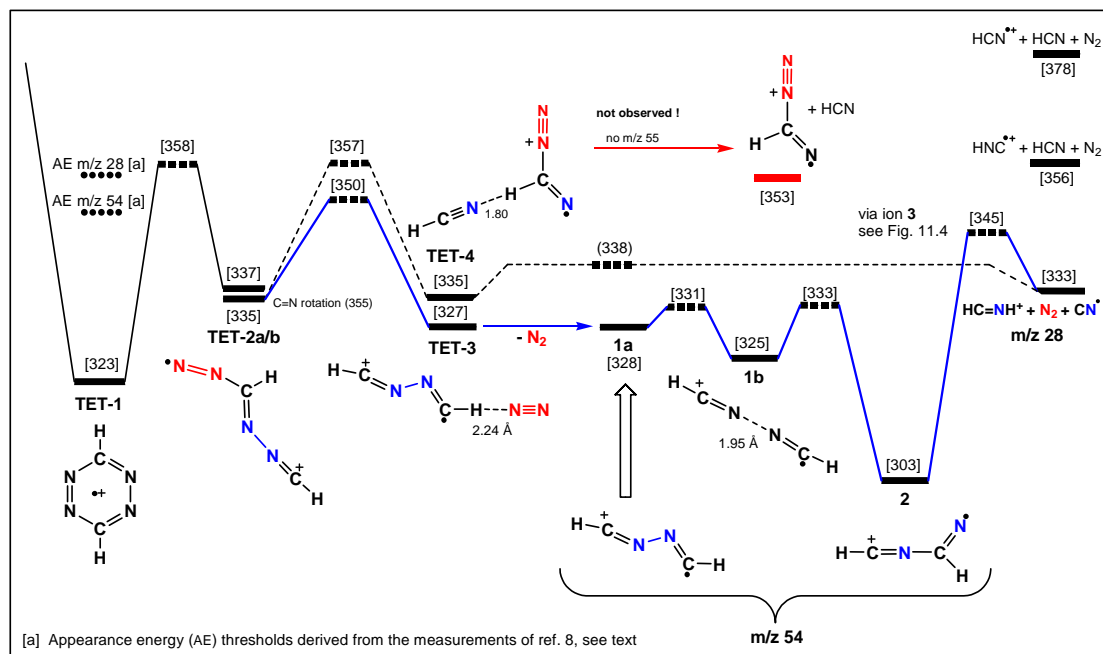


Figure 11.2 Mechanistic proposal for the formation of m/z 54 and m/z 28 ions from low-energy s -tetrazine ions (**TET-1**). Numbers in square and round brackets refer to 298 K enthalpies (in kcal mol^{-1}) derived from CBS-APNO and CBS-QB3 calculations respectively.

Nevertheless, there does not seem to be a mechanistic alternative for loss of N_2 from **TET-1**. Cleavage of an N–N bond is an energy demanding process that does not lead to a stable intermediate but rather the three-body dissociation $\text{TET-1} \rightarrow \text{HC}\equiv\text{N}^{++} + \text{HC}\equiv\text{N} + \text{N}_2$: a potential energy surface scan (B3LYP/CBSB7 level of theory) indicates that the TS lies at $384 \text{ kcal mol}^{-1}$. Likewise, the ylid-ion of s -tetrazine (**TET-5** of Table 11.1) is not accessible because the associated 1,2-H shift at $415 \text{ kcal mol}^{-1}$ is far too high in energy. This leaves **TET-2** as the only reasonable intermediate involved in the loss of N_2 .

Ion **TET-2** may also account for the formation of the m/z 28 $\text{HC}=\text{NH}^+$ ions in the TPEPICO experiments of Nenner *et al.* [8]. The associated pathway involves migration of its HCN moiety to form the hydrogen-bridged radical cation **TET-4**. The HCN component of **TET-4** is not readily lost: the m/z 55 ion of Figure 11.2 at $353 \text{ kcal mol}^{-1}$ is *not* generated. Rather, the HCN component abstracts a proton to generate $\text{HC}=\text{NH}^+ + \text{CN}^{\bullet} + \text{N}_2$ in a three-body dissociation, via the low barrier at $338 \text{ kcal mol}^{-1}$.

Table 11.1 Energetic data [a] derived from CBS-QB3 and CBS-APNO calculations of stable ions and connecting transition states involved in the dissociation chemistry of ionized *s*-tetrazine (**TET-1**) and *s*-triazine (**TRI-1**).

Isomer	CBS-QB3 E(total) [OK]	QB3 $\Delta_f H_{298}^0$	APNO $\Delta_f H_{298}^0$	Transition State	CBS-QB3 E(total) [OK]	QB3 $\Delta_f H_{298}^0$	APNO $\Delta_f H_{298}^0$
TET-1N	-295.88997	113	115	TS TET-1 \rightarrow 2a	-295.50459	356	358
TET-1 (Fig. 11.2)	-295.56158	320	323	TS TET-1 \rightarrow 5	-295.41019	415	[b]
TET-2a (Fig. 11.2)	-295.53399	338	337	TS TET-2a \rightarrow 2b	-295.50624	355	353
TET-2b (Fig. 11.2)	-295.53765	336	335	TS TET-2a \rightarrow 3	-295.51678	349	350
TET-3 (Fig. 11.2)	-295.55186	328	327	TS TET-2b \rightarrow 4	-295.50543	356	357
TET-4 (Fig. 11.2)	-295.53628	338	335	TS TET-4 \rightarrow <i>m/z</i> 28	-295.53599	338	[b]
TET-5	-295.49927	359	363				
TRI-1N	-279.92379	53	54	TS TRI-1 \rightarrow 2	-279.46077	345	344
TRI-1 (Fig. 11.3)	-279.55593	284	287	TS TRI-1 \rightarrow 3a	-279.49436	324	324
TRI-2 (Fig. 11.3)	-279.55938	282	282	TS TRI-3a \rightarrow 3b	-279.48846	328	329
TRI-3a (Fig. 11.3)	-279.49832	322	322	TS TRI-3b \rightarrow 4	-279.48652	330	330
TRI-3b (Fig. 11.3)	-279.48743	329	329	TS TRI-4 \rightarrow 5	-279.50159	320	320
TRI-4 (Fig. 11.3)	-279.51222	314	313	TS TRI-5 \rightarrow 6	-279.46200	345	345
TRI-5 (Fig. 11.3)	-279.50147	321	321				
TRI-6 (Fig. 11.3)	-279.52859	304	303	TS 1a \rightarrow 1b	-186.14924	333	331
				TS 1b \rightarrow 2	-186.14301	334	333
1a (Fig. 11.4)	-186.14947	330	328	TS 1 \rightarrow 4	-186.07977	374	373
1b (Fig. 11.4)	-186.15870	324	325	TS 2 \rightarrow 3	-186.12317	346	345
2 (Fig. 11.4)	-186.19198	303	303	TS 3 \rightarrow 4	-186.13342	340	341
3 (Fig. 11.4)	-186.20232	298	296	TS 3 \rightarrow 5	-186.16536	319	318
4 (Fig. 11.4)	-186.17289	315	315	TS 2 \rightarrow <i>m/z</i> 53	-186.11015	354	354
5 (Fig. 11.4)	-186.20589	294	294	TS 5 \rightarrow <i>m/z</i> 53	-186.13525	339	339

[a] E(total) in Hartrees, all other components in kcal mol⁻¹. [b] The desired transition states could not be located using the CBS-APNO model chemistry.

The TPEPICO study concludes that the *m/z* 28 ions are (primarily) generated by the step-wise process: **TET-1** (*m/z* 82) \rightarrow *m/z* 54 \rightarrow *m/z* 28. This is reasonable considering that *m/z* 28 is the base peak in the CID mass spectrum of the *m/z* 54 ions in Figure 11.1b. On the other hand, the consecutive and the three-body dissociation reactions share the rate-determining transition state, TS **TET-1/2**, raising the possibility that the three-body

dissociation is competitive in a narrow band of energies close to the onset for m/z 28 formation. In this context we note that a pure three-body fragmentation mechanism describes the dissociation of *neutral s*-tetrazine [10].

Figure 11.2 indicates that the linear dimer ion **1a** is a minimum on the potential energy surface albeit that a mere 3 kcal mol⁻¹ of energy leads to interconversion with its more stable long-bonded variant HC=N---N=CH⁺⁺ (**1b**). This ion serves as the precursor to the nitrene type isomer **2**, via a 1,2-HCN shift at 333 kcal mol⁻¹. This facile rearrangement is expected to convert the majority of the incipient ions **1a/b** into ions HC=N–C(=N)H⁺⁺ (**2**), which contain an exposed N atom. This may account for the pronounced N atom loss in the *Helium* CID spectrum as shown by the peak at m/z 40 in the inset of Figure 11.2b.

In this context we note that the relative intensity of m/z 40 in the m/z 38 – 40 cluster of peaks is much higher when O₂ is used as the collision gas. This so-called ‘Oxygen effect’ (for which a tentative explanation has been proposed [11]) has also been reported for the C₂H₂N₂⁺⁺ isomer HN=C=C=NH⁺⁺ [7, 12]. However, for this species, which does not contain an exposed N atom, the prominent m/z 40 peak in its O₂ CID mass spectrum becomes vanishingly small when He is used as the collision gas.

Thus theory and experiment seem to suggest that the majority of the source-generated m/z 54 ions from *s*-tetrazine rearranges into HC=N–C(=N)H⁺⁺ (**2**) prior to the collision event. To probe whether a small fraction retains its initial connectivity, the dissociation characteristics of ions **2** having a low internal energy content were examined. As shown in the next section, such ions can be conveniently generated by the dissociative ionization of *s*-triazine.

11.2.2 The structure of the C₂H₂N₂⁺⁺ ions generated from *s*-triazine

Figure 11.3 predicts that the m/z 54 ions generated by dissociative ionization of *s*-triazine (see Figure 11.1e) are C₂H₂N₂⁺⁺ ions of structure HC=N–C(=N)H⁺⁺ (**2**). These can be generated at the thermochemical threshold, by the route: **TRI-1** → **TRI-3** → **2** + HCN. Prior to dissociation, ions **TRI-3** may rearrange into hydrogen-bridged radical cations **TRI-4/5**

and ion–dipole complexes of ion **2** and HCN. The small kinetic energy release associated with the HCN loss ($T_{0.5} \leq 1$ meV) supports this scenario.

An HCN molecule departing from **TRI-5** could in principle transform ion **2** into the mixed dimer ion $\text{H}-\text{C}=\text{N}-\text{C}=\text{N}-\text{H}^{++}$ (**3**) by proton-transport catalysis (PTC) [13,14].

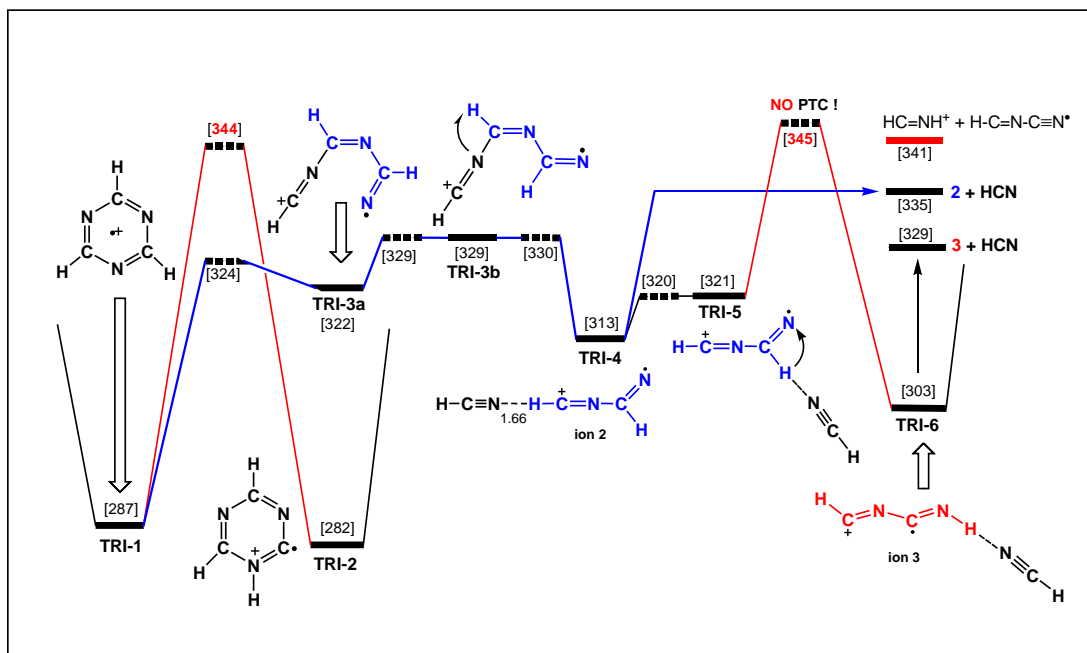


Figure 11.3 Mechanistic proposal for the formation of m/z 54 ions from low-energy *s*-triazine ions (**TRI-1**).

However, the barrier calculated for this process lies well above the threshold for dissociation, as does the unassisted 1,2-H shift in **TRI-4**. Figure 11.4 shows that the isomerization **2** \rightarrow **3** also requires a barrier of the same magnitude and that this reaction leads to dissociation. In the same vein, the 1,2-H shift transforming ion **2** into $\text{H}-\text{C}-\text{N}(\text{H})\text{C}\equiv\text{N}^{++}$ is prohibitively high, while the resulting (as yet unidentified) ionized carbene is *c.* 20 kcal mol⁻¹ higher in energy.

These findings suggest that the $\text{C}_2\text{H}_2\text{N}_2^{++}$ ions generated by loss of HCN from low-energy (metastable) *s*-triazine molecular ions are isomerically pure ions **2**.

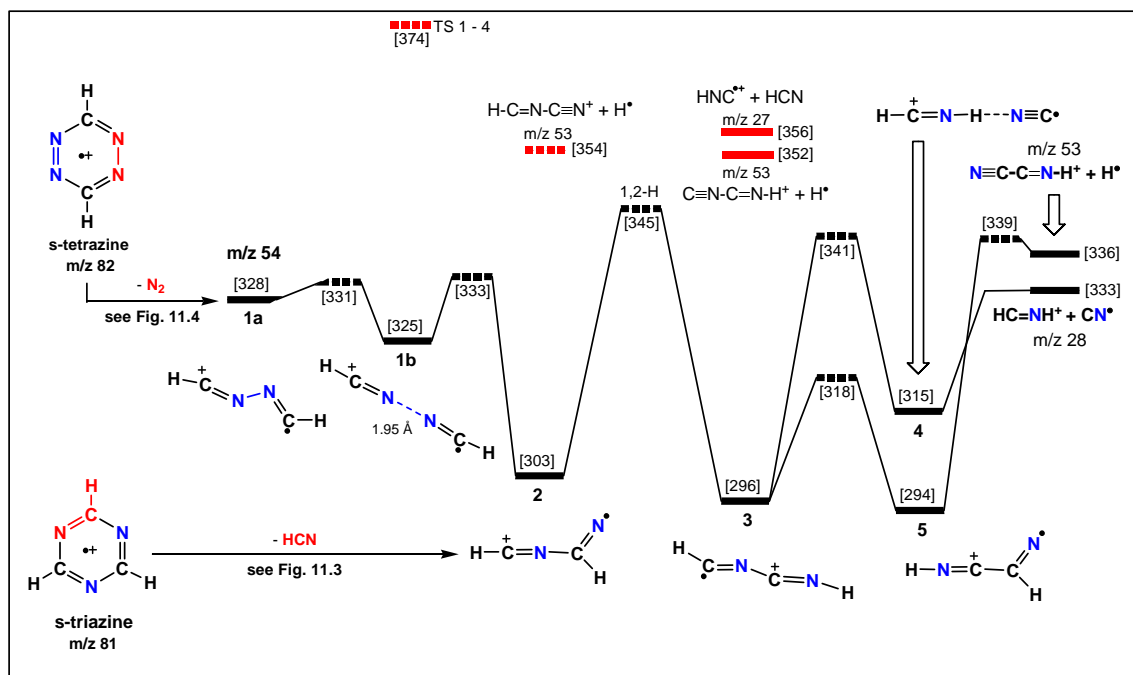


Figure 11.4 Mechanistic proposal for the formation of m/z 28 ions and m/z 53 ions from the low-energy HCN dimer ions 1 and 2. The numbers refer to CBS-APNO derived 298 K enthalpies in kcal mol⁻¹.

11.2.3 Dissociation characteristics of the dimer ions from TRI-1 vs those from TET-1

Metastable m/z 54 ions 2 from *s*-triazine and 1/2 from *s*-tetrazine lose CN^\bullet and H^\bullet with a similar ratio (1.7) but with elevated KER values for the latter ions ($T_{0.5} = 25$ vs 40 meV for loss of CN^\bullet and 120 vs 160 meV for loss of H^\bullet).

Figure 11.4 proposes that loss of CN^\bullet from ion 2 is initiated by an energy demanding 1,2-H shift, at 345 kcal mol⁻¹, to generate energy-rich ions $HC=N-C=NH^+$ (3). These readily further rearrange into transient hydrogen-bridged radical cations $HC=N-H\cdots N=C^+$ (4) which lose CN^\bullet by direct bond cleavage. The competing H^\bullet loss follows the route 2 \rightarrow 3 \rightarrow 5, which then loses H^\bullet via a small reverse barrier to yield $HN=C=C=N^+$, the global minimum on the $C_2HN_2^+$ potential energy surface [15]. Further, metastable ions 1 are expected to follow the same routes: they must rearrange into 2 prior to the loss of CN^\bullet

because the 1,2-H shift connecting **1** directly with **4** lies far too high in energy (TS at 374 kcal mol⁻¹ in Figure 11.4).

This mechanism provides an entirely reasonable description of the low energy dissociations of ions **2** and **1** because the highest barrier lies well below the thresholds calculated in Table 11.2 for direct H[•] loss from the various intermediates. This scenario implies that the differences between the MI and the O₂ CID spectra of the *s*-tetrazine and *s*-triazine derived *m/z* 54 ions (elevated KERs and more intense *m/z* 28 peaks for the former, see Fig. 11.1) provide no direct evidence for the co-generation of stable ions **1** from TET-1. The differences may simply reflect that (meta)stable ions **2** from *s*-tetrazine are generated with elevated internal energies (see Section 11.2.1) while those from *s*-triazine may populate the entire deep energy well.

Table 11.2 Energetic data [a] derived from CBS-QB3 and CBS-APNO calculations of the various dissociation products of ionized *s*-tetrazine (TET-1) and *s*-triazine (TRI-1).

Species	CBS-QB3 E(total) [0K]	QB3 $\Delta_f H_{298}^0$	APNO $\Delta_f H_{298}^0$	Species	CBS-QB3 E(total) [0K]	QB3 $\Delta_f H_{298}^0$	APNO $\Delta_f H_{298}^0$
HC(=N)N₂⁺⁺ + HCN	-	352	353	HCNH⁺ + N=N-C≡N[•]	-	350	344
HC(=N)N ₂ ⁺⁺	-202.22669	320	321	HCNH⁺ + HC=N-C≡N[•]	-	341	341
HCN	-93.28754	32	32	HCNH⁺ + CN[•]	-	333	333
				HCNH ⁺	-93.55869	227	226
H-C=N-C≡N⁺⁺ + H[•] [b]	-	351	351	N=N-C≡N[•]	-201.95878	124	117[c]
C≡N-C=N-H⁺⁺ + H[•]	-	352	352	H-C=N-C≡N[•]	-185.91171	114	115
H-C=N-N≡C⁺⁺ + H[•]	-	393	394	CN[•]	-92.58761	107	106
H-N=C-C≡N⁺⁺ + H[•]	-	336	336				
H-C=N-C≡N ⁺⁺	-185.61705	299	299	HCN⁺⁺ + HCN	-	378	378
C≡N-C=N-H ⁺⁺	-185.61689	300	300	HNC⁺⁺ + HCN	-	356	356
H-C=N-N≡C ⁺⁺	-185.55273	340	340	HCN ⁺⁺	-92.78703	346	347
H-N=C-C≡N ⁺⁺	-185.64141	284	284	HNC ⁺⁺	-92.82224	324	324

[a] E(total) in Hartrees, enthalpies are in kcal mol⁻¹; [b] The computed values for H are 52.1 kcal mol⁻¹. [c] The remarkable divergence of the calculated enthalpies is reflected in the optimized geometries. Note that this radical is thermodynamically unstable with respect to its dissociation products N₂ + CN[•].

Nevertheless, the m/z 38 – 40 regions of the *Helium* CID spectra of Figures 11.1b/f (insets) show a structure diagnostic difference: the peak at m/z 40 is more pronounced in the spectrum of the *s*-triazine derived ions **2**. That the high energy N atom loss from the TET-1 derived ions is diminished by comparison, indicates that some non-dissociating ions retain their initial structure, **1**. The spectra of m/z 54 ions generated from *metastable* precursor ions show the same trend: compare Figures 11.1c/g. That the N atom loss is more pronounced in Fig. 11.1g than in Fig. 11.1f reflects the lower propensity of low-energy precursor ions **2** to interconvert with ions **1**. This reinforces our proposal that the m/z 40 peak is a structure diagnostic peak of the nitrene ion **2** and that its prominence provides a yardstick for the co-generation of ion **1** from TET-1.

11.2.4 The neutral counterparts of ions **1** and **2** probed by theory and NRMS

The neutralization-reionization (NR) mass spectra of the m/z 54 ions generated from *s*-tetrazine and *s*-triazine are shown in Figures 11.1d/h. The absence of a peak at m/z 54 in the spectrum of Figure 11.1h indicates that ion **2** does not ‘survive’ the neutralization process, but rather dissociates prior to collisional reionization. This result is in line with our model chemistry calculations, which predict that the incipient neutrals **2N** dissociate into two HCN molecules. This explains why peaks at m/z 27 and 26 dominate the NR mass spectrum.

Prima facie, the weak survivor peak in the NR mass spectrum of the *s*-tetrazine derived ions could be taken as evidence that ions **1**, generated as a minor component in admixture with ions **2**, have a stable neutral counterpart (**1N**). However, theory predicts that **1N** is not a minimum either and a more detailed analysis [16] shows that ~ 60 % of the survivor peak of Figure 11.1d originates from neutrals generated from the ^{13}C and ^{15}N isotopologues of the m/z 53 ion $\text{H}-\text{C}=\text{N}-\text{C}=\text{N}^+$. The remaining contribution most likely stems from an isobaric impurity in the sample as witnessed by the weak peaks at m/z 51 and 52.

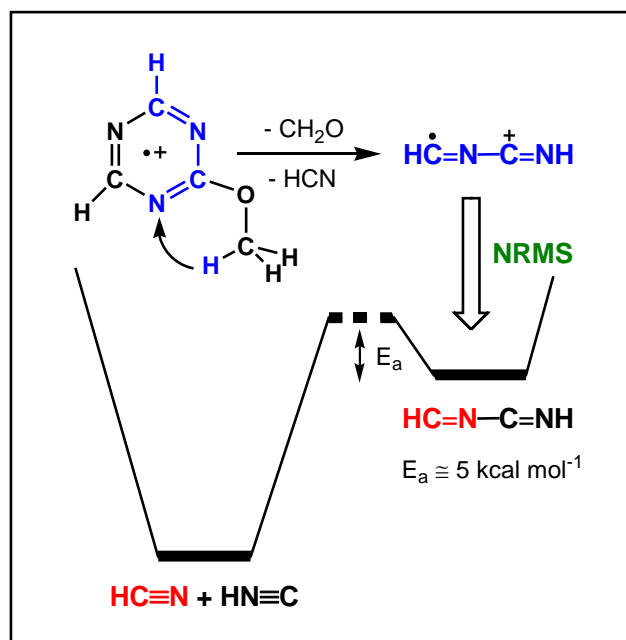
The absence of a genuine survivor peak in the NR spectra supports our identification of two new isomers, because all previously reported $C_2H_2N_2^{++}$ ions have stable neutral counterparts.

References

- [1] F. Pichieri, Chem. Phys. Lett. 353 (2002) 383 and references cited therein.
- [2] A. Horn, H. Mollendal, O. Sekiguchi, E. Uggerud, H. Roberts, E. Herbst, A.A. Vigiano, T. Fridgen. Astrophys. J. 611 (2004) 605.
- [3] K. Ishii, A. Tajima, T. Taketsugu, K. Yamashita. Astrophys. J. 636 (2006) 927.
- [4] R.A. Evans, P. Lorencak, T-K. Ha, C. Wentrup. J. Am. Chem. Soc. 113 (1991) 7261.
- [5] C. Wentrup, P. Lorencak, A. Maquestiau, R. Flammang, Chem. Phys. Lett. 137 (1987) 241.
- [6] R.A. Evans, S.M. Lacombe, M.J. Simon, G. Pfister-Guillouzo, C. Wentrup, J. Phys. Chem. 96 (1992) 4801.
- [7] K.J. Jobst, M.R. Hanifa, J.K. Terlouw, Chem. Phys. Lett. 462 (2008) 152.
- [8] I. Nenner, O. Dutuit, M. Richard-Viard, P. Morin, A.H. Zewail, J. Am. Chem. Soc. 110 (1988) 1093.
- [9] J.L. Holmes, C. Aubry, P.M. Mayer. Assigning Structures to Ions in Mass Spectrometry, CRC Press, Boca Raton, 2007. Chapter 1.
- [10] L. Nahon, P. Morin, M. Larzilliere, I. Nenner, J. Chem. Phys. 96 (1992) 3628.
- [11] C. Aubry, J.L. Holmes, J. Am. Soc. Mass Spectrom. 12 (2001) 23.
- [12] R. Flammang, Y. Van Haverbeke, S. Laurent, M. Barbieux-Flammang, M.W. Wong, C. Wentrup, Rapid Commun. Mass Spectrom. 98 (1996) 232.
- [13] C.Y. Wong, P.J.A. Ruttink, P.C. Burgers, J.K. Terlouw, Chem. Phys. Lett. 390 (2004) 176.
- [14] C.Y. Wong, P.J.A. Ruttink, P.C. Burgers, J.K. Terlouw, Chem. Phys. Lett. 387 (2004) 204.
- [15] S. Petrie, J. Phys. Chem. A 102 (1998) 7835.
- [16] L.N. Heydorn, C.Y. Wong, R. Srinivas, J.K. Terlouw, Int. J. Mass Spectrom. 225 (2003) 11.

Chapter 12

The covalently bound dimer ion $\text{HC=N-C=NH}^{\bullet+}$ and its neutral counterpart



Model chemistry calculations (CBS-QB3 and CBS-APNO methods) and tandem mass spectrometry based experiments indicate that dissociative ionization of 2-methoxy-*s*-triazine (consecutive losses of CH_2O and HCN) yields the elusive covalently bound [H,C,N] dimer ion $\text{HC=N-C=NH}^{\bullet+}$, a species of interest in astrochemistry. Neutralization-Reionization Mass Spectrometry (NRMS) experiments indicate that its neutral counterpart, HC=N-C=NH , is a kinetically stable molecule in the rarefied gas-phase.

The work described here has been published previously in an article under the same title : K.J. Jobst, J.K. Terlouw, Chem. Phys. Lett. 497 (2010) 7 - 11.

12.1 Introduction

The [H,C,N] pair of isomers and their ionized counterparts are prominent species in various regions of the interstellar medium [1]. Their covalently bound dimers [2] and other C₂H₂N₂ isomers are therefore of interest as potential interstellar and also prebiotic species [3].

The C₂H₂N₂ isomers CH₂=N–C≡N and HN=C(H)–C≡N (*N*- and *C*-cyanomethanamine) were the first to be generated and thoroughly characterized as stable molecules in the gas-phase using various spectroscopic techniques [3-5]. An early attempt to generate a third isomer, NH₂–C–C≡N (aminocyanocarbene), involved the thermal or photolytic decomposition of the alkali metal salts of 1-cyanoformamide tosylhydrazone [6]. However, the exhaustive studies of Refs. 3-5 leave little doubt that the above reaction yields *C*-cyanomethanimine instead.

In a more recent study [7], we have used the technique of Neutralization-Reionization Mass Spectrometry (NRMS) [8, 9] to show that one electron reduction of NH₂–C–C≡N⁺ generates the elusive aminocyanocarbene as a stable molecule in the rarefied gas-phase. The same strategy was employed to probe the structure and stability of the covalently-bound HN≡C dimer HN=C=C=NH (ethenediimine) [7] and the HC≡N dimers HC=N–N=CH and HC=NC(=N)H [10]. The experimental findings of these studies confirm the predictions from theory that the HN≡C dimer is a kinetically stable molecule whereas the HC≡N dimers are not.

In the present study, we report on the generation of the as yet unidentified stable dimer ion HC=N–C=NH⁺, by dissociative ionization of 2-methoxy-*s*-triazine. NRMS experiments and model chemistry calculations agree that the neutral counterpart of this ion is a (marginally) stable molecule.

12.2 Results and discussion

12.2.1 Generation of the mixed dimer ion $\text{HC}=\text{NC}=\text{NH}^{*+}$ (2)

The EI mass spectrum of 2-methoxy-*s*-triazine, see Fig. 12.1, shows a prominent peak at m/z 54 ($\text{C}_2\text{H}_2\text{N}_2^{*+}$). From MS/MS spectra (not shown) it follows that these ions are generated in a stepwise process : m/z 111 \rightarrow m/z 81 \rightarrow m/z 54. As shown in Figure 12.2, we propose that a 1,4-H shift in the molecular ion initiates loss of CH_2O to produce ion **TRI-2**, a 1,2-H shift isomer of ionized *s*-triazine **TRI-1**. Our recent study [8] of **TRI-1** leaves little doubt that HCN loss therefrom yields the HCN dimer ion $\text{HC}=\text{N}-\text{C}(=\text{N})\text{H}^{*+}$ (**1**) and we surmise that loss of HCN from ion **TRI-2** would generate the ‘mixed’ dimer ion $\text{HC}=\text{N}-\text{C}=\text{NH}^{*+}$ (**2**).

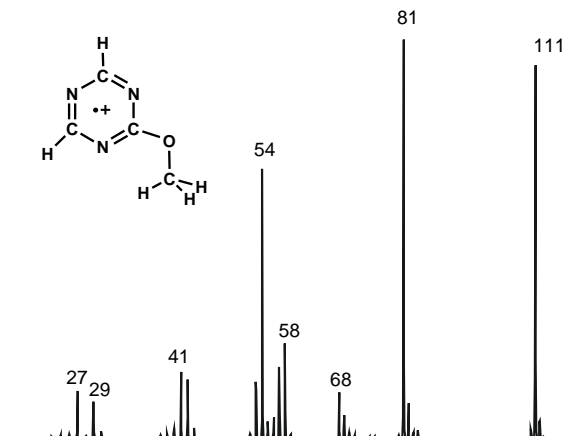


Figure 12.1 EI mass spectrum of 2-methoxy-*s*-triazine

This proposal is corroborated by the model chemistry calculations of Figure 12.2, which indicate that low-energy ions **TRI-1** and **TRI-2** do not interconvert prior to dissociation : the associated 1,2-H shift lies well above the energy requirements of the direct bond cleavage reactions producing ions **1** and **2**. Ions **TRI-1** and **TRI-2** may instead rearrange into hydrogen bridged radical cations [11] (**HBRC-1** and **HBRC-2** respectively) in which ions **1** and **2** are complexed with HCN. In line with this [10], the two ions appear to

dissociate with only a small kinetic energy release : for **TRI-1**, the KER is 0.2 meV [12], while our measured KER for **TRI-2** is ~ 0.5 meV. This difference is compatible with the proposal that the two ions dissociate via different mechanisms.

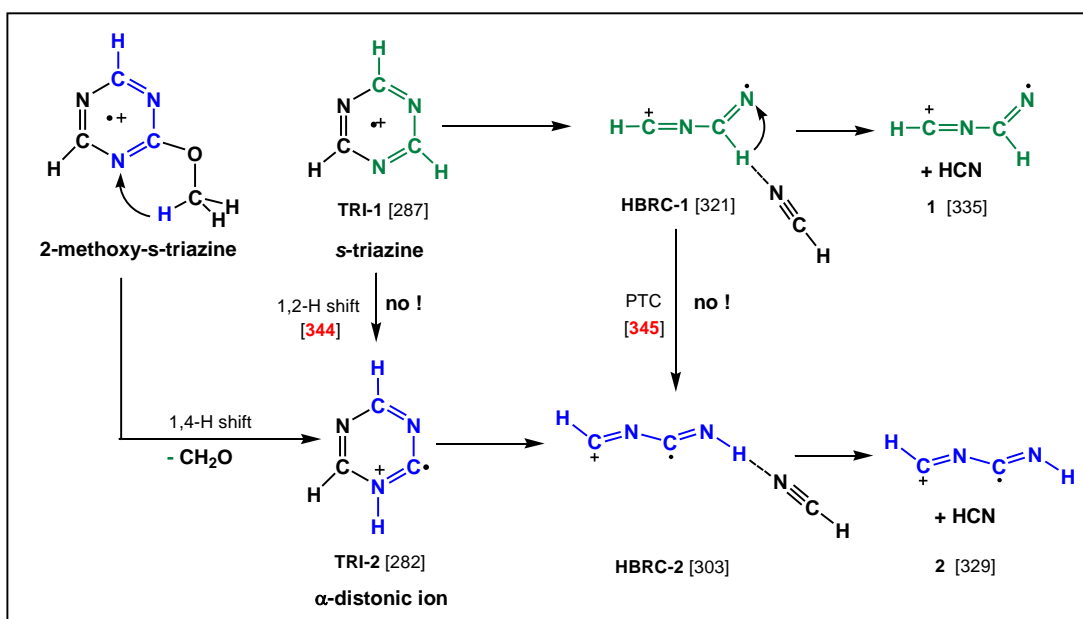


Figure 12.2 The formation of $C_2H_2N_2^{++}$ ions **1** and **2** by dissociative ionization of *s*-triazine and 2-methoxy-*s*-triazine. The numbers in square brackets are 298 K enthalpies in kcal mol^{-1} . These have been obtained from CBS-APNO calculations reported in our recent study of Ref. 10.

The involvement of the HBRCs also raises the question whether the departing HCN molecule can catalyze the interconversion of ions **1** and **2** by proton-transport catalysis (PTC) [13,14]. However, theory predicts that both the catalyzed and unassisted 1,2-H shift reactions connecting **HBRC-1** and **HBRC-2** are too energy demanding [10].

Compelling evidence that ion **2** is generated in the dissociation of **TRI-2** is provided by its collision-induced dissociation (CID) mass spectrum shown in Fig. 12.3b : the spectrum shows structure diagnostic peaks at m/z 41 and 15, indicative of the $HC=$ and $=NH$ connectivity in $HC=N-C=NH^{++}$, which are absent in the spectrum of ion **1** (Fig. 12.3a).

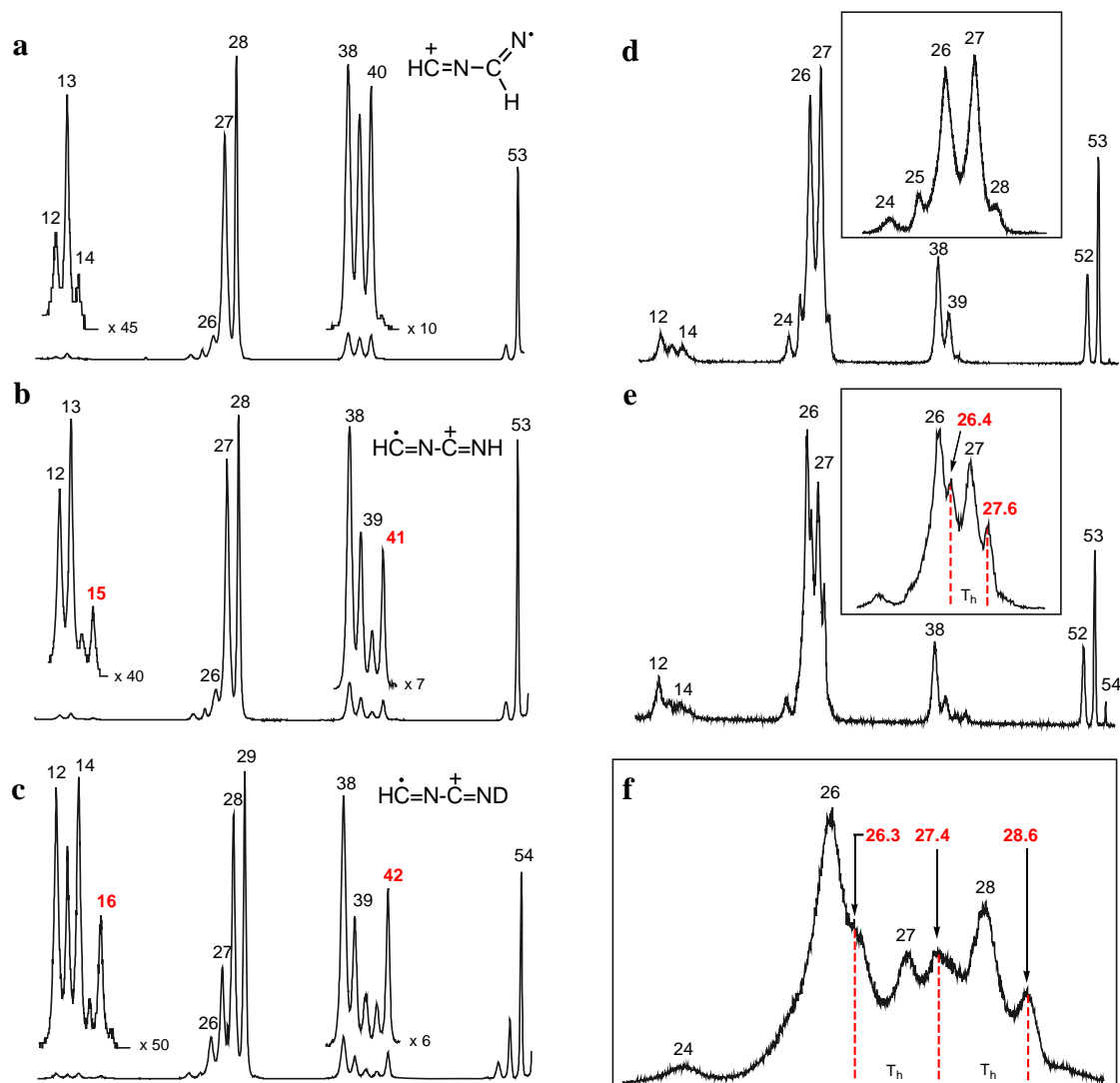


Figure 12.3 (left) CID mass spectra of the m/z 54 ions generated from (a) *s*-triazine; (b) 2-methoxy-*s*-triazine and (c) CD_3 -labelled 2-methoxy-*s*-triazine. (right) NR mass spectra of the m/z 54 ions generated from (d) *s*-triazine and (e) 2-methoxy-*s*-triazine. Item (f) shows the m/z 20 – 30 region of the NR mass spectrum of $\text{HC}=\text{N}-\text{C}=\text{ND}^{+\cdot}$.

In contrast, the spectrum of the nitrene ion **1**, see Fig. 12.3a, shows a characteristic peak at m/z 40 for loss of N.

Fig. 12.3c shows the CID mass spectrum of the isotopologue $\text{HC}=\text{N}-\text{C}=\text{ND}^{+\cdot}$, generated from CD_3O -labelled 2-methoxy-*s*-triazine and, in accordance with the proposal of Figure

12.2, the m/z 15 (NH^+) and 41 (CH-loss) peaks in Fig. 12.3b are shifted to m/z 16 (ND^+) and 42 (CH-loss). As further evidence of the $\text{DN}=\text{C}^-$ structure motif, Fig. 12.3c shows a peak at m/z 28 that is significantly more intense than the peak at m/z 27. This is readily understood, considering [8] that the dissociation of the labelled dimer ion $\text{HC}=\text{N}-\text{C}=\text{ND}^{\bullet+}$ into $\text{DN}=\text{C}^{\bullet+}$ (m/z 28) is energetically more favourable than its dissociation into $\text{HC}\equiv\text{N}^{\bullet+}$ (m/z 27).

Finally, a comparison of the CID mass spectrum of Fig. 12.3b with reference spectra [7,10] of the ions $\text{HN}=\text{C}=\text{C}=\text{NH}^{\bullet+}$, $\text{NH}_2-\text{C}-\text{CN}^{\bullet+}$ and $\text{HC}=\text{N}-\text{N}=\text{CH}^{\bullet+}$ leaves little doubt that we are dealing with the elusive mixed dimer ion $\text{HC}=\text{N}-\text{C}=\text{NH}^{\bullet+}$ (**2**).

12.2.2 The dissociation chemistry of ion **2** and its neutral counterpart

The CID experiments of Section 12.2.1 unambiguously show that ions **1** and **2** do not readily interconvert. This is consistent with the computational results of Figure 12.4 (top), which indicate that the energy required for the associated 1,2-H shift is higher than that for the rearrangement and dissociation reactions: $\mathbf{2} \rightarrow \mathbf{3} \rightarrow \mathbf{4} \rightarrow \text{HN}=\text{C}-\text{C}\equiv\text{N}^+ (m/z\ 53) + \text{H}^\bullet$ and $\mathbf{2} \rightarrow \mathbf{HB1} \rightarrow \text{HC}=\text{NH}^+ (m/z\ 28) + \text{CN}^\bullet$. These processes represent the dissociation reactions of lowest energy requirement as witnessed by the peaks at m/z 28 and 53 in the metastable ion (MI) mass spectrum of ion **2** (not shown). The MI mass spectrum of **1** also shows only two peaks at m/z 28 and 53 and, in our previous study [10], it was proposed that these dissociations are initiated by the isomerization reaction $\mathbf{1} \rightarrow \mathbf{2}$. In line with this, the magnitude of the kinetic energy released in the H^\bullet loss from **1** is considerably greater than that from **2** (140 vs 104 meV). The computational results of Figure 12.4 (top) do indicate that ions **2**, **3** and **4** may interconvert, but only at elevated internal energies. Thus, we contend that the majority of non-dissociating m/z 54 ions generated from 2-methoxy-*s*-triazine retain the structure of ion **2**.

Figure 12.4 (bottom) predicts that the neutral dimer $\text{HC}=\text{N}-\text{C}=\text{NH}$ (**N2**) lies $\sim 40 \text{ kcal mol}^{-1}$ above the thermochemical energy level of the monomers $\text{HCN} + \text{HNC}$. Nevertheless, theory predicts that a barrier of $\sim 5 \text{ kcal mol}^{-1}$ inhibits the dimer's dissociation. The

calculations further indicate that the neutral dimer N3, a cyclic isomer of N2, is a stable species whose de-dimerization is prevented by an energy barrier of 15 kcal mol⁻¹. However, N3 is unlikely to be generated in the NR experiment because of the prohibitively high barrier connecting N2 and N3.

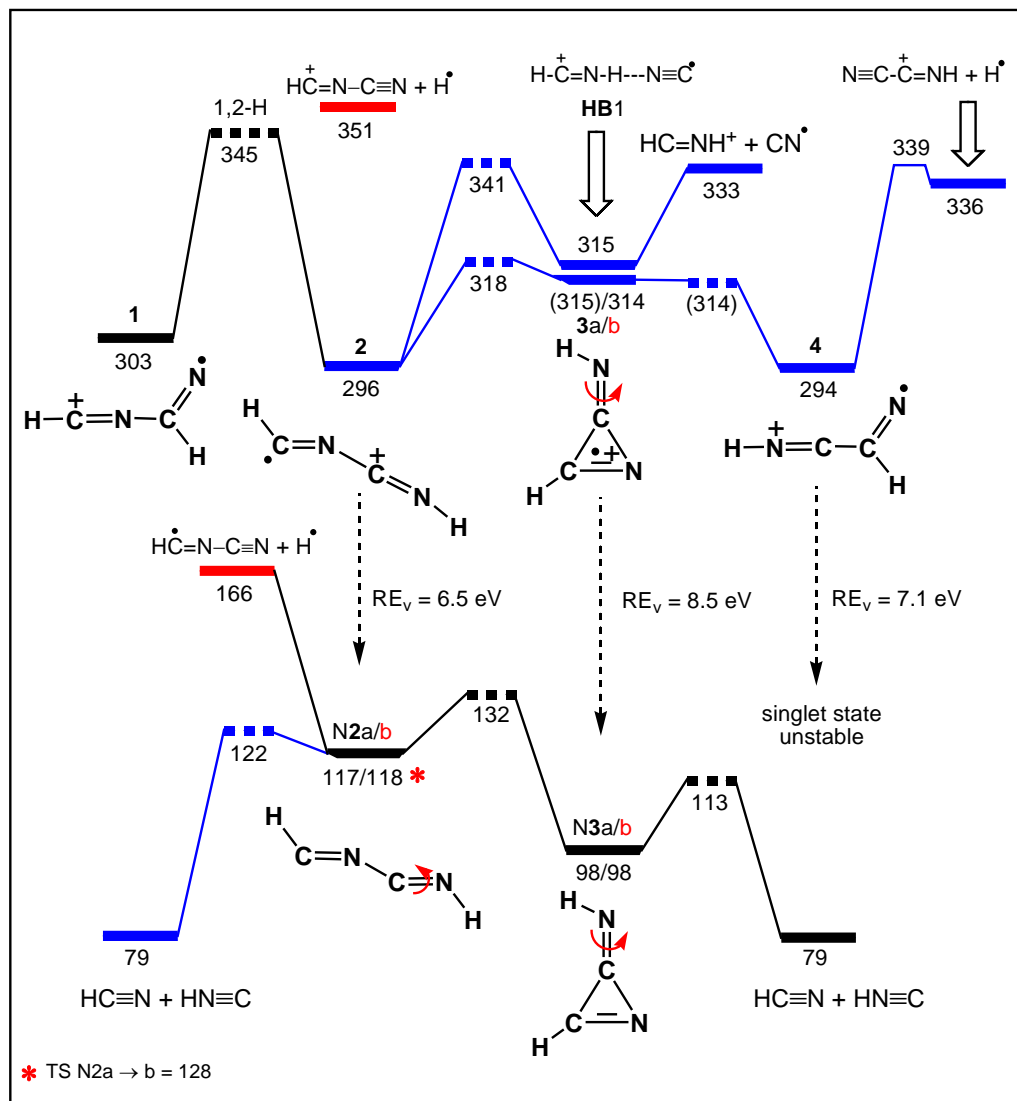


Figure 12.4 Model chemistry results of Table 12.1 showing the dissociation and isomerization chemistry of $C_2H_2N_2^{++}$ ions **1** - **4** and their neutral counterparts. The 298 K enthalpies are in kcal mol⁻¹; the vertical recombination energies (RE_v) shown are in eV.

The charge-transfer in a Neutralization-Reionization experiment is a vertical Frank-Condon process [9]. Assuming that resonant charge exchange occurs, a crude estimate of the internal energy of the incipient neutral N₂ is obtained from the difference between the adiabatic ionization energy (IE_a) and the vertical recombination energy (RE_v) of its ionic counterpart **2**. Thus, from the calculated IE_a and RE_v values reported in the Table, it is expected that the majority of the neutrals N₂, generated in the charge-transfer reaction, have ~30 kcal mol⁻¹ of internal energy. While this level of excitation is sufficient to cause dissociation of the majority of the incipient neutrals, a fraction thereof may well be generated as stable molecules. Experiments to probe this possibility are discussed in the next Section.

Table 12.1 Enthalpies of formation (kcal mol⁻¹) and total energies (Hartree) derived from CBS-QB3 and CBS-APNO calculations [a].

Species		CBS-QB3 E(total) [0K]	QB3 Δ _f H ⁰ ₂₉₈	APNO Δ _f H ⁰ ₂₉₈	RE _v [b]	Transition State	CBS-QB3 E(total) [0K]	QB3 Δ _f H ⁰ ₂₉₈	APNO Δ _f H ⁰ ₂₉₈
HC=N-C(=N)H ⁺	1	-186.19198	302.9	302.8	7.8	1 → 2	-186.12317	346.4	345.4
HC=N-C=NH ⁺	2	-186.20232	296.8	296.4	6.5	2 → HB1	-186.13342	340.4	341.6
HN=C-N=CH ⁺	3a	-186.17276	314.9	[c]	8.5	2 → 3a	-186.16536	319.4	318.0
HN=C-N=CH ⁺	3b	-186.17397	314.2	314.6	8.5	3a → b	-186.17412	314.0	[c]
HN=C-C(=N)H ⁺	4	-186.20589	294.2	294.6	7.1	3b → 4	-186.17624	312.6	[c]
HC=N-H ⁺ ---N≡C ⁺	HB1	-186.17289	315.5	315.4	-	4 → HN=C-C≡N ⁺	-186.13525	338.9	339.3
HC=N-C≡N ⁺		-185.61705	299	299	-	+ H ⁺ [d]			
HC=N-C=NH	N2a	-186.48777	117.4	117.3	7.8	N2a → b	-186.47119	127.9	127.9
HC=N-C=NH	N2b	-186.48707	118.0	118.0	7.7	N2b → HCN + HNC	-186.47789	123.6	121.9
HN=C-N=CH	N3a	-186.51766	98.1	98.4	-	N2a → N3a	-186.46520	131.4	131.9
HN=C-N=CH	N3b	-186.51922	97.1	97.6	9.4	N3a → HCN + HNC	-186.49067	115.3	114.4
HC=N-C≡N ⁺		-185.91171	114	115	-	N3a → b	-186.48556	118.6	119.1
						N3b → HCN + HNC	-186.49403	113.2	112.6

[a] E(total) in Hartrees, all other components in kcal mol⁻¹. [b] Vertical recombination and ionization energies in eV from calculations at the B3LYP/CBSB7 level of theory; [c] conformer **3a** is not a minimum at the CBS-APNO level of theory : it ring opens into ion **4** ; [d] The computed values for H⁺, CN⁺, HCN, HNC and HC=NH⁺ are 52.1, 106, 32, 46.5 and 226 kcal mol⁻¹ in excellent agreement with experiment, see ref. 8.

12.2.3 Generation of HC=NC=NH (N₂) by neutralization-reionization experiments

The NR mass spectra of ions **1** and **2**, are shown in Figs. 12.3d/e. A remarkable feature of Fig. 12.3e, but not of Fig. 12.3d, is the pair of peaks at m/z 26.4 and 27.6, which represent the ‘horns’ of a dish-shaped peak [8] centered at m/z 27. The substantial kinetic energy release associated with this peak ($T_h \cong 30 \text{ kcal mol}^{-1}$) shows that the corresponding dissociation involves a sizable reverse barrier. Since we do not observe such a broad m/z 27 peak in the CID or MI mass spectra of ions **2**, the peak must relate to the dissociation of *neutralized* ions HC=N–C=NH⁺ whose dissociation products, HN≡C + HC≡N, are subsequently re-ionized. In support of this interpretation, the relevant part of the NR mass spectrum of the HC=N–C=ND⁺ isotopologue presented in Fig. 12.3f, shows two dish-shaped peaks of equal intensity, centered at m/z 27 (HC≡N⁺) and 28 (DN≡C⁺). We note in passing that these results further attest to the proposed structure integrity of ions **2**.

As discussed in Section 12.2.2, our calculations predict that the de-dimerization of the neutralized ions involves a barrier of *c.* 5 kcal mol⁻¹ whereas a crude estimate indicates that the incipient neutrals have $\sim 30 \text{ kcal mol}^{-1}$ of internal energy. These findings support the interpretation of the NR experiment that most of the incipient neutrals have an internal energy that exceeds the barrier leading to de-dimerization with the release of a large amount of kinetic energy.

The weak survivor signal at m/z 54 may well result from the reionization of the small fraction of neutrals N₂ that has insufficient internal energy to dissociate. To verify this possibility, we probed the structure of the (mass selected) m/z 54 survivor ions by collision-induced dissociation. In such an experiment, the non-dissociating neutrals are reionized (yielding the survivor ions), mass selected and subsequently induced to dissociate by collision with He to yield the NR-CID mass spectrum. If the neutralized ions retain their structure integrity, their NR-CID mass spectrum is expected to be very close to the conventional CID mass spectrum of the original ions.

The prominent m/z 27 ($\text{HNC}^{\bullet+}$) peak and the structure diagnostic peaks at m/z 15 and 41 in the m/z 54 NR-CID mass spectrum of Fig. 12.5a indicate that $\text{C}_2\text{H}_2\text{N}_2^{\bullet+}$ ions of structure **2** are indeed regenerated in the NR process. However, the intensities of the peaks at m/z 12, 14, 26, 28, 38 and 40 in Fig. 12.5a are significantly higher than those in the CID mass spectrum of ions **2** (Fig. 12.5b). This we ascribe to the presence of an isobaric impurity in the m/z 54 $\text{C}_2\text{H}_2\text{N}_2^{\bullet+}$ survivor ion signal, *viz.* C_2NO^+ ions of the connectivity $\text{C}=\text{N}-\text{C}=\text{O}^+$, a structure motif in the 2-methoxy-*s*-triazine precursor molecule of this study. Considering the results of our earlier NR study of the C_2NO^+ system of ions [16], it appears that the CID characteristics of the stable $\text{C}=\text{N}-\text{C}=\text{O}^+$ isomer may readily account for the deviation of the spectrum of Fig. 12.5a from that of Fig. 12.5b, if it is assumed that c. 25 % of the beam of NR survivor ions consists of ions $\text{C}=\text{N}-\text{C}=\text{O}^+$.

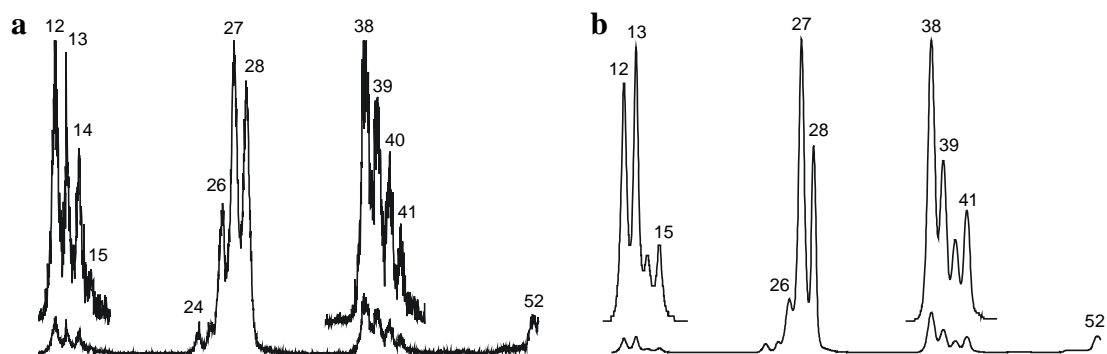


Figure 12.5 (a) NR-CID and (b) 3ffr CID mass spectra of the m/z 54 ions from 2-methoxy-*s*-triazine.

In this context we note that the proposed isobaric $\text{C}=\text{N}-\text{C}=\text{O}^+$ impurity only plays a role in the interpretation of the NR-CID mass spectrum of the survivor ions of putative structure **2**, not in its CID mass spectrum. This is because the estimated NR efficiency [15] of the $\text{C}=\text{N}-\text{C}=\text{O}^+$ ions [16] is more than a factor of 100 higher than that of the $\text{C}_2\text{H}_2\text{N}_2^{\bullet+}$ ions **2**. This concurs with the result of an experiment using a Micromass GC-TOF instrument in the EI mode at a mass resolution of 4000 : the m/z 54 ions yielded a symmetric peak centered at m/z 54.022, which confirms that their elemental composition is $\text{C}_2\text{H}_2\text{N}_2$ and that

potential isobaric (C_2NO) impurities lie well below the 1 % level and that the conventional CID mass spectrum is essentially that of “pure” $C_2H_2N_2^{*+}$ ions.

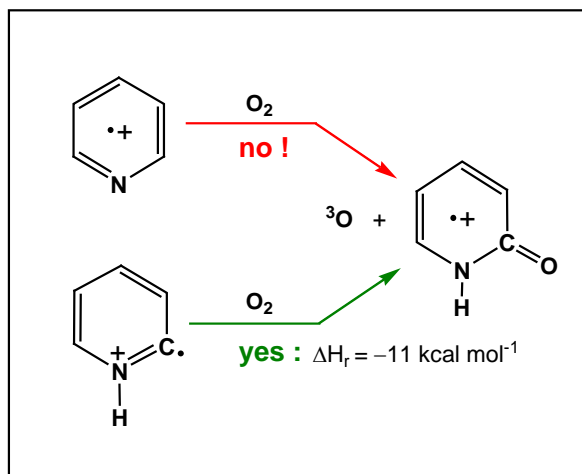
In summary, we conclude that the elusive $C_2H_2N_2^{*+}$ isomer $HC=N-C=NH^{*+}$ (**2**) is a remarkably stable species in the diluted gas-phase whereas, in agreement with predictions from theory, its neutral counterpart $HC=N-C=NH$ (**2N**) is only marginally stable.

References

- [1] F. Pichieri, Chem. Phys. Lett. 353 (2002) 383 and references cited therein.
- [2] For a recent study of non-covalently bound dimers see : A. Heikkilä, J. Lundell, J. Phys. Chem. A 104 (2000) 6637.
- [3] R.A. Evans, P. Lorencak, T-K. Ha, C. Wentrup. J. Am. Chem. Soc. 113 (1991) 7261.
- [4] C. Wentrup, P. Lorencak, A. Maquestiau, R. Flammang, Chem. Phys. Lett. 137 (1987) 241.
- [5] R.A. Evans, S.M. Lacombe, M.J. Simon, G. Pfister-Guillouzo, C. Wentrup, J. Phys. Chem. 96 (1992) 4801.
- [6] R.E. Moser, J.M. Fritsch, T.L. Westman, R.M. Kliss, C.N. Matthews, J. Am. Chem. Soc. 89 (1967) 5673.
- [7] K.J. Jobst, M.R. Hanifa, J.K. Terlouw, Chem. Phys. Lett. 462 (2008) 152.
- [8] J.L. Holmes, C. Aubry, P.M. Mayer. Assigning Structures to Ions in Mass Spectrometry, CRC Press, Boca Raton, 2007. Chapter 1.
- [9] F. Tureček, Top. Curr. Chem. 225 (2003) 77.
- [10] K.J. Jobst, M.R. Hanifa, P.J.A. Ruttink, J.K. Terlouw, Chem. Phys. Lett. 473 (2009) 257.
- [11] P.C. Burgers, J.K. Terlouw, in: N.M.M. Nibbering (Ed.), Encyclopedia of Mass Spectrometry, vol. 4, Elsevier, Amsterdam, 2005, p. 173.
- [12] R.G. Cooks, J.H. Beynon, R.M. Caprioli, G.R. Lester. Metastable Ions, Elsevier Scientific Pub. Co., Amsterdam, 1973. p. 61.
- [13] C.Y. Wong, P.J.A. Ruttink, P.C. Burgers, J.K. Terlouw, Chem. Phys. Lett. 390 (2004) 176.
- [14] C.Y. Wong, P.J.A. Ruttink, P.C. Burgers, J.K. Terlouw, Chem. Phys. Lett. 387 (2004) 204.
- [15] L.N. Heydorn, C.Y. Wong, R. Srinivas, J.K. Terlouw, Int. J. Mass Spectrom. 225 (2003) 11.
- [16] G.A. McGibbon, C.A. Kingsmill, J.K. Terlouw, P.C. Burgers, Int. J. Mass Spectrom. 121 (1992) R11.

Chapter 13

Differentiation of the pyridine radical cation from its distonic isomers by ion-molecule reactions with dioxygen



In a previous study on the pyridine ion (1) and the pyridine-2-ylid isomer (2), we reported that ions 2 readily react with H_2O to produce 2-pyridone ions at m/z 95, by O-atom abstraction. The mechanism for this intriguing reaction, however, was not established. This prompted us to use model chemistry calculations (CBS-QB3) to probe various mechanistic scenarios and to perform complementary experiments with the new, more versatile, ion-molecule reaction chamber of the Mons Autospec 6F mass spectrometer. It appears that H_2O is not the reacting neutral that produces the 2-pyridone ion of the above reaction, but rather O_2 from air co-introduced with the water vapour. Theory and experiment agree that the exothermic reaction of O_2 with the pyridine-2-ylid ion leads to loss of 3O from a stable peroxide-type adduct ion at m/z 111. Similarly, pyridine-3-ylid ions (3) generate 3-pyridone ions, but the reaction in this case is thermoneutral. The m/z 111 : 95 peak intensity ratios in the spectra of the ion-molecule products from ions 2 and 3 may serve to differentiate the isomers.

The work described here has been published previously in an article under the same title : K.J. Jobst, J. De Winter, R. Flammang, J.K. Terlouw, P. Gerbaux, *Int. J. Mass Spectrom.* 286 (2009) 83 - 88.

13.1 Introduction

Differentiation of a gaseous organic ion from its isomers is commonly based upon high-energy collision induced dissociation (CID) mass spectra of mass selected ions. However, this approach may be difficult or even impossible to realize if a set of isomeric ions only displays common dissociation pathways [1]. As an alternative, the reactivity of the ion under investigation may be probed by interactions with selected neutral molecules. Apart from charge exchange and protonation reactions, highly structure specific associative ion-molecule reactions may occur, which readily distinguish the ion from its structural isomers [1]. This is especially true for distonic ions, because of their unique tendency to exhibit radical-type reactivity [2, 3].

A case in point concerns our previous work [4a-c] on the pyridine ion and its distonic (1,2-H shift) isomers shown in Figure 13.1. The distonic isomers are remarkably stable relative to ionized pyridine but are separated by high interconversion barriers. Consequently, these isomers can be differentiated on the basis of the m/z 28 (HCNH^+) : 26 ($\text{C}_2\text{H}_2^{+\bullet}$) peak intensity ratio in their high-energy CID mass spectra [4a,b].

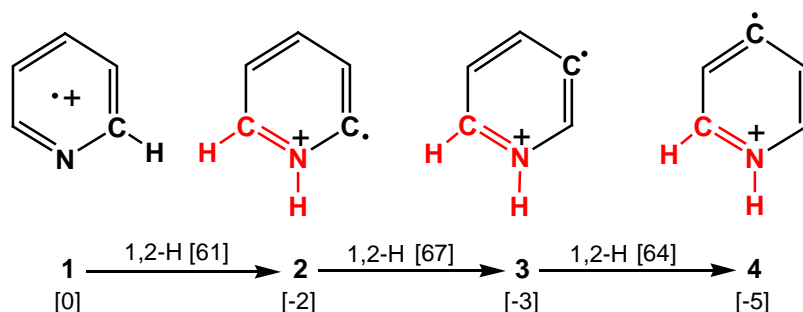


Figure 13.1 Structures of the pyridine ion **1** and its α -, β - and γ -distonic isomers **2** – **4**. Relative energies are in kcal mol^{-1} and taken from Ref. 4.

However, an easier differentiation was achieved in our more recent study of this system [4c,5] by associative ion-molecule reactions involving a variety of neutral reagents,

including H₂O. Neutral water does not react with the pyridine ion, but its α -distonic isomer was found to readily generate the 2-pyridone ion, by an O-atom transfer [4c].

The mechanism for this intriguing reaction, however, was not established. This prompted us to use model chemistry calculations (CBS-QB3) to probe various mechanistic scenarios and also to perform complementary experiments with the new, more versatile, ion-molecule reaction chamber of the Mons Autospec 6F instrument. It will be shown that H₂O is not the reacting neutral that produces the 2-pyridone ion of the above reaction, but rather O₂ from air co-introduced with the water vapour in the ion-molecule reaction chamber.

13.2 Results and discussion

13.2.1 The associative ion-molecule reaction of the pyridine-2-ylid ion with H₂O

Pyridine-2-ylid ions (**2**) are readily generated in the dissociative ionization of 2-acetylpyridine [5] by the route depicted in Figure 13.2.

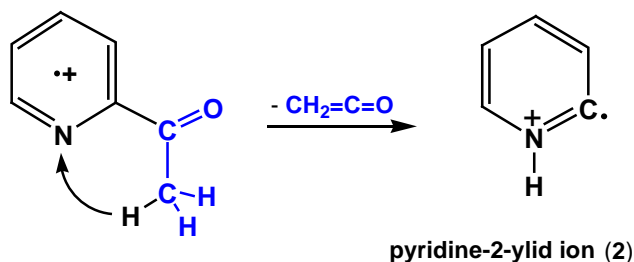


Figure 13.2 The generation of pyridine-2-ylid ions by dissociative ionization of 2-acetylpyridine.

In good agreement with the results of our previous study [4c], the reaction of mass selected ions **2** with H₂O vapour in the hexapole reaction chamber of our mass spectrometer leads to the formation of m/z 95 product ions, as witnessed by the spectrum of Fig. 13.3a. Under the same conditions, pyridine ions (**1**) are unreactive.

The (high-energy) CID mass spectrum of these m/z 95 product ions, see Figure 13.3d, is closely similar to that of the molecular ions produced in the EI mass spectrum of the 2-

hydroxy-pyridine/pyridine-2-one system of tautomers [6]. This result, and the fact that the reaction with D₂O as the reagent exclusively generates m/z 95 ions, led to the proposal [4c] that the 2-pyridone ion is the major reaction product from the m/z 97 adduct ion comprised of H₂O and ion 2.

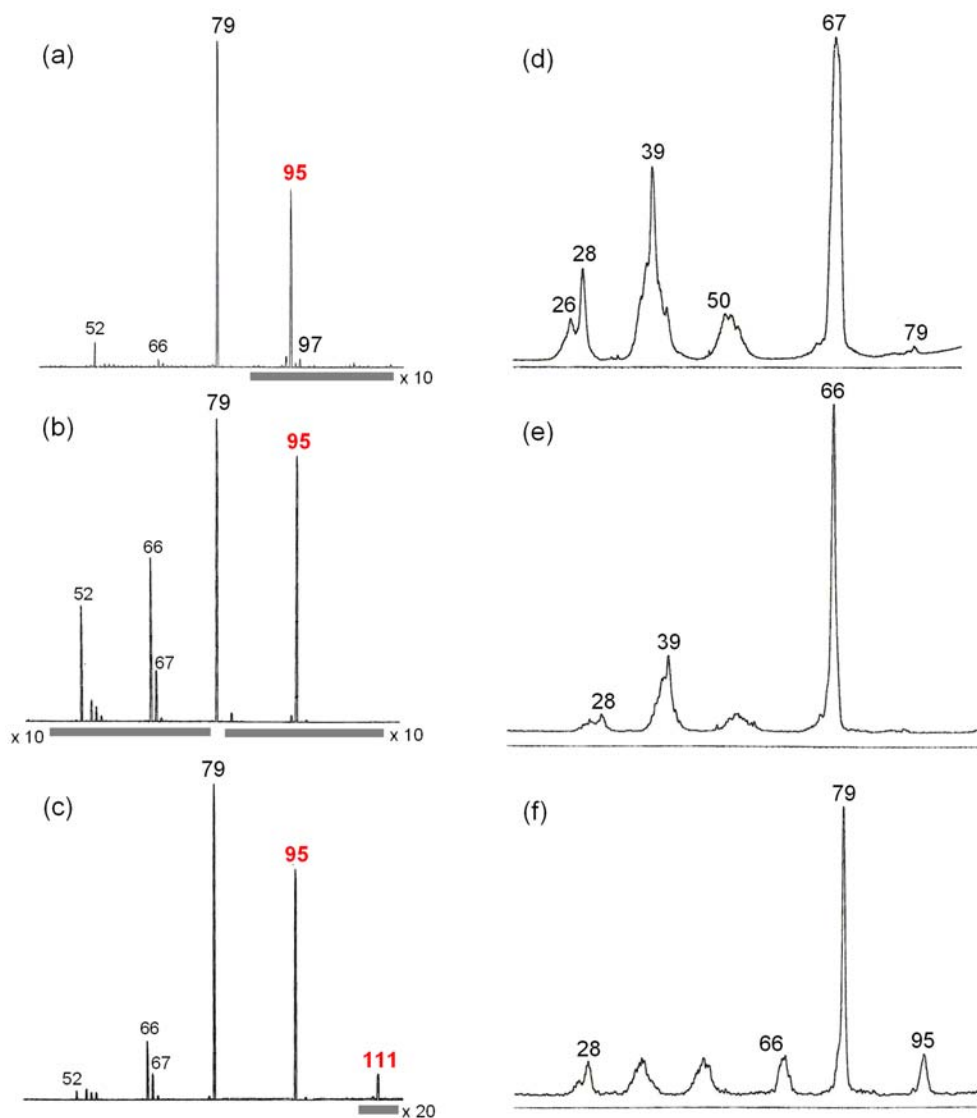


Figure 13.3 Mass spectra of the products of the ion-molecule reactions of pyridine-2-ylid ions with : (a) water vapour; (b) dioxygen [O_2 pressure = 2×10^{-4} mbar] and (c) dioxygen [O_2 pressure = 8×10^{-4} mbar]. Items (d), (e) and (f) are CID mass spectra of the m/z 95, m/z 94 and m/z 111 ions, generated in the above ion-molecule reaction with dioxygen.

The model chemistry calculations of Figure 13.4 show that the interaction of a single water molecule with ion **2** may yield hydrogen-bridged radical cation [7] **HBRC1**. This ion could be envisaged to isomerize into **D1a** or **D1b** but neither pathway appears to be energetically feasible :

(i) the isomerization of **HBRC1** into **D1a** involves a prohibitively high TS at 197 kcal mol⁻¹ for the formation of the intermediate ion **HBRC2**. This ion, see Table 13.1, is predicted to dissociate by loss of OH[•] (which is not experimentally observed !) rather than rearrange into ion **D1a**. (ii) adduct ion **D1b**, generated by C-O bond formation, is not even a minimum. Finally, the subsequent 1,2- and 1,1-H₂ elimination reactions from **D1a** and **D1b** are expected to have considerable energy barriers.

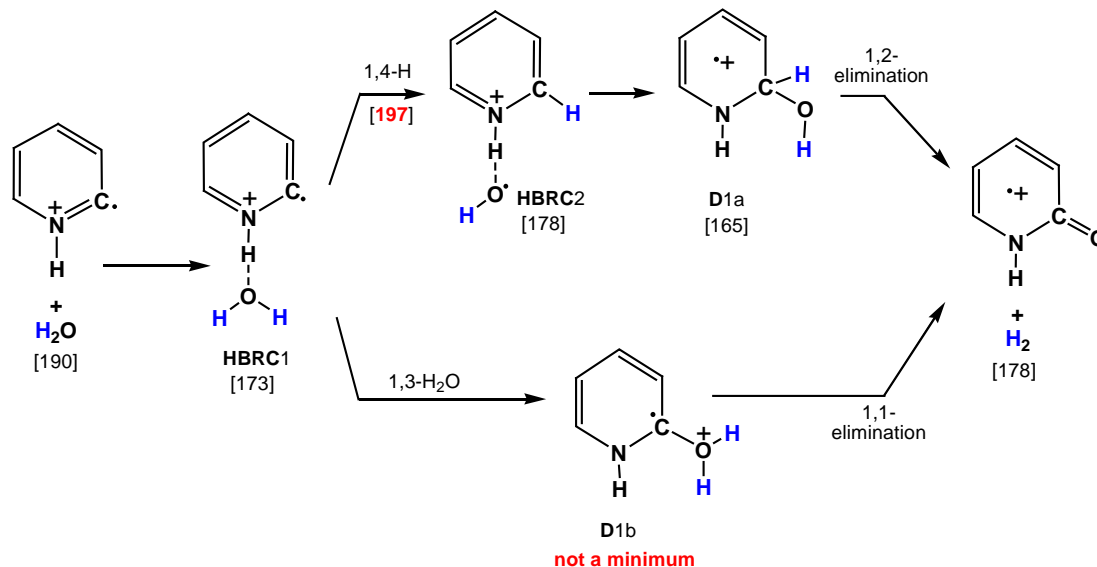


Figure 13.4 The ion-molecule reaction of the pyridine-2-ylid ion **2** with H₂O. The numbers refer to 298 K enthalpies in kcal mol⁻¹ derived from CBS-QB3 calculations.

Thus, despite the exothermicity of the reaction, the scenario of Figure 13.4 predicts that the bulk of the *m/z* 97 adduct ions dissociate by loss of water. In line with this prediction, the *m/z* 97 adduct ions do not lose H₂ to any significant extent in their CID mass spectrum (not shown). Instead, these ions primarily back-dissociate into ions **2** and H₂O. It is

therefore highly unlikely that the 2-pyridone ion is generated in the reaction of a water molecule with ion **2**.

Table 13.1 Energetic data from CBS-QB3 calculations for the ion-molecule reactions of pyridine-2-ylid and pyridine-3-ylid ions described in Figures 13.3 and 13.5 [a].

Structure	CBS-QB3 E(total) [0K]	QB3 $\Delta_f H_{298}^0$	EXPT [b] $\Delta_f H_{298}^0$
Ion 1 (pyridine ion)	-247.49012	248	247
Ion 2 (pyridine-2-ylid ion)	-247.49103	247.5	-
Ion 3 (pyridine-3-ylid ion)	-247.49293	246	-
Ion 2 + H ₂ O	-	189 [c]	-
HBRC1	-323.85403	173	-
TS HBRC1 → 2	-323.81641	197	-
HBRC2	-323.84658	178	-
Ion D1a	-323.86587	165	-
protonated pyridine + [•] OH	-	187 [c]	-
protonated pyridine	-248.18185	178	-
2-Pyridone ion + H ₂	-	178	176
2-Pyridone ion	-322.68334	178	176
Ion D2	-397.72966	199	-
2-Pyridone ion + ³ O	-	237 [c]	236
TS 2-pyridone ion → pyrrole ion	-322.60929	283 [d]	-
Pyrrole ion + CO + ³ O	-	249 [c]	248
Pyrrole ion	-209.48311	217	215
Ion D3	-397.72565	202	-
3-Pyridone ion + ³ O	-	246	-
TS 3-pyridone ion → pyrrole ion	-322.56735	310 [d]	-
3-Pyridone ion	-322.66798	187	-

[a] $E_{\text{(total)}}$ in Hartrees, all other components are in kcal mol⁻¹; Enthalpies derived from this and other model chemistries are expected to be of chemical accuracy (± 2 kcal mol⁻¹). However, as pointed out by a reviewer, for the peroxy type ions **D2** and **D3** the performance of the method may be compromised by an inadequate wave function. [b] Ref. 13; [c] The CBS-QB3 derived enthalpies for H₂O, [•]OH, ³O and CO are -58.2, 8.8, 59.4 and -26.9 kcal mol⁻¹; [d] The decarbonylation involves two transition states (ring-opening and loss of CO from the resulting intermediate) : the quoted TS refers to the second step.

This led us to consider the possibility that the 2-pyridone ion is generated by another reagent. A plausible candidate would be triplet (biradical) O_2 molecules from air co-introduced with the water vapour. Such a reaction would not be unprecedented: reactions of distonic ions and O_2 have been observed previously [8,9]. Indeed, a drawback of the present inlet system is that, despite multiple freeze/pump cycles, air may be co-introduced into the hexapole cell when dealing with reagents of low volatility. This prompted us to examine the interaction of pyridine-2-ylid ions with pure oxygen.

13.2.2 The associative ion-molecule reaction of ion 2 with dioxygen

Fig. 13.3b shows the mass spectrum of the products of the ion-molecule reaction of pyridine-2-ylid ions (m/z 79) and pure oxygen. That 2-pyridone ions are readily generated in the reaction is revealed by the intense peak at m/z 95 and its corresponding CID mass spectrum, which is identical with that shown in Fig. 13.3d.

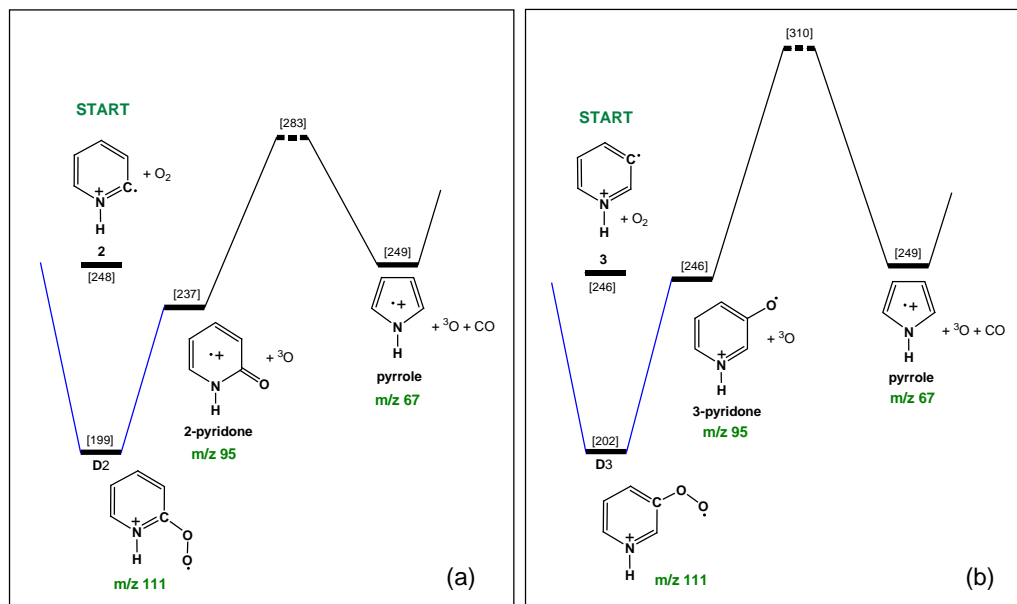


Figure 13.5 Potential energy diagrams describing the associative ion-molecule reactions of (a) the pyridine-2-ylid ion **2** and (b) the pyridine-3-ylid ion **3** with dioxygen. Numbers in square bracket refer to CBS-QB3 derived 298 K enthalpies in kcal mol^{-1} .

These observations are rationalized by the model chemistry calculations of Figure 13.5a, which show that the initial interaction between ion **2** and O₂ leads to the remarkably stable covalently-bound species **D2**. This peroxide-type ion enjoys considerable stabilization, c. 50 kcal mol⁻¹, relative to the combined enthalpies of ion **2** and O₂. Our calculations further show that loss of ³O from ion **D2** yields the 2-pyridone ion in a process that is continuously exothermic by 11 kcal mol⁻¹ relative to the combined enthalpies of **2** and O₂. The spectrum of Fig. 13.3b also shows peaks at *m/z* 52, 66 and 67, whose formation deserves comment. The signal at *m/z* 52 (C₄H₄⁺⁺) is readily attributed to the spontaneous and collision induced loss of HCN from the mass-selected 2-ylid ions [4a], but the other two ions must result from associative ion-molecule reactions between the **2** and O₂.

The *m/z* 67 ion, readily identified as the pyrrole ion on the basis of its CID mass spectrum (not shown), likely originates from decarbonylating 2-pyridone ions : see the CID mass spectrum of Fig. 13.3d, where *m/z* 67 is the base peak. The calculated TS for the decarbonylation is quite high (283 kcal mol⁻¹), in line with the results of a previous study on isomeric C₃H₅NO⁺ ions [6].

This raises the question as to why this energy demanding reaction is observed. First, we note that the EI generated 2-ylid reactant ions may have up to ~70 kcal mol⁻¹ of internal energy, the estimated energy requirement for the spontaneous loss of HCN [4a,d]. Thermalization of these ions by (unreactive) collisions with the neutral reagent takes place in the hexapole cell but this process may be rather inefficient in our experimental set-up. Perhaps more likely, ions entering the hexapole cell have a minimum translational energy of ~5 eV, so that collision-induced dissociation may still compete with collisional cooling. In line with this, Fig. 13.3c shows that the relative intensity of the *m/z* 67 (and *m/z* 52) peak decreases considerably when the O₂ pressure is raised.

The spectrum of Fig. 13.3c indicates that the *m/z* 66 ion also results from a high energy process. Its CID mass spectrum (not shown) may be that of a C₄H₄N⁺ isomer for which, unfortunately, reference spectra are not available. Several pathways for its formation can

be envisaged, but in the absence of further information, these remain highly speculative. The CID mass spectrum of Fig. 13.3e, indicates that one route may involve decarbonylation of the weakly detected m/z 94 ions in Fig. 13.3b.

The most important feature of Fig. 13.3c is that at the elevated O_2 pressure, the m/z 111 adduct ion (**D2**) becomes observable. The fact that its CID mass spectrum shows a significant peak at m/z 95, see Fig. 13.3f, underlines our proposal that dioxygen, rather than water, reacts with the pyridine-2-ylid ion.

13.2.3 The associative ion-molecule reaction of ion **3** with dioxygen

We have also studied the reaction of pyridine-3-ylid ions **3** with dioxygen to see if the distonic isomers **2** and **3** can be differentiated. Ions **3** can conveniently be generated by the dissociative ionization of 2,3-diacetylpyridine, as depicted in Figure 13.6.

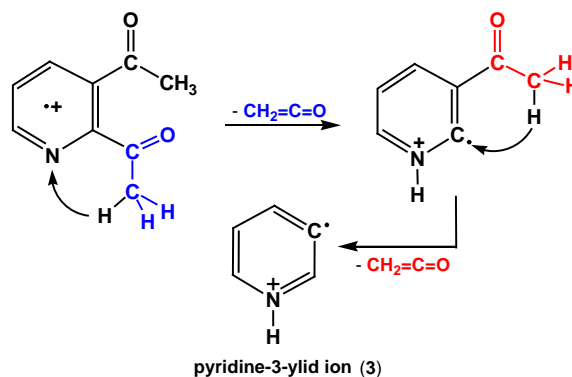


Figure 13.6 The generation of pyridine-3-ylid ions by dissociative ionization of 2,3-diacetylpyridine.

In line with the calculations of Figure 13.5b, which predict that the O-atom abstraction of dioxygen by the radical site of ion **3** is a thermoneutral reaction, Fig. 13.7a displays a sizeable peak at m/z 95 for the reaction of ion **3** with dioxygen. The CID mass spectrum of these m/z 95 ions is shown in Fig. 13.7c. The spectrum is virtually the same as that of the 3-pyridone ions generated by demethylation of protonated 3-methoxy-pyridine [6].

However, the CID mass spectra of 2- and 3-pyridone reported in Ref. 6 are closely similar and the same obtains for the CID spectra of Figures 13.3d and 13.7c.

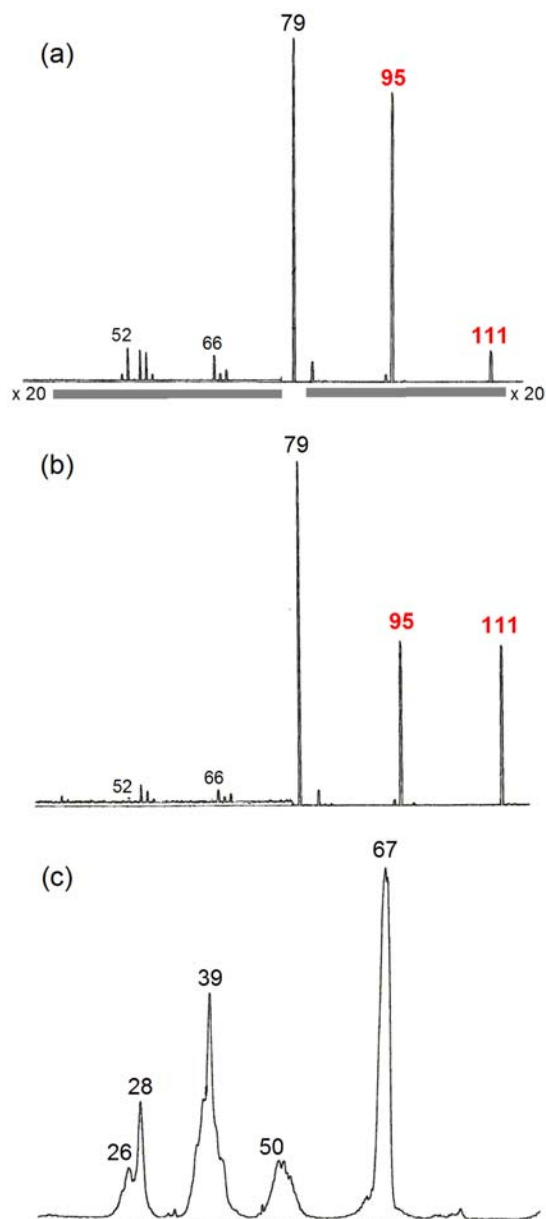


Figure 13.7 Mass spectra of the products of the ion-molecule reactions of pyridine-3-ylid ions with dioxygen : (a) $[O_2 \text{ pressure} = 2 \times 10^{-4} \text{ mbar}]$ and (b) $[O_2 \text{ pressure} = 8 \times 10^{-4} \text{ mbar}]$; (c) CID mass spectrum of the m/z 95 ions generated in the above ion-molecule reaction.

Thus, ions **2** and **3** cannot be differentiated on the basis of the CID mass spectra of the m/z 95 ions. However, there is a striking difference in the relative abundance of the m/z 111 and 95 ions generated in the two reactions. Comparison of Figures 13.7a and 13.3b shows that at a relatively low O_2 pressure, the m/z 111 adduct ion is observed with ion **3** but not with ion **2**. This is in agreement with our calculations, namely that the O-atom abstraction is exothermic for ion **2** and thermoneutral for ion **3**. Thus, incipient ions **D2** are more prone to dissociate prior to collisional stabilization than ions **D3**. This trend is paralleled in the mass spectra of Figures 13.7b and 13.3c where a higher oxygen pressure was used in the hexapole cell. The m/z 111 : 95 peak intensity ratio may therefore serve to differentiate ions **2** and **3**.

Finally, we note that adduct ions **D2** or **D3** are unlikely to further react with O_2 under our experimental conditions. Exploratory calculations indicate that the reaction of **D2** with O_2 is exothermic (by c. 15 kcal mol⁻¹), and that dissociation of the resulting [**D2**-O=O]⁺ adduct ion into 2-pyridone⁺ + O_3 is more energy demanding (by c. 25 kcal mol⁻¹) than back-dissociation into **D2** + O_2 .

13.3 Conclusions

The previously reported [4c] formation of the 2-pyridone ion from the pyridine-2-ylid ion and H_2O appears to refer to the reaction of O_2 from air co-introduced with the water vapour. Theory and experiment agree that this exothermic reaction leads to loss of 3O from a stable peroxide-type adduct ion at m/z 111. Similarly, pyridine-3-ylid ions (**3**) generate 3-pyridone ions, but the reaction in this case is thermoneutral. The m/z 111 : 95 peak intensity ratios in the spectra of the ion-molecule products from ions **2** and **3** reflect the different energy requirements and may serve as a diagnostic tool to differentiate the isomers.

The reported O-atom abstraction may well represent a general reaction of distonic heterocyclic ions : work in progress shows that the distonic ions of pyrimidine [10],

imidazole [11] and thiazole [11] show the same behaviour. The reaction of O₂ with the distonic ions of the prebiotic pyrimidine molecule may be of interest to astrochemistry [12].

References

- [1] J.L. Holmes, C. Aubry, P.M. Mayer, *Assigning Structures to Ions in Mass Spectrometry*. CRC Press: Boca Raton, FL, 2007.
- [2] K.M. Stirk, L.K.M. Kiminkinen, H.I. Kenttämä, *Chem.Rev.* 92 (1992) 1649.
- [3] (a) J.S. Brodbelt, *Mass Spectrom. Rev.* 16 (1997) 91; (b) S. Gronert, *Chem. Rev.*, 101 (2001) 329; (c) P. Gerbaux, P. Wantier, P.N. Cam, M.T. Nguyen, G. Bouchoux, R. Flammang, *Eur. J. Mass Spectrom.* 10 (2004) 889 ; (d) Y.E. Corilo, M.N. Eberlin, *J. Mass Spectrom.* 43 (2008) 1636.
- [4] (a) D. Lavorato, J.K. Terlouw, T.K. Dargel, W. Koch, G.A. McGibbon, H. Schwarz, *J. Am. Chem. Soc.* 118 (1996) 11898 ; (b) D. Lavorato, J.K. Terlouw, T.K. Dargel, G.A. McGibbon, W. Koch, H. Schwarz, *Int. J. Mass Spectrom.* 179/180 (1998) 7 ; (c) P. Gerbaux, M. Barbieux-Flammang, J.K. Terlouw, R. Flammang, *Int. J. Mass Spectrom.* 206 (2001) 91; (d) P.C. Burgers, J.L. Holmes, *Int. J. Mass Spectrom. Ion Processes*, 58 (1984) 15.
- [5] P. Gerbaux, M. Barbieux-Flammang, Y. Van Haverbeke, R. Flammang, *Rapid Commun. Mass Spectrom.* 13 (1999) 1707.
- [6] M.A. Trikoupi, P. Gerbaux, D.J. Lavorato, R. Flammang, J.K. Terlouw, *Int. J. Mass Spectrom.* 217 (2002) 1.
- [7] P.C. Burgers, J.K. Terlouw, in : N.M.M. Nibbering (Ed.), *Encyclopedia of Mass Spectrometry*, vol. 4, Elsevier, Amsterdam, 2005, p. 173.
- [8] S.J. Yu, C.L. Holliman, D.L. Rempel, M.L. Gross, *J. Am. Chem. Soc.* 115 (1993) 9676.
- [9] (a) P.G. Wenthold, J. Hu, R.R. Squires, *J. Mass Spectrom.* 33 (1998) 796; (b) D.G. Harman, S.J. Blanksby, *Org. Biomol. Chem.* 5 (2007) 3495.
- [10] D. J. Lavorato, T.K. Dargel, W. Koch, G.A. McGibbon, H. Schwarz, J.K. Terlouw, *Int. J. Mass Spectrom.* 210/211 (2001) 43.
- [11] R. Flammang, M.T. Nguyen, G. Bouchoux, P. Gerbaux, *Int. J. Mass Spectrom.* 202 (2000) A8.
- [12] H.K. Ervasti, K.J. Jobst, P.C. Burgers, P.J.A. Ruttink, J.K. Terlouw, *Int. J. Mass Spectrom.* 262 (2007) 88.
- [13] S.G. Lias, J.E. Bartmess, J.F. Liebman, J.L. Holmes, R.D. Levin, W.G. Mallard, *J. Phys. Chem. Ref. Data* 17 Suppl. 1 (1988).

Chapter 14

Experimental and computational methods

14.1 The VG Analytical ZAB-R Mass Spectrometer

The tandem mass spectrometry-based experiments performed at McMaster University involved the VG Analytical ZAB-R instrument [1]. This custom built mass spectrometer is a three sector instrument of BE_1E_2 geometry (B = magnet, E = electrostatic analyzer), whose design is based on the standard, non-extended geometry of its predecessor, the ZAB-2F [2].

The ion source, which is kept under high vacuum using a 160/170 Diffstak, is equipped with three inlet systems for sample introduction : (i) an all glass heated inlet system (AGHIS) used for volatile compounds; (ii) an all quartz direct insertion probe used for less volatile compounds; (iii) a direct solids insertion probe used for solid samples.

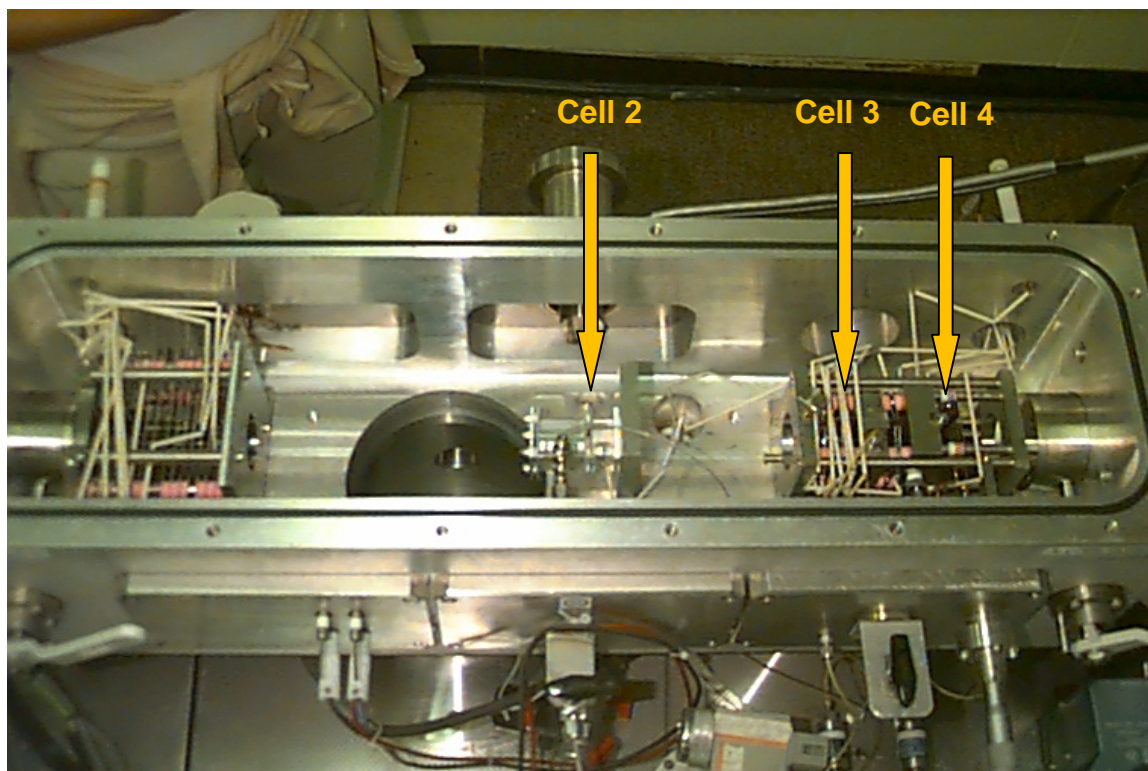
Viscous liquids of low volatility (such as N-formylethanolamine of Chapter 9) are best introduced with the solids insertion probe or alternatively by putting a smear of the sample on the tip of the quartz probe. The AGHIS and the quartz probe both possess reservoirs from which the sample steadily evaporates and/or sublimes. Consequently, the temperature of the bulk sample can easily be varied to obtain a desired source pressure.

The first of five collision cells is located in the first field region (1ffr) of the instrument. An Autospec magnet precedes the second field free region (2ffr) housing, which has the form of a 79 x 23 x 23 cm rectangular box. The box may be quickly isolated from its two diffusion pumps and the other sectors using four valves. Easily removable top and side panels enables rapid access to the three collision chambers (cells 2 – 4 of Figure 1.1) and lens assemblies mounted inside the 2ffr. Cell 3 is a home-built chamber, with the dimensions 30(l) x 3(w) x 14(h) mm, used for neutralization with organic vapours such as



The VG ZAB-R Mass Spectrometer

N,N-dimethylaniline. Cell 4 [20(l) x 1(w) x 10(h) mm], which is also electrically isolated and equipped with a y-focus/deflection lens assembly, is used for 'standard' reionization and collision-induced dissociation (CID) experiments. Cells 2 - 4 are situated at distances of 240, 44 and 10 mm from the focal point of the ion beam at the intermediate slit, which is located next to the glass window on top of the 2ffr box. Immediately following the first electrostatic analyzer (E_1), there is a box type collector housing in which the 3ffr collision chamber (cell 5) is located in front of a small Autospec ESA (E_2 , 12.7 cm radius, 72.5°). This housing contains two photomultiplier type detectors and a fifth 160/700 Diffstak is used to pump this region.

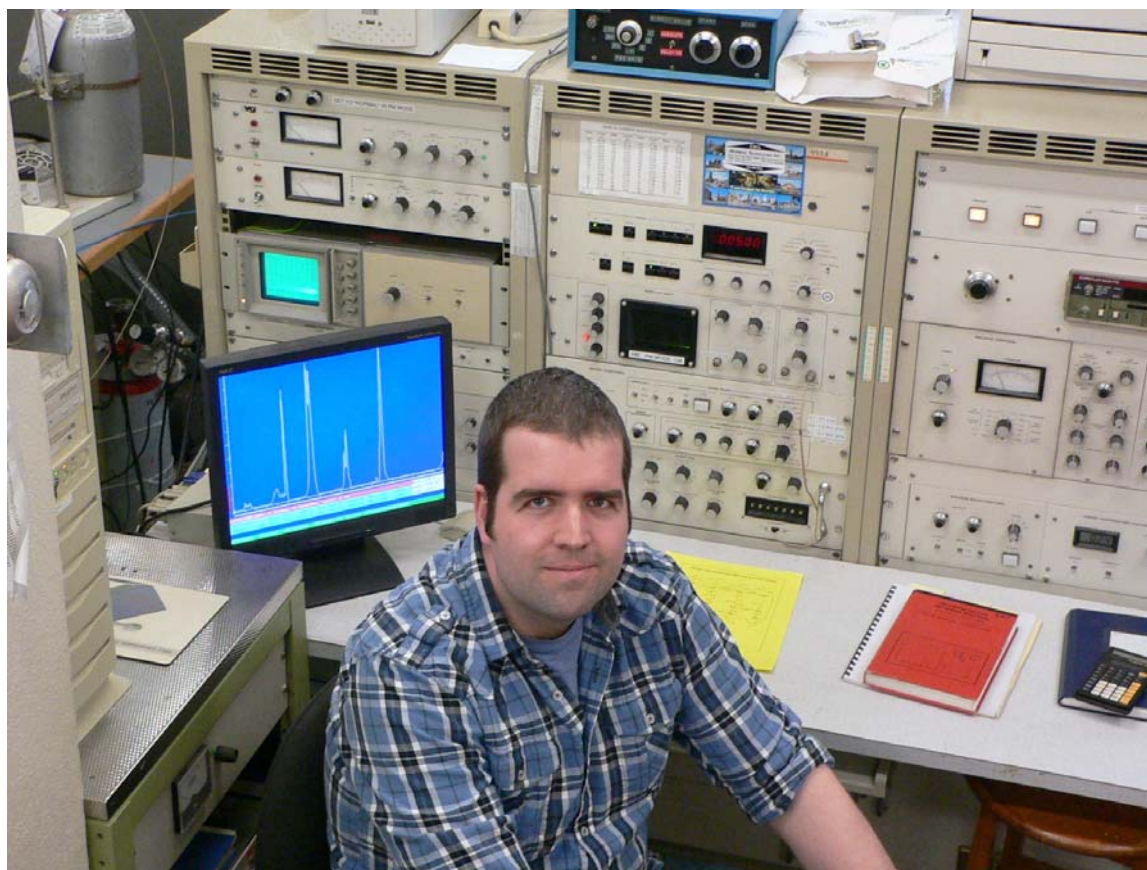


The second-field-free region (2ffr) with the top panel removed.

14.2 Experimental Conditions

The electron ionization (EI) mass spectra were obtained under the following conditions : electron energy : 70 eV; emission current : 0.5 mA; source temperature : 100 – 120 °C. The accelerating voltage (4 - 10 kV) used in the collision experiments is indicated in the Figure captions in the Chapters. The vapour pressure of the sample in the source, typically 10^{-7} - 10^{-5} Torr, is monitored by a remote ionization gauge.

The chemical ionization (CI) experiments of Chapters 3 and 5 were performed at a source pressure of c. 10^{-4} Torr, while maintaining the other parameters noted above. The repeller voltage was held close to 0 V and the primary ionization was accomplished with 100 eV electrons.



The control console and data acquisition system.

All spectra were recorded using a PC-based data acquisition system (ZABCAT) developed by Mommers Technologies Inc. (Ottawa, Canada). The spectra represent an accumulation of 5 – 30 individual scans.

The metastable ion (MI) mass spectra were obtained in the 2ffr unless otherwise indicated. The kinetic energy release (KER) values were estimated from the width at half-height ($T_{0.5}$) of the metastable peak by means of a standard equation (see Chapter 1) and corrected for the width at half height of the main beam [3].

The collision-induced dissociation (CID) mass spectra were obtained in the 2- or 3ffr and the MS/MS/MS experiments (MI/CID, CID/CID and NR/CID) were all obtained in the 3ffr.

Unless indicated otherwise, all CID experiments were performed using either O₂ or He as the collision target at a main beam transmittance of 70%.

The neutralization (NR) mass spectra were obtained in the 2ffr using N,N-dimethylaniline as the neutralization target (cell 3, main beam transmittance of 70%) and O₂ (cell 4) for reionization. For all NR experiments, a total analyzer pressure of 5×10^{-5} Torr was used. A charged deflector electrode is located between cells 3 and 4 to separate the ions from the beam of neutrals.

The CIDI spectra were obtained (in the 2ffr) using the instrumental setup for a CID experiment but with the deflector electrode located in front of the collision gas chamber set at 1 kV.

14.3 The AutoSpec 6F Mass Spectrometer

The ion-molecule reactions of mass-selected ion (Chapters 2, 5 and 13) were performed using the Mons AutoSpec 6F [4], a six-sector magnetic deflection instrument of EBEEBE geometry. The instrument is equipped with three cells (C₁₋₃) to realize high-energy collision-induced dissociations and an rf-only hexapole (HEX) reaction chamber for studies of associative ion-molecule reactions so that the present configuration is: C₁E₁B₁C₂E₂-HEX-E₃B₂C₃E₄, see Fig. 1.9 of Chapter 1.

In brief, the experiment involves mass selection of a beam ions (8 keV) using the first three sectors. Next, the ions are decelerated to ~ 5 eV in front of the hexapole cell to optimize the yield of associative ion-molecule reactions with target gas vapour – at a pressure of ~ 5×10^{-4} mbar, as measured with a Pirani gauge located inside the cell. Following reacceleration to 8 keV, ions leaving the hexapole cell may be mass analyzed by scanning the field of B₂, or mass selected and subjected to collision-induced dissociation with O₂ in chamber C₃. The CID mass spectrum of the mass-selected ions is obtained by scanning sector E₄.

14.4 Computational methods

The calculations were performed using the Gaussian 03 and Gaussian 09 suites of programs [5] on SHARCNET. Enthalpies of formation for the various ions and neutrals were obtained from the CBS-QB3 [6] model chemistry. For selected species, the much more computationally demanding CBS-APNO [7] method was used. The identity of local minima and connecting transition states (TS) was confirmed by frequency analysis. Unless stated otherwise, all enthalpies presented in the text and in the schemes refer to CBS-QB3 derived $\Delta_f H_{298}^\circ$ values in kcal mol⁻¹.

The CBS-QB3 model chemistry is expected to yield enthalpy values with chemical accuracy (± 2 kcal mol⁻¹) [8]. However, several of the open-shell ions of this work show $\langle S^2 \rangle$ values beyond the “acceptable” range of circa 5% of the theoretical value. It is difficult to assess the effect of strong spin-contamination on the errors in the CBS-QB3 derived energies but the incorporation of a spin-correction factor and the use of DFT derived geometries are expected to mitigate adverse effects [9]. Further, in all cases the potential energy diagrams of this study are not significantly different from those obtained at the B3LYP/CBSB7 level of theory, where spin-contamination is not an issue. In this context we note that, see Tables in the Chapters, the available experimental $\Delta_f H_{298}$ values for are gratifyingly close to the calculated values.

14.5 Preparation of Precursor Molecules

All commercially available precursor molecules (Aldrich, Alfa Aesar, TCI, CDN Isotopes Canada) were used without further purification. The procedures for all synthesized precursor molecules are briefly presented below by Chapter. Where necessary, the identity and purity of the compound was verified by a GC-MS experiment using a Micromass GC-TOF instrument at its standard resolution of ~ 5000 (50% valley definition).

Chapter 4

The D-labeled nitriles $\text{CD}_2=\text{CH}-\text{C}\equiv\text{N}$ and $\text{CH}_2=\text{CD}-\text{C}\equiv\text{N}$ were purchased from CDN Isotopes Canada. $\text{CD}_2=\text{CH}-\text{C}\equiv\text{N}$ was obtained from $\text{CD}_2=\text{CD}-\text{C}\equiv\text{N}$ by back exchange with H_2O under alkaline conditions [10]. A sample of pyridazine-3-carboxylic acid, the precursor for the pyridazine ylid-ion, was available from a previous study [11].

Chapter 5

H^{13}CN was synthesized from K^{13}CN (BOC) and H_2SO_4 using a standard procedure [12]. Gattermann [12b] recommends that the operator smoke during the preparation, for he found that a trace of HCN is sufficient to give the tobacco smoke a highly characteristic flavour. This preliminary warning is useful in case of leaky apparatus or a faulty hood. All necessary precautions were taken during the synthesis.

Chapter 6

The deuterium labelled isotopomer $\text{CH}_3\text{C}(=\text{O})\text{NDOD}$ was obtained from the unlabelled compound by repeated exchange with methanol-OD.

Chapter 7

The 2-aminoxyethanol sample was synthesized from 2-bromoethanol and N-hydroxyphthalimide by an established procedure [13], but using N,N-dimethylformamide rather than dimethyl sulfoxide as the solvent. Its isotopologue $\text{ND}_2\text{OCH}_2\text{CH}_2\text{OD}$ was obtained therefrom by repeated exchange with methanol-OD.

Chapter 8

The reduction of simple nitrocompounds to the corresponding amines may be accomplished by a wide variety of means without difficulty, but the partial reduction to form hydroxylamines is far less straightforward. Hence, the desired precursor molecule of this study, 2-hydroxyaminoethanol, has not even been described in the literature. However, in a joint project with Dr. R.D. Bowen, a synthetic procedure was devised starting from 2-nitroethanol that is described in the experimental of Ref. 14. Isolation of

2-hydroxyaminoethanol as the free base ($\text{HOCH}_2\text{CH}_2\text{NHOH}$) was found to be impractical, but its hydrochloride could be generated in situ during the reaction work up and be isolated as a hygroscopic solid.

The samples were introduced into the ion source of the mass spectrometer (kept at 120 °C) via a solids probe held at 80 °C. Since the compound is prone to decompose and/or polymerize upon heating, the finely powdered sample was put into a 15 mm quartz probe tube into which a 17 mm gold wire was inserted to promote a better heat transfer to the sample [15].

Repeated exchange of the unlabelled hydrochloride with a five fold excess of anhydrous methanol-OD was used to prepare a sample of $\text{DOCH}_2\text{CH}_2\text{NDOD}\cdot\text{DCl}$. The isotopologue $\text{HOCH}_2\text{CD}_2\text{NHOH}\cdot\text{HCl}$ was obtained from the D-labelled 2-nitroethanol $\text{HOCH}_2\text{CD}_2\text{NO}_2$, whose synthesis is also described in Ref. 14.

Chapter 9

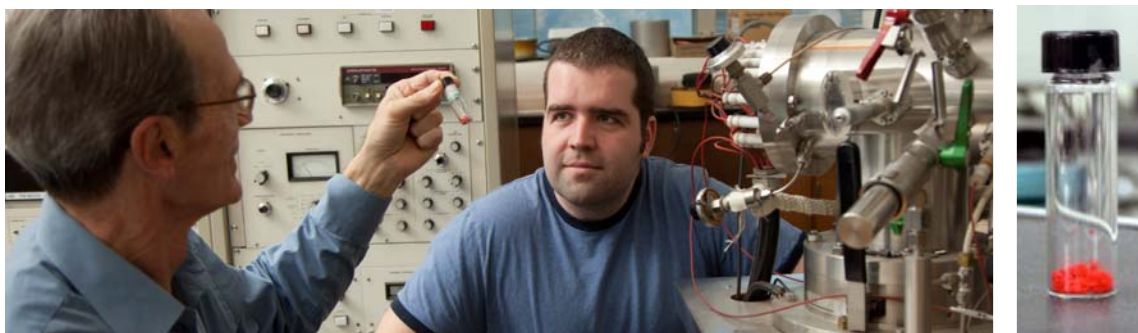
The synthesis of N-formylethanolamine (NFE) from ethanolamine was performed using methyl formate, rather than ethyl formate as stipulated in the procedure of Tip *et al.* [16]. Methyl formate (100 mg, 1.7 mmol) was added slowly to a solution of ethanolamine (100 mg, 1.7 mmol) dissolved in methanol (1.8 mL) while cooling the mixture with an ice water bath. The solvent was removed under reduced pressure but the prescribed [16] vacuum distillation of the resulting high-boiling residue was not performed because it appears that 2-oxazoline is generated as a persistent impurity by thermal decomposition of the sample. This point is discussed further in Chapter 9. Repeated exchange of the labile hydrogens of NFE with MeOD yielded $\text{DOCH}_2\text{CH}_2\text{NDCHO}$. The D-labelled compound $\text{HOCD}_2\text{CD}_2\text{NHCHO}$ was synthesized using ethanolamine- d_4 (CDN Isotopes) in the above procedure.

The D-, ^{18}O -, and mixed D/ ^{18}O -isotopologues $\text{HOCH}_2\text{CH}_2\text{NHCDO}$, $\text{HOCH}_2\text{CH}_2\text{NHCH}^{18}\text{O}$ and $\text{HOCH}_2\text{CH}_2\text{NHCD}^{18}\text{O}$ were prepared from the labelled methyl formates CH_3OCDO (Aldrich) $\text{CH}_3\text{OCH}^{18}\text{O}$ and $\text{CH}_3\text{OCD}^{18}\text{O}$. A 5 : 2 : 1 molar mixture of MeOH, H_2^{18}O , and (D-

labelled) formic acid was kept at room temperature for 5 days and thereafter distilled to obtain $\text{CH}_3\text{OCH}^{18}\text{O}$ and $\text{CH}_3\text{OCD}^{18}\text{O}$. O-methoxy-N-formylethanolamine and its isotopologue $\text{CH}_3\text{OCH}_2\text{CH}_2\text{NHCH}^{18}\text{O}$ were synthesized from O-methoxyethanolamine (Aldrich > 99%) in a procedure analogous to that used for the preparation of NFE.

Chapter 11

Until recently, physicochemical studies of *s*-tetrazine were hampered by great difficulties to obtain reasonably pure samples. In this study, we have used a new procedure [17] proposed in 1998 that is based upon the reaction of formamidine acetate with hydrazine hydrate in acetic acid. The dihydro-tetrazine generated is subsequently oxidized in situ with KNO_2 to produce *s*-tetrazine as a bright red crystalline compound that was isolated by extraction and further purified by sublimation.



Chapter 12

Decarboxylation of ionized *s*-triazine-2-carboxylic acid followed by loss of HCN is expected to yield the distonic dimer ion $\text{HC}=\text{N}-\text{C}=\text{NH}^{\bullet+}$ discussed in Chapter 12. However, this compound was not available and an attempted expensive custom synthesis was aborted. Instead we synthesized a sample of 2-methoxy-*s*-triazine from *s*-triazine and $\text{NH}_2\text{C}(=\text{NH})\text{OCH}_3\cdot\text{HCl}$ (2-methylpseudourea hydrochloride) using the method described in Ref. 18. As shown in Chapter 12, this precursor molecule also generates the desired ion, by the consecutive loss of $\text{CH}_2=\text{O}$ and HCN.

References

- [1] H.F. van Garderen, P.J.A. Ruttink, P.C. Burgers, G.A. McGibbon, J.K. Terlouw, *Int. J. Mass Spectrom. Ion Proc.* 121 (1992) 159.
- [2] R.P. Morgan, J.H. Beynon, R.H. Bateman and B.N. Green, *Int. J. Mass Spectrom. Ion Phys.* 28 (1978) 171.
- [3] J.L. Holmes, C. Aubry, P.M. Mayer. *Assigning Structures to Ions in Mass Spectrometry*, CRC Press, Boca Raton, 2007. Chapter 1.
- [4] (a) R.H. Bateman, J. Brown, M. Lefevre, R. Flammang, Y. Van Haverbeke, *Int. J. Mass Spectrom. Ion Processes* 115 (1992) 205; (b) R. Flammang, Y. Van Haverbeke, C. Braybrook, J. Brown, *Rapid Commun. Mass Spectrom.* 9 (1995) 795; (c) L. Trupia, N. Dechamps, R. Flammang, G. Bouchoux, M.T. Nguyen, P. Gerbaux, *J. Am. Soc. Mass Spectrom.* 19 (2008) 126.
- [5] M. J. Frisch et al. *Gaussian 09*, Gaussian, Inc., Wallingford CT, 2004.
- [6] J.A. Montgomery, Jr., M.J. Frisch, J.W. Ochterski, G.A. Petersson, *J. Chem. Phys.* 112 (2000) 6532.
- [7] J.W. Ochterski, G.A. Petersson, J.A. Montgomery, Jr., *J. Chem. Phys.* 104 (1996) 2598.
- [8] L.N. Heydorn, Y. Ling, G. de Oliveria, J.M.L. Martin, Ch. Lifshitz, J.K. Terlouw. *Zeitschrift für Physikalische Chemie*, 215 (2001) 141.
- [9] P.M. Mayer, C.J. Parkinson, D.M. Smith, L. Radom, *J. Chem. Phys.* 108 (1998) 604.
- [10] M.G. Fatica, H.J. Harwood, *J. Macromol. Sci. Chem.*, A12(8) (1978) 1099.
- [11] T. Karapanayiotis, G. Dimopoulos-Italiano, R.D. Bowen, J.K. Terlouw, *Int. J. Mass Spectrom.* 236 (2004) 1.
- [12] (a) K. Ziegler, *Organic Syntheses*, 1 (1941) 314; (b) L. Gattermann, *Ann.*, 357 (1907) 318.
- [13] D. Dhanak, C.B. Reese, S. Romana, G. Zappia, *J. Chem. Soc., Chem. Commun.* (1986) 903.
- [14] K.J. Jobst, S. Jogee, R.D. Bowen, J.K. Terlouw, *Int. J. Mass Spectrom.* (2011) in press.
- [15] L.M. Fell, J.T. Francis, J.L. Holmes, J.K. Terlouw, *Int. J. Mass Spectrom. Ion Proc.* 165/166 (1997) 179.
- [16] L. Tip, C. Versluis, J.W. Dallinga, W. Heerma, *Anal. Chim. Acta*, 241 (1990) 219.
- [17] J. Sauer, D.K. Heldmann, J. Hetzenegger, J. Krauthan, H. Sichert, J. Schuster, *Eur. J. Org. Chem.* 12 (1998) 2885.
- [18] F.C. Schaefer, G.A. Peters, *J. Am. Chem. Soc.* 81 (1959) 1470.

Summary

This thesis explores the role of catalysis by a single molecule in the course of both association and dissociation reactions of organic radical cations in the rarefied gas-phase. The first Chapter introduces the combined experimental and theoretical approach used in the studies of this thesis. It also provides a brief description of the various tandem mass spectrometry based experiments and the model chemistries derived from theory

In Chapter 2, it is shown that a very high barrier prohibits the cyanamide ion, $\text{H}_2\text{N}-\text{C}\equiv\text{N}^{\bullet+}$, to isomerize into the elusive carbodiimide ion $\text{HN}=\text{C}=\text{NH}^{\bullet+}$, the most stable member of the family of $\text{CH}_2\text{N}_2^{\bullet+}$ ions. However, experiment and theory agree that a single H_2O molecule catalyzes the transformation $\text{H}_2\text{N}-\text{C}\equiv\text{N}^{\bullet+} \rightarrow \text{HN}=\text{C}=\text{NH}^{\bullet+}$.

Chapter 3 discusses the ion-molecule reaction of the acrylonitrile ion $\text{CH}_2=\text{CH}-\text{C}\equiv\text{N}^{\bullet+}$ with its neutral counterpart. It appears that hydrogen-bridged radical cations (HBRCs) and ion-dipole complexes are initially formed, which do not undergo self-catalysis. Instead, the HBRCs undergo self-protonation or else isomerize into a very stable covalently bound ‘head-to-tail’ dimer ion, which acts as the starting configuration for the reactions that lead to the losses of H^{\bullet} , HCN and C_2H_2 . The latter process involves a crucial cyclization step that ultimately yields ionized pyrimidine, in admixture with its α -distonic isomer. This process may be relevant in the context of the quest for the prebiotic pyrimidine molecule in astrochemistry.

Chapter 4 shows that $\text{CH}_2=\text{C}=\text{C}=\text{NH}^{\bullet+}$ and $\text{CH}=\text{CH}-\text{N}=\text{CH}^{\bullet+}$ are the most stable members of the family of $\text{C}_3\text{H}_3\text{N}^{\bullet+}$ isomers and that they cannot interconvert with the acrylonitrile ion. This leads to the proposal that the interaction of $\text{C}_2\text{H}_2^{\bullet+}$ and HCN , a reaction of potential interest in astrochemistry, yields the distonic ion $\text{CH}=\text{CH}-\text{N}=\text{CH}^{\bullet+}$, rather than $\text{CH}_2=\text{CH}-\text{C}\equiv\text{N}^{\bullet+}$. In Chapter 5, it is shown that the interaction of a single HCN molecule with an acrylonitrile ion does *not* lead to cyclization into the pyrimidine ion, but instead efficiently promotes the isomerization of $\text{CH}_2=\text{CH}-\text{C}\equiv\text{N}^{\bullet+}$ into $\text{CH}_2=\text{C}=\text{C}=\text{NH}^{\bullet+}$.

Chapter 6 discusses the unexpected dissociation of low energy N-hydroxyacetamide radical cations, $\text{CH}_3\text{C}(=\text{O})\text{NHOH}^{\bullet+}$, into $\text{CH}_3\text{C}=\text{O}^+ + \text{NH}_2\text{O}^\bullet$. The key transformation comprises the ion-catalyzed rearrangement $\text{HNOH}^\bullet \rightarrow \text{NH}_2\text{O}^\bullet$, where $\text{CH}_3\text{-C}=\text{O}^+$ acts as the catalyst in a quid-pro-quo process. In this reaction the acetyl cation donates a *proton* to the N atom of HNOH^\bullet and then the O-H *proton* of the incipient $\text{NH}_2\text{OH}^{\bullet+}$ radical cation is donated back.

Chapter 7 presents the remarkably rich dissociation chemistry of 2-aminoxyethanol ions $\text{HOCH}_2\text{CH}_2\text{ONH}_2^{\bullet+}$. The metastable ions generate $\text{HOCH}_2\text{CH}(\text{OH})^+$, protonated glycolaldehyde; $\text{HOCH}_2\text{C}(=\text{O})\text{H}^{\bullet+}$, the glycolaldehyde ion; $\text{HC}(\text{OH})\text{NH}_2^+$, protonated formamide; $\text{CH}_2\text{OH}_2^{\bullet+}$, the methylene oxonium ion, and NH_4^+ , the ammonium cation.

The challenging mechanistic analysis indicates that a 1,4-H shift yields distonic ions $\text{HOCHCH}_2\text{ONH}_3^{\bullet+}$, which serve as the common intermediate of all pathways. They readily isomerize into several interconverting HBRCs of which ionized glycolaldehyde- NH_3 complexes are key species. The latter also account for the partial conversion of the glycol-aldehyde ions into their more stable enol counterpart $\text{HOC}(\text{H})=\text{C}(\text{H})\text{OH}^{\bullet+}$, by proton-transport catalysis

Chapter 8 argues that the prominent H_2O loss from metastable 2-hydroxyaminoethanol ions $\text{HOCH}_2\text{CH}_2\text{NHOH}^{\bullet+}$ generates 1,2-oxazetidine ions. A mechanistic analysis indicates that the dissociation of the molecular ions is initiated by a 1,5-H transfer that leads to the formation of ionized 1,2-oxazetidine via a HBRC intermediate.

The study of Chapter 9 reveals that both distonic ions and HBRCs play a key role in the dissociation chemistry of the N-formylethanolamine ion, $\text{HOCH}_2\text{CH}_2\text{NHC}(\text{H})=\text{O}^{\bullet+}$.

The primary fragmentations involving the losses of CH_2O and $\text{C}_2\text{H}_3\text{O}^\bullet$ yield the distonic ion $^\bullet\text{CH}_2\text{N}(\text{H})\text{CHOH}^+$ and O-protonated formamide $\text{HC}(\text{OH})\text{NH}_2^+$. The competing H_2O loss yields a mixture of N-vinylformamide ions and its cyclized distonic isomer.

It is proposed that part of the molecular ions, via C–C bond cleavage, rearrange into HBRC $[\text{CH}_2\text{N}(\text{H})\text{C}(\text{H})=\text{O}-\text{H}^{\bullet+}-\text{O}=\text{CH}_2]^{\bullet+}$, which serves as the direct precursor to CH_2O loss. The competing $\text{C}_2\text{H}_3\text{O}^\bullet$ and H_2O losses are initiated by a 1,5-H shift in the molecular ions to

produce the distonic ion $\text{HOCHCH}_2\text{N(H)C(H)OH}^{\bullet+}$.

Loss of $\text{C}_2\text{H}_3\text{O}^\bullet$ therefrom involves a “McLafferty + 1” type reaction in which HBRCs are key intermediates. The radical lost in this reaction is $\text{CH}_2=\text{C(H)O}^\bullet$ but a quid-pro-quo catalysis may lead to the co-generation of the more stable acetyl radical $\text{CH}_3\text{C}=\text{O}^\bullet$.

The H_2O loss involves communication with ion-molecule complexes of vinyl alcohol and formimidic acid, whose components may recombine to form $\text{HOCH(CH}_2\text{)N(H)C(H)OH}^{\bullet+}$. This distonic ion may undergo a 1,5-H shift to produce a HBRC of the N-vinylformamide ion and H_2O . Facile cyclization of the N-vinylformamide ion may occur in the hydrogen-bridged complex prior to the loss of H_2O .

The studies of Chapters 10 – 12 demonstrate that the covalently bound $[\text{H,C,N}]$ dimer ions $\text{HN}=\text{C}=\text{C}=\text{NH}^{\bullet+}$, $\text{HC}=\text{N}-\text{C}=\text{NH}^{\bullet+}$ and $\text{NH}_2-\text{C}-\text{C}\equiv\text{N}^{\bullet+}$ have a stable neutral counterpart in the rarefied gas phase, which may be of relevance to interstellar chemistry. It is further shown that interaction of $\text{NH}_2-\text{C}-\text{C}\equiv\text{N}^{\bullet+}$ with an HNC molecule leads to the catalyzed isomerization of both the neutral and the ion into HCN and $\text{HN}=\text{C}=\text{C}=\text{NH}^{\bullet+}$.

The elusive HCN dimer ion $\text{HC}=\text{N}-\text{N}=\text{CH}^{\bullet+}$ is stable in the rarefied gas-phase, albeit that it readily interconverts, via a 1,2-HCN shift, with its nitrene isomer $\text{HC}=\text{NC}(=\text{N})\text{H}^{\bullet+}$. However, unlike the HNC dimer ion $\text{HN}=\text{C}=\text{C}=\text{NH}^{\bullet+}$, theory and experiment agree that the HCN dimer ions $\text{HC}=\text{N}-\text{N}=\text{CH}^{\bullet+}$ and $\text{HC}=\text{NC}(=\text{N})\text{H}^{\bullet+}$ have no stable neutral counterpart.

In Chapter 13, it is shown that the 2- and 3-ylid isomers of the pyridine ion react with O_2 to produce the 2- and 3-pyridone ions at m/z 95. Theory and experiment agree that these reactions lead to losses of ^3O from stable peroxide-type adduct ions at m/z 111. The reaction is exothermic with the 2-ylid ion and thermoneutral with the 3-ylid ion. This makes it possible to use the m/z 111 : 95 peak intensity ratios in the spectra of the ion-molecule products as a diagnostic tool to differentiate the isomers.

The reported O-atom abstraction may well represent a general reaction of distonic heterocyclic ions : work in progress shows that the distonic ions of pyrimidine, imidazole and thiazole behave in the same way.